Identification of critical process parameters for the downstream processing of cell culture-derived Orf virus particles

Dissertation

Zur

Erlangung des akademischen Grades der Doktorin der Ingenieurwissenschaften

(Dr.-Ing.)

dem Promotionszentrum für Ingenieurwissenschaften

am Forschungscampus Mittelhessen

vorgelegt von

Friederike Eilts, M.Sc.

Datum der Disputation: 29. November 2023

München, den 04. Dezember 2023

PREFACE

Finally -these are the pages with the work of the last five years. To write this is a surreal and exciting moment, which was only possible to achieve with the support of many people.

First, I want to thank my supervisors, Prof. Dr. Michael Wolff from Technische Hochschule Mittelhessen and Prof. Dr. Bernhard Spengler from Justus-Liebig-Universität Gießen, for the opportunity to pursue my doctoral degree and for the valuable feedback on scientific questions. Furthermore, I want to thank Prof. Dr. Peter Czermak for his guidance as head of the Institute for Bioprocessing and Pharmaceutical Technology at THM and his readiness to step in as co-referee and chair of the examination board. Further thanks go to Prof. Dr. Udo Reichl and PD. Dr. Olga Dolnik for agreeing to be part of the examination board. Additionally, I want to name the people, who took the time to comment on this manuscript and improved it a great deal: Michael, Keven, Lasse, and DJ.

In particular, I want to thank Michael for his continuous support, open-door policy, and trust in me to follow my research ideas and learn scientific intuition. Next to the position for this dissertation project, Michael offered me many exceptional opportunities: to experience GMP production, to participate in (international) conferences, and, notably, to travel to Rensselaer Polytechnic Institute in Troy, NY, USA, for a research stay. My time at RPI was devotedly supported by professors Robert Linhardt, Fuming Zhang, and Jonathan Dordick. To work with these remarkable scientists was an honor and taught me many more things than pure knowledge.

Thinking of my workplaces, I am grateful for the environment that offered space for research. At IBPT, I especially want to thank Prof. Dr. Peter Czermak and Prof. Dr. Denise Salzig for providing a well-structured and excellently equipped work environment, which we shared and filled with Michael's downstream equipment. The attitude to offer space and equipment between the groups of the institute was incredibly valuable and offered me to spend time in Michael's downstream processing lab as well as Peter's cell culture, bioprocess engineering, and membrane technology labs, and Prof. Dr. Frank Runkel's biopharmaceutical technology lab.

These places were filled with people who shared my daily research life - many thanks to all (unnamed) colleagues from CBIS at RPI and IBPT at THM. The community support and the common interests facilitated my path toward finishing my PhD, which I only have brought to this point with. At IPBT, I spent most of my lab time in the shared downstream processing and cell culture lab. I immensely enjoyed the advice and encouragement that all members offered at all times. An open door and day/night-long chats about research and beyond were understood by everyone. This extended to countless extracurricular activities, which were always a blast. Within this group of workmates, I want to name those who shared an office with me over time, in chronological order, Jasmin Leber, Gundula Sprick, Stefan Schönherr, Nele, Daniel Humpert, Keven Lothert, Lotti, and Carolin Lappöhn. Exceptional gratitude belongs to Stefan, with whom I experienced many discussions on subjects we did (not) agree on; to Keven, who was an indispensable support in all projects and problems with laughter and pragmatism; and to Florian Petry, the self-made office mate, who was a constant advisor in all questions of research and life. From next door's, Julie Harnischfeger and Pablo should not be left unmentioned, which spent hours of friendship with me at and outside of work. From IBPT, I also want to thank all students I supervised, who diligently generated data and knowledge for several publications. Their achievements significantly advanced the progress of this dissertation project and my personal development.

Next, several people kindly supported my research as collaborators and partners by supplying material, scientific equipment, and advice. Exceptional thanks are due to Felix Pagallies, Dr. Ralf Amann, and Dr. Achim Rziha from Universitätsklinikum Tübingen for the shared work on the Orf virus; to the group of Dr. Martin Hardt from Biomedizinisches Forschungszentrum Seltersberg for their support on transmission electron microscopy; to Dr. Jennifer Labisch and Dr. Karl Pflanz from Sartorius Stedim Biotech GmbH for the common interest in the steric exclusion chromatography; to Lisa Jordan and Prof. Dr. Anna Becker from Friedrich-Alexander-Universität Nürnberg-Erlangen as well as to Prof. Dr. Sven Bergmann from Friedrich-Loeffler-Institut for the shared project on purifying the koi herpes virus; to Dr. Robert Vogel for the joint work on tunable resistive pulse sensing, and to Prof. Dr. Patrick Elter and Dr. Claus Moseke for the opportunity to work with scanning electron microscopy.

Throughout my life and my scientific career, I was encouraged by many inspiring individuals and encounters. I met friends who always have my back and taught me lessons for life. Some of these friends date back to my school time in Augsburg and Braunschweig and will hopefully last for life. Throughout my Bachelor's and Master's studies, the unconditional support of the Bioings and now the Festivalalteramtive group was my savior. My studies in Waterloo, ON, Vancouver, BC, Canada, and Bogotá, Colombia, introduced me to new values and unforgettable people. Throughout the time of my PhD, the exchange with new friends and my mentoring peer group were extremely valuable in finding ground. Eventually, I learned the most long-lasting lessons from my late horses, Luna and Fibi, and the people around them, who offered conversations about personal development and purpose.

The final thanks belong to the people without whom I would not have reached this point: my parents, who always believe in me and offer me every opportunity there is, who are my role models for handcrafting, enthusiasm, asking the *why* questions, and letting be; my sister Anna, whom I talked to the most hours (according to my telephone bill), and who is the most valuable opposite of me I could wish for; and Lasse, my silent supporter and soul mate, who shares every adventure with me no matter what.

Already now, while finishing this text, many unnamed people, and the reasons for my gratitude to them, pop up in my head. Please know that I also thought of you!

München, July 24th 2023

Friederike Eilts

TABLE OF CONTENTS

DECLARATION OF AUTHORSHIP & EIDESSTATTLICHE ERKLÄRUNG

I declare that I have completed this dissertation single-handedly without the unauthorized help of a second party and only with the assistance acknowledged therein. I have appropriately acknowledged and cited all text passages derived verbatim from or based on the content of published work of others and all information relating to verbal communications. I consent to the use of anti-plagiarism software to check my thesis. I have abided by the principles of good scientific conduct laid down in the regulations of the leading university, which were delivered to me in carrying out the investigations described in the dissertation.

Ich erkläre: Ich habe die vorgelegte Dissertation selbstständig und ohne unerlaubte, fremde Hilfe und nur mit den Hilfen angefertigt, die ich in der Dissertation angegeben habe. Alle Textstellen, die wörtlich oder sinngemäß aus veröffentlichten Schriften entnommen sind, und alle Angaben, die auf mündlichen Auskünften beruhen, sind als solche kenntlich gemacht. Ich stimme einer eventuellen. Überprüfung meiner Dissertation durch eine Antiplagiat-Software zu. Bei den von mir durchgeführten und in der Dissertation erwähnten Untersuchungen habe ich die Grundsätze guter wissenschaftlicher Praxis, wie sie in der entsprechenden Satzung der federführenden Hochschule niedergelegt sind und die mir ausgehändigt wurde, eingehalten.

München, July 24th 2023

Friederike Eilts

ABSTRACT

The COVID-19 (coronavirus disease 2019) pandemic has shown the importance of ready-at-hand- tools to bring pharmaceutical products to market. This includes the availability of platforms to target new diseases as well as their production process. Such a platform could be available with the Orf virus (ORFV), a promising viral vector with applications as gene therapeutic, antiviral, oncolytic, immunomodulatory, and vaccination agent. However, production processes for the ORFV are not established yet. A recent publication on a lab-scale purification process of the ORFV suggested the use of the steric exclusion chromatography (SXC) with high infectious virus yields and impurity removal. This rather new method is closely related to the conventional polyethylene glycol (PEG) precipitation, however, including a porous chromatographic media in the process. By preferential and steric exclusion mechanisms, the precipitates accrete inside the stationary phase and are retained. Several critical process parameters of the method are known and easily controlled, i.e., the PEG composition, the buffer composition as well as the pH and the ionic strength, the mixing technique prior to column loading, the flow rate, and the stationary phase. Nevertheless, high variability between different runs is frequently observed. In this work, three unexplored parameters for ORFV processing with SXC were identified: the pore size of the stationary phase, the incubation time and mixing strategy of the PEG / ORFV solution, and the addition of salts. Here, small pore sizes and long incubation times induced filtration effects, which cause pressure surges. The pressure is often a constraint in SXC application due to the high viscosity of the PEG. Therefore, a reduction of the PEG concentration while maintaining high yields is desirable. This could be achieved by adding different chaotropic ions to the PEG/ORFV mixture as proven for Mg^{2+}. Furthermore, characterization of degrading and stabilizing conditions on the infectivity of the new platform virus was rarely published. In this work, this gap was addressed by an extensive study of mechanical, chemical, and thermal stress conditions on ORFV infectivity. In summary, the ORFV is extremely robust against degradation under conditions routinely applied for pharmaceutical virus production. Nevertheless, care should be taken with heat and the implementation of ultrasonication in the production process. Generally, the ORFV should be stored under refrigerated conditions (4 °C), although the virus showed no substantial loss of infectivity if stored at 37 °C for two days or frozen. With regards to ion typically applied in purification processes, only ammonium salts should be avoided. Further stabilization is expected by the addition of proteins, sugars, and some amino acids. Based on these findings, a formulation buffer for ORFV storage with 1 % recombinant human serum albumin and 5 % sucrose was proposed. In the case of extended storage under heated conditions, albumin can be substituted with arginine. In conclusion, this comprehensive study of preferable process and storage conditions and critical process parameters of the SXC for the ORFV can inform future scale-up options to successfully implement SXC in pharmaceutical ORFV production processes with high infectious titer recoveries.

KURZFASSUNG

Die COVID-19 (coronavirus disease 2019) Pandemie hat die Wichtigkeit hervorgehoben pharmazeutische Produkte auf dem Markt schnell zur Verfügung stellen zu können. Dies kann unter anderem mit Plattformen gelingen, die an neue Krankheiten adaptiert werden können, und deren Produktionsprozess etabliert ist. Eine mögliche neue Plattformlösung kann das Orf virus (ORFV) sein. Als viraler Vektor dient das ORFV beispielweise als Gentherapeutikum, Impfstoff oder antiviraler, onkolytischer und immunomodulatorischer Wirkstoff. Bisher wurde jedoch kein etablierter Großproduktionsprozess für das ORFV entwickelt, der eine Anwendung als Plattform ermöglicht. In der Produktion im Labormaßstab wurde die Sterische Exklusionschromatographie (SXC) als Teilschritt der Produktreinigung vorgeschlagen und zeigte hohe Ausbeuten an infektiösem Virus mit hoher Reinheit. Die SXC ist eine vor wenigen Jahren entwickelte Methode, die nahe mit konventioneller Polyethylenglykol-(PEG)-präzipitation verwandt ist, wobei ein poröses Chromatographiemedium Teil des Fällungsprozesses ist, an das sich Präzipitate anlagern und hier zurückgehalten werden. Die dafür verantwortlichen präferentiellen und sterischen Exklusionsmechanismen sind durch eine Vielzahl an Prozessparametern bestimmt, wie beispielsweise die PEG-Zusammensetzung, den Puffer inklusive des pH-Werts und der Ionenstärke, und die Inkubationszeit der Komponenten. In dieser Arbeit wurden drei bisher wenig erforschte Parameter als kritisch für die Applikation der SXC auf das ORFV identifiziert: die Porengröße der stationären Phase, die Mischungsstrategie der Komponenten, und die Zugabe verschiedener Salze zum Laufpuffer. Im Detail verursachten kleine Porengrößen und lange Inkubationszeiten Porenverblockungen und damit Filtrationseffekte, welche die Operation der SXC durch starke Druckanstiege limitierten. Dies ist besonders relevant, da die SXC durch die hohe Viskosität der PEG-Lösungen mit erhöhtem Grunddruck betrieben wird. Daher ist eine Reduktion der PEG-Konzentration erwünscht, was durch den Zusatz von verschiedenen chaotropen Salzen, gezeigt für Mg^{2+}, ermöglicht werden könnte. Als weiterer relevanter Punkt des Reinigungsprozesses von ORFV, wurde der Einfluss von degradierenden und stabilisierenden Parametern auf die Infektiosität des Virus untersucht. Zusammengefasst zeigte das ORFV eine hohe Robustheit gegenüber den Bedingungen klassischer pharmazeutischer Produktionsprozesse. Nichtsdestotrotz sollte Hitzeexposition und Ultraschall nur nach gründlicher Prüfung eingesetzt werden und eine Lagerung bei gekühlten Bedingungen (4 °C) präferiert werden. In Bezug auf Ionen, die in üblichen Prozessschritten der Separation eingesetzt werden, wurde der Einsatz von Ammoniumsalzen als kritisch identifiziert. Eine Stabilisierung des ORFV hingegen wurde mit dem Zusatz von verschiedenen Proteinen, Zuckern und einigen Aminosäuren erreicht. Hieraus wurde ein Formulierungspuffer für das ORFV vorgeschlagen mit 1 % rekombinantem humanem Serumalbumin und 5 % Saccharose. Als Option für längere Lagerung bei erhöhten Temperaturen, konnte gezeigt werden, dass das Albumin durch Arginin ersetzt werden kann. Zusammenfassend kann diese umfassende Studie von stabilisierenden Lagerbedingungen und kritischen Prozessparametern der SXC für das ORFV die erfolgreiche Etablierung eines großskaligen pharmazeutischen Produktionsprozesses mit hohen infektiösen Titern ermöglichen.

LIST OF ABBREVATIONS

AAV	adeno-associated virus
Approx.	approximately
CE	cellulose
CIM	convective interaction media
conc.	concentration
DSP	downstream processing
ELISA	enzyme-linked immunosorbent assay
dsDNA	double-stranded DNA
GMP	Good Manufacturing Practice
HA	hemagglutinin
HBSS	Hank's balanced salt solution
HCP	host cell protein
HEPES	4-(2-hydroxyethyl)-1-piperazineethanesulfonic acid
HSA	human serum albumin
IU	infectious units
MES	2-(N-morpholino)ethanesulfonic acid
MW	molecular weight
MVA	modified vaccinia Ankara
N/A	not available
ORFV	Orf virus
PBS	phosphate buffered saline
PCR	polymerase chain reaction
PEG	polyethylene glycol
PFU	plaque-forming units
ref.	reference
rHSA	recombinant HSA
SARS-CoV-2	severe acute respiratory syndrome coronavirus 2
STORM	stochastic optical reconstruction microscopy
SXC	steric exclusion chromatography
$TCID_{50}$	50 % tissue culture infectious dose
TRIS	tris(hydroxymethyl)aminomethane
USP	upstream processing
VLP	virus-like particle

CHAPTER 1: Introduction

The development and production of vaccines have been a renewed subject of major public attention since the start of the SARS-CoV-2 (severe acute respiratory syndrome coronavirus 2) pandemic in January 2020. In an unprecedented pace, the duration from initial idea to first vaccine shot against SARS-CoV-2 took less than one year. Two and a half years later, nearly twenty vaccines have been approved by different health agencies [2]. Nevertheless, hundreds of candidates did not make it to market due to side-effects, reduced effectivities, and unestablished production processes [2]. Due to the complexity of the virions, the lack of an established production process is a common problem for new virus targets. Unlike production processes for proteins, e.g., antibodies, those for viruses are not easily adaptable due to the viruses' diversity. Additionally, for so-called live (attenuated) viruses, the activity or efficacy relies on the infectivity, resulting in the need for gentle process conditions to ensure high infectivity yields. This multi-layered issue was the key driver for this dissertation's research project. It aimed to identify critical parameters for the purification of the Orf virus (ORFV) as part of a pharmaceutical production process. In the first chapter, a broad overview of biological nanoparticles as well as an introduction to virus(-like) products are given (**section 1**). This is followed by a description of common production and especially purification processes of viral pharmaceuticals (**section 2**). In the subsequent sections, the steric exclusion chromatography (SXC) as a purification step is described (**section 3**), along with its implementation in the ORFV production process (**section 4**). Finally, the motivation for this dissertation project is brought into context and elaborated (**section 5**).

1. The use of biological nanoparticles as biotechnological products

Biological nanoparticles are diverse in their functions and applications. Among those are submicron bacteria, viruses, viral vectors, virus-like particles (VLPs) as well as exosomes and other vesicles [3]. In this group, pathogenic viruses (and bacteria) are a research target for centuries. The first use of viruses as pharmaceutical products dates back 500 years. Although the causative agent was still undetected, the first vaccines against smallpox were developed in the 17th century [4]. In the late 18th century, Edward Jenner started to inoculate humans with cowpox instead of smallpox to confer immunity against smallpox itself [4]. Following this effort, the term *vaccination* (from Latin *vacca*, cow) was born. Several more vaccines against bacterial and viral diseases were developed in the following 150 years, e.g., against cholera, anthrax, tetanus, diphtheria, and pertussis [5]. In the second half of the 20th century, methods to use *in vitro* viral tissue and cell culture started to develop. Additionally, images of viruses, and thus direct proof, became possible [6]. Until the end of the 20th century, the scientific world described viral nanoparticles only as pathogens. This perception started to change with improvements in analytical tools and the use of molecular genetics [5]. Today, viruses, VLPs, and viral vectors are used in various biotechnological applications, such as pharmaceutical [7,8] and agricultural [9] products (**Figure 1**). Although

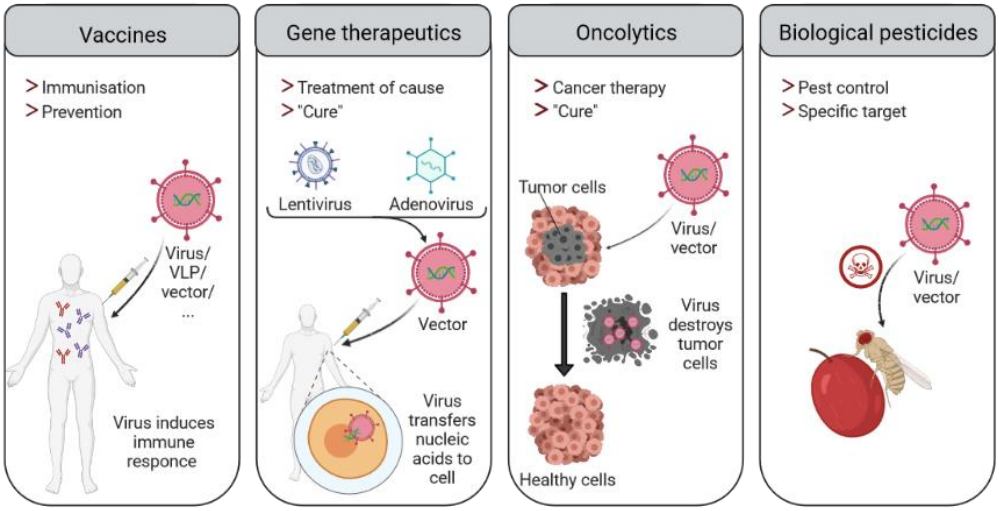

Figure 1: Application examples of virus (-like) biotechnological products. Most of the common applications of viruses, VLPs, and viral vectors are treatments of diseases, either as a preventative measure in form of vaccines, or as a putative cure, e.g., as gene therapeutic or oncolytic agent. Out of this scope is the agricultural application such as biological pesticides. In all cases, the specific infection of cells is the foundation for the working principle. The figure is an adapted version of a conference presentation [1], and was prepared using *biorender.com* under the agreement number UT24CAN25X.

all three nanoparticles can be described by their viral origin, their production and applications differ considerably.

Defining virus (-like) particles and viral vectors

Viruses are a group of submicron, intracellular parasites, with sizes ranging from a few nanometers to hundreds of nanometers. They store their genome in a capsid, which shields it from environmental influences. However, the lack of a functional translational machinery means that viruses cannot replicate without using a host, which provides the tools for multiplying the virions [11]. Such hosts can be cells from animals, plants, and bacteria, or, in rare cases, even other viruses [10]. Most viruses have a restricted host range [11], i.e., host tropism. To use a cell as a replication machinery, virions start by attaching to the host cell, which is commonly achieved through the binding of the viral surface proteins to specific cell receptors. The latter are often strongly conserved proteins and present across multiple cells, important for fundamental cellular functions [11]. The next step in the replication cycle is the uptake into the cell: the endocytosis. In this step, the virion disintegrates to release its genomic information from the capsid [12], which, in some cases, is wrapped by additional membranes or envelopes [13]. After obligate intracellular replication by the host cell, maturation begins by reconstituting into full virus particles [12], which are then released from the cell and can infect new hosts [11]. The complete replication process varies between different virus families and is extremely complex [11].

The application of viruses as a biotechnological product relies on the viral host tropism and the parasitic infection inducing cell death. Today, the host cell-restriction of viruses can be lifted by genetic techniques such as incorporating foreign receptor-binding proteins into viruses, called

pseudotyping. An example is the expression of glycoprotein G of the vesicular stomatitis virus on the natively insect-infecting baculovirus [14,15], which enables the baculovirus to efficiently infect or transduce a broad range of mammalian cell types [14]. Thus, genetically engineered viruses open new possibilities for targeting specific cells for treatment.

This technique to modulate viral surface proteins is also used for VLPs. These nanostructures are assembled by proteins derived from viral envelopes, surfaces, or cores; however, they do not contain genomic information, which means they cannot replicate [16]. As such, VLPs resemble virions on the outside with modified surfaces, and they can be used for a variety of applications, e.g., immunotherapy, vaccination, and drug delivery [16].

Another technique for engineering viruses is the insertion of genes into the viral genome, which are transferred into the target cell during the transduction process [17]. In this approach, the virus acts as vehicle for delivery, thereby becoming a viral vector. The transferred genes may express proteins, which can release their therapeutic effect in the targeted tissues. Furthermore, viral vectors are applied as gene therapeutics, i.e., by modifying the expression of genes or correcting dysfunctional genes in the host [18]. This can offer a cure for currently untreatable cancer types [19] or hereditary diseases [20]. Common viral vectors are based on the adenovirus [21], the adeno-associated virus (AAV) [22,23], the γ-retrovirus [24], the lentivirus [25], or the baculovirus [14,26]. An emerging platform for viral vector-based gene therapeutics is the ORFV.

The Orf virus

The ORFV belongs to the genus *Parapoxvirus*, family *Poxviridae*. One of its closest relatives is the modified vaccinia Ankara (MVA) virus, an *Orthopoxvirus*, which is historically applied for immunization against the variola virus, the causative agent of smallpox. All members of the family *Poxviridae* belong to the largest known viruses of up to 400 nm and have a rod- or brick-like shape [27]. The ORFV virions are approximately 140 – 200 nm wide and 220 – 300 nm long [28–30] and of ovoid-shape (**Figure 2**). The virus is covered with characteristic surface filaments, which are tubule-like structures that surround the virions in a left-turning spiral and has resulted in the virus being often described as a ball of wool [31]. Other times, it is described by a criss-cross pattern [32]. This is due to the superimposition of the lower and upper surface of single virions, which is visible under transmission electron microscopy using negative staining [33] (**Figure 2A**). The ORFV is a DNA virus, encoding approximately138 kbp [34], with its genome stored in a complex core with two lateral bodies. It replicates in the cell's cytoplasm [35] and throughout the morphogenesis several forms of viral particles are produced [27,36]. The first mature and fully infectious ORFV form is the intracellular mature virion, which is enveloped by a membrane derived from the cellular endoplasmic reticulum. These virions are further wrapped by two additional membranes, likely from Golgi-origin. Eventually, the wrapped viral particles fuse with the cell membrane, acquire an envelope in this budding process, and are then released as extracellular mature virions (**Figure 2B**). Thus, at least two forms of infectious ORFV particles may be produced [35]: one type carrying an inner membrane, the intracellular mature virion,

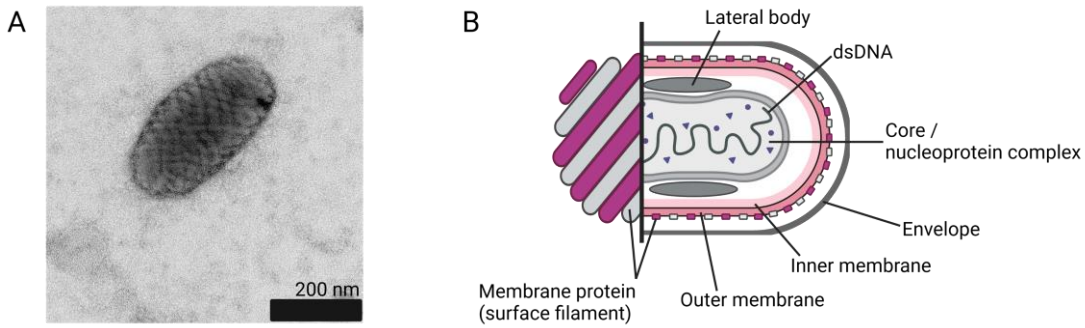

Figure 2: Structure of the ORFV. (A) Image of an ORFV virion, taken with a transmission electron microscope using negative staining (2 % uranyl acetate). Note the characteristic criss-cross pattern of the genus *Parapoxvirus*. The image was taken at the *Biomedizinisches Forschungszentrum Seltersberg* with the kind support of Dr. Martin Hardt. (B) Schematic diagram of an ORFV virion, showing the surface structure on the left and a cross-section through the center on the right. The figure was prepared using *biorender.com* under the agreement number MB25O6XTEK.

which is released by cell lysis; and one type with an outer membrane and an envelope, extracellular mature virion, which is released by budding.

The ORFV, in its wild form, is a zoonotic virus, which mainly infects sheep and goats [30], and rarely humans [35]. Like all poxviruses, the ORFV primarily targets epithelial cells. It causes the orf disease, which manifests as highly contagious skin lesions [37]. In humans, however, these lesions are localized, and the disease is self-limited. Thus, the ORFV never reached the attention of its relative, the variola virus.

Several vaccines against the orf disease have been developed, which are mainly based on attenuated ORFV virions [37–40]. However, vaccination success was limited as hosts can be infected repeatedly, indicating a short-lived immunity and the necessity of repeated immunization [38,41–43]. This observation has brought attention to the ORFV as potential viral vector for human and veterinary pharmaceutical application [34]. Other factors include a narrow host tropism, a lack of systemic spread, a strong humoral and cellular immune response against the expressed antigens without attacking the vector itself, and immunomodulatory effects even in non-permissive hosts [44]. In several studies, the ORFV vector has been evaluated as recombinant vaccine [45–49], including against SARS-CoV-2 [50], oncolytic and antiviral therapeutic [34,51–53], and immunomodulatory agent [41,54–56]. Most of the applications are based on the highly attenuated ORFV strain D1701-V [44]. This recombinant vector lacks key virulence factors and allows for encoding up to three transgenes, which can be expressed even in the absence of ORFV replication [48].

The multitude of applications for the recombinant ORFV vector as pharmaceutical product highlights its versatility. However, therapeutic application is only possible with an efficient ORFV production yielding high virus titers, appropriate storage conditions as well as an effective delivery of infectious virions to the patient.

2. Production processes of viral pharmaceuticals

The need for production processes of viral pharmaceuticals arose with the first development of vaccines. The early smallpox vaccines were based on infectious material from fresh pustules or scab taken from humans suffering from smallpox or cowpox [4]. The practice of generating vaccines from living organisms, e.g., rabbits, horses, and chicken embryos, remained a standard procedure until the second half of the 20th century, when cell culture methods were developed [57]. While a considerable number of viral vaccines are still produced in chicken embryos today, production processes have successively adapted to cell culture-based virus replication [58]. Throughout the late 20th century, impurity-based safety and efficiency concerns induced an extension of the production processes from sole virus propagation to include a subsequent purification step [58]. Although changed fundamentally, the following classification to describe the production process is still valid today: upstream processing (USP) and downstream processing (DSP) (**Figure 3**). While the USP incorporates the production of the target itself, the DSP aims to separate the target selectively from impurities. Thus, the DSP is also often referred to as purification. The framework for this set-up is the safety of the pharmaceutical product, which is controlled by Good

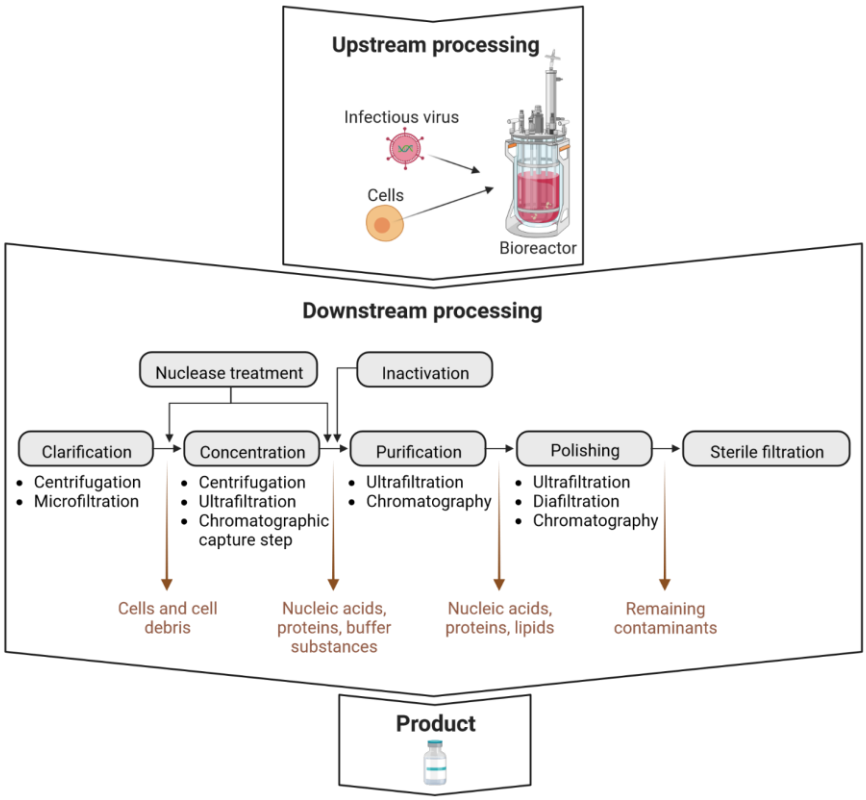

Figure 3: Schematic example production process of a viral pharmaceutical product. The process is performed from top to bottom: upstream processing, downstream processing, and final product processes. The boxes in downstream processing indicate individual steps, which are connected in their consecutive order. The red arrows describe substances leaving the processing train as impurities. Nuclease treatment is usually implemented before or after a concentration step or, in some cases, even prior to clarification. An inactivation step is not mandatory for all products and only applied for some vaccines. Product processes include formulation as well as fill-and-finish. The figure was adapted from Wolff and Reichl [62], and was prepared using *biorender.com* under the agreement number FP24CAMUDA.

Manufacturing Practice (GMP) guidelines and standards [59]. Both USP and DSP are constantly advancing, driven by new developments and the need for efficient and economically profitable processes. Platform technologies are typically desired as they can be rapidly adapted to a variety of targets [60,61], offer high yields and purity, and scalable throughput as well as the preservation of the target product [62,63].

In this chapter, the steps of production processes for viral pharmaceuticals is explained with focus on the DSP and the characterization of viral targets.

Upstream processing of viral pharmaceuticals

The USP aims to produce the target in high concentrations and quantities. For viruses (and viral vectors), propagation is performed in cells. To take advantage of the cell culture production, optimal growth conditions for the cells, which support cell proliferation and virus replication, must be provided. Therefore, different forms of bioreactors are used to supply a controlled and sterile environment, which allows for online monitoring and control of critical parameters, e.g., oxygen saturation, pH, temperature, and nutrient supply. After successful virus production, the cell culture broth is harvested with the target virus as well as impurities, e.g., residual growth media and additives, cells, cell debris, cell-derived by-products and impurities, e.g., host cell protein (HCP) and DNA, media components, and un-assembled or defect virus particles [61].

Downstream processing methods for viral pharmaceuticals

The next step, the DSP, aims to isolate the target from process- and product related impurities [61]. Evidently, a high virus yield, a high virus concentration, and a low residual impurity content are the main goals of the DSP. Worldwide, health agencies regulate the threshold values for residual HCP and host cell DNA tolerable in cell culture-derived vaccines. Although exact numbers are often not stated [64], the concentration of double-stranded DNA (dsDNA) of 200 pb or longer is frequently recommended below 10 ng per dose, and for HCP below 50 [65] or 100 µg mL^{-1} [66,67]. Similar values are recommended for gene therapy vectors [68–70]. To achieve such impurity removal as well as appropriate product concentrations, the DSP for viral pharmaceuticals is usually split into several steps: clarification, concentration, potential nuclease treatment, purification, polishing, and in some cases sterile filtration [61] (**Figure 3**). Clarification is the first process step after the cell culture harvest, and its aim is to eliminate large contaminants, e.g., cells and cell debris, using filtration or centrifugation. The subsequent concentration step is frequently implemented to reduce the volume of the liquid to be processed while also reducing contaminant levels by utilizing a selective unit operation, e.g., with centrifugation or chromatographic methods. To reduce the residual host cell DNA concentration, a nuclease treatment is often implemented before or after the concentration step to enzymatically degrade the DNA, which facilitates its separation from the target. The treatment requires specific buffer conditions as well as long holding times, which can impair the target quality. Additionally, the removal of the nuclease must be ensured throughout the subsequent DSP steps. The inactivation of virus aims to eliminate virus

infectivity, which is only applied if virus replication in the host is not necessary or desired, e.g., for different vaccines. Common methods are gamma irradiation or heat as physical treatment as well as formaldehyde or ethylenimine as chemical treatment [71]. Testing for effective inactivation is a mandatory procedure and ensures vaccine safety [71]. Challenges in inactivation may be the conservation of the vaccine's immunogenicity, which often is compensated by adjuvants [72].

Following the optional nuclease treatment and virus inactivation, purification and polishing steps are implemented to selectively separate the target from residual impurities, e.g., by applying precipitation, filtration, or chromatographic techniques. While sterile filtration can be used to eliminate microbial contaminations, it often causes high virus losses. Alternatively, a completely aseptic process can be implemented [73]. Finally, the product is formulated, meaning different supplements are added to stabilize the virions for storage and transport, and then the formulated product is filled into appropriate containers. The typical unit operations for the described steps are illustrated in the following sections and their (dis-)advantages summarized in **Table 1.**

Centrifugation

Centrifugation-based process steps involve the concentration of the target or a specific separation task such as impurity removal, e.g., cell debris. The method depends on differences in the density and buoyancy between product and impurities. Although large-scale continuous centrifuges exist, their use is limited by scaling and high investment costs [61]. Membrane-based filtration can be an effective alternative [74].

Filtration

In filtration processes, selectivity is achieved by varying the pore size of the filter. Two main types of filtration set-ups are available: depth filtration, also called dead-end filtration, and cross-flow filtration, often referred to as tangential-flow or diafiltration [60]. In depth filtration, the feed is completely processed through the filter membrane, and all particles or molecules smaller than the filter-specific cut-off pass through in the permeate [75]. The permeate usually contains the product, separated from the retained substances. The pore size further defines the type of depth-filtration. Filtration with micrometer-sized pores is common for clarification (microfiltration), while submicron pores for sterile filtration or purification steps (ultrafiltration) [76]. Cross-flow filtration, on the contrary, uses a feed flow parallel to the filter membrane. Hence, the retained molecules cannot build up on the filter, but are washed off. Generally, the target is desired to remain in the retentate, and can be concentrated by repeated cycling [14]. The impurities are washed out in the permeate. With this set-up, concentration, buffer-exchange, and polishing steps can be achieved [77].

Precipitation

Precipitation is a very complex method, historically used for protein and antibody purification [78,79]; however, unspecific precipitation of by-products along with the target molecules can reduce the purity of the target [61]. To induce flocculation, a precipitation agent, e.g., salts or polyethylene glycol (PEG), is introduced. After a hold-time, the precipitates can be separated by either centrifugation or filtration. Additional removal of the precipitation agent is necessary. The

fundamental concepts of this method will be described in detail later, when the closely related SXC is introduced (**section 3**).

Table 1: Summary of advantages and disadvantages of typical downstream processing methods for viral pharmaceuticals.

Method	Advantages	Disadvantages
Centrifugation	+ Cheap batch operation + Robust processing + Continuous set-up available + Mild processing conditions	- High investment costs - Scale limited by set-up - Low to medium selectivity
Filtration	+ Robust processing + Variety of unit operations with set-up + Semi-continuous processing possible	- Medium-prized consumables - Scale limited by filter size - Low selectivity - Potential loss of biological activity due to shear forces
Precipitation	+ Cheap batch operation + Medium to high selectivity + Easy scaling + Applicable for both selective product and contaminant separation	- Removal of precipitation agent necessary - Potential loss of biological activity due to precipitation agent - Sensitive to changes in educt composition
Chromatography	+ High selectivity + Cheap operation + Semi-continuous processing possible + Often mild processing conditions	- Cost-intensive consumables - Limited scaling - Buffer exchange often necessary - Potential loss of biological activity depending on buffer composition - Sensitive to changes in educt composition

Chromatography

Chromatographic methods are defined as the separation of different components based on the difference in the speed with which they pass through a medium. The distinct retention times can be induced by different flow-paths, adsorption to the media, or affinities [61]. To take advantage of any of these mechanisms, a suitable media, e.g., resin, membrane, or monolith, is needed. Historically, resins have been the standard stationary phase for chromatographic applications, and are usually supplied as easily modifiable, synthetic micrometer-sized beads [80]. The beads themselves are highly porous, increasing their total surface area by orders of magnitudes. Most of the resin-based columns were developed for protein purification, which limits their application for viruses [80]. Although viruses contain proteins, they are also composed of lipids and nucleic acids. Additionally, viruses are several orders of magnitude bigger than most proteins. Thus, they cannot penetrate resin pores due to their size and may precipitate in the void space within the

packed resin bed. Mass transfer in resin beds is driven by diffusion, while convection occurs only around the beads. However, for virus applications, convective mass transport is desired as they are too big for diffusive transport. This favors the use of membranes and monoliths in viral DSP applications [61]. Although the described differences between proteins and viruses induce the need for new chromatographic methods, they can also be advantageous in separating target viruses from protein impurities.

A universally applied method to separate targets by size is size exclusion chromatography, in which compounds of different size will have different retention times across the resin. The pore size determines whether the compounds can enter certain pores and thereby defines the total accessible volume. Smaller molecules are retained longer, being able to diffuse into more space, while bigger molecules are eluted first. Thus, target virus and impurities are expected to yield different elution times in size exclusion chromatography. For viruses, this method is often used as a gentle purification method or in a multi-modal approach [81].

Apart from size exclusion, selectivity in chromatography may be based in binding to the stationary phase, i.e., via flow-through as well as bind-and-elute methods. The latter two operate with the retention of either impurities (flow-through) or the target (bind-and-elute) on the stationary phase, while the respective other part is found in the flow-through fraction. Elution is purposely induced by changing the binding conditions depending on the methods operating principle of ion exchange, hydrophobic interaction or affinity chromatography.

Ion exchange chromatography is a standard approach for virus purification [80]. It is based on electrostatic interaction between the target and the ligand on the stationary phase. As such, anion and cation exchangers are available. The binding can be reversed by increasing the salt concentration and displacing the virions, or by changing the charge of the viruses, e.g., by adjusting the pH. However, both approaches may reduce virus infectivity.

Hydrophobic interaction chromatography takes advantage of the virus composition, including proteins and lipids. These have a hydrophobic component, which becomes dominant in certain environments, e.g., by adding kosmotropic salts [82]. Thus, the virus particles hydrophobically bind to the stationary phase and are released by eliminating the additional salt. The high salt concentrations can be a challenge for preserving virus infectivity and need to be evaluated carefully.

Affinity chromatography is one of the most specific methods available [83]. In this modality, viruses are retained due to their selective binding to the affinity ligand, e.g., heparin. Reversing the affinity binding, however, is more challenging, and harsh conditions have to be applied often, which might impair the product's integrity. Furthermore, affinity columns are often expensive [61]. This approach, as well as ion exchange and hydrophobic interaction chromatography, is most often employed in bind-and-elute mode [83].

Multi-modal, or mixed-mode, applications are advancing rapidly with new DSP challenges, improved computational modelling approaches, and a better understanding of multi-modal interactions [84]. They are a powerful tool, leveraging several target characteristics for retention by combining aforementioned chromatographic principles, e.g., as ion exchange and hydrophobic

interaction chromatography or combinations with size exclusion chromatography, often referred to as restricted access matrices (RAM) [84].

The choice of a suitable purification process is dictated by the target characteristics. As described in the different DSP methods, selectivity can be based on size (and the density), specific surface composition, e.g., charge distribution, hydrophobicity, and specific affinity [63,80,81]. However, a thorough virus characterization is necessary to take advantage of any of these traits. Additionally, virus quantification methods need implementation for surveillance of the yields in each unit operation.

Formulation and stabilization approaches

Throughout the extensive production processing, the infectious virions are exposed to a variety of degrading conditions, e.g., shear, heat, salt, or pH stress. Hence, measures need to be taken to preserve the virus infectivity [85]. The same accounts for preserving virus infectivity during handling and storage after processing is complete, which is essential to ensure the delivery of a safe and effective pharmaceutical product to the patient. To achieve this goal, an appropriate formulation of the virus is generated by adding excipients, such as buffers, salts, amino acids, osmolytes, sugars, proteins, antioxidants, and surfactants [86,87]. To investigate the efficacy of a formulation, storage and forced degradation studies may be undertaken [88]. Suitable components are often selected based on their capability to preserve the virus stability, safety in pharmaceuticals, degree of interference with unit operations, economic considerations, and the simplicity of the formulation. Analysis of the viral infectivity and aggregation are often the basis for the decision.

Characterization of viral targets

Viruses are complex submicron structures. Even within one strain, differences can be profound, e.g., induced by the production cell line or the cultivation media [89]. Thus, the characterization of the virion particles is essential for the development of the production process, in particular the DSP and the formulation. For virion characterization, common initial traits of interest are the size (and the dimensions), the concentration of virions, the charge (and the isoelectric point) as well as the hydrophobicity. More advanced characterization methods target certain epitopes, e.g., surface proteins. Along with virus characterization, virus recoveries also need to be quantified throughout the production to inform the selection of pertinent processing steps. Multiple options of analysis are available for these tasks and a selection of the most common methods is summarized in **Table 2**.

Quantification of virions can be performed either directly or indirectly [90]. Direct methods are based on counting the particle number, e.g., using imaging, nanoparticle tracking, tunable resistive pulse sensing, or flow virometry. However, they are not able to differentiate between infectious and non-infectious particles, an important characteristic for viral products. Indirect quantification may be based on virion infectivity as well as specific epitopes or content. Furthermore,

Table 2: Methods for virus characterization and quantification. Evaluation of the specific methods was done qualitatively with a range from beneficial (+++) to disadvantageous (+) traits. Only the need for a standard is categorized as required (+) and not required (-). The table was adapted from Lothert et al. [90]. ELISA, enzyme-linked immunosorbent assay; PCR, polymerase chain reaction; ref., reference; STORM, stochastic optical reconstruction microscopy; $TCID_{50}$; 50 % tissue culture infectious dose.

Trait	Methods	Throughput	Virion quantification		Comment	Ref.
			Reliability	Standard required		
Size / dimensions and concentration of virus particles	Dynamic light scattering	+++	+	+	Concentration measurements only with multi-angle approaches	[91–93]
	Imaging approaches	+	+++	-	Specific (e.g. electron microscopy) or unspecific (e.g. STORM) quantification	[94,95]
	Nanoparticle tracking analysis	+++	++	-	Specific quantification with marker	[96,97]
	Tunable resistive pulse sensing	++	++	+		[96,98]
	Flow virometry	+++	++	-	Markers required	[99]
	(Capillary) electrophoresis *	++	++	+		[100]
	Analytical centrifugation *	++	++	+	Standard needs to be of similar density and dimensions	[95,101]
	Analytical chromatography *	+++	++	+		[69]
Concentration of infectious viruses	$TCID_{50}$ assay	+	+	-		[102]
	Plaque titration / focus forming assay	+	+	-		[103]
	Flow cytometric titration	++	++	+		[99]
Specific epitopes / content	Antibody-based assays (e.g. ELISA)	++	+++	+	Antibodies required	[104]
	Surface plasmon resonance spectrometry	+++	+++	+	Preparation of flow cell for each target	[105,106]
	PCR techniques	++	+++	(+)	Modern digital PCR techniques operate without standard	[104,107]
	Protein-specific assays	++	+++	+	e.g., hemagglutinin (HA)	[108]
	Analytical chromatography *	++	++	+		[69]

Charge	Tunable resistive pulse sensing	++	++	+		[109]
	Electrophoretic light scattering	+++	+	-		[95]
	(Capillary) electrophoresis *	++	++	-		[104,110]
	In-silico prediction	+	(+++)	-	Knowledge of protein structure necessary	[111]
Hydrophobicity	Probe spectrofluorometry	+++	++	-		[112]
	Contact angle determination	++	++	-		[113]
	Analytical chromatography	++	+	+		[112]
	In-silico prediction	+	(+++)	-	Knowledge of protein structure necessary	[112]

* Preparative methods for detection and quantification, e.g., by UV- or light scattering detector or mass spectrometry.

simple detection methods such as UV-absorbance or more complex analysis such as mass spectrometry are implemented for quantification.

In general, virus characterization and quantification depend on well-prepared samples. Such preparation should prevent interference of measurement and bias of the results caused by the presence of impurities. Examples for impurities are nanoparticles of similar size that could affect size-determination or unassembled viral subunits that might interfere with epitope-characterization. The only exceptions from this limitation are assays based on viral infectivity, or in some cases methods that use markers, e.g., antibodies. Thus, to perform physicochemical characterization of charge, hydrophobicity, and for most size analysis methods, virions must be highly purified [114,115]. In most cases, size-based methods such as ultracentrifugation are recommended for this preparation task [113,116]. However, a method re-evaluation is necessary for every new target as the sample preparation is as complex as conventional DSP development.

3. The steric exclusion chromatography

As mentioned in **section 2**, the SXC is closely related to PEG-precipitation. The method combines the adaptability of precipitation to nearly every biomolecule [117] with the following advantages of a chromatographic approach: simplified scale-up, adjustable flow rates and throughput as well as the option for continuous processing [80,118].

Although the SXC itself was first mentioned in 2012, the implementation of precipitating agents in other chromatographic methods was reported before. Such approaches can be categorized as

multi-modal and include size exclusion, hydrophobic interaction, and ion exchange chromatography [119,120]. The use of precipitation as the only driving force of chromatographic separation was first described by Lee et al. [121] for the purification of biological macromolecules. Since then, a variety of SXC applications has been published [122], i.e., for immunoglobulins [118,121,123,124], nucleic acids [125], and viruses [121,126–135]. Of special interest for this work are the latter SXC applications, which proved the methods' exceptional contaminant removal and virus yield (**Table 3**).

The working principle behind the steric exclusion chromatography

As the name SXC suggests, the separation of viruses from contaminants by retaining the viruses on the stationary phase is achieved by mutual steric exclusion without direct chemical interactions [121]. The theoretical foundation of this complex process dates back to the works of Timasheff's laboratory on protein solvent interactions [119] and Ogston's laboratory on excluded volume [136]. The conclusion was drawn that the exclusion of cosolvents from protein surfaces stabilizes proteins, e.g., by applying sugars. On the contrary, protein denaturants, e.g., urea, bind to unfolded proteins [119]. Thus, preferential inclusion (or binding) and preferential exclusion determine the interaction of cosolvents among each other. The origin of the exclusion effects has been explained by (1) strong hydration, (2) preferential exclusion, and (3) steric exclusion [119,136]. (1) Strong hydration prevents cosolvents from binding to the protein surface, leading to a deficient cosolvent concentration in the hydration layer. (2) The reverse effect is known from strongly hydrated salts, which can be preferentially excluded from protein surfaces due to their own hydration sheath. Other examples include certain amino acids, e.g., glycine and alanine. (3) Polymers, e.g., PEG, the most commonly applied polymer in SXC, may be sterically excluded from the protein surface

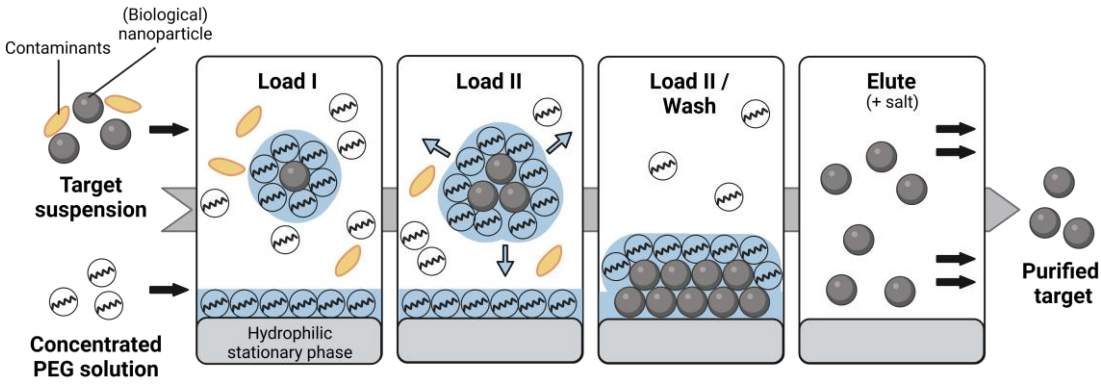

Figure 4: Working principle of the SXC. Target with contaminants is mixed with a concentrated PEG solution and loaded onto the stationary phase. The target virus and the stationary phase are covered in a PEG-deficient zone (blue). The thickness of this zone is determined by the hydrodynamic diameter of the PEG molecules (**Load I**). With increasing duration of residence time, targets associate according to their size to reduce the contact area of the PEG-deficient zone and the high-PEG bulk surrounding. Excess water is released due to the self-association (arrows), which reduces the PEG concentration in the bulk phase (**Load II**). The virions associate at the stationary phase to further reduce the contact area (**Load III**), and contaminants can be washed out (**Wash**). By reducing the PEG concentration, the self-association of the targets is reversed and a concentrated, purified product is eluted (**Elute**). The figure was adapted from Eilts et al. [126], and was prepared using *biorender.com* under the agreement number RD25O6XL3Q.

due to their big hydrodynamic radius compared to water molecules. Imagining them as spheres, they cannot fully occupy the hydration sheaths around proteins, which is filled with solvent (water molecules). This leads to a polymer-deficiency in this layer (**Figure 4, panel *Load I***). The last effect (3) is the main cause for precipitation. In classical SXC, the presence of a polymer- / PEG-deficient zone creates an osmotic pressure, which has been described to induce a depletion interaction mechanism. By self-association of the proteins, excess water is released, and the interface of the bulk zone and the deficient zone is reduced, leading to a favorable decrease of free energy (**Figure 4, panel *Load II***). Such intermolecular association occurs throughout precipitation and SXC [137]. In the case of SXC, a porous stationary phase with a large surface area is a dominant component in the system. Thus, proteins and their precipitates associate with each other without a direct form of affinity and accrete at the stationary phase (**Figure 4, panel *Load III/Wash***) [121]. For multi-modal SXC applications, preferential exclusion itself is an additive force to the fundamental interaction of the protein with the stationary phase [119,120]. At this point, it should be mentioned that SXC has also been shown to work in a bulk approach, in which magnetic particles covered in cellulose offered the surface area for accretion instead of a stationary phase on a column [123]. While the targets accrete on the stationary phase, contaminants of smaller size than the target are washed out (**Figure 4, panel *Load III/Wash***). Finally, the PEG concentration can be reduced or completely omitted, which removes exclusion effects, which allows the target to elute from the column in a purified and concentrated state (**Figure 4, panel *Elute***). As can be assumed from this introduction, the selectivity of binding in SXC is determined by a variety of parameters.

Defining critical process parameters for the steric exclusion chromatography

To exploit the precipitation process, PEG must be the most abundant compound in the system besides water. Thus, it is not surprising that any cosolvent interaction with PEG alters the precipitation efficiency. The size of the PEG molecules determines the size of the molecules that can be excluded [136,137]. With increasing PEG molecular weight and concentration, target molecules of smaller size can be excluded. Conversely, with increasing size and concentration of the target, the PEG concentration may be reduced [117,138–140].

This is straightforward as the size of the PEG molecules determines the thickness of the PEG-deficient zone and the PEG concentration increases the osmotic pressure, which drives the molecular self-association. The self-associating nature of the target is defined by its interaction with the solutes. Strongly hydrophobic targets interact with the slightly hydrophobic PEG, thus counteracting the preferential exclusion and limiting the binding to the hydrophilic stationary phase [138]. In another case, a high surface charge increases target repulsion, but it can be resolved by increasing the concentration or molecular weight of the PEG or by changing the buffer pH towards neutral target charge [123,137,141]. Electrostatic repulsion can also be counteracted by increasing the ionic strength of the solvent, i.e., introducing salt-induced charge shielding into the system. However, specific salt ions act differently on proteins and PEG with regards to solubility, specific binding, charge shielding, and compacting of the PEG molecules [81,137,138,141]. Thus, the ad-

Table 3: Summary of recent column-based SXC applications to purify viruses. Alphabetically listed targets were applied in the SXC in a pre-purified state, i.e., either using clarification (in some cases including nuclease treatment) (= clarified) or after clarification and primary purification (= purified). The load was diluted with a PEG-enriched solution, either prior to sample loading (offline) or continuously throughout column loading in the tubing of the chromatographic system (in-line). The pore size of the stationary phase is given in brackets. The loading was stopped after a certain binding capacity was reached. The consecutive elution was analyzed for the virus yield and the contaminant removal of HCP and DNA compared to the loading sample. The total virus recovery describes the combined virus content in all chromatographic fractions, i.e., flow-through, wash, and elution (**Figure 4**). Approx., approximately; CE, cellulose; CIM, convective interaction media; conc., concentration; IU, infectious units; MES, 2-(N-morpholino)ethanesulfonic acid; MW, molecular weight; N/A, not available; PBS, phosphate buffered saline; PFU, plaque-forming units; TRIS, tris(hydroxymethyl)aminomethane.

Target		**Load**	**Loading conditions**					**Elution buffer**	**Flow rate**	**Stationary phase**	**Binding capacity**	**Virus recovery**		**Impurity removal**		**Ref.**
Type	**Size**	-	**PEG conc.**	**PEG MW**	**Buffer**	**Dilution factor**	**Mixing**	-	-	-	-	**Yield**	**Total**	**HCP**	**DNA**	
-	**[nm]**	-	**%[-]**	**[Da]**	-	**[-]**	-	-	**[mL min^{-1}]**	-	-	**%[-]**	**%[-]**	**%[-]**	**%[-]**	
AAV (serotypes AAV2, AAV6, AAV-1P5, AAV-9A2)	25	clarified	10	6000	PBS pH 7.4	2 - 3.2	in-line	PBS pH 7.4	5-10	100 cm^2 (0.4 mL) CE membrane (1 µm)	Approx. 2.9 x 10^9 virus genomes / cm$^2_{membrane}$ (0.7 x 10^{12} virus genomes / mL $_{membrane}$)	> 95	126	80-85	94-98	[131]
Bacteriophage M13K07	7 x 900	clarified	6	6000	50 mM MES + 600 mM NaCl pH 6	2	in-line	50 mM MES + 100 mM NaCl pH 6	10	1 mL CIM-OH monolith (2 µm)	6.2 x 10^9 PFU / mL$_{monolith}$ at 10 % breakthrough	> 90	N/A	99.8	93	[121]
Baculovirus (genotype Ac-MNPV-VSVG)	20 x 260	clarified	8	8000	PBS pH 7.4	2	offline	PBS + 500 mM NaCl pH 7.4	3.2	20 cm^2 (0.14 mL) CE membrane (3 - 5 µm)	5 x 10^7 PFU / cm$^2_{membrane}$ (7 x 10^9 PFU / mL$_{membrane}$) at 10 % breakthrough	91	> 95	99	85	[129]
										20 cm^2 (0.14 mL) Polyamide membrane (5 µm)	N/A	81		> 99.99	81	[129]
										20 cm^2 (0.13 mL) Glass microfiber membrane (5 µm)	N/A	73		93	45	[129]

Hepatitis C virus (genotype 1a and 5a)	40 - 80	purified	8	6000	20 mM TRIS-HCl + 180 mM NaCl pH 9	4	offline	20 mM TRIS-HCl + 400 mM NaCl pH 7.4	2	13 cm^2 (0.09 mL) CE membrane (1 µm)	4 x 10^8 units / $cm^2_{membrane}$ (5.7 x 10^{10} units / $mL_{membrane}$) at 10 % breakthrough	>91	>95	84	>99	[126]
Influenza A virus	80 - 120	clarified	8	6000	50 mM TRIS-HCl + 150 mM NaCl or PBS pH 7.4	4	offline	50 mM TRIS-HCl + 150 mM NaCl or PBS pH 7.4	5	17 cm^2 (0.07 mL) CE membrane (1 µm)	N/A	>95	N/A	92.4	99.7	[130]
									10	75 cm^2 (0.3 mL) CE membrane (1 µm)	3.4 μg_{HA} / $cm^2_{membrane}$ (907 μg_{HA} / $mL_{membrane}$)	>98	N/A	88-92	77-99	[130]
									4	0.34 mL CIM-OH monolith (2 µm)	N/A	71	N/A	92	98	[130]
Lentivirus	80 - 100	clarified	12.5	4000	50 mM TRIS-HCl + 150 mM pH 7.4	2	inline	50 mM TRIS-HCl + 150 mM pH 7.4	6-7	35 or 70 cm^2 CE membrane (2.5 - 3 µm)	1.1 - 2.1 x 10^{12} virus particles/ $cm^2_{membrane}$	88	>90	81	79	[132]
MVA virus	250 x 300 x 120	purified	7.2	6000	PBS + NaCl, NaBr, KCl (700 mM) pH 7.4	N/A	N/A	PBS + NaCl, NaBr, KCl (700 mM) pH 7.4	8.2	70 cm^2 (0.3 mL) CE membrane (1 µm)	Approx. 2 - 5 x 10^8 $TCID_{50}$ / $cm^2_{membrane}$ (4.7 – 11.7 x 10^{10} $TCID_{50}$ / $mL_{membrane}$) at 5 % breakthrough	>95	N/A	>90	90	[134]
ORFV (2 genotypes)	140 x 300	clarified	8	8000	20 mM TRIS-HCl + 180 mM NaCl pH 7.4	4	offline	20 mM TRIS-HCl + 400 mM NaCl pH 7.4	3	13 cm^2 (0.09 mL) CE membrane (1 µm)	1.3 x 10^6 IU/ $cm^2_{membrane}$ (1.8 x 10^8 IU / $mL_{membrane}$) at 10 % breakthrough	84-91	>95	99	63-81	[128]
Yellow fever virus (strains 17DD and 17D-204)	40 - 50	clarified	10	6000	N/A	N/A	N/A	N/A	5	100 cm^2 (0.4 mL) CE membrane (1 µm)	6 x 10^7 PFU / $cm^2_{membrane}$ (1.5 x 10^{10} PFU / $mL_{membrane}$) at 10 % breakthrough	101-109	106-113	92	62-73	[133]
Yellor fever VLP	30 - 40	clarified	8	6000	PBS pH 8.0	2	inline	PBS pH N/A	6	N/A	N/A	72	N/A	>99	60	[133]

dition of salts must be evaluated carefully. On the processing side, the critical parameters include the flux and thus retention time, the purity of the applied sample, and the type of the stationary phase. The accretion of the precipitates is enhanced on a hydrophilic stationary phase due to the slightly hydrophobic nature of PEG [119]. For common SXC applications, membranes, monoliths, or cryogels have been successfully applied.

To explore critical process parameters in chromatography, model systems are often employed [142,143]. While doing so, the differences between the model system and the final application are essential for method transfer and should be considered to answer scientific questions. Furthermore, statistical design of experiments offers the opportunity to detect unheralded limitations and explore their impact on the processing success.

Review of limitations and open questions

Although the SXC has proven its efficacy in purifying biological macromolecules in a variety of applications, all these were of lab-scale. To implement the method in a large-scale pharmaceutical production, limitations must be well defined, some of which have been addressed in recent publications and are summarized in the following.

- Resins as **stationary phase** which are often packed in columns, offer most of the surface for binding within the porous beads, which is reached by diffusion. However, these are not penetrable by most viruses [61]. Additionally, PEG increases the viscosity and makes diffusion too slow to take advantage of the pores [119]. While reduced flow rates can counteract this limitation, this would lead to an increased residence time, which in turn would cause precipitation in the column void space and limit further processing by rapid pore blockage. Hence, macro-porous systems, such as membranes or monoliths, are preferable for SXC applications, especially for viruses, as they operate with convective mass transport [118], and at higher flux which reduces the chance of precipitate-induced pore blockage.
- Additionally, an increase in **flux** can help increase the throughput of the process. However, it reduces the residence time in the column and the contact time of the virus with the stationary phase, which directly correlates with the chance for accretion and retention. This is likely significant for systems with larger pore sizes, which would have reduced contact areas. Such stationary phases may be implemented to reduce the system pressure further and increase the throughput [118]. Hence, this is an optimization problem not easily solved. Labisch et al. [135] proposed to use the membrane area of the first layer as scaling factor.
- Another open question concerning the **pore size** is the space for precipitation. Larger pore sizes allow for more layers of target molecules to build up without blocking the pores. It has been postulated for the immunoglobulin M that a finite number of layers accretes inside the pores until an equilibrium of molecules being washed out and new adherence is established [121]. This effect has not yet been observed for viruses, as they tend to build up until the pores are blocked and the resulting filtration effects increase the column pressure exponentially [121,126].
- **Mixing** the PEG-enriched solution with the target before loading the column has been performed in SXC for some viruses applications without issues [126–129,131]. However, concerns of this strategy were risen and in-line mixing recommended [119,131]. In the first approach, it can be assumed that precipitates form around nuclei such as cell debris

before column loading. Whether they disintegrate due to shear forces in the pores and where these precipitates deposit in the column are open for investigation. However, some insight was provided by Tao et al. [118], who showed that γ-globulin precipitates can form inside cryogel monolith pores when using in-line mixing. Two studies with influenza viruses [133] and lentiviruses [135],both using in-line mixing, revealed that the virus particles are primarily retained on the top layers of membrane columns. The latter suggests the presence of filtration effects, which are a limitation to the SXC method.

To pave the path for a platform application of the SXC, these urgent questions need further investigation.

4. Production of Orf virus pharmaceuticals

The first therapeutics based on the ORFV were vaccines against the orf disease, developed in the 1930s [37]. Today, approved drugs using ORFV are only available for veterinary applications, e.g., as immunomodulatory agent in horses [56]. However, the literature at the time of this writing is sparse with respect to the corresponding production processes, including USP and DSP.

Upstream processing of the Orf virus

The propagation of ORFV can be performed *in vivo* or *in vitro*. For orf disease vaccines, attenuated live ORFV has been cultivated in tissue culture or live virus extracted from animal scab [37]. *In vitro* replication was reported to occur in ovine and bovine cells for wild type ORFV and in certain cell lines for adapted ORFV isolates [43]. The highest infectious titers were reported for sheep skin fibroblast cells and OA3.T sheep epithelial cells, while an order of magnitude less was reported for human embryonic kidney (HEK-293) cells or primary ovine fetal turbinate cells [144].

Downstream processing of the Orf virus

The DSP of scab-based material is unsophisticated. Scabs are desiccated, ground to powder, and stored frozen or in the fridge [40]. It should be recognized that the risk of contaminations, e.g., bacteria from secondary infections, is high with this approach [37]. Thus, standards for pharmaceutical products, especially for human use, are not met. Therefore, cell culture-based production processes followed by a complete DSP train are preferable.

In lab-based studies, sucrose density gradient centrifugation is regularly used for ORFV purification [31,33,144–146]. This method yields high infectious ORFV titers and excellent purities. Another centrifugation approach, yielding lower purity [114], is the sucrose cushion ultracentrifugation [42,53]. While ORFV samples from centrifugal approaches have been used for preclinical animal studies [51], their exact purities were not discussed. Another lab-based, micro-scale approach to generate material for preclinical studies is plaque-purification [46,147]. To replace these

single-step purification processes, a lab-based DSP train was recently proposed for the preparation of high-titer ORFV samples for preclinical murine models [144]. First, a centrifugal clarification step was recommended. To release additional virus, the cell pellet was processed by freeze-thawing coupled with sonication and then centrifuged again. Both supernatants were combined for a nuclease treatment and a subsequent two-step filtration process, i.e., depth and tangential-flow filtration, followed by an iodixanol ultracentrifugation, a dialysis, and a PEG concentration step. Recoveries of 85 % and higher were determined for both filtration steps. However, no quantification of impurities was performed.

A study on the comparison of different purification methods for pre-clarified ORFV was published by Lothert et al. [128], in which they evaluated steric exclusion, cation and anion exchange, hydrophobic interaction, pseudo-affinity (sulfated cellulose), and multi-modal (Capto Core 700), i.e., ion exchange and size exclusion, chromatography. The report showed that anion exchange and SXC resulted in the highest ORFV yields (> 80 %) as the primary chromatographic purification step. The SXC, however, offered the highest contaminant removal, i.e., > 99 % total protein and 62 % dsDNA. As a secondary unit operation, the multi-modal resin performed best with 90 % ORFV yield and an additional 36 % dsDNA removal. The two-step purified ORFV eluate yielded roughly 80 % infectious ORFV, while containing a residual contaminant content of 24 ng mL^{-1} dsDNA (78 % removal) and a HCP concentration below the limit of detection (25 µg mL^{-1}). However, the final dsDNA content achieved with this process setup was above the regulatory limits of 10 ng per dose. Therefore, a follow-up study implemented the combination of SXC and multimodal chromatography in a full lab-scale DSP set-up for pharmaceutical application [127]. This included a freeze-thaw cell lysis step, a two-step depth filtration train, nuclease treatment, and the two chromatographic steps SXC and multimodal. The implementation of the additional unit operations increased the dsDNA removal to 94 %. Accordingly, the residual content was approximately 1 ng per 10^6 IU ORFV, conforming to regulatory limitations up to 10^7 IU ORFV per dose. Additionally, the infectious virus yield in the chromatographic set-up was increased to 90 %, resulting in a yield of 64 % for the overall process.

Although the presented study by Lothert et al. [127] reveals exceptional ORFV recoveries, a large-scale application remains to be evaluated. Scale-up procedures often introduce unexpected changes of degradation forces. Past studies have evaluated the stress-related response of infectious ORFV particles throughout such processing steps. The virus is expected to remain infective for months when preserved in scab material; however, exposure to environmental conditions inactivates it quickly [43]. Other stress factors such as UV-C irradiation [53] and substances like binary ethylamine [51] can reduce the ORFV infectivity. Thermal inactivation studies showed that heating at 56 °C [43] is unfavorable, while freeze-thawing had little impact on the virus activity [128,144]. Further studies on thermal, chemical, or mechanical stress are scarce for the ORFV, but available for other poxviruses [148]. Nonetheless, some conclusions may be drawn from available pharmaceutical products based on the ORFV or the closely related MVA virus.

Selected Orf virus formulation options

Formulations for ORFV-based products aim towards the preservation of infectivity and the prevention of virus aggregation. In the reviewed pharmaceutical products, ORFV and MVA, a close relative of the ORFV, virus stability is conserved using excipients such as protein (HSA, lactalbumin, casein, gelatin), sugars (trehalose, sucrose, lactose, dextran), sugar alcohols (sorbitol and mannitol), and a suitable buffer system of near neutral pH (**Table 4**).

Table 4: Formulation compositions of ORFV- and MVA virus-related pharmaceutical products. Products are listed with and without health agency approval. For lyophilized products, only the buffer for the freeze-drying is described, if not stated otherwise. HBSS, Hank's balanced salt solution; HEPES, 4-(2-hydroxyethyl)-1-piperazineethanesulfonic acid; HSA, human serum albumin.

Virus strain	Product type	Trade name	Storage condition	Excipients	Ref.
ORFV Muk 59/05	orf disease vaccine (ovine)	N/A	lyophilized	5 % lactalbumin 10 % trehalose or sucrose HBSS	[39]
ORFV D1701	immunomodulatory agent (equine)	*ZYLEXIS*	lyophilized	8 % dextran n40 6 % casein hydrolysate 8 % lactose 9 % sorbitol NaOH for neutralization	[55]
MVA virus	smallpox vaccine (human)	*ACAM2000*	lyophilized	2 % HSA 5 % mannitol 0.5-0.7 % NaCl 6-8 mM HEPES	[149,150]
MVA virus	smallpox vaccine (human)	*JYNNEOS*	lyophilized	140 mM NaCl 10 mM TRIS HCl for neutralization	[151]
MVA virus	smallpox vaccine (human)	*Imvanex*	lyophilized	gelatine NaCl TRIS HCl for neutralization	[152]
MVA virus	Ebola vaccine (human)	*Ad26.ZEBOV/ MVA-BN - Filo*	liquid, frozen	NaCl TRIS NaOH for neutralization	[153,154]

In the reviewed pharmaceutical products, ORFV and MVA, a close relative of the ORFV, virus stability is conserved using excipients such as protein (HSA, lactalbumin, casein, gelatin), sugars (trehalose, sucrose, lactose, dextran), sugar alcohols (sorbitol and mannitol), and a suitable buffer system of near neutral pH (**Table 4**). Additionally, sugars like sucrose were reported to prevent the aggregation of concentrated ORFV [144]. The dominance of lyophilized products suggests the ORFV stability throughout a freezing process compared to liquid storage. Proteins and sugars stabilize proteins during the phase transition and provide a matrix for the ORFV in the pulverized form. In this state, some MVA vaccines are stable for years [150–152].

5. Motivation of the dissertation project

The development time of new pharmaceutical products until they reach market approval is an essential factor for rapid action against emerging diseases, as SARS-CoV-2 has clearly illustrated. To prevent bottlenecks in the production process, limitations should be identified and eliminated early on. Such constraints can generate reduced yields or loss of activity. For viral vectors, which are commonly applied for gene therapeutic, oncolytic, or vaccine applications, the infectivity determines the efficiency of the product. One such vector with potential pharmaceutical application is the ORFV. The virus has gained increasing attention in the recent years for a variety of therapeutic applications. However, studies on the ORFV infectivity stability are scarce. Such studies will aid in identifying relevant excipients for a stable product formulation and suitable additives for infectivity preservation throughout the production process, where unforeseen deviations in the process may occur. Additionally, suitable unit operations can be selected to reduce the impact of mechanical and chemical stresses on infectivity stability. Thus, the objective of this dissertation project is to extensively characterize the degrading conditions and stabilizing environments of the ORFV. Therefore, pertinent sample preparation techniques must be identified and evaluated.

In the past, a full lab-scale production process implementing the SXC has been proposed for the ORFV to achieve high yields. However, little is known about the critical process parameters and limitations for scale-up of the SXC with the ORFV. A deeper understanding of these questions will likely improve the adoption of the SXC, as well as the full DSP, to different ORFV genotypes in reduced time. Therefore, this dissertation project focuses on the identification of undescribed critical process parameters in the SXC processing of the ORFV and their impact on the recoveries.

The elucidation of ORFV infectivity stability and SXC processing is proposed to the successful implementation of a full, scalable DSP with high yields along with an effective formulation of the final product.

References

[1] F. Eilts, M. Steger, K. Lothert, F. Pagallies, R. Amann, M.W. Wolff, The impact of purification on the particle integrity of the Orf virus analyzed for an established downstream process, ACHEMA Pulse Congress 2021. DECHEMA. Online, 15.06.2021.

[2] J.S. Tregoning, K.E. Flight, S.L. Higham, Z. Wang, B.F. Pierce, Progress of the COVID-19 vaccine effort: viruses, vaccines and variants versus efficacy, effectiveness and escape, Nat. Rev. Immunol. 21 (2021) 626–636. https://doi.org/10.1038/s41577-021-00592-1.

[3] S. Stanley, Biological nanoparticles and their influence on organisms, Curr Opin Biotech 28 (2014) 69–74. https://doi.org/10.1016/j.copbio.2013.11.014.

[4] S. Riedel, Edward Jenner and the history of smallpox and vaccination, Proc. (Bayl Univ. Med. Cent) 18 (2005) 21–25. https://doi.org/10.1080/08998280.2005.11928028.

[5] S. Plotkin, History of vaccination, Proc Natl Acad Sci USA 111 (2014) 12283–12287. https://doi.org/10.1073/pnas.1400472111.

[6] H.-W. Ackermann, The first phage electron micrographs, Bacteriophage 1 (2011) 225–227. https://doi.org/10.4161/bact.1.4.17280.

[7] C. Varanda, M.d.R. Félix, M.D. Campos, P. Materatski, An Overview of the Application of Viruses to Biotechnology, Viruses 13 (2021). https://doi.org/10.3390/v13102073.

[8] M. Wang, S. Gao, W. Zeng, Y. Yang, J. Ma, Y. Wang, Plant Virology Delivers Diverse Toolsets for Biotechnology, Viruses 12 (2020). https://doi.org/10.3390/v12111338.

[9] V. Prasad, S. Srivastava, Insect Viruses, in: Omkar (Ed.), Ecofriendly Pest Management for Food Security, Academic Press Elsevier, Amsterdam, 2016, pp. 411–442.

[10] D. Raoult, P. Forterre, Redefining viruses: lessons from Mimivirus, Nat Rev Microbiol 6 (2008) 315–319. https://doi.org/10.1038/nrmicro1858.

[11] C.J. Burrell, C.R. Howard, F.A. Murphy, Virus Replication, in: C.J. Burrell, C.R. Howard, F.A. Murphy (Eds.), Fenner and White's Medical Virology, fifth ed., Elsevier, 2017, pp. 39–55.

[12] R. Wolkowicz, M. Schaechter, What makes a virus a virus?, Nat Rev Microbiol 6 (2008) 643; author reply 643. https://doi.org/10.1038/nrmicro1858-c1.

[13] C.J. Burrell, C.R. Howard, F.A. Murphy, Virion Structure and Composition, in: C.J. Burrell, C.R. Howard, F.A. Murphy (Eds.), Fenner and White's Medical Virology, fifth ed., Elsevier, 2017, pp. 27–37.

[14] F. Eilts, J. Harnischfeger, D. Loewe, M.W. Wolff, D. Salzig, P. Czermak, Production of Baculovirus and Stem Cells for Baculovirus-Mediated Gene Transfer into Human Mesenchymal Stem Cells, in: B.A. Pfeifer, A. Hill (Eds.), Vaccine Delivery Technology, Springer US, New York, NY, 2021, pp. 367–390.

[15] G. Sprick, T. Weidner, D. Salzig, P. Czermak, Baculovirus-Induced Recombinant Protein Expression in Human Mesenchymal Stromal Stem Cells: A Promoter Study, N Biotechnol 39 (2017) 161–166. https://doi.org/10.1016/j.nbt.2017.08.006.

[16] H. Tariq, S. Batool, S. Asif, M. Ali, B.H. Abbasi, Virus-Like Particles: Revolutionary Platforms for Developing Vaccines Against Emerging Infectious Diseases, Front Microbiol 12 (2021) 790121. https://doi.org/10.3389/fmicb.2021.790121.

[17] R. Mulligan, The Basic Science of Gene Therapy, Science 260 (1993) 926–932. https://doi.org/10.1126/science.8493530.

[18] Z. Zhao, A.C. Anselmo, S. Mitragotri, Viral vector-based gene therapies in the clinic, Bioeng. Transl. Med. 7 (2022) e10258. https://doi.org/10.1002/btm2.10258.

[19] T. Wirth, N. Parker, S. Ylä-Herttuala, History of gene therapy, Gene 525 (2013) 162–169. https://doi.org/10.1016/j.gene.2013.03.137.

[20] R. Gardlík, R. Pálffy, J. Hodosy, J. Lukács, J. Turna, P. Celec, Vectors and delivery systems in gene therapy, Med Sci Monit 11 (2005) RA110-21.

[21] W.S.M. Wold, K. Toth, Adenovirus vectors for gene therapy, vaccination and cancer gene therapy, Curr Gene Ther 13 (2013) 421–433.

[22] J.J. Bower, L. Song, P. Bastola, M.L. Hirsch, Harnessing the Natural Biology of Adeno-Associated Virus to Enhance the Efficacy of Cancer Gene Therapy, Viruses 13 (2021). https://doi.org/10.3390/v13071205.
[23] M.F. Naso, B. Tomkowicz, W.L. Perry, W.R. Strohl, Adeno-Associated Virus (AAV) as a Vector for Gene Therapy, BioDrugs 31 (2017) 317–334. https://doi.org/10.1007/s40259-017-0234-5.
[24] Y. Yi, M. Jong Noh, K. Hee Lee, Current Advances in Retroviral Gene Therapy, Curr Gene Ther 11 (2011) 218–228. https://doi.org/10.2174/156652311795684740.
[25] M.C. Milone, U. O'Doherty, Clinical use of lentiviral vectors, Leukemia 32 (2018) 1529–1541. https://doi.org/10.1038/s41375-018-0106-0.
[26] A.C. Chambers, M. Aksular, L.P. Graves, S.L. Irons, R.D. Possee, L.A. King, Overview of the Baculovirus Expression System, Curr Protoc Protein Sci 91 (2018) 5.4.1-5.4.6. https://doi.org/10.1002/cpps.47.
[27] G. McFadden, Poxvirus tropism, Nat Rev Microbiol 3 (2005) 201–213. https://doi.org/10.1038/nrmicro1099.
[28] J. Nagington, R.W. Horne, Morphological Studies of Orf and Vaccinia Viruses, Virology 16 (1962) 248–260. https://doi.org/10.1016/0042-6822(62)90245-3.
[29] A. Nitsche, H.R. Gelderblom, K. Eisendle, N. Romani, G. Pauli, Pitfalls in Diagnosing Human Poxvirus Infections, J Clin Virol 38 (2007) 165–168. https://doi.org/10.1016/j.jcv.2006.11.013.
[30] R. Wang, S. Luo, Orf Virus: A New Class of Immunotherapy Drugs, in: D. Vlachakis (Ed.), Systems Biology, IntechOpen, London, 2019.
[31] D. Spehner, S. de Carlo, R. Drillien, F. Weiland, K. Mildner, D. Hanau, H.-J. Rziha, Appearance of the Bona Fide Spiral Tubule of ORF Virus is Dependent on an Intact 10-Kilodalton Viral Protein, J Virol 78 (2004) 8085–8093. https://doi.org/10.1128/JVI.78.15.8085-8093.2004.
[32] C.J. Burrell, C.R. Howard, F.A. Murphy, Poxviruses, in: C.J. Burrell, C.R. Howard, F.A. Murphy (Eds.), Fenner and White's Medical Virology, fifth ed., Elsevier, 2017, pp. 229–236.
[33] J. Nagington, A.A. Newton, R.W. Horne, The structure of orf virus, Virology 23 (1964) 461–472. https://doi.org/10.1016/0042-6822(64)90230-2.
[34] R. Wang, Y. Wang, F. Liu, S. Luo, Orf virus: A promising new therapeutic agent, Rev Med Virol 29 (2019) e2013. https://doi.org/10.1002/rmv.2013.
[35] C. Bergqvist, M. Kurban, O. Abbas, Orf virus infection, Rev. Med. Virol. 27 (2017) e1932. https://doi.org/10.1002/rmv.1932.
[36] D. Haig, A.A. Mercer, Parapoxviruses, in: B.W.J. Mahy, M.H.V. van Regenmortel (Eds.), Encyclopedia of virology, third. ed., Elsevier, Amsterdam, 2008, pp. 57–63.
[37] A.M. Bukar, F.F.A. Jesse, C.A.C. Abdullah, M.M. Noordin, Z. Lawan, H.K. Mangga, K.N. Balakrishnan, M.-L.M. Azmi, Immunomodulatory Strategies for Parapoxvirus: Current Status and Future Approaches for the Development of Vaccines against Orf Virus Infection, Vaccines 9 (2021). https://doi.org/10.3390/vaccines9111341.
[38] J.A. Bala, K.N. Balakrishnan, A.A. Abdullah, R. Mohamed, A.W. Haron, F.F.A. Jesse, M.M. Noordin, M.L. Mohd-Azmi, The re-emerging of orf virus infection: A call for surveillance, vaccination and effective control measures, Microb Pathog 120 (2018) 55–63. https://doi.org/10.1016/j.micpath.2018.04.057#.
[39] D.P. Bora, V. Bhanupraka, G. Venkatesan, V. Balamuruga, M. Prabhu, R. Yogisharad, Effect of Stabilization and Reconstitution on the Stability of a Novel Strain of Live Attenuated Orf Vaccine (ORFV MUK59/05), Asian J Anim Vet Adv 10 (2015) 365–375. https://doi.org/10.3923/ajava.2015.365.375.
[40] J.M.B. Musser, C.A. Taylor, J. Guo, I.R. Tizard, J.W. Walker, Development of a contagious ecthyma vaccine for goats, Am J Vet Res 69 (2008) 1366–1370. https://doi.org/10.2460/ajvr.69.10.1366.
[41] A. Friebe, A. Siegling, S. Friederichs, H.-D. Volk, O. Weber, Immunomodulatory effects of inactivated parapoxvirus ovis (ORF virus) on human peripheral immune cells: induction of cytokine secretion in monocytes and Th1-like cells, J Virol 78 (2004) 9400–9411. https://doi.org/10.1128/JVI.78.17.9400-9411.2004.
[42] A. Reguzova, M. Ghosh, M. Müller, H.-J. Rziha, R. Amann, Orf Virus-Based Vaccine Vector D1701-V Induces Strong CD8+ T Cell Response against the Transgene but Not against ORFV-Derived Epitopes, Vaccines 8 (2020) 295. https://doi.org/10.3390/vaccines8020295.
[43] H.-J. Rziha, M. Büttner, Parapoxviruses, in: Reference Module in Life Sciences, Elsevier, 2020, p. 1505.
[44] H.-J. Rziha, J. Rohde, R. Amann, Generation and Selection of Orf Virus (ORFV) Recombinants, Methods Mol Biol 1349 (2016) 177–200. https://doi.org/10.1007/978-1-4939-3008-1_12.

[45] R. Amann, J. Rohde, U. Wulle, D. Conlee, R. Raue, O. Martinon, H.-J. Rziha, A new rabies vaccine based on a recombinant ORF virus (parapoxvirus) expressing the rabies virus glycoprotein, J Virol 87 (2013) 1618–1630. https://doi.org/10.1128/JVI.02470-12.

[46] J. Rohde, H. Schirrmeier, H. Granzow, H.-J. Rziha, A new recombinant Orf virus (ORFV, Parapoxvirus) protects rabbits against lethal infection with rabbit hemorrhagic disease virus (RHDV), Vaccine 29 (2011) 9256–9264. https://doi.org/10.1016/j.vaccine.2011.09.121.

[47] J. Rohde, R. Amann, H.-J. Rziha, New Orf virus (Parapoxvirus) recombinant expressing H5 hemagglutinin protects mice against H5N1 and H1N1 influenza A virus, PLoS ONE 8 (2013) e83802. https://doi.org/10.1371/journal.pone.0083802.

[48] H.-J. Rziha, M. Büttner, M. Müller, F. Salomon, A. Reguzova, D. Laible, R. Amann, Genomic Characterization of Orf Virus Strain D1701-V (Parapoxvirus) and Development of Novel Sites for Multiple Transgene Expression, Viruses 11 (2019) 127. https://doi.org/10.3390/v11020127.

[49] E. van Rooij, F. Rijsewijk, H.W. Moonen-Leusen, A. Bianchi, H.-J. Rziha, Comparison of different prime-boost regimes with DNA and recombinant Orf virus based vaccines expressing glycoprotein D of pseudorabies virus in pigs, Vaccine 28 (2010) 1808–1813. https://doi.org/10.1016/j.vaccine.2009.12.004.

[50] A. Reguzova, M. Sigle, F. Pagallies, F. Salomon, H.-J. Rziha, Z. Bittner-Schrader, B. Verstrepen, K. Böszörményi, E. Verschoor, K. Elbers, M. Esen, A. Manenti, M. Monti, M. Derouazi, H.-G. Rammensee, M. Löffler, R. Amann, A novel multi-antigenic parapoxvirus-based vaccine demonstrates efficacy in protecting hamsters and non-human primates against SARS-CoV-2 challenge, researchsquare preprint (2023). https://doi.org/10.21203/rs.3.rs-2832501/v1.

[51] A. Friebe, A. Siegling, O. Weber, Inactivated Orf-virus shows disease modifying antiviral activity in a guinea pig model of genital herpesvirus infection, J Microbiol Immunol Infect 51 (2018) 587–592. https://doi.org/10.1016/j.jmii.2017.03.002.

[52] M.P. O'Leary, A.H. Choi, S.-I. Kim, S. Chaurasiya, J. Lu, A.K. Park, Y. Woo, S.G. Warner, Y. Fong, N.G. Chen, Novel oncolytic chimeric orthopoxvirus causes regression of pancreatic cancer xenografts and exhibits abscopal effect at a single low dose, J Transl Med 16 (2018) 110. https://doi.org/10.1186/s12967-018-1483-x.

[53] J.L. Rintoul, C.G. Lemay, L.H. Tai, M.M. Stanford, T.J. Falls, S.C.T. de, B.W. Bridle, M. Daneshmand, P.S. Ohashi, Y. Wan, B.D. Lichty, A.A. Mercer, R.C. Auer, H.L. Atkins, J.C. Bell, ORFV: a novel oncolytic and immune stimulating parapoxvirus therapeutic, Mol. Ther. 20 (2012) 1148–1157. https://doi.org/10.1038/mt.2011.301.

[54] S.B. Fleming, L.M. Wise, A.A. Mercer, Molecular genetic analysis of orf virus: a poxvirus that has adapted to skin, Viruses 7 (2015) 1505–1539. https://doi.org/10.3390/v7031505.

[55] E. Ons, R. Raue WO 2015/057777 Al, 2015.

[56] R. Paillot, A systematic review of the immune-modulators Parapoxvirus ovis and Propionibacterium acnes for the prevention of respiratory disease and other infections in the horse, Vet Immunol Immunopathol 153 (2013) 1–9. https://doi.org/10.1016/j.vetimm.2013.01.010.

[57] S.A. Plotkin, S.L. Plotkin, The development of vaccines: how the past led to the future, Nat Rev Microbiol 9 (2011) 889–893. https://doi.org/10.1038/nrmicro2668.

[58] P. Palese, Making better influenza virus vaccines?, Emerging Infect Dis 12 (2006) 61–65. https://doi.org/10.3201/eid1201.051043.

[59] K. Patel, N. Chotai, Documentation and Records: Harmonized GMP Requirements, J Young Pharm 3 (2011) 138–150. https://doi.org/10.4103/0975-1483.80303.

[60] D. Hoffmann, J. Leber, D. Loewe, K. Lothert, T. Oppermann, J. Zitzmann, T. Weidner, D. Salzig, M.W. Wolff, P. Czermak, Purification of New Biologicals Using Membrane-Based Processes, in: A.B. Basile, C. Charcosset (Eds.), Current trends and future developments on (bio-) membranes: Membrane processes in the pharmaceutical and biotechnological field, Elsevier, Amsterdam, 2019, pp. 123–150.

[61] M.W. Wolff, U. Reichl, Downstream Processing of Cell Culture-Derived Virus Particles, Expert Rev Vaccines 10 (2011) 1451–1475. https://doi.org/10.1586/erv.11.111.

[62] L. Pedro, S.S. Soares, G.N.M. Ferreira, Purification of Bionanoparticles, Chem Eng Technol 31 (2008) 815–825. https://doi.org/10.1002/ceat.200800176.

[63] M.M. Segura, A.A. Kamen, A. Garnier, Overview of current scalable methods for purification of viral vectors, Methods Mol Biol 737 (2011) 89–116. https://doi.org/10.1007/978-1-61779-095-9_4.

[64] K. Pilely, M.R. Johansen, R.R. Lund, T. Kofoed, T.K. Jørgensen, L. Skriver, E. Mørtz, Monitoring process-related impurities in biologics-host cell protein analysis, Anal Bioanal Chem 414 (2022) 747–758. https://doi.org/10.1007/s00216-021-03648-2.

[65] C.L.Z. de Zafra, V. Quarmby, K. Francissen, M. Vanderlaan, J. Zhu-Shimoni, Host cell proteins in biotechnology-derived products: A risk assessment framework, Biotechnol Bioeng 112 (2015) 2284–2291. https://doi.org/10.1002/bit.25647.

[66] K. Champion, H. Madden, J. Dougherty, E. Shacter, Defining Your Product Profile and Maintaining Control Over It, Part 2: Challenges of Monitoring Host Cell Protein Impurities, 2005.

[67] EMA, CPMP position statement on DNA and host cell proteins (HCP) impurities, routine testing versus validation studies (1997).

[68] FDA, Chemistry, Manufacturing, and Control (CMC) Information for Human Gene Therapy Investigational New Drug Applications (INDs): Draft Guidance for Industry (2018).

[69] P. Kramberger, L. Urbas, A. Štrancar, Downstream processing and chromatography based analytical methods for production of vaccines, gene therapy vectors, and bacteriophages, Hum Vaccin Immunother 11 (2015) 1010–1021. https://doi.org/10.1080/21645515.2015.1009817.

[70] J.F. Wright, Product-Related Impurities in Clinical-Grade Recombinant AAV Vectors: Characterization and Risk Assessment, Biomedicines 2 (2014) 80–97. https://doi.org/10.3390/biomedicines2010080.

[71] B. Sanders, M. Koldijk, H. Schuitemaker, Inactivated Viral Vaccines, in: B.K. Nunnally, V.E. Turula, R.D. Sitrin (Eds.), Vaccine Analysis: Strategies, Principles, and Control, Springer, Berlin, Heidelberg, 2015, pp. 45–80.

[72] J.B. Ulmer, U. Valley, R. Rappuoli, Vaccine manufacturing: challenges and solutions, Nat Biotechnol 24 (2006) 1377–1383. https://doi.org/10.1038/nbt1261.

[73] T. Vicente, C. Peixoto, M.J.T. Carrondo, P.M. Alves, Purification of recombinant baculoviruses for gene therapy using membrane processes, Gene Ther. 16 (2009) 766–775. https://doi.org/10.1038/gt.2009.33.

[74] T.A. Grein, R. Michalsky, M. Vega López, P. Czermak, Purification of a recombinant baculovirus of Autographa californica M nucleopolyhedrovirus by ion exchange membrane chromatography, J Virol Methods 183 (2012) 117–124. https://doi.org/10.1016/j.jviromet.2012.03.031.

[75] P. Nestola, C. Peixoto, R.R.J.S. Silva, P.M. Alves, J.P.B. Mota, M.J.T. Carrondo, Improved virus purification processes for vaccines and gene therapy, Biotechnol Bioeng 112 (2015) 843–857. https://doi.org/10.1002/bit.25545.

[76] M. Prashad, K. Tarrach, Depth filtration: Cell clarification of bioreactor offloads, Filtr Separat 43 (2006) 28–30. https://doi.org/10.1016/S0015-1882(06)70950-8.

[77] T. Vicente, A. Roldão, C. Peixoto, M.J.T. Carrondo, P.M. Alves, Large-scale production and purification of VLP-based vaccines, J Invertebr Pathol 107 Suppl (2011) S42-8. https://doi.org/10.1016/j.jip.2011.05.004.

[78] K.C. Ingham, Precipitation of proteins with polyethylene glycol: Characterization of albumin, Arch Biochem Biophys 186 (1978) 106–113. https://doi.org/10.1016/0003-9861(78)90469-1.

[79] K.C. Ingham, [23] Precipitation of proteins with polyethylene glycol, in: M.P. Deutscher (Ed.), Guide to Protein Purification, Elsevier, 1990, pp. 301–306.

[80] R. Morenweiser, Downstream Processing of Viral Vectors and Vaccines, Gene Ther 12 Suppl 1 (2005) 103-10. https://doi.org/10.1038/sj.gt.3302624.

[81] P. Gagnon, Chromatographic Purification of Virus Particles, in: M.C. Flickinger (Ed.), Encyclopedia of Industrial Biotechnology, John Wiley & Sons, Inc, Hoboken, NJ, USA, 2009.

[82] P. Gagnon, E. Grund, T. Lindbäck, Large Scale Process Development for Hydrophobic Interaction Chromatography, Part 1: Gel Selection and Development of Binding Condition, BioPharm 8 (1995) 21–29.

[83] M. Zhao, M. Vandersluis, J. Stout, U. Haupts, M. Sanders, R. Jacquemart, Affinity Chromatography for Vaccines Manufacturing: Finally Ready for Prime Time?, Vaccine (2018) Corrected Proof. https://doi.org/10.1016/j.vaccine.2018.02.090.

[84] G.-A. Junter, L. Lebrun, Polysaccharide-based chromatographic adsorbents for virus purification and viral clearance, J Pharm Anal 10 (2020) 291–312. https://doi.org/10.1016/j.jpha.2020.01.002.

[85] D. Clénet, T. Vinit, D. Soulet, C. Maillet, F. Guinet-Morlot, A. Saulnier, Biophysical Virus Particle Specific Characterization to Sharpen the Definition of Virus Stability, Eur J Pharm Biopharm 132 (2018) 62–69. https://doi.org/10.1016/j.ejpb.2018.08.006.

[86] S. Ohtake, Y. Kita, T. Arakawa, Interactions of formulation excipients with proteins in solution and in the dried state, Adv Drug Deliver Rev 63 (2011) 1053–1073. https://doi.org/10.1016/j.addr.2011.06.011.
[87] J.L. Tlaxca, S. Ellis, R.L. Remmele, Live attenuated and inactivated viral vaccine formulation and nasal delivery: potential and challenges, Adv Drug Deliver Rev 93 (2015) 56–78. https://doi.org/10.1016/j.addr.2014.10.002.
[88] F.M.C. Cardoso, D. Petrovajová, T. Horňáková, Viral vaccine stabilizers: status and trends, Acta Virol 61 (2017) 231–239. https://doi.org/10.4149/av_2017_301.
[89] F. Hämmerling, M.M. Pieler, R. Hennig, A. Serve, E. Rapp, M.W. Wolff, U. Reichl, J. Hubbuch, Influence of the Production System on the Surface Properties of Influenza A Virus Particles, Eng Life Sci 17 (2017) 1071–1077. https://doi.org/10.1002/elsc.201700058.
[90] K. Lothert, F. Eilts, M.W. Wolff, Quantification methods for viruses and virus-like particles applied in biopharmaceutical production processes, Expert Rev Vaccines 21 (2022) 1029–1044. https://doi.org/10.1080/14760584.2022.2072302.
[91] C.M. Maguire, M. Rösslein, P. Wick, A. Prina-Mello, Characterisation of particles in solution – a perspective on light scattering and comparative technologies, Sci Technol Adv Mat 19 (2018) 732–745. https://doi.org/10.1080/14686996.2018.1517587.
[92] W. Anderson, D. Kozak, V.A. Coleman, Å.K. Jämting, M. Trau, A Comparative Study of Submicron Particle Sizing Platforms: Accuracy, Precision and Resolution Analysis of Polydisperse Particle Size Distributions, J Colloid Interface Sci 405 (2013) 322–330. https://doi.org/10.1016/j.jcis.2013.02.030.
[93] S. Falke, C. Betzel, Dynamic Light Scattering (DLS), in: A.S. Pereira, P. Tavares, P. Limão-Vieira (Eds.), Radiation in Bioanalysis, Springer International Publishing, Cham, 2019, pp. 173–193.
[94] J. Xu, H. Ma, Y. Liu, Stochastic Optical Reconstruction Microscopy (STORM), Curr Protoc Cytom 81 (2017) 12.46.1-12.46.27. https://doi.org/10.1002/cpcy.23.
[95] S. Bhattacharjee, DLS and Zeta Potential - What They Are and What They Are Not?, J Control Release 235 (2016) 337–351. https://doi.org/10.1016/j.jconrel.2016.06.017.
[96] S. Heider, C. Metzner, Quantitative Real-Time Single Particle Analysis of Virions, Virology 462-463 (2014) 199–206. https://doi.org/10.1016/j.virol.2014.06.005.
[97] P. Kramberger, M. Ciringer, A. Štrancar, M. Peterka, Evaluation of nanoparticle tracking analysis for total virus particle determination, Virol J 9 (2012) 265. https://doi.org/10.1186/1743-422X-9-265.
[98] L. Yang, T. Yamamoto, Quantification of Virus Particles Using Nanopore-Based Resistive-Pulse Sensing Techniques, Front Microbiol 7 (2016) 1500. https://doi.org/10.3389/fmicb.2016.01500.
[99] J.L.R. Zamora, H.C. Aguilar, Flow virometry as a tool to study viruses, Methods 134-135 (2018) 87–97. https://doi.org/10.1016/j.ymeth.2017.12.011.
[100] E. van Tricht, L. Geurink, F. Galindo Garre, M. Schenning, H. Backus, M. Germano, G.W. Somsen, C.E. Sänger-van de Griend, Implementation of at-line capillary zone electrophoresis for fast and reliable determination of adenovirus concentrations in vaccine manufacturing, Electrophoresis 40 (2019) 2277–2284. https://doi.org/10.1002/elps.201900068.
[101] L.L. Bondoc Jr, S. Fitzpatrick, Size Distribution Analysis of Recombinant Adenovirus Using Disc Centrifugation, J Ind Microbiol Biot 20 (1998) 317–322. https://doi.org/10.1038/sj.jim.2900529.
[102] C. Lei, J. Yang, J. Hu, X. Sun, On the Calculation of TCID50 for Quantitation of Virus Infectivity, Virol Sin 36 (2021) 141–144. https://doi.org/10.1007/s12250-020-00230-5.
[103] S.T. Abedon, T.I. Katsaounis, Detection of Bacteriophages: Statistical Aspects of Plaque Assay, in: D.R. Harper, S.T. Abedon, B.H. Burrowes, M.L. McConville (Eds.), Bacteriophages, Springer International Publishing, Cham, 2021, pp. 539–560.
[104] B. Buszewski, E. Maślak, M. Złoch, V. Railean-Plugaru, E. Kłodzińska, P. Pomastowski, A new approach to identifying pathogens, with particular regard to viruses, based on capillary electrophoresis and other analytical techniques, Trends Analyt Chem 139 (2021) 116250. https://doi.org/10.1016/j.trac.2021.116250.
[105] A.M. Shrivastav, U. Cvelbar, I. Abdulhalim, A comprehensive review on plasmonic-based biosensors used in viral diagnostics, Commun Biol 4 (2021) 70. https://doi.org/10.1038/s42003-020-01615-8.
[106] P.K.R. Kumar, Monitoring Intact Viruses Using Aptamers, Biosensors 6 (2016). https://doi.org/10.3390/bios6030040.
[107] A.A. Morley, Digital PCR: A brief history, Biomol Detect Quantif 1 (2014) 1–2. https://doi.org/10.1016/j.bdq.2014.06.001.

[108] S. Levine, T.T. Puck, B.P. Sagik, An absolute method for assay of virus hemagglutinins, J Exp Med 98 (1953) 521–531. https://doi.org/10.1084/jem.98.6.521.
[109] R. Vogel, A.K. Pal, S. Jambhrunkar, P. Patel, S.S. Thakur, E. Reátegui, H.S. Parekh, P. Saá, A. Stassinopoulos, M.F. Broom, High-Resolution Single Particle Zeta Potential Characterisation of Biological Nanoparticles using Tunable Resistive Pulse Sensing, Sci Rep 7 (2017) 17479. https://doi.org/10.1038/s41598-017-14981-x.
[110] L. Kremser, G. Bilek, D. Blaas, E. Kenndler, Capillary electrophoresis of viruses, subviral particles and virus complexes, J Sep Sci 30 (2007) 1704–1713. https://doi.org/10.1002/jssc.200700105.
[111] J. Heffron, B.K. Mayer, Virus Isoelectric Point Estimation: Theories and Methods, Appl Environ Microb 87 (2021). https://doi.org/10.1128/AEM.02319-20.
[112] C.L. Heldt, A. Zahid, K.S. Vijayaragavan, X. Mi, Experimental and computational surface hydrophobicity analysis of a non-enveloped virus and proteins, Colloid Surface B 153 (2017) 77–84. https://doi.org/10.1016/j.colsurfb.2017.02.011.
[113] H. Shi, V.V. Tarabara, Charge, size distribution and hydrophobicity of viruses: Effect of propagation and purification methods, J Virol Methods 256 (2018) 123–132. https://doi.org/10.1016/j.jviromet.2018.02.008.
[114] K.T. James, B. Cooney, K. Agopsowicz, M.A. Trevors, A. Mohamed, D. Stoltz, M. Hitt, M. Shmulevitz, Novel High-Throughput Approach for Purification of Infectious Virions, Sci Rep 6 (2016) 36826. https://doi.org/10.1038/srep36826.
[115] B. Michen, T. Graule, Isoelectric Points of Viruses, J Appl Microbiol 18 (2010) 290. https://doi.org/10.1111/j.1365-2672.2010.04663.x.
[116] C. Dika, C. Gantzer, A. Perrin, J.F.L. Duval, Impact of the virus purification protocol on aggregation and electrokinetics of MS2 phages and corresponding virus-like particles, Phys Chem Chem Phys 15 (2013) 5691–5700. https://doi.org/10.1039/c3cp44128h.
[117] S.-L. Sim, T. He, A. Tscheliessnig, M. Mueller, R.B.H. Tan, A. Jungbauer, Branched polyethylene glycol for protein precipitation, Biotechnol Bioeng 109 (2012) 736–746. https://doi.org/10.1002/bit.24343.
[118] S.-P. Tao, J. Zheng, Y. Sun, Grafting Zwitterionic Polymer onto Cryogel Surface Enhances Protein Retention in Steric Exclusion Chromatography on Cryogel Monolith, J Chromatogr A 1389 (2015) 104–111. https://doi.org/10.1016/j.chroma.2015.02.051.
[119] T. Arakawa, P. Gagnon, Excluded Cosolvent in Chromatography, J Pharm Sci 107 (2018) 2297–2305. https://doi.org/10.1016/j.xphs.2018.05.006.
[120] P. Gagnon US 9,809,639 B2, 2012.
[121] J. Lee, H.T. Gan, S.M.A. Latiff, C. Chuah, W.Y. Lee, Y.-S. Yang, B. Loo, S.K. Ng, P. Gagnon, Principles and Applications of Steric Exclusion Chromatography, J Chromatogr A 1270 (2012) 162–170. https://doi.org/10.1016/j.chroma.2012.10.062.
[122] J.J. Labisch, G.P. Wiese, K. Pflanz, Steric Exclusion Chromatography for Purification of Biomolecules—A Review, Separations 10 (2023) 183. https://doi.org/10.3390/separations10030183.
[123] P. Gagnon, P. Toh, J. Lee, High Productivity Purification of Immunoglobulin G Monoclonal Antibodies on Starch-Coated Magnetic Nanoparticles by Steric Exclusion of Polyethylene Glycol, J Chromatogr A 1324 (2014) 171–180. https://doi.org/10.1016/j.chroma.2013.11.039.
[124] C. Wang, S. Bai, S.-P. Tao, Y. Sun, Evaluation of Steric Exclusion Chromatography on Cryogel Column for the Separation of Serum Proteins, J Chromatogr A 1333 (2014) 54–59. https://doi.org/10.1016/j.chroma.2014.01.059.
[125] A. Levanova, M.M. Poranen, Application of Steric Exclusion Chromatography on Monoliths for Separation and Purification of RNA Molecules, J Chromatogr A 1574 (2018) 50–59. https://doi.org/10.1016/j.chroma.2018.08.063.
[126] K. Lothert, A.F. Offersgaard, A.F. Pihl, C.K. Mathiesen, T.B. Jensen, G.P. Alzua, U. Fahnøe, J. Bukh, J.M. Gottwein, M.W. Wolff, Development of a downstream process for the production of an inactivated whole hepatitis C virus vaccine, Sci Rep 10 (2020) 3018. https://doi.org/10.1038/s41598-020-72328-5.
[127] K. Lothert, F. Pagallies, F. Eilts, A. Sivanesapillai, M. Hardt, A. Moebus, T. Feger, R. Amann, M.W. Wolff, A scalable downstream process for the purification of the cell culture-derived Orf virus for human or veterinary applications, J Biotechnol 323 (2020) 221–230. https://doi.org/10.1016/j.jbiotec.2020.08.014.
[128] K. Lothert, F. Pagallies, T. Feger, R. Amann, M.W. Wolff, Selection of chromatographic methods for the purification of cell culture-derived Orf virus for its application as a vaccine or viral vector, J Biotechnol 323 (2020) 62–72. https://doi.org/10.1016/j.jbiotec.2020.07.023.

[129] K. Lothert, G. Sprick, F. Beyer, G. Lauria, P. Czermak, M.W. Wolff, Membrane-Based Steric Exclusion Chromatography for the Purification of a Recombinant Baculovirus and its Application for Cell Therapy, J Virol Methods 275 (2020) 113756. https://doi.org/10.1016/j.jviromet.2019.113756.

[130] P. Marichal-Gallardo, M.M. Pieler, M.W. Wolff, U. Reichl, Steric Exclusion Chromatography for Purification of Cell Culture-Derived Influenza A Virus Using Regenerated Cellulose Membranes and Polyethylene Glycol, J Chromatogr A 1483 (2017) 110–119. https://doi.org/10.1016/j.chroma.2016.12.076.

[131] P. Marichal-Gallardo, K. Börner, M.M. Pieler, V. Sonntag-Buck, M. Obr, D. Bejarano, M.W. Wolff, H.-G. Kräusslich, U. Reichl, D. Grimm, Single-use capture purification of adeno-associated viral gene transfer vectors by membrane-based steric exclusion chromatography, Hum Gene Ther 32 (2021) 959–974. https://doi.org/10.1089/hum.2019.284.

[132] J.J. Labisch, M. Kassar, F. Bollmann, A. Valentic, J. Hubbuch, K. Pflanz, Steric exclusion chromatography of lentiviral vectors using hydrophilic cellulose membranes, J Chromatogr A (2022) 463148. https://doi.org/10.1016/j.chroma.2022.463148.

[133] P.A. Marichal-Gallardo, Chromatographic purification of biological macromolecules by their capture on hydrophilic surfaces with the aid of non-ionic polymers, Universitäts- und Landesbibliothek Sachsen-Anhalt, 2019.

[134] G. Gränicher, M. Babakhani, S. Göbel, I. Jordan, P. Marichal-Gallardo, Y. Genzel, U. Reichl, A high cell density perfusion process for Modified Vaccinia virus Ankara production: Process integration with inline DNA digestion and cost analysis, Biotechnol Bioeng 118 (2021) 4720–4734. https://doi.org/10.1002/bit.27937.

[135] J.J. Labisch, R. Paul, G. Wiese, K. Pflanz, Scaling Up of Steric Exclusion Membrane Chromatography for Lentiviral Vector Purification, Membranes 13 (2023) 149. https://doi.org/10.3390/membranes13020149.

[136] D.H. Atha, K.C. Ingham, Mechanism of Precipitation of Proteins by Polyethylene Glycols. Analysis in Terms of Excluded Volume, J Biol Chem 256 (1981) 12108–12117. https://doi.org/10.1016/S0021-9258(18)43240-1.

[137] S.I. Miekka, K.C. Ingham, Influence of self-association of proteins on their precipitation by poly(ethylene glycol), Arch Biochem Biophys 191 (1978) 525–536. https://doi.org/10.1016/0003-9861(78)90391-0.

[138] S.-L. Sim, T. He, A. Tscheliessnig, M. Mueller, R.B.H. Tan, A. Jungbauer, Protein precipitation by polyethylene glycol: a generalized model based on hydrodynamic radius, J Biotechnol 157 (2012) 315–319. https://doi.org/10.1016/j.jbiotec.2011.09.028.

[139] J.C. Lee, L.L. Lee, Preferential Solvent Interactions Between Proteins and Polyethylene Glycols, J Biol Chem 256 (1981) 625–631. https://doi.org/10.1016/S0021-9258(19)70019-2.

[140] I.M. Kuznetsova, K.K. Turoverov, V.N. Uversky, What macromolecular crowding can do to a protein, Int J Mol Sci 15 (2014) 23090–23140. https://doi.org/10.3390/ijms151223090.

[141] Broide, Tominc, Saxowsky, Using phase transitions to investigate the effect of salts on protein interactions, Phys Rev E 53 (1996) 6325–6335. https://doi.org/10.1103/PhysRevE.53.6325.

[142] J. Giesler, L. Weirauch, J. Thöming, M. Baune, G.R. Pesch, Separating microparticles by material and size using dielectrophoretic chromatography with frequency modulation, Sci Rep 11 (2021) 16861. https://doi.org/10.1038/s41598-021-95404-w.

[143] J. op de Beeck, W. de Malsche, J. Vangelooven, H. Gardeniers, G. Desmet, Hydrodynamic chromatography of polystyrene microparticles in micropillar array columns, J Chromatogr A 1217 (2010) 6077–6084. https://doi.org/10.1016/j.chroma.2010.07.031.

[144] J.P. van Vloten, J.A. Minott, T.M. McAusland, J.C. Ingrao, L.A. Santry, G. McFadden, J.J. Petrik, B.W. Bridle, S.K. Wootton, Production and purification of high-titer OrfV for preclinical studies in vaccinology and cancer therapy, Mol Ther Methods Clin Dev 23 (2021) 434–447. https://doi.org/10.1016/j.omtm.2021.08.004.

[145] W.K. Joklik, The purification of four strains of poxvirus, Virology 18 (1962) 9–18. https://doi.org/10.1016/0042-6822(62)90172-1.

[146] N. Nashiruddullah, D.C. Pathak, N.N. Barman, J.A. Ahmed, P. Borah, S.S. Begum, S. Islam, In Vitro and in Vivo Assessment of Orf Virus (ORFV) by Electron Microscopy, Vet. arhiv. (Veterinarski arhiv) 88 (2018) 847–861. https://doi.org/10.24099/vet.arhiv.0229.

[147] T. Fischer, O. Planz, L. Stitz, H.-J. Rziha, Novel recombinant parapoxvirus vectors induce protective humoral and cellular immunity against lethal herpesvirus challenge infection in mice, J Virol 77 (2003) 9312–9323. https://doi.org/10.1128/jvi.77.17.9312-9323.2003.

[148] F.v. Rheinbaben, J. Gebel, M. Exner, A. Schmidt, Environmental resistance, disinfection, and sterilization of poxviruses, in: A.A. Mercer, A. Schmidt, O. Weber (Eds.), Poxviruses, Birkhäuser Basel, Basel, 2007, pp. 397–405.

[149] O.S. Kumru, S.B. Joshi, D.E. Smith, C.R. Middaugh, T. Prusik, D.B. Volkin, Vaccine Instability in the Cold Chain: Mechanisms, Analysis and Formulation Strategies, Biologicals 42 (2014) 237–259. https://doi.org/10.1016/j.biologicals.2014.05.007.

[150] FDA, Product Information ACAM2000. https://www.fda.gov/media/75792/download (accessed 29 April 2022).

[151] Bavarian Nordic A/S, Package insert JYNNEOS, 2021. https://www.fda.gov/media/131078/download (accessed 5 August 2021).

[152] European Medicines Agency, Assessment report IMVANEX, 2013. https://www.ema.europa.eu/en/documents/assessment-report/imvanex-epar-public-assessment-report_en.pdf (accessed 4 August 2021).

[153] M.A.H. Capelle, L. Babich, J.P.E. van Deventer-Troost, D. Salerno, K. Krijgsman, U. Dirmeier, B. Raaby, J. Adriaansen, Stability and suitability for storage and distribution of Ad26.ZEBOV/MVA-BN®-Filo heterologous prime-boost Ebola vaccine, Eur J Pharm Biopharm 129 (2018) 215–221. https://doi.org/10.1016/j.ejpb.2018.06.001.

[154] EMA, Product Information MVA-BEA. https://www.ema.europa.eu/en/documents/product-information/mvabea-epar-product-information_en.pdf (accessed 6 August 2022).

CHAPTER 2: Physicochemical characterization of the Orf virus

The characterization of active pharmaceutical compounds is an important step in the development of therapeutic products and their production processes. Not only from an economical perspective are high yields and little losses desirable. Concerning active viral targets, the infectivity is frequently the defining characteristic. Loss of infectivity can occur throughout the virus propagation (USP), the purification (DSP) as well as the storage and distribution. Thus, degrading forces and ways to stabilize the virions need to be identified. Concerning the processing itself, thermal, mechanical, and chemical stress are most commonly causes for infectivity loss. Throughout storage and distribution, thermal and mechanical extrema should be characterized as well as the duration of the storage. For such tests, suitable samples need to be prepared to guarantee representative results. Preparations should be of high infectious titer and intact virus particles as well as free of interfering substances. After the characterization of the virus target and the identification of degradation conditions, a formulation with stabilizing excipients can be tested. Additives commonly applied for viral targets include proteins, amino acids, salts, detergents, antioxidants, or buffers. Some of these may even be implemented throughout the production process if they do not limit the unit operations, supplying additional protection against infectious virus loss.

For the ORFV, few authors published results on ORFV-specific characteristics, infectivity stability, and degrading conditions as well as methods to prepare samples to study these traits. However, to ensure a streamlined process set-up, a thorough study of these research questions is expedient, which is covered in this chapter. Here, three consecutive studies engaging with virus characterization and formulation are presented. In **part A**, the preparation of samples that are suitable to perform a characterization of ORFV were evaluated. For this purpose, three different methods were compared concerning the infectious ORFV yield and recovery, impurity removal, economic and preparation concerns as well as by using size and electrophoretic mobility measurements. The SXC and ultracentrifugation were identified as suitable. These two methods were applied in the studies in **part B and C**. Here, critical degradation parameters in common vaccine production processes were tested (**B**) and stabilizing excipients evaluated (**C**). In short, the ORFV is very stable against most environmental influences and can be easily stabilized with a protein at neutral pH. If proteins are not applicable throughout the processing, several sugars and amino acids revealed preserving effects on the ORFV.

In conclusion, the studies undertaken equip the reader with tools to prepare the ORFV for further analysis and a thorough knowledge of degrading conditions. Additionally, options to stabilize the virus against infectivity loss in such environments is presented, which might be adapted for formulation finding or throughout the processing.

Part A: Sample preparation methods for Orf virus characterization

Eilts, F.; Steger, M.; Pagallies, F.; Rziha, H.-J.; Hardt, M.; Amann, R.; Wolff, M. W. (2022). Comparison of sample preparation techniques for the physicochemical characterization of Orf virus particles. Journal of Virological Methods 310, 114614. doi: 10.1016/j.jviromet.2022.114614

Journal of Virological Methods 310 (2022) 114614

Contents lists available at ScienceDirect

Journal of Virological Methods

journal homepage: www.elsevier.com/locate/jviromet

Protocols

Comparison of sample preparation techniques for the physicochemical characterization of Orf virus particles

Friederike Eilts [a], Marleen Steger [a], Felix Pagallies [b], Hanns-Joachim Rziha [b], Martin Hardt [c], Ralf Amann [b,d], Michael W. Wolff [a,e,*]

[a] Institute of Bioprocess Engineering and Pharmaceutical Technology, University of Applied Sciences Mittelhessen (THM), Wiesenstr.14, 35390 Giessen, Germany
[b] Department of Immunology, University of Tuebingen, Auf der Morgenstelle 15, 72076 Tuebingen, Germany
[c] Imaging Unit, Biomedical Research Centre Seltersberg, Justus Liebig University, Schubertstraße 81, 35392 Giessen, Germany
[d] PRiME Vector Technologies, Herrenberger Straße 24, 72070 Tuebingen, Germany
[e] Fraunhofer Institute for Molecular Biology and Applied Ecology (IME), Ohlebergsweg 12, 35392 Giessen, Germany

ARTICLE INFO

Keywords:
Isoelectric point
Orf virus
Surface charge
Transmission electron microscopy
Viral vector vaccine
Zeta potential

ABSTRACT

The determination of the electrostatic charge of biological nanoparticles requires a purified, mono-disperse, and concentrated sample. Previous studies proofed an impact of the preparation protocol on the stability and electrohydrodynamics of viruses, whereas commonly used methods are often complex and do not allow the required sample throughput. In the present study, the application of the (I) steric exclusion chromatography (SXC) for the Orf virus (ORFV) purification and subsequent physicochemical characterization was evaluated and compared to (II) SXC followed by centrifugal diafiltration and (III) sucrose cushion ultracentrifugation. The three methods were characterized in terms of protein removal, size distribution, infectious virus recovery, visual appearance, and electrophoretic mobility as a function of pH. All preparation techniques achieved a protein removal of more than 99 %, and (I) an infectious ORFV recovery of more than 85 %. Monodisperse samples were realized by (I) and (III). In summary, ORFV samples prepared by (I) and (III) displayed comparable quality. Additionally, (I) offered the shortest operation time and easy application. Based on the obtained data, the three procedures were ranked according to eight criteria of possible practical relevance, which delineate the potential of SXC as virus preparation method for physicochemical analysis.

1. Introduction

To study the mechanisms of virus interaction with surfaces and their aggregation behavior, an extensive physicochemical characterization is often a necessity (Langlet et al., 2008). This is the case for environmental applications as well as for pharmaceutical production, especially downstream processing. However, the implementation of unpurified virus material from a cell culture supernatant for this task is biased by impurities, e.g., host cell protein, cell debris, and immature virions (James et al., 2016; Michen and Graule, 2010). Thus, virus samples need to be purified, preferably in short preparation times, with minimum losses and without affecting the virus composition (James et al., 2016). Now, a chicken-egg-question arises: An efficient sample preparation procedure is indispensable for a thorough characterization of the target nanoplexes, however, every procedure depends on various properties of the same, potentially changing the sample composition. Generally spoken, a sample preparation must be reproducible and robust to ensure the purification of the target virions from different origins, while avoiding the accumulation of sub-groups selected by, e.g., size or charge. Such an evaluation of the suitability of virus sample preparation strategies for the physicochemical characterization of different bacteriophages was performed by Dika et al. (2013a) and Shi and Tarabara (2018), who compared density gradient centrifugation, diafiltration (DF), dialysis, and polyethylene glycol (PEG) precipitation. Both studies

Abbreviations: AM, ammonium molybdate; CPB, citrate phosphate buffer; DF, diafiltration; DLS, dynamic light scattering; Elu, elution; IU, infectious units; MWCO, molecular weight cut-off; ORFV, Orf virus; PBS, phosphate buffered saline; PEG, polyethylene glycol, PEG8000 corresponds to 8000 Da; PDI, polydispersity index; pI, isoelectric point; SC, sucrose density gradient centrifugation; SXC, steric exclusion chromatography; SXC-DF, steric exclusion chromatography with subsequent diafiltration; TEM, transmission electron microscopy; UAc, uranyl acetate.

* Correspondence to: Wiesenstr.14, 35390 Giessen, Germany.
E-mail addresses: friederike.eilts@lse.thm.de (F. Eilts), michael.wolff@lse.thm.de (M.W. Wolff).

https://doi.org/10.1016/j.jviromet.2022.114614
Received 7 July 2022; Received in revised form 4 September 2022; Accepted 5 September 2022
Available online 6 September 2022
0166-0934/© 2022 Elsevier B.V. All rights reserved.

concluded that the presence of residual contaminants and viral aggregates interfered with electrophoretic mobility measurements, and only density gradient centrifugation fulfilled the requisites. However, the application is very time-consuming and of limited sample throughput. This underlines the need for alternative techniques.

A method that has not yet been evaluated for the task of sample preparation for physicochemical analysis is the steric exclusion chromatography (SXC). In the past, SXC has gaines increasing popularity as a time- and cost-effective, easy-to-use, and efficient preparative purification method for nanoparticles and macromolecules, such as viruses (Labisch et al., 2022; Lothert et al., 2020a, 2020b, 2020c, 2020d; Marichal-Gallardo et al., 2017, 2021), latex nanoparticles (Eilts et al., 2022), bacteriophages (Lee et al., 2012), nucleic acids (Levanova and Poranen, 2018), and globulins (Gagnon et al., 2014; Lee et al., 2012; Tao et al., 2015; Wang et al., 2014). An extensive description of the methods' theory can be found elsewhere (Gagnon et al., 2014; Lee et al., 2012). These previous publications showed the methods' high capacity to deplete protein (> 99 %) and double-stranded DNA (> 50 %) as well as to isolate and concentrate particles depending, on their size and charge. Common drawbacks of the related PEG precipitation (Shi and Tarabara, 2018), such as residual PEG concentration in the final sample, have not been investigated for the SXC so far. However, a recent study on the Orf virus (ORFV) showed a monodisperse size distribution and high purity samples after SXC application (Lothert et al., 2020b). Additionally, charge measurements were performed successfully. Due to these promising results, and the ORFV application as a versatile recombinant vaccine (Amann et al., 2013; Rohde et al., 2011; Rziha et al., 2019; van Rooij et al., 2010) and oncolytic therapy (Rintoul et al., 2012), this virus was chosen for the presented study as a model virus. The ORFV is an ovoid-shaped DNA-virus of the genus *Parapoxvirus*, family *Poxviridae*, that measures approximately 140 – 200 nm in width and 220 – 300 nm in length (Nagington and Horne, 1962; Nitsche et al., 2007; Wang and Luo, 2019). The characteristic virion surface resembles a ball of wool, due to the tubule-like structure, which surrounds the envelope in a spiral fashion (Spehner et al., 2004).

Usually ORFV has been prepared by sucrose density gradient centrifugation (Joklik, 1962; Nagington et al., 1964; Nashiruddullah et al., 2018; Spehner et al., 2004; van Vloten et al., 2021). The routinely and standardized application make the centrifugation the current gold-standard for lab-scale purification, allowing a concentration of the virus to high titers with excellent purities. ORFV preparation only by SC alone is used repeatedly (Reguzova et al., 2020; Rintoul et al., 2012).

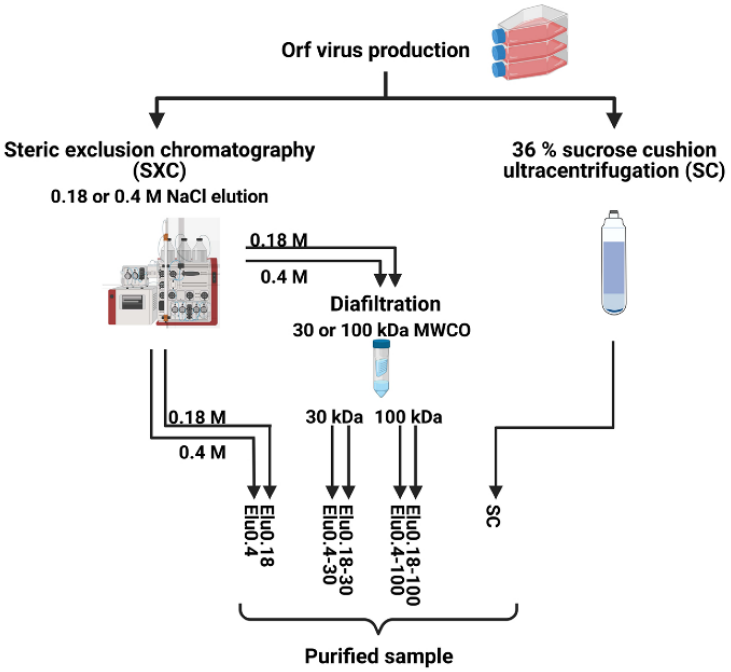

Fig. 1. Overview and terms of sample preparation methods to purify the Orf virus (ORFV) for physicochemical analysis. After ORFV production, the clarified supernatant was processed either by ultracentrifugation a 36 % sucrose cushion (SC), or by steric exclusion chromatography (SXC). The latter was performed with a 0.18 or 0.4 M NaCl elution. After the SXC elution, half of the samples of both elutions were subjected to an additional diafiltration step (DF) with cellulose membrane filters of 30 kDa or 100 kDa molecular weight cut-off (MWCO). Hence, seven different preparation strategies were applied. For example, a sample purified by SXC, eluted (Elu) with 0.4 M NaCl and subsequent DF with a 30 kDa filter unit, is referred to as Elu0.4–30. Figure created with *BioRender.com*.

Abbreviation	Primary purification	Secondary purification
Elu0.4	SXC, elution buffer 0.4 M NaCl	-
Elu0.4-30		DF with 30 kDA MWCO
Elu0.4-100		DF with 100 kDA MWCO
Elu0.18	SXC, elution buffer 0.18 M NaCl	-
Elu0.18-30		DF with 30 kDA MWCO
Elu0.18-100		DF with 100 kDA MWCO
SC	Ultracentrifugation through 36 % sucrose cussion	-

The method aims to semi-purify and concentrate the viral particles from cell debris and host-cell protein (James et al., 2016). Like the SXC, the sole application of SC is less time-consuming than the density gradient centrifugation procedure, but concurrently generates samples of lower purity levels. To our knowledge, no studies on the recovery or purity levels of ORFV samples purified by SC have been published yet.

In the presented study, three sample preparation methods with a relatively low execution time were evaluated by comparing the purification of the ORFV in terms of the impact on viral aggregation, viral recovery, sample purity, and the determination of the electrophoretic mobility as a function of pH. The tested methods were SXC, SXC followed by DF (SXC-DF), and SC (Fig. 1). DF was applied as a secondary preparation step to investigate the possibility to further purify and concentrate the samples from SXC. To evaluate the prepared samples by transmission electron microscopy (TEM), different staining protocols were tested to visualize the single ORFV particles in their native buffer. The results of the virus sample characterization were used to rank the three preparation techniques according to an extended list of criteria of potential practical relevance adapted from Shi and Tarabara (2018), i.e., monodispersity, size selectivity for ORFV, recovery and concentration of infectious ORFV, protein removal, determination of zeta potential and pI, execution time, and sample economics.

2. Materials and methods

2.1. Propagation and purification of the model virus

The production of ORFV in Vero cells was conducted as previously described (Rziha et al., 2016). The attenuated ORFV strain D1701-V expressing the green fluorescent protein AcGFP (Rziha et al., 2019) was used in this study. After successful infection, the cell-culture was subjected to one freeze-thaw cycle (−80 °C) and centrifuged for cell debris removal. Afterwards, the supernatant was stored at − 80 °C until further use. An overview of the sample preparation procedures for ORFV purification (Sections 2.1.1 – 2.1.3) is displayed in Fig. 1, where the nomenclature of the ORFV samples is defined.

2.1.1. Sucrose cushion ultracentrifugation (SC)

SC was carried out as described by (Rziha et al., 2016). The purification started with either 150 mL or 900 mL clarified cell culture supernatant, and the final volume for resuspension was 1 or 2 mL in phosphate buffered saline (PBS), generating a 150- to 450-times concentration, respectively.

2.1.2. Steric exclusion chromatography (SXC)

The ORFV was purified via SXC as described before (Lothert et al., 2020b) with minor changes. After harvest, the virus-cell-suspension was clarified by stepwise centrifugation at 4 °C (300 x *g*, 5 min, and 4500 x *g*, 30 min) (Multifuge X1R, Heraeus). Briefly, every SXC run was performed using freshly prepared regenerated cellulose membrane stacks with a diameter of 47 mm and 1 µm nominal pore diameter (Whatman RC60, GE Healthcare). The loading and wash steps of SXC purification were unchanged to the cited protocol, but the elution was performed either with 0.4 M NaCl as stated by Lothert et al. (2020b), or 0.18 M NaCl. The elution volume was 20 mL, 10 % of the load volume, aiming for 10 x concentration. Samples, eluted from SXC, contained up to 1 % PEG due to the residual loading buffer in the chromatographic column.

2.1.3. Centrifugal diafiltration (DF)

DF of the two different SXC elution fractions (0.18 and 0.4 M NaCl) was performed to concentrate the virions and exchange the sample buffer. Commercially available Amicon Ultra-4 spin column filters (Merck Millipore) with a regenerated cellulose membrane and a molecular weight cut-off (MWCO) of 30 kDa or 100 kDa were used. The active filter membrane surface area was 3 cm^2. According to the manufacturer's instructions, 4 mL of virus suspension was centrifuged and washed twice using a 20 mM TRIS buffer (pH 7.4) containing 180 mM NaCl. Centrifugation was performed for at least 30 min until no changes in the volume were detected anymore. For the highest concentration, only the white-colored sediment was used for further experiments, which was 100 µL for 100 kDa and 250 µL for 30 kDa membranes, reaching a concentration of approximately 15 x and 40 x for the respective units.

2.2. Size and structural analysis

2.2.1. Transmission electron microscopy (TEM)

The virus particle size and integrity were further evaluated by TEM using conventional negative staining. After purification, the different ORFV samples were treated equally, i.e., stored at − 80 °C until further use. The 300-mesh copper grids (Plano) were prepared with polymer support films of 1.2 % Formvar (Science Services), carbon-coated, and ionized by glow-discharge. Negative staining was either performed by the so-called *drop-to-drop* or the *on-drop* method, illustrated in Fig. 2. In the *drop-to-drop* method, one drop of unfixed virus solution was directly applied onto the copper grids and incubated for 3 – 7 min for adsorption (Figs. 2, 1a and1b). The excess liquid was poured off by blotting (Figs. 2, 1c). Afterwards the grids were negatively stained by incubating the grid for 5 s on a drop of a heavy metal-containing solution for three cycles, while blotting in between (Fig. 2, 2). Finally, the sample was washed in the same style with distilled water, blotted, and left for air-drying (Figs. 2, 3). The *on-drop* method was varied by some details. First, the copper grids were incubated on a drop of unfixed virus solution for 3–7 min (Figs. 2, 1a and 1b). Here, as well, the excess liquid was taken off by blotting (Figs. 2, 1c and 1d). Afterwards, the grids were negatively stained by incubating for 7 min on a drop of a heavy metal-containing solution, but only for one cycle (Figs.. 2, 2a and 2b). Finally, the grid was blotted (Figs. 2, 2c and 2d), no washing undertaken, and left for air-drying (Figs. 2, 3). All grids were stored under the exclusion of light until visualization in the transmission electron microscope.

Furthermore, to evaluate the appropriate virus structure resolution of SXC and SC samples, different heavy metal-containing stains were tested. The stains were aqueous solutions of 2% ammonium molybdate (AM) (Agar Scientific), NanoW (Nanoprobes), and 1 % (SXC samples) or 2 % (SC samples) uranyl acetate (UAc) (Electron Microscopy Sciences). All stains were 0.2 µm filtered. NanoW is a commercially available ready-to-use stain based on tungsto acid with a neutral pH. The 2 % AM stain was titrated to pH 7 ± 0.5 with 5 M NaOH. The UAc stain (1 or 2 %) was prepared as an 0.15 M oxalic acid solution (Merck Millipore), and the pH adjusted with 25 % ammonia (Carl Roth). No post-staining fixation was done. Preparations were finally inspected by using a EM912a/b (Zeiss) at 120 kV under zero-loss conditions, and images were recorded with a slight under-focus using a 2k x 2k ssCCD camera (TRS 'Tröndle Restlichtverstärkersysteme', Moorenweis, Germany) (Lothert et al., 2020b). For image analysis and quantitative measurements, the iTEM package (Olympus) was used.

2.2.2. Dynamic light scattering

The measurements of the purified virus samples' size distribution were conducted via dynamic light scattering (DLS) with a Zetasizer Nano ZS90 (Malvern Panalytical) as described by Lothert et al. (2021). The refractive index and viscosity values of the 0.2 µm filtered buffers were assumed to be equal to water. The polydispersity index (PDI) itself was calculated by the Zetasizer software and indicates the width of a size distribution with a single mean diameter (Malvern Instruments Ltd., 2017).

2.3. Infectivity analysis

The quantification of infectious viral particles was conducted by fluorescence-activated cell counting in a flow cytometer (Guava® easyCyte HT, Merck Millipore), adapted without viability staining from

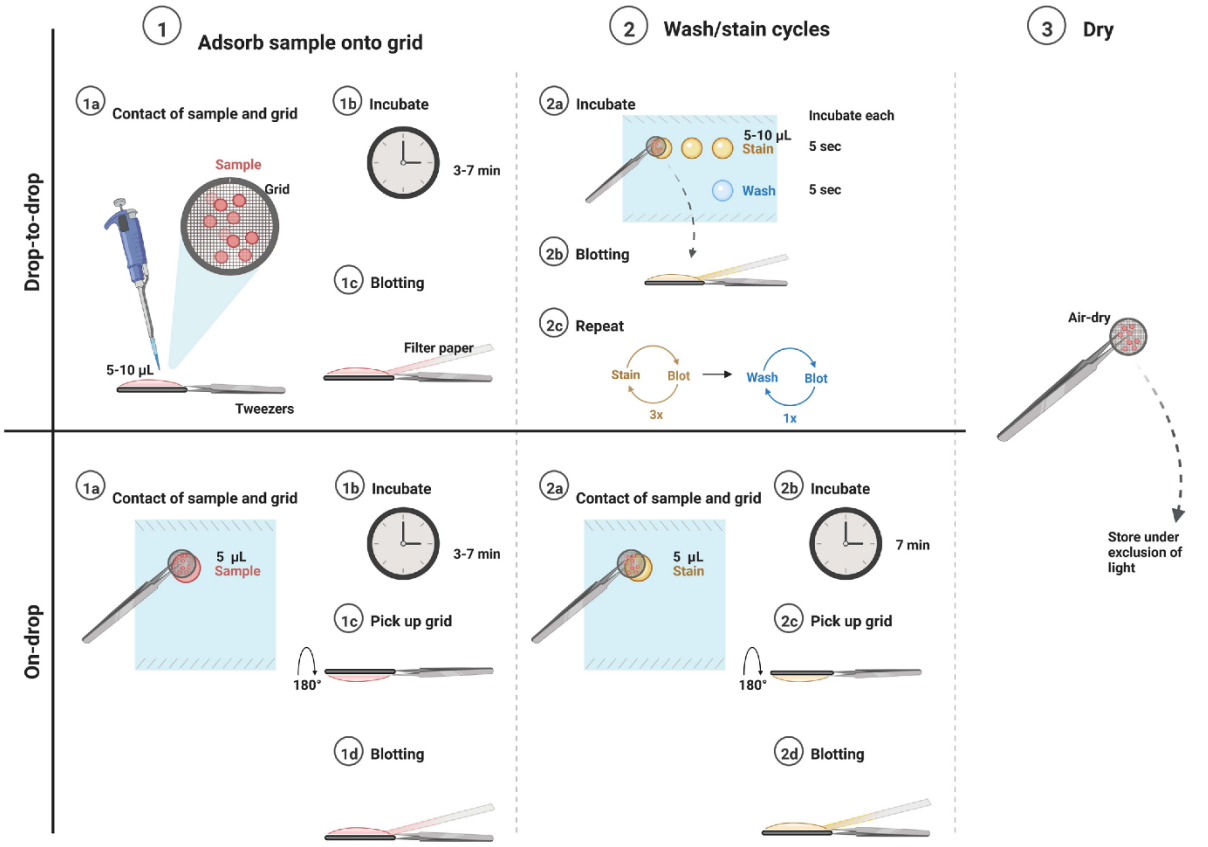

Fig. 2. Preparation of grids by negative staining for transmission electron microscopy (TEM) analysis. All Orf virus (ORFV) samples prepared by negative staining were either processed using (I) the so-called *drop-to-drop* (see upper illustration), or (II) the *on-drop* method (see lower illustration). Both methods were structured first by a step for adsorption of the virus sample (1), followed by a washing/staining (2), and a drying step (3). The unfixed virus solution was freshly thawed, and a drop of sample was brought into contact with the prepared 300-mesh copper grids, either (I) by application directly onto the grid, or (II) by lying on the drop. After incubation, the grids were stained either (I) in three cycles, each lasting 5 s, with a final wash step, or (II) by incubation on a drop of stain without washing. Last, all grids were air-dried and stored under the exclusion of light until visualization in TEM. Figure created with *BioRender.com*.

Rziha et al. (2019). The infection rate, i.e., the percentage of green fluorescent (infected) cells was standardized by virus plaque titration in triplicates.

2.4. Total protein assay

Quantification of the total protein content via the Pierce BCA Protein Assay Kit (Thermo Fisher Scientific) was undertaken according to (Lothert et al., 2020c). The quantification limit is 25 µg mL^{-1}. The measurements were conducted in triplicates.

2.5. Measurement of the electrophoretic mobility

The measurements of the particles' electrophoretic mobility, and indirectly their zeta potential, were conducted using phase analysis light scattering with a Zetasizer Nano ZS90, adapted from Lothert et al. (2020c). All samples were diluted at least 1:10 to reduce the influence of the sample buffer. If not stated otherwise, 0.1 M citrate phosphate buffer (CPB) of varying pH was used as diluent to determine the isoelectric point (pI). The conductivity of the CPB was adjusted to 15 mS cm^{-1} using NaCl. The virus samples were analyzed in triplicates, and the obtained data was processed using the Smoluchowski model ($f(\kappa a) = 1.50$) to calculate the zeta potential values from the electrophoretic mobility values.

3. Results

3.1. Electron microscopy of ORFV

For TEM analysis, a staining protocol is preferable, which allows for electron microscopical resolution of ORFV particles in the presence of the same buffer used for virus preparation. To this end, the on-drop and drop-to-drop technique were compared as negative staining protocols (see Fig. 2). The micrographs showed little difference in stain distribution, the resolution of viral particles, and the intactness of the support films. Hence, to simplify the negative staining procedure, the on-drop method was applied for all further preparations. Next, using the on-drop method, the evaluation of the three different stains, AM, Nano W, and UAc, resulting in the best integrity of ORFV particles prepared by SC or SXC, was conducted. We observed an increased stability of the ORFV's integrity under neutral conditions. Therefore, all stains were adjusted to pH 7 ± 0.5, including UAc in oxalic acid solution (mostly UAc is applied in aqueous solutions at acidic pH 4–5).

The SC-prepared samples (Fig. 3A1 to A3) indicated that staining with 2 % UAc and NanoW displayed a good resolution of the characteristic criss-cross pattern of intact mature ORFV, although NanoW-staining resulted in some deformation of viral particles (Fig. 3A2). The best presentation of mature ORFV particles, demonstrating intact tubules formed to the characteristic ball-of-wool, was obtained with 2 %

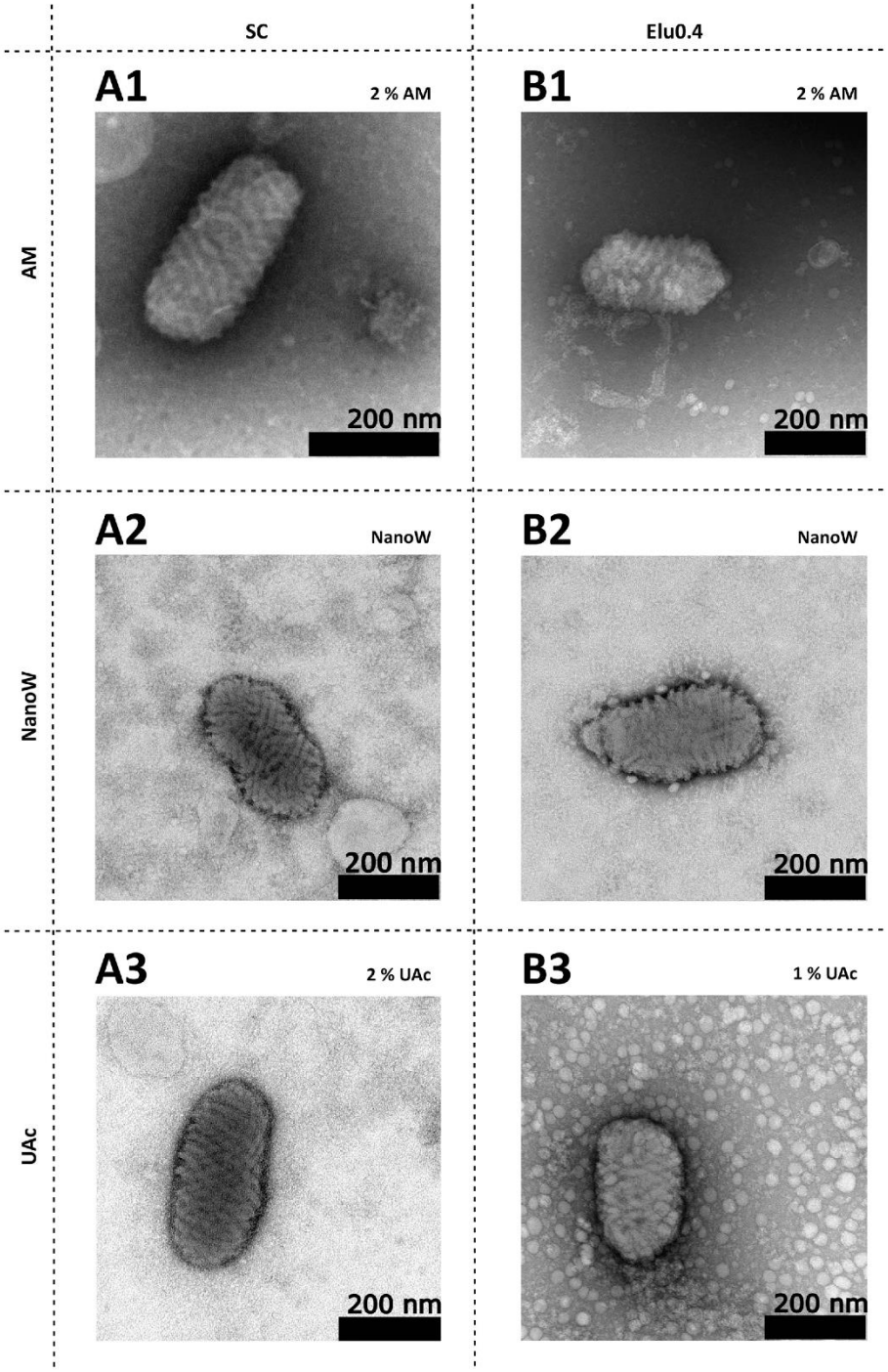

Fig. 3. Comparison of negative staining solutions for transmission electron microscopic (TEM) analysis. The TEM preparations of the Orf virus (ORFV) were prepared as described in the materials and methods section, and the staining was conducted by the *on-drop* method (see Fig. 2). Virus prepared by ultracentrifugation through a 36 % sucrose cushion (SC) was stained with 2 % ammonium molybdate (AM) (A1), NanoW (A2), or 2 % UAc (A3). Samples from steric exclusion chromatography (SXC) with a 0.4 M NaCl elution (Elu0.4) were stained with 2 % AM (B1), NanoW (B2), or 1 % UAc (B3). The bars depict the indicated sizes.

UAc staining (Fig. 3A3).

Next, we tested ORFV prepared by SXC and elution with 0.4 M NaCl (Elu0.4), containing 1 % PEG. The presence of salt and PEG seemed to slightly affect the integrity of the ORFV particles, independent from the used stain. In all cases, the criss-cross pattern of the outer tubules was not completely preserved anymore (Fig. 3 B1 to B3). Staining with NanoW resulted in additional small globules (10–20 nm in size) attached to the virus particles (Fig. 3 B2). The UAc staining led to the creation of larger beads (20–50 nm in size) deposited on the supporting film on the grid. In summary, these results favored the use of the UAc-staining for the electron microscopic analysis of the different ORFV preparation procedures.

TEM inspection was performed to evaluate the purity and integrity of ORFV, prepared by the different SXC procedures. Here, no highly purified virus was analyzed, which allows the visualization of ORFV samples that still contain aggregated virus and contaminating cellular material. For comparison, SC-prepared ORFV is represented in Fig. 4A. As can be seen in Fig. 4 (B and C) all samples from SXC and SXC-DF exhibited the described white globules or beads (20–50 nm) on the supporting film of the grid, reducing the particle's contrast. Comparing the preparation by SXC, using 0.18 (B1) or 0.4 M NaCl (C1), similar quantities of single mature and intact ORFV particles were detected. Although the visible number of virus particles appeared approximately 10–100 times lower as compared to the SC samples, the degree of cellular contaminants was reduced.

Furthermore, the application of DF was tested for a possible increase of virus purity. However, the use of filters of either 30 or 100 kDa exclusion size markedly impaired the photographic illustration of ORFV particles (Fig. 4B2, B3, C2, and C3). This treatment resulted in a pronounced accumulation of virus particles and the formation of electron-dense layers, which impeded the recognition of the characteristic ORFV. In addition, a closer inspection indicated that the DF also led to the deformation or damage of the criss-cross order of the ORFV tubules (Fig. 4B3 or C2 or C3).

3.2. Size measurements of ORFV samples by TEM and DLS

The size distributions of the ORFV samples were determined orthogonally by TEM and DLS. The TEM analysis allowed the measurement of the typical ORFV particles' dimensions. DLS, on the other hand, was applied to analyze the size distribution of the whole samples, which can be used to identify aggregates and contaminants present in the samples.

The TEM analysis showed an ORFV length between 292 and 331 nm and a width of 177–193 nm, respectively (Fig. 5A). Significant differences of mean length values ($\alpha = 0.05$) were only found between the Elu0.4- and Elu0.18–30-preparations. In general, the determined particle sizes were in good agreement with those reported in the literature, displayed in Fig. 5A (Nagington and Horne, 1962; Nitsche et al., 2007; Wang and Luo, 2019).

The DLS analysis revealed mean diameters of the virus samples ranging from 183 to 254 nm with significant differences between almost all preparations ($\alpha = 0.05$) (Fig. 5B). Note that the ORFV is a rod-shaped virus, but the calculation of the particle's diameter from DLS measurements assumes a sphere. Thus, the values of virus size obtained from DLS, range between the width- and the length- values measured in TEM. Samples from SXC, SC, and Elu0.18–30 showed the largest values (241–269 nm), while measurements of Elu0.4–30, Elu0.4–100, and Elu0.18–100 resulted in significantly smaller sizes (184–212 nm). Purification with 100 kDa MWCO, compared to 30 kDa, led to a reduced cumulative mean diameter by 43 nm for a preceding 0.18 M NaCl elution and a reduction by 19 nm for an elution with 0.4 M NaCl. Furthermore, the mean PDI indicated the monodispersity of the measurements, with a commonly stated border of 0.5. Samples from SXC (0.32 and 0.36) as well as from SC (0.38) were well below (> 0.1) this border. SXC-DF-prepared samples showed values in this range for Elu0.4–100 (0.37), whereas the other three procedures were close to 0.5 (0.49, 0.53, and 0.48).

3.3. Infectivity and protein content of the different ORFV preparations

The level of residual contaminants of the prepared ORFV samples was assessed by a total protein analysis (Table 1). All preparation methods led to reductions of more than 99 % of the total protein load of the final sample compared to the initial clarified cell culture supernatant. Starting with approximately 1.9 mg mL^{-1} protein, the protein concentration after SXC purification was below the assay detection limit (LOD) (25 µg mL^{-1}). Concentrating the SXC samples by DF resulted in residual protein concentrations of 124–130 µg mL^{-1}, and 57–64 µg mL^{-1} for a SXC elution with 0.18 M and 0.4 M NaCl, respectively. The apparent increase of the SXC-DF's protein concentrations is due to the volume reduction after SXC by DF application. Samples from SC contained 166 µg mL^{-1} residual protein.

The recovery of the infectious ORFV particles varied between the different preparation methods. Considering a 10-fold volumetric concentration by SXC application, using 0.18 M NaCl for elution (Elu0.18), the starting total of 14.7×10^7 IU (infectious units) was recovered with 86 % of infectious titer, resulting in 6.3×10^6 IU mL^{-1} (12.6×10^7 IU). A recovery of 89 % infectious titer was found after an elution with 0.4 M NaCl (Elu0.4), as 5.3×10^6 IU mL^{-1} (10.6×10^7 IU) was recovered from the total applied 12.3×10^7 IU. Using DF for additional purification and concentration of SXC, the samples showed approximately one log higher viral titers than the respective starting material after an initial SXC purification, i.e., 2.2–8.5 × 10^7 IU mL^{-1}. However, the application of DF on SXC samples resulted in a reduction of the infectious titer recoveries. DF of Elu0.18 yielded a 29 % recovery of infectious virus for 100 kDa MWCO (Elu0.18–100), whereas 53 % were recovered using a 30 kDa filter unit (Elu0.18–30). The DF of the Elu0.4-preparation obtained recoveries of 25 % or 28 % of infectious ORFV for 30 kDa (Elu0.4–30) or 100 kDa (Elu0.4–100) cut-off filters, respectively. Lastly, using starting materials of 2.1–3.6 × 10^7 IU mL^{-1}, the SC samples had the highest concentration of infectious particles with 1.1×10^9 IU mL^{-1}, with an infectious particle recovery of approximately 9–31 %. The range refers to both implemented initial cell culture volumes (150 and 900 mL).

3.4. Productivity of the preparation methods

Concerning the throughput of the preparation methods, the initial volume for SXC was approximately 200 mL, and the processing time approximately two hours, with an operation at 2 mL min^{-1}. The duration of the handling for this method increases linearly with the loading volume to the maximum loading capacity of the column. DF and SC on the contrary, are limited by the design of the centrifuges. As DF was used for a secondary processing of the SXC samples, the initial volume of 200 mL was assumed for further calculations. Additional processing times of two to three hours can be expected depending on the number of washing steps. For SC-preparation, the crude sample was either150 or 900 mL, and both needed the same handling time of 24–48 h.

With these parameters, the volumetric concentration factors of the SXC, SXC+DF, and SC application were calculated, based on the initial crude cell culture supernatant volume and the final sample volume after purification (Table 1). The SXC procedure achieved a 10-fold volume reduction, SC between 150- and 450-fold, SXC-DF with 30 kDa membranes 150-fold, and SXC-DF with 100 kDa membranes 400-fold. As previously mentioned, the concentration factor of the latter combined the SXC- and DF-related shares.

3.5. Measurement of the electrophoretic mobility of purified ORFV

Data on the electrophoretic mobility of the different ORFV eluates prepared by SXC, SXC-DF, and SC (Fig. 1) were collected as a function of pH. This data was used for the zeta potential calculation and determination of the pI of the virus, the point of zero charge, visualized at $y = 0$.

First, no pI for the SXC-DF samples with 0.4 M NaCl elution (Elu0.4–30 and Elu0.4–100) was determined, i.e., the zeta potential in the assessed pH range from 2.6 to 7.6 yielded negative values. Therefore, the point of an overall neutral charge could not be determined.

For the other five sample preparation procedures, the pH-dependent functions of the zeta potential exhibited positive potentials at pH values lower than the pI, and negative potentials at greater pH values (Fig. 6). Both preparations derived from SXC, Elu0.18 and Elu0.4, had similar pH-dependent potentials with a pI at pH 3.4 and pH 3.6, respectively. The SC-purified sample showed higher moduli for the same pH value than the SXC samples. Its pI was determined at pH 3.5. Last, the samples

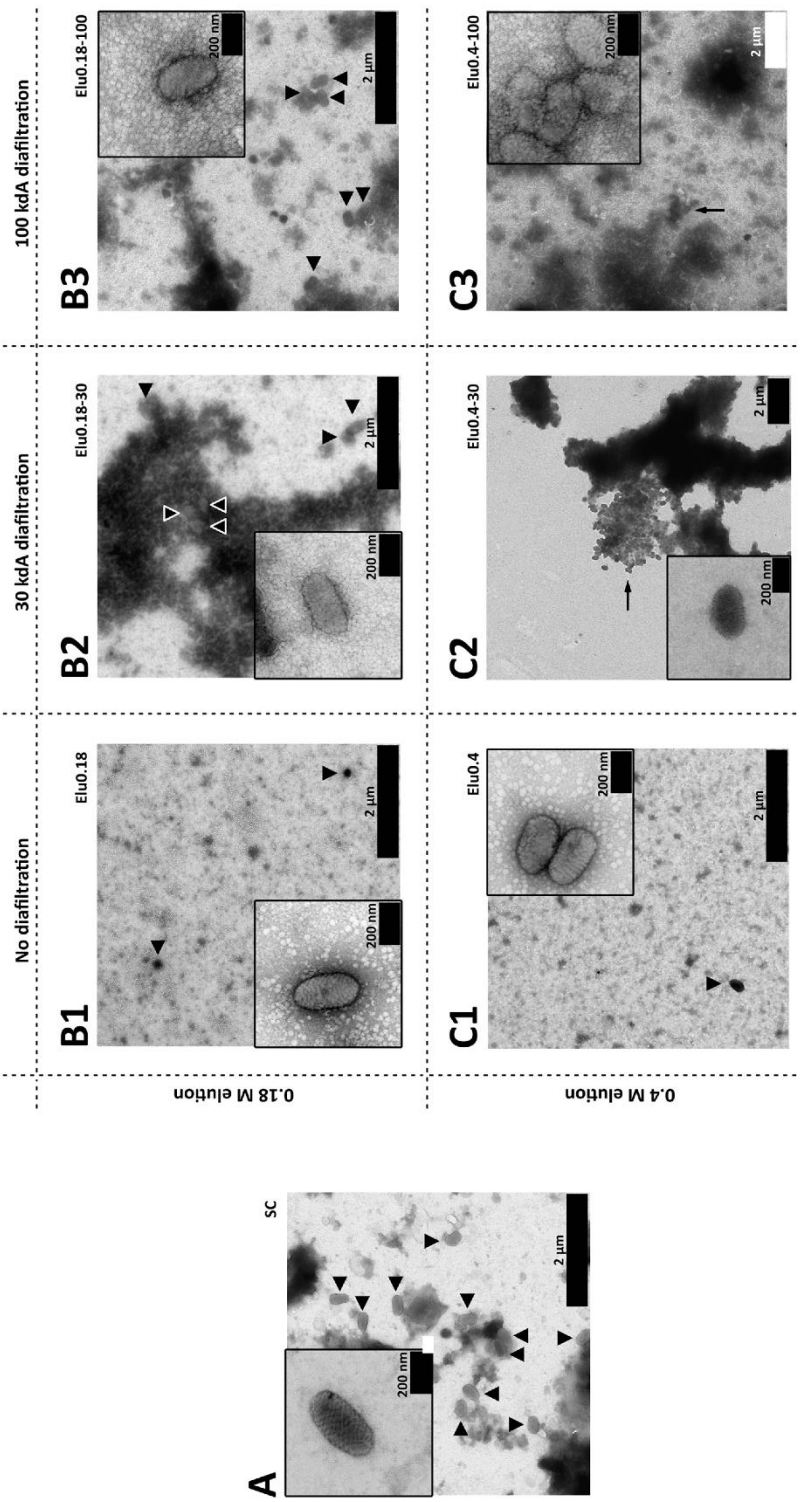

Fig. 4. Transmission electron microscopy (TEM) images of the different Orf virus (ORFV) preparations. For negative staining of the virus, prepared by ultracentrifugation through 36 % sucrose cushion (SC), (A) 2 % uranyl acetate (UAc) was used, but the steric exclusion chromatography (SXC) purifications were stained with 1 % UAc (B and C). Arrowheads point to single ORFV particles (B1 to B3 and C1), and arrows mark clusters of ORFV particles (C2 and C3). The inserts show magnified views of virions. (A) shows ORFV obtained by SC, (B1 and C1) demonstrate ORFV purified by SXC, (B2 and B3) show ORFV from SXC with a 0.18 M NaCl elution followed by diafiltration (DF), and (C2 and C3) demonstrate ORFV after SXC with a 0.4 M NaCl elution and DF. The DF was performed with either 30 kDa (B2 and C2) or with 100 kDa (B3 and C3) centrifugal filter units. The bars depict the indicated sizes.

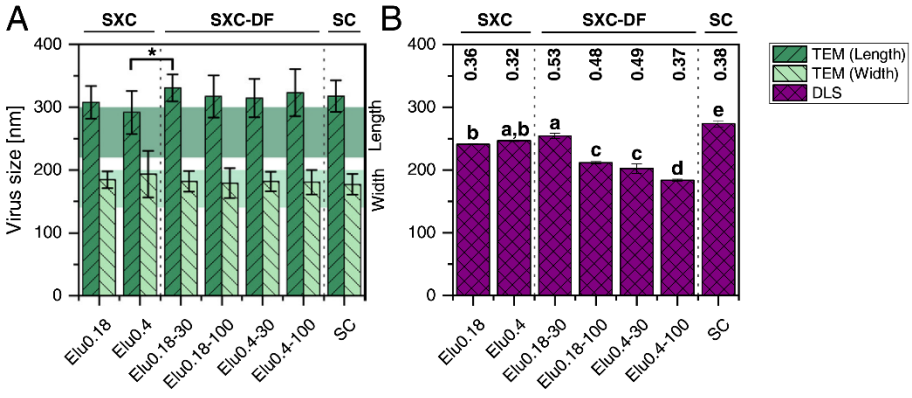

Fig. 5. Comparison of size measurements of samples containing Orf virus (ORFV) after sample preparation. The ORFV was purified by the preparation strategies described in Fig. 1. Size measurments of the virus samples were performed by transmission electron microscopy (TEM) (A, green), and dynamic light scattering (DLS) (B, purple). The viral particle's length (dark green bars) and width (light green bars) were measured by TEM of detectable intact mature ORFV particles (A). Behind the bars, the published length and width measurements of ORFV are indicated as dark and light green shaded areas, respectively (Nagington and Horne, 1962; Nitsche et al., 2007; Wang and Luo, 2019). By applying DLS to the virus samples, the obtained mean diameter of the whole sample was assessed (B). The values above the bars indicate the average polydispersity index of these measurements. ANOVA, Tukey test; $n = 3$; * $\alpha = 0.05$. the same letters indicate no significance according to the Tukey test table (B). Columns show the mean values, and error bars show the standard deviations from at least 50 ORFV particles measured in TEM and 9 DLS measurements. Elu, elution; SC, 36 % sucrose cushion ultracentrifugation, SXC, steric exclusion chromatography; SXC-DF, steric exclusion chromatography followed by diafiltration. (For interpretation of the references to color in this figure legend, the reader is referred to the web version of this article.)

Table 1
Overview of protein and infectious Orf virus (ORFV) concentrations after purification. After sample preparation, the protein and the infectious ORFV concentration was assessed. Additionally, the final volume was noted to calculate each concentration factor. Hence, the protein reduction and the infectious ORFV recovery are normalized to the concentration factors. Values in brackets state the respective infectious particle recovery only for the secondary preparation step (diafiltration, DF). For nomenclature, see Fig. 1.

Sample	Concentration factor[a]	Total protein		Protein reduction	Infectious ORFV		Recovery of infectious ORFV
	mL mL^{-1}	µg mL^{-1}		% (µg µg^{-1})	IU mL^{-1}		% (IU IU^{-1})
	-	MV	SD	MV	MV	SD	
Elu0.18	10	< LOD[b]	–	>99	6.3 E + 06	5.08 E + 05	86
Elu0.4	10	< LOD[b]	–	>99	5.3 E + 06	5.76 E + 05	89
Elu0.18–30	150	124	4.00	>99	5.8 E + 07	8.24 E + 06	53 (61)
Elu0.18–100	400	130	2.00	>99	8.5 E + 07	3.40 E + 06	29 (34)
Elu0.4–30	150	64	2.79	>99	2.2 E + 07	6.27 E + 06	25 (28)
Elu0.4–100	400	57	3.31	>99	6.6 E + 07	1.45 E + 06	28 (31)
SC	150–450	166	8.80	>99	1.1 E + 09	1.54 E + 09	9–31

n = 3.
IU, infectious units; LOD, limit of detection; MV, mean value; SD, standard deviation; SC, ultracentrifugation through 36 % sucrose cushion.
[a] The concentration factor is the volumetric ratio of the initial cell culture supernatant and final sample.
[b] LOD for the Pierce BCA Protein Assay is 25 µg mL^{-1}.

purified by DF, after an 0.18 M NaCl elution from SXC, had the highest pI at pH 3.8 and pH 4.1 for 100 kDa (Elu0.18–100) and 30 kDa (Elu0.18–30) cut-offs, respectively.

4. Discussion

An important prerequisite for the charge measurements and the isoelectric point determination of biological nanoparticles is a pure and homogenous sample. As a consequence of our recent achievements of chromatographic ORFV preparation (Lothert et al., 2020b, 2020c), this work compares the three methods, SXC, SXC-DF and SC, in regard to their ability to generate ORFV samples for physicochemical analysis. The methods were assessed in terms of an extended list of criteria from Shi and Tarabara (2018), including monodispersity, size selectivity, recovery and concentration of infectious virus, protein removal, determination of zeta potential and pI value, processing time, and sample economics. In addition, the integrity of ORFV particles was evaluated by TEM. A comparison of different negative staining reagents revealed UAc as the best option for the electron microscopic imaging of mature virions after SXC or SC-preparation. The staining at neutral pH increased the integrity of virions, presumably due to the sensitivity of ORFV to acidic pH. NanoW, a tungsten acid-based stain, caused some deformation of the ORFV viral particles. This is in accordance with earlier findings for the penetration of phosphotungstic acid penetrating into ORFV particles (Nagington et al., 1964).

The resolution quality of the ORFV particles by TEM depended on the preparation technique. So far, a structural integrity assessment of SC-prepared ORFV (Reguzova et al., 2020; Rintoul et al., 2012) was not performed. The SC-derived samples showed very good imaging of the characteristic criss-cross pattern of intact mature ORFV. In contrast, the presentation of ORFV particles prepared by SXC as well as by SXC-DF seemed to be affected by the presence of salt and PEG, exhibiting irregularities of the surface tubules. Furthermore, the imaging of SXC-prepared ORFV showed a lack of the particle's contrast due to white globules or beads covering the supporting film of the grid, which presumably consisted of PEG and salt crystals. A similar effect on the particles' contrast was reported for 1 % trehalose and 0.1 % PEG (Carlo and de Harris, 2011). Previous results of imaging of ORFV by TEM reported similar findings for AM-staining (Lothert et al., 2020b). SXC-DF samples had an increased density of white globules as compared to SXC without DF (Fig. 3). This was not expected, because the DF devices of 30 and 100 kDa were applied to reduce the PEG and salt concentration.

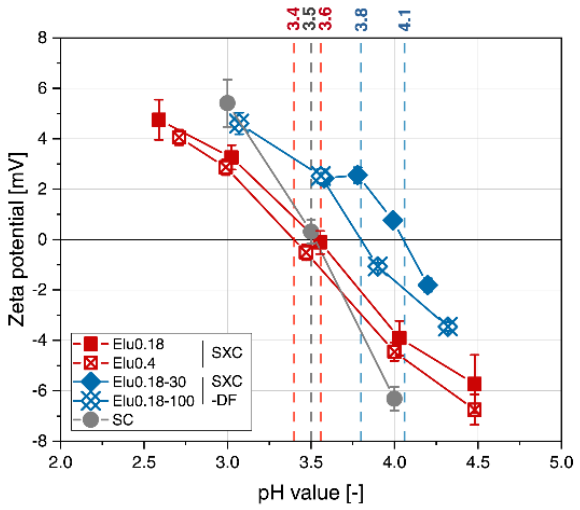

Fig. 6. pH-dependent zeta potential of purified Orf virus (ORFV). The prepared ORFV samples (see Fig. 1) were analyzed concerning their pH-dependent electrophoretic mobility. The latter values were used to calculate the zeta potentials using the Smoluchowski model. The steric exclusion chromatography (SXC) preparation was performed with an elution of either 0.18 M or 0.4 M NaCl (squares), Elu0.18 and Elu0.4, respectively. Both variants were further processed by diafiltration (SXC-DF) with 30 kDa or 100 kDa filter units (diamonds), Elu0.18–30 and Elu0.18–100, respectively. The samples from ultracentrifugation through 36 % sucrose cushion (SC) (circles) were not modified any further. All samples were diluted 1:10 in a pH-adjusted citrate phosphate buffer (15 mS cm^{-1}). Lines are a guide to the eye. The numbers above the graph indicate the approximate isoelectric point ($y = 0$). The data shown are mean values ($n = 3$) and their respective standard deviations.

Presumably, due to volume exclusion by membrane fouling or preferential hydration, the coiled structure of PEG was retained (Baek et al., 2017). To prove this hypothesis, residual PEG should be quantified by, e.g., HPLC-based methods. Additional stains, such as osmium tetroxide, could be tested for improved contrasting of ORFV obtained by SXC and SXC-DF.

The assessment of the ORFV particle size yielded similar results for all purification techniques, indicating no preferential purification of smaller virus size subpopulations. The presented results of the size of ORFV (Fig. 5) were in agreement with reported values ranging 140 – 200 nm in width and 220–300 nm in length (Nagington and Horne, 1962; Nitsche et al., 2007; Wang and Luo, 2019). The TEM analysis and the DLS measurements further indicated aggregation of ORFV particles after DF-preparation, conforming with literature reports (Shi and Tarabara, 2018).

The determination of infectivity was another important criterion for the quality of ORFV prepared by SXC or SXC-DF. The highest concentration of infectious virus was achieved by SC, but with regard to the applied input virus amount, the lowest recovery of 9–13 % was obtained with this method. Conversely, high recoveries were achieved by SXC (86–89 %), albeit the concentration of infectious ORFV was the lowest. Lower virus titers after SXC are due to a limitation of the applicable input volume, limited by the chromatographic column. A reduction of regained infectivity by SXC-DF (25–53 %) might be caused by virus adhesion to and virus entrapment in the membrane material. The formation of virus aggregates after DF (Fig. 4) might also decrease virus infectivity. Comparing the presented data with reports on other viruses of similar sizes as, for example, measles virus (100–250 nm) or mumps virus (150 nm), centrifugal DF with 100 kDa DF membranes showed slightly higher recoveries as compared to ultracentrifugation (Sviben et al., 2016). However, both methods reached less than 40 % recovery, which is in the magnitude of the here presented results. After DF, the ORFV concentration was increased by a factor of 15 and 40 for 30 kDa and 100 kDa units, respectively (Table 1). The difference is presumably due to the smaller pore size of the 30 kDa units, which might enhance membrane fouling by increased protein retention, and consequently a reduced flux (Loewe et al., 2019; Sviben et al., 2016).

Residual host cell protein is an unwanted contaminant in virus purification. In this study, all preparation procedures reduced the detectable protein content of the final eluate by more than 99 %. The SXC-preparations yielded the lowest protein contamination (below LOD), conforming to previous results (Lothert et al., 2020c). The relative protein levels of the preparations conformed with the visualization of protein in TEM imaging. Concerning the residual protein in DF-preparations, presumably an increase of the active filter area of the centrifugal filter units might improve contaminant removal. A high salt concentration can be used in SXC to increase virus recovery by diminishing electrostatic interactions (Lothert et al., 2020d). However, this also increases the protein load, which is non-specifically bound to the stationary phase and to the virions, and hence, co-eluted with elevated salt levels. Therefore, a higher protein load in the Elu0.4 samples after DF had been expected, which, however, was not the case (Table 1). One explanation could be a facilitated protein passage through the DF membranes in the presence of a higher salt concentration (Callahan et al., 2014).

The use of the zeta potential to describe the surface charge of soft particles, e.g., viruses in contrast to hard colloids, can be questioned (Dika et al., 2013b, 2015). Nevertheless, the practical application of the zeta potential and the pI value is common in biotechnological industry, and was therefore used in the present study. The measurement of the pH-dependent zeta potential of the prepared samples identified the pI of ORFV. Coinciding pI values between pH 3.4 and 3.6 were found for the samples prepared by SXC and SC (Fig. 5). Elution after SXC with an increased salt concentration resulted in a slightly reduced pI value. This could indicate an interaction of salt with the viral surface (Langlet et al., 2008).

Concerning SXC-DF-prepared samples, no pI was determined for samples from the 0.4 M NaCl elution, and the pI for 0.18 M NaCl elution was at pH 3.8 and 4.1. Additionally, the moduli of the zeta potentials of ORFV in the SXC-DF samples were lower than for SC- and SXC-derived samples. This could be attributed to an increased PEG concentration. PEG coating covered the charge of MS2 phages and their inner capsids (Dika et al., 2013a). Conclusively, the deviating values of the different ORFV preparation methods are explained by a higher residual protein concentration and polydispersity after DF-preparation (Shi and Tarabara, 2018).

The previously reported higher pI value of approximately pH 4.6 for the ORFV strain D1701-V (Lothert et al., 2020b) might be due to the used TRIS buffer, which has a poor buffer capacity below pH 7.4. The present work measured the pI value in CPB that can buffer between pH 2.6 and pH 7.6. A reduced electrophoretic mobility indicating a higher pI was reported for TRIS-$MgCl_2$, compared to NaCl (Shi and Tarabara, 2018). Additionally, phosphates in the CPB are known to form complexes with amino functional groups of viral proteins, thereby potentially neutralizing the positive charge and leading to a relative decrease in pI (Langlet et al., 2008; Michen and Graule, 2010; Yuan et al., 2008). This stresses that the zeta potential as well as the pI value are systemic parameters dependent on the solvent (Langlet et al., 2008). Described pI values of other poxviruses, range between pH 2.3 and 5.9 (Michen and Graule, 2010). Interestingly, lower pI values were obtained for viruses of higher purity, e.g., prepared by differential centrifugation combined with density gradient centrifugation, or by using trichlorotrifluoroethane (Douglas et al., 1966, 1969). A similar effect is suggested for the results of the present study.

The obtained results were ranked by eight criteria (Table 2) adopted from Shi and Tarabara (2018). The SXC and SC showed an equally good monodispersity of the samples (+++). SXC-DF samples revealed a high

Table 2
Ranking of the three preparation methods for physiochemical characterization of the Orf virus (ORFV). The different preparation techniques were compared concerning their suitability for preparing ORFV samples for physicochemical characterization. The criteria were adapted from Shi and Tarabara (2018). In this overview, the sample preparation methods were summarized as steric exclusion chromatography (SXC) for both 0.18 and 0.4 M NaCl elution strategies, and the SXC followed by diafiltration (SXC-DF) combining the four procedures, Elu0.18–30, Elu0.18–100, Elu0.4–30, and Elu0.4–100. The last method was ultracentrifugation through 36 % sucrose cushion (SC). For nomenclature, see Fig. 1.

Criterion	Preparation method		
	Steric exclusion chromatography (SXC)	Steric exclusion chromatography + diafiltration (SXC-DF)	36% sucrose cushion ultracentrifugation (SC)
Mono-dispersity of particle size distribution	+++	+	+++
Size selectivity for ORFV	+++	+++	+++
Recovery of infectious ORFV particles	+++	++	+
Concentration of infectious ORFV particles	+	++	+++
Reduction of protein concentration	+++	++	++
Determination of zeta potential and isoelectric point	+++	+	+++
Expenditure of time	+++	++	+
Costs	+++	++	+++

+++ corresponds to highest ranking. Costs were estimated without equipment.

polydispersity (PDI ~ 0.5) and small cumulative mean diameters (-), which is probably caused by present residual protein. The dimensions of the ORFV, measured by TEM, were comparable to literature values for all three preparation methods (+++). The recovery rate of the obtained ORFV infectivity favored SXC (+++), combined with the lowest final protein contamination (+++). The concentration of infectious ORFV was the highest for SC (+++), and the lowest for SXC (+). The determination of the zeta potential and the pI value of SXC- and SC-derived samples showed values within 0.2 pH steps (+++), while the DF-preparation caused deviations, or prevented the determination of a pI (+). However, the accuracy of these measurements needs confirmation using ORFV that is prepared by isopycnic centrifugation, or in different solution compositions. Finally, the criteria regarding time and cost investment per sample also favored the SXC method (+++). Concerning the application time, the preparation by SXC is 30–120 min, depending on the loading volume, while DF adds an additional 3 h. However, compared to other methods, such as SC (1–2 days), both procedures are rapid. Conclusively, the SXC method represents an attractive alternative to other conventional ultracentrifugation techniques to prepare pure ORFV not only for analytical purposes.

5. Conclusion

The presented results show that the preparation of *Parapoxvirus* ORFV by the chromatographic method SXC is suitable for physicochemical characterization. The analysis of the zeta potential allowed the determination of a pI value of 3.4. Infectious virus was obtained with a high recovery of almost 90 % of the input infectivity. TEM imaging showed mature virions of the characteristic morphology of ORFV, which contained very low or absent residual cell protein. The high monodispersity indicates the absence of aggregates. Altogether, the SXC was superior to the compared methods of SXC-DF or SC. Thus, it represents an alternative method to the commonly used differential and density gradient ultracentrifugation, which are time-consuming and allow for only a limited sample throughput. Furthermore, SC, without the following density gradient centrifugation, can be a valuable preparation method, while saving time and costs for purification.

Funding

This work was financially supported by the Heinrich Böll Foundation with a doctoral scholarship to FE and the strategic research fund of the University of Applied Sciences Mittelhessen, Giessen, Germany. Further funding for the experimental execution was provided by an EXIST-Forschungstransfer grand (03EFKBW171) of the German Federal Ministry for Economic Affairs and Energy. The funding sources were not involved in the research or preparation of the article.

Declaration of Competing Interest

The authors declare the following financial interests/personal relationships which may be considered as potential competing interests: Ralf Amann is CEO of PRiME Vector Technologies, a company developing pharmaceuticals based on the Orf virus vector. Friederike Eilts was part-time employed by PRiME Vector Technologies before the time of this study. All other authors have declared no conflicts of interest.

Acknowledgements

The authors would like to thank Keven Lothert for the valuable scientific discussions, Yasmina MJ Harsy for assistance with the analytical work, and Anna Moebus for facilitating the electron microscopy imaging. Additionally, the thorough proof-reading of the manuscript by Catharine Meckel-Oschmann is greatly acknowledged. The presented manuscript is part of FE's dissertation at the Graduate Centre for Engineering Sciences under the aegis of the Justus-Liebig-University Giessen, Germany, in cooperation with the University of Applied Sciences Mittelhessen, Giessen, Germany. The graphical abstract, Fig. 1, and Fig. 2 were generated with *biorender.com*.

References

Amann, R., Rohde, J., Wulle, U., Conlee, D., Raue, R., Martinon, O., Rziha, H.-J., 2013. A new rabies vaccine based on a recombinant ORF virus (parapoxvirus) expressing the rabies virus glycoprotein. J. Virol. 87 (3), 1618–1630.
Baek, Y., Yang, D., Singh, N., Arunkumar, A., Ghose, S., Li, Z.J., Zydney, A.L., 2017. pH variations during diafiltration due to buffer nonidealities. Biotechnol. Prog. 33 (6), 1555–1560.
Callahan, D.J., Stanley, B., Li, Y., 2014. Control of protein particle formation during ultrafiltration/diafiltration through interfacial protection. J. Pharm. Sci. 103 (3), 862–869.
Carlo, S., de Harris, J.R., 2011. Negative staining and cryo-negative staining of macromolecules and viruses for TEM. Micron 42 (2), 117–131.
Dika, C., Duval, J.F.L., Francius, G., Perrin, A., Gantzer, C., 2015. Isoelectric point is an inadequate descriptor of MS2, Phi X 174 and PRD1 phages adhesion on abiotic surfaces. J. Colloid Interface Sci. 446, 327–334.
Dika, C., Gantzer, C., Perrin, A., Duval, J.F.L., 2013a. Impact of the virus purification protocol on aggregation and electrokinetics of MS2 phages and corresponding virus-like particles. Phys. Chem. Chem. Phys. 15 (15), 5691–5700.
Dika, C., Ly-Chatain, M.H., Francius, G., Duval, J., Gantzer, C., 2013b. Non-DLVO adhesion of F-Specific RNA Bacteriophages to abiotic surfaces: importance of surface roughness, hydrophobic and electrostatic interactions. Colloid. Surf. A 435, 178–187.
Douglas, H.W., Rondle, C.J., Williams, B.L., 1966. Micro-electrophoresis of cowpox and vaccinia viruses in molar sucrose. J. Gen. Microbiol. 42 (1), 107–113.
Douglas, H.W., Williams, B.L., Rondle, C.J.M., 1969. Micro-electrophoresis of pox viruses in molar sucrose. J. Gen. Virol. 5 (3), 391–396.
Eilts, F., Steger, M., Lothert, K., Wolff, M.W., 2022. The Suitability of latex particles to evaluate critical process parameters in steric exclusion chromatography. Membranes 12 (5), 488.

Gagnon, P., Toh, P., Lee, J., 2014. High productivity purification of immunoglobulin G monoclonal antibodies on starch-coated magnetic nanoparticles by steric exclusion of polyethylene glycol. J. Chromatogr. A 1324, 171–180.
James, K.T., Cooney, B., Agopsowicz, K., Trevors, M.A., Mohamed, A., Stoltz, D., Hitt, M., Shmulevitz, M., 2016. Novel high-throughput approach for purification of infectious virions. Sci. Rep. 6, 36826.
Joklik, W.K., 1962. The purification of four strains of poxvirus. Virology 18 (1), 9–18.
Labisch, J.J., Kassar, M., Bollmann, F., Valentic, A., Hubbuch, J., Pflanz, K., 2022. Steric exclusion chromatography of lentiviral vectors using hydrophilic cellulose membranes. J. Chromatogr. A, 463148.
Langlet, J., Gaboriaud, F., Duval, J.F., Gantzer, C., 2008. Aggregation and surface properties of F-specific RNA phages: implication for membrane filtration processes. Water Res. 42 (10–11), 2769–2777.
Lee, J., Gan, H.T., Latiff, S.M.A., Chuah, C., Lee, W.Y., Yang, Y.-S., Loo, B., Ng, S.K., Gagnon, P., 2012. Principles and applications of steric exclusion chromatography. J. Chromatogr. A 1270, 162–170.
Levanova, A., Poranen, M.M., 2018. Application of steric exclusion chromatography on monoliths for separation and purification of RNA molecules. J. Chromatogr. A 1574, 50–59.
Loewe, D., Grein, T.A., Dieken, H., Weidner, T., Salzig, D., Czermak, P., 2019. Tangential flow filtration for the concentration of oncolytic measles virus: the influence of filter properties and the cell culture medium. Membranes 9 (12), 160.
Lothert, K., Dekevic, G., Loewe, D., Salzig, D., Czermak, P., Wolff, M.W., 2021. Upstream and downstream processes for viral nanoplexes as vaccines. In: Pfeifer, B.A., Hill, A. (Eds.), Vaccine Delivery Technology, 2183. Springer, New York, NY, US, pp. 217–248.
Lothert, K., Offersgaard, A.F., Pihl, A.F., Mathiesen, C.K., Jensen, T.B., Alzua, G.P., Fahnøe, U., Bukh, J., Gottwein, J.M., Wolff, M.W., 2020a. Development of a downstream process for the production of an inactivated whole hepatitis C virus vaccine. Sci. Rep. 10 (1), 3018.
Lothert, K., Pagallies, F., Eilts, F., Sivanesapillai, A., Hardt, M., Moebus, A., Feger, T., Amann, R., Wolff, M.W., 2020b. A scalable downstream process for the purification of the cell culture-derived Orf virus for human or veterinary applications. J. Biotechnol. 323, 221–230.
Lothert, K., Pagallies, F., Feger, T., Amann, R., Wolff, M.W., 2020c. Selection of chromatographic methods for the purification of cell culture-derived Orf virus for its application as a vaccine or viral vector. J. Biotechnol. 323, 62–72.
Lothert, K., Sprick, G., Beyer, F., Lauria, G., Czermak, P., Wolff, M.W., 2020d. Membrane-based steric exclusion chromatography for the purification of a recombinant baculovirus and its application for cell therapy. J. Virol. Methods 275, 113756.
Malvern Instruments Ltd, 2017. What does polydispersity mean?: Material Talks. (https://www.materials-talks.com/wp-content/uploads/2017/10/What-does-polydispersity-mean.pdf). (Accessed 19 November 2021).
Marichal Gallardo, P., Börner, K., Pieler, M.M., Sonntag Buck, V., Obr, M., Bejarano, D., Wolff, M.W., Kräusslich, H.-G., Reichl, U., Grimm, D., 2021. Single-use capture purification of adeno-associated viral gene transfer vectors by membrane-based steric exclusion chromatography. Hum. Gene Ther. 32 (17–18), 959–974.
Marichal-Gallardo, P., Pieler, M.M., Wolff, M.W., Reichl, U., 2017. Steric exclusion chromatography for purification of cell culture-derived influenza A virus using regenerated cellulose membranes and polyethylene glycol. J. Chromatogr. A 1483, 110–119.
Michen, B., Graule, T., 2010. Isoelectric points of viruses. J. Appl. Microbiol 18, 290.
Nagington, J., Horne, R.W., 1962. Morphological studies of orf and vaccinia viruses. Virology 16 (3), 248–260.
Nagington, J., Newton, A.A., Horne, R.W., 1964. The structure of orf virus. Virology 23 (4), 461–472.
Nashiruddullah, N., Pathak, D.C., Barman, N.N., Ahmed, J.A., Borah, P., Begum, S.S., Islam, S., 2018. In vitro and in vivo assessment of Orf virus (ORFV) by electron microscopy. Vet. Arh. (Vet. Arh.) 88 (6), 847–861.
Nitsche, A., Gelderblom, H.R., Eisendle, K., Romani, N., Pauli, G., 2007. Pitfalls in diagnosing human poxvirus infections. J. Clin. Virol. 38 (2), 165–168.
Reguzova, A., Ghosh, M., Müller, M., Rziha, H.-J., Amann, R., 2020. Orf virus-based vaccine Vector D1701-V induces strong CD8− T cell response against the transgene but not against ORFV-derived epitopes. Vaccines 8 (2), 295.
Rintoul, J.L., Lemay, C.G., Tai, L.H., Stanford, M.M., Falls, T.J., de, S.C.T., Bridle, B.W., Daneshmand, M., Ohashi, P.S., Wan, Y., Lichty, B.D., Mercer, A.A., Auer, R.C., Atkins, H.L., Bell, J.C., 2012. ORFV: a novel oncolytic and immune stimulating parapoxvirus therapeutic. Mol. Ther. 20 (6), 1148–1157.
Rohde, J., Schirrmeier, H., Granzow, H., Rziha, H.-J., 2011. A new recombinant Orf virus (ORFV, Parapoxvirus) protects rabbits against lethal infection with rabbit hemorrhagic disease virus (RHDV). Vaccine 29 (49), 9256–9264.
Rziha, H.-J., Büttner, M., Müller, M., Salomon, F., Reguzova, A., Laible, D., Amann, R., 2019. Genomic characterization of Orf virus strain D1701-V (Parapoxvirus) and development of novel sites for multiple transgene expression. Viruses 11 (2), 127.
Rziha, H.-J., Rohde, J., Amann, R., 2016. Generation and selection of Orf virus (ORFV) recombinants. Methods Mol. Biol. 1349, 177–200.
Shi, H., Tarabara, V.V., 2018. Charge, size distribution and hydrophobicity of viruses: effect of propagation and purification methods. J. Virol. Methods 256, 123–132.
Spehner, D., Carlo, S., de, Drillien, R., Weiland, F., Mildner, K., Hanau, D., Rziha, H.-J., 2004. Appearance of the bona fide spiral tubule of ORF virus is dependent on an intact 10-Kilodalton viral protein. J. Virol. 78 (15), 8085–8093.
Sviben, D., Forčić, D., Kurtović, T., Halassy, B., Brgles, M., 2016. Stability, biophysical properties and effect of ultracentrifugation and diafiltration on measles virus and mumps virus. Arch. Virol. 161 (6), 1455–1467.
Tao, S.-P., Zheng, J., Sun, Y., 2015. Grafting Zwitterionic polymer onto cryogel surface enhances protein retention in steric exclusion chromatography on cryogel monolith. J. Chromatogr. A 1389, 104–111.
van Rooij, E., Rijsewijk, F., Moonen-Leusen, H.W., Bianchi, A., Rziha, H.-J., 2010. Comparison of different prime-boost regimes with DNA and recombinant Orf virus based vaccines expressing glycoprotein D of pseudorabies virus in pigs. Vaccine 28 (7), 1808–1813.
van Vloten, J.P., Minott, J.A., McAusland, T.M., Ingrao, J.C., Santry, L.A., McFadden, G., Petrik, J.J., Bridle, B.W., Wootton, S.K., 2021. Production and purification of high-titer OrfV for preclinical studies in vaccinology and cancer therapy. Mol. Ther. Methods Clin. Dev. 23, 434–447.
Wang, C., Bai, S., Tao, S. P., Sun, Y., 2014. Evaluation of steric exclusion chromatography on cryogel column for the separation of serum proteins. J. Chromatogr. A 1333, 54–59.
Wang, R., Luo, S., 2019. Orf virus: a new class of immunotherapy drugs. In: Vlachakis, D. (Ed.), Systems Biology. IntechOpen, London.
Yuan, B., Pham, M., Nguyen, T.H., 2008. Deposition kinetics of bacteriophage MS2 on a silica surface coated with natural organic matter in a radial stagnation point flow cell. Environ. Sci. Technol. 42 (20), 7628–7633.

Part B: Critical process parameters for Orf virus infectivity stability

Eilts, F.; Labisch, J. J.; Orbay, S.; Harsy, Y. M. J.; Steger, M.; Pagallies, F.; Amann, R.; Pflanz, K.; Wolff, M. W. (2023). Stability studies for the identification of critical process parameters for a pharmaceutical production of the Orf virus. Vaccine 41 (32), 4731-4742. doi: 10.1016/j.vaccine.2023.06.047

Vaccine 41 (2023) 4731–4742

Contents lists available at ScienceDirect

Vaccine

journal homepage: www.elsevier.com/locate/vaccine

Stability studies for the identification of critical process parameters for a pharmaceutical production of the Orf virus

Friederike Eilts [a], Jennifer J. Labisch [b,c], Sabri Orbay [a], Yasmina M.J. Harsy [a], Marleen Steger [a], Felix Pagallies [d], Ralf Amann [d,e], Karl Pflanz [b], Michael W. Wolff [a,*]

[a] Institute of Bioprocess Engineering and Pharmaceutical Technology, University of Applied Sciences Mittelhessen (THM), Wiesenstr.14, 35390 Giessen, Germany
[b] Lab Essentials Applications Development, Sartorius Stedim Biotech GmbH, August-Spindler-Straße 11, 37079 Goettingen, Germany
[c] Institute of Technical Chemistry, Leibniz University Hannover, Callinstraße 3-9, 30167 Hannover, Lower Saxony, Germany
[d] Department of Immunology, University of Tuebingen, Auf der Morgenstelle 15/3.008, 72076 Tuebingen, Germany
[e] Prime Vector Technologies, Herrenberger Straße 24, 72070 Tuebingen, Germany

ARTICLE INFO

Article history:
Received 19 October 2022
Received in revised form 1 June 2023
Accepted 12 June 2023
Available online 21 June 2023

Keywords:
Downstream processing
Forced degradation studies
Formulation
Parapox Orf virus
Viral vector vaccine

ABSTRACT

A promising new vaccine platform is based on the Orf virus, a viral vector of the genus *Parapoxvirus*, which is currently being tested in phase I clinical trials. The application as a vaccine platform mandates a well-characterised, robust, and efficient production process. To identify critical process parameters in the production process affecting the virus' infectivity, the Orf virus was subjected to forced degradation studies, including thermal, pH, chemical, and mechanical stress conditions. The tests indicated a robust virus infectivity within a pH range of 5–7.4 and in the presence of the tested buffering substances (TRIS, HEPES, PBS). The ionic strength up to 0.5 M had no influence on the Orf virus' infectivity stability for NaCl and $MgCl_2$, while NH_4Cl destabilized significantly. Furthermore, short-term thermal stress of 2 d up to 37 °C and repeated freeze-thaw cycles (20 cycles) did not affect the virus' infectivity. The addition of recombinant human serum albumin was found to reduce virus inactivation. Last, the Orf virus showed a low shear sensitivity induced by peristaltic pumps and mixing, but was sensitive to ultrasonication. The isoelectric point of the applied Orf virus genotype D1707-V was determined at pH 3.5. The broad picture of the Orf virus' infectivity stability against environmental parameters is an important contribution for the identification of critical process parameters for the production process, and supports the development of a stable pharmaceutical formulation. The work is specifically relevant for enveloped (large DNA) viruses, like the Orf virus and like most vectored vaccine approaches.

© 2023 Elsevier Ltd. All rights reserved.

1. Introduction

Since the beginning of 2020, the world-wide endeavour to develope vaccines against COVID-19 exhibited the importance of rapidly available vaccines and production platforms, such as mRNA or viral vectors. A promising viral vector to possibly fulfill such a task is the Orf virus (ORFV), a member of the genus *Parapoxvirus*, which contains a linear double-stranded DNA and measures approximately 140–200 nm in width and 220–300 nm in length [1–3]. Its ovoid form is enveloped by a characteristic tubule-like structure, assembled in a left-turning spiral around the virus [4]. The wild-type ORFV causes contagious ecthyma, also known as Orf, a zoonotic disease, which affects mainly sheep and goats worldwide [3]. Several live vaccines were developed against the disease [5–7], but the vaccination success is limited especially due to a short-lived immunity [7–10]. This feature is a key advantage for the use as a vector vaccine that can be administered multiple times. The highly attenuated ORFV strain D1701-V offers the advantage of a viral vector with a potent immune response [11,12], which is accompanied by a short-lived duration of the ORFV-specific immunity, allowing re-immunization [8,9,13,14]. Other favourable properties of D1701-V are a restricted host range, the induction of strong B- and T-cell immune responses to express antigens, and the lack of systemic spread [9,12,14]. In recent years, attenuated ORFV-strains gained increased attention as a

Abbreviations: CPB, citrate-phosphate buffer; DLS, dynamic light scattering; DMEM, Dulbecco's Modified Eagle's Medium; DSP, downstream processing; FCS, fetal calf serum; GFP, green fluorescent protein; IU, infectious unit; MVA, Modified Vaccinia Ankara; ORFV, Orf virus; PBS, phosphate buffered saline; PCTRL, positive control; pI, isoelectric point; rHSA, recombinant human serum albumin.

* Corresponding author.
E-mail address: michael.wolff@lse.thm.de (M.W. Wolff).

https://doi.org/10.1016/j.vaccine.2023.06.047
0264-410X/© 2023 Elsevier Ltd. All rights reserved.

pharmaceutical for human and veterinary applications [15]. Studies showed its versatility as an oncolytic treatment [13,16,17], an immunomodulatory agent [18], and as a viral vector platform [12,19–24]. A recent study explores its potential as anti-SARS-CoV-2 vaccine [25].

Previously, we established a lab-scale downstream processing (DSP) train for an ORFV vector including clarification, capture, and polishing [26,27]. However, to be implemented as a robust production process, data on critical process parameters and degradation forces that could possibly reduce the ORFV infectivity recovery is lacking. Such parameters can be investigated by applying forced degradation studies as recommended by the ICH (International Conference of Harmonisation) guidelines for the pharmaceutical industry [28]. The employment of these guidelines is aimed at revealing important degradation pathways, which might be indicators for a potency loss of biological drugs or the formation of impurities of concern, thus, ensuring an adequate quality of biopharmaceutical products [29]. Forced degradation studies are undertaken for an intentional breakdown of a specific biological drug under suitable stress conditions, which lead to an accelerated chemical and physical degradation [30]. Examples for the application of such studies are the evaluation of process-related stress factors for viral pharmaceuticals [28,31–34], the identification of potential formulation additives and storage conditions [29,31,32], as well as the development of analytical methods [29,30].. However, few studies have been published on degradation pathways and the underlying factors of the ORFV. Relevant articles include investigations on the stress-related response of infectious ORFV particles with regard to three freeze-thaw cycles [27], lyophilisation [5], and the addition of stabilizers, such as lactalbumin, trehalose, or sucrose [5]. Further literature data indicated a complete virus inactivation by UV-C irradiation for 300 s [13] or binary ethylamine [21]. Certainly, the documented results are an asset for the development of stable formulations and the sample handling for analytics, but to our knowledge no essential information about thermal, chemical, or mechanical stress studies of the ORFV is available. Concerning other poxviruses, which are known to be very stable, an extensive review was published by Rheinbaben *et al.* [35].

To unveil possible sources of inactivation, often encountered in pharmaceutical production, we performed a series of forced degradation studies on the ORFV. Concerning the DSP, this especially accounts for thermal stress in the bioreactor cultivation, mechanical stress by stirrers, pumps, and membranes, as well as chemical stress due to potentially occurring variations in pH, ionic strength, and additives. Hence, this work targeted relevant parameters such as temperature, freeze-thaw cycles, shear stress, and buffer compositions, including ionic strength, inorganic salts, additives as well as pH. As the ORFV serves as an infective viral vector, changes in the infectious titer were the focus of this work and *stability* was used as synonym for the preservation of infectivity. The results from this work are an important tool for the optimization of the existing production process of the ORFV for vaccine applications, as well as for an acceleration of future process and formulation developments.

2. Results

The degradation investigations were executed with cell culture-derived ORFV, purified either using ultracentrifugation [36] or an established DSP train [26]. According to a recent study, ORFV prepared from such protocols was of comparable quality with high infectivity recoveries and morphological integrity [37]. The grade of purity of the total protein and the dsDNA content was comparable in both purification protocols [37].

2.1. Temperature-dependent infectivity

In this study, the ORFV was incubated over a period of 14 d at 4 and 37 °C, and samples were taken after 1, 2, 7, and 14 d. The temperature were chosen to represent long-term storage (4 °C) and cultivation/production in a bioreactor environment (37 °C). Additionally, the influence of an rHSA supplementation at 0.25 % and 0.5 % was investigated. The reduction of infectivity was compared to the ORFV initial titer of 4.5×10^6 IU mL^{-1} (IU, infectious unit). The data related to incubation at 4 °C indicated no significant change in the viral titer for the sampling intervals 1, 2, and 7 d (Fig. 1**A**). After 14 d, a significant ORFV infectivity decrease was observed at 4 °C for the non-supplemented sample ($\alpha = 0.05$) to approximately 2.6×10^6 IU mL^{-1} (0.2 log). Both rHSA concentrations stabilized the virus in the same time interval, showing no significant reduction of the infectivity losses. Furthermore, we observed that at 22 °C the ORFV titer was comparable to storage at 4 °C over a period of 14 d (data not published).

At 37 °C, the viral titer showed no significant alteration after 1 and 2 d of incubation (Fig. 1**B**). After 7 d, the ORFV infectious titer of the non-supplemented sample decreased to 1.3×10^6 IU mL^{-1} (0.3 log) and after 14 d to 0.4×10^6 IU mL^{-1} (1 log), indicating a significance at $\alpha = 0.05$ and $\alpha = 0.01$, respectively. As was observed for 4 °C, the addition of rHSA stabilized the ORFV at 37 °C, showing no pronounced decline after 7 d for both rHSA concentrations, 0.25 % and 0.5 %. After 14 d, however, only the samples with 0.5 % rHSA showed a significant stabilization, whereas the samples with 0.25 % rHSA exhibited a titer reduction of roughly 0.3 log to 1.4×10^6 IU mL^{-1}. Hence, the results indicated that virus processing without a noteworthy ORFV infectious titer loss can be performed safely without a supplementation of rHSA at 4 °C for a period of up to 7 d and at 37 °C up to 2 d.

2.2. Freeze-thaw induced changes in size and infectivity

The ORFV was subjected to 2, 5, and 8 freeze-thaw cycles, and the infectivity of the samples was determined. The influence of rHSA on this process was investigated as for the previous studies by the addition of 0.25 % or 0.5 %, compared to a non-supplemented sample with an initial infectious titer of 4.5×10^6 - IU mL^{-1}. The experiment showed no significant loss of titer for any rHSA concentration, 0 %, 0.25 %, and 0.5 %, ($\alpha = 0.05$) after the applied eight freeze-thaw cycles (Fig. 2**A**), with titers ranging from 3.2×10^6 IU mL^{-1} to 4.5×10^6 IU mL^{-1}. A supplementary study investigated the size distribution of the ORFV after 1, 5, and 20 freeze-thaw cycles without rHSA addition applying dynamic light scattering (DLS) (Fig. 2**B**). The measure for statistical comparison was the ORFV size determined after one freeze-thaw cycle. While the size after one freeze-thaw cycle ranged between 160 and 220 nm, a significant increase was detected after five cycles to 220–340 nm ($\alpha = 0.01$), and further after 20 repetitions to 280–440 nm. To conclude, the ORFV titer was not affected by up to eight freeze-thaw cycles, but a significant increase in the sample size distribution was observed after five freeze-thaw cycles.

2.3. The isoelectric point (pI) of the ORFV

To determine the ORFV's point of zero charge, the pI, all samples were diluted in pre-titrated buffers. The pH-dependent charge distribution on the ORFV surface showed a positive charge for pH 3.0–3.4 and a negative charge for pH 3.8–7.4, indicating the location of the pI between pH 3.4 and pH 3.8 (Fig. 3**A**). Using a polynomial fit, the pI was presumed to be approximately pH 3.5. A comparable charge distribution was determined for 6 °C and 22 °C.

The location of the pI was further investigated by size-based measurements. Fig. 3**B** depicts the size distribution of the ORFV

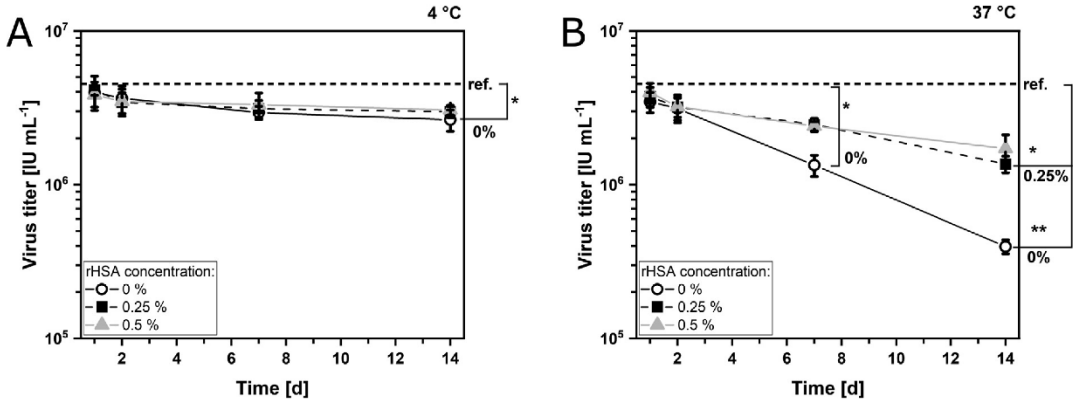

Fig. 1. Influence of the incubation temperature on the Orf virus (ORFV) infectivity. ORFV aliquots were non-supplemented (open circles) or supplemented with 0.25 % (black squares) and 0.5 % (grey triangles) recombinant human serum albumin (rHSA) and stored at 4 °C (**A**) and 37 °C (**B**) over the course of 14 d. The reference value (ref.) represents the initial infectious virus concentration on 0 d. The lines are guide to the eye. ANOVA, Tukey; $n = 3$; *$\alpha = 0.05$; **$\alpha = 0.01$. Data are mean values with standard deviations as error bars.

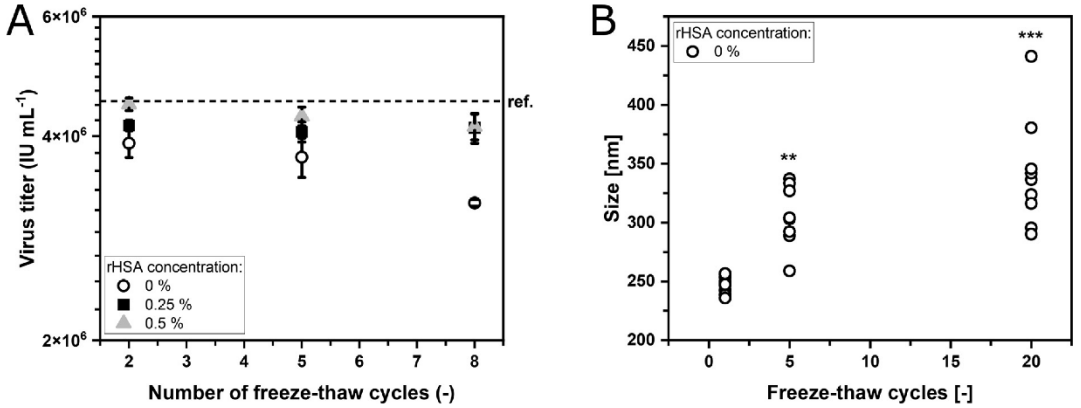

Fig. 2. Freeze-thaw stability (-80 °C, 22 °C) of the Orf virus' (ORFV) infectivity. ORFV aliquots were unsupplemented (open circles) or supplemented with 0.25 % (black squares) and 0.5 % (grey traingles) recombinant human serum albumin (rHSA). All samples were frozen at −80 °C and thawed in a water bath at room temperature (22 °C), representing one cycle. The influence on the infectivity compared to a reference value (ref.) after one freeze-thaw cycle is shown in (**A**). Here, data are mean values with the respective standard deviation as error bars. (**B**) represents the size distribution of the ORFV depending on the number of freeze-thaw cycles. All measurements are shown and compared to one freeze-thaw cycle. ANOVA, Tukey; $n = 3$; **$\alpha = 0.01$; *** $\alpha = 0.001$.

samples as a function of the pH for an incubation time of up to15 min, while Fig. 3**C** displays the full kinetics over 5 h for pH 2, 3, 4, and 5. After 15 min of incubation (Fig. 3**B**), a significant increase in size, as compared to the ORFV size determined at pH 7.4, was observed, at pH 2 (α = 0.05) to approximately 800 nm, at pH 3 (α = 0.001) to 1600–3000 nm, and at pH 4 (α = 0.001) to 1500–2700 nm. Further, the size distribution at pH 5, 6, and 7.4 remained monodisperse and stable at roughly 250 nm for this time interval. A similar picture as for the size distributions after 15 min of incubation was detected for the pH-dependent kinetics over the course of 5 h (Fig. 3**C**). These illustrated a stable size at pH 5 (250 nm) and a size increase to approximately 1000 nm for pH 2, and several micrometers for pH 3 and 4. These summarized results indicated an acidic pI at approximately pH 3.5 of the ORFV.

2.4. pH stress and buffering system

In order to study suitable ranges of pH and possible buffering substances for production, the ORFV was incubated at 4 °C for up to 60 d at pH 2–10 (for the composition of the buffers see **section 5.4.4**). Furthermore, the buffers HEPES, TRIS, PBS (phosphate buffered saline), and CPB (citrate–phosphate buffer) were tested. No excipients, e.g., rHSA, were added. Additionally, the ORFV was incubated in DMEM (Dulbecco's Modified Eagle's Medium), which was supplemented with 5 % fetal calf serum (FCS), as a positive control (PCTRL). The point of reference for statistical analysis was the initial ORFV sample on day zero with 10.0×10^5 IU mL^{-1}. After 1 d of incubation, the ORFV infectivity was reduced significantly for pH 2–4 (α = 0.001) below the limit of detection (10^4 IU mL^{-1}), and for pH 10 (α = 0.001) by 0.5 log to 5.4×10^5 IU mL^{-1} (Fig. 4**A**). The titer of the ORFV incubated at pH 10 was further reduced after 2 d to 2.0×10^5 IU mL ^{1}. Concerning the other tested pH values, pH 5, 6, and 7.4 had an insignificant influence on the ORFV infectious titer after 1 d of storage, but rather exhibited a significant viral titer loss after 2 d (α = 0.001). pH 6 showed the highest infectious virus recoveries for 1 d (9.7×10^5 IU mL^{-1}) and 2 d of incubation (7.4×10^5 IU mL^{-1}), whereas after 14 d, differences between pH 5, 6, and 7.4 were insignificant. Last, the control samples (PCTRL) revealed an increased stabilization of the ORFV infectivity

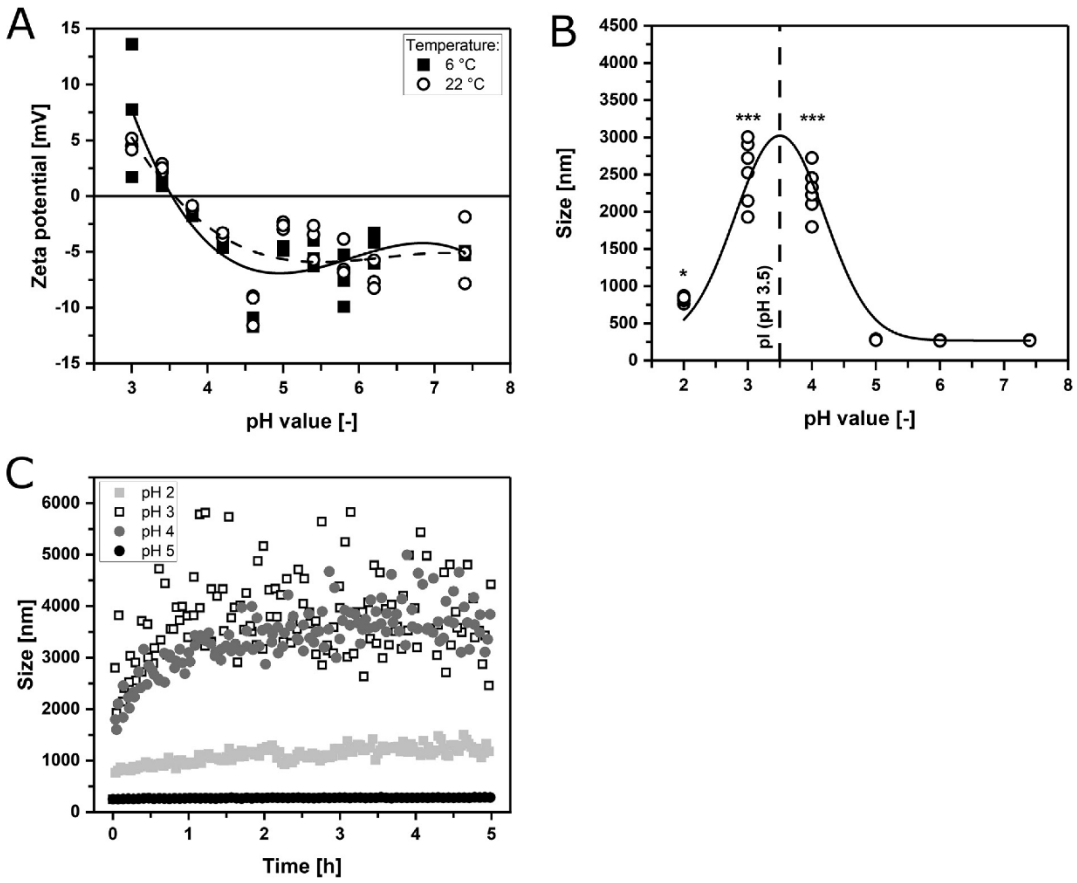

Fig. 3. Measurements of the isoelectric point (pI) of the Orf virus (ORFV). (**A**) The charge of the ORFV was measured depending on the pH at 6 °C (black squares) and 22 °C (open circles). All aliquots were diluted 1:20 in titrated 0.1 M citrate-phopshate buffer. A third-order polynomial fit is plotted for 6 °C (solid line) and 22 °C (dashed line), both exhibiting y = 0 at pH 3.5, showing the pI, the point of zero charge. (**B**) and (**C**) depict pH-dependent measurements of the ORFV's size distribution after 15 min (**B**) and as kinetic over 5 h (**C**) at 22 °C including the data from (**B**). ORFV aliquots were diluted 1:20 in titrated 0.1 M KCl-HCL buffer (pH 2) (grey squares) or 0.1 M citrate-phopshate buffer (pH 3–7.4) (open squares (pH 3), grey circles (pH 4), black circles (pH 5) and measured by dynamic light scattering (DLS).*The solid line in (**B**) serves as a guide to the eye, while the dashed line represents the pH value for the net zero charge (pI) from (**A**). The size distribution at* pH *7.4 served as a reference for the statistical analysis. ANOVA, Tukey; n = 3; *α = 0.05; *** α = 0.001. All data points are shown.*

in the presence of DMEM + 5 % FCS compared to an untreated sample on day zero. Unlike the incubation without FCS, the infectious titer of the ORFV remained stable for 14 d and reduced by 0.3 log to 7.4×10^5 IU mL^{-1} ($\alpha = 0.01$) after 30 d, and by 0.4 log to 6.6×10^5 - IU mL^{-1} ($\alpha = 0.001$) after 60 d. In both time intervals, the infectious titer for all other samples was below the limit of detection. Concerning the four buffers tested, only for CPB a significant influence of the buffering system by a 0.2 log reduction to 8.2×10^5 IU mL^{-1} was detected after 24 h, compared to an untreated sample ($\alpha = 0.05$) (Fig. 4**B**). After 48 h. HEPES samples preserved the highest infectious titer (7.9×10^5 IU mL^{-1}), followed by PBS (7.3×10^5 - IU mL^{-1}), TRIS (6.3×10^5 IU mL^{-1}), and CPB (5.5×10^5 IU mL^{-1}). In conclusion, the ORFV showed the highest stability for pH 5, 6, and 7.4, while the buffers HEPES, PBS, and TRIS could be used without any significant infectivity reduction.

2.5. Influence of ionic strength and salt type

The aim of this investigation was to evaluate the stability of the ORFV in the presence of NH_4Cl, NaCl, $MgCl_2$, while three different conductivities were chosen: 15, 35, and 45 mS cm^{-1}, corresponding to one-, two-, and three-time physiological conditions. The corresponding molarity can be obtained from Table 1. For statistical analysis, the samples were compared to an untreated ORFV sample on day zero with 10.0×10^5 IU mL^{-1}. The conducted experiments indicated an insignificant difference of the ORFV infectivity in the presence of NaCl and $MgCl_2$ compared to the reference value of up to 24 h (Fig. 5**A + B**). Furthermore, for these two salts, the infectivity reduction was independent of the ionic strength for up to 48 h, but showed a pronounced decrease compared to the initial ORFV concentration of 0.3–0.4 log to 6.3–7.3 $\times$ 10^5 IU mL^{-1} ($\alpha = 0.001$). After 7 d, a significant difference developed between the highest (45 mS cm^{-1}) and the other two (15 and 35 mS cm^{-1}) ionic strengths for NaCl, and between the highest and lowest ionic strength (15 and 45 mS cm^{-1}) for $MgCl_2$ ($\alpha = 0.001$). The lowest titers were observed for the samples containing 45 mS cm^{-1} salt, i.e., 2.5×10^5 IU mL^{-1} and 2.2×10^5 IU mL^{-1} for NaCl and $MgCl_2$, respectively. The incubation with NH_4Cl reduced the ORFV significantly after 24 h by 0.7 log to 3.0×10^5 IU mL^{-1} for 15 mS cm^{-1}, which lowered to 1.2×10^5 IU mL^{-1} after 7 d incubation time (Fig. 5**C**). Concerning 35 mS cm^{-1}, the infectious titer was 0.3×10^5 IU mL^{-1} after 24 h, leveling to the limit of detection (10^4 - IU mL^{-1}) after 48 h, whereas the highest concentration was below the detection limit at all sampling times. The impact of NH_4Cl on

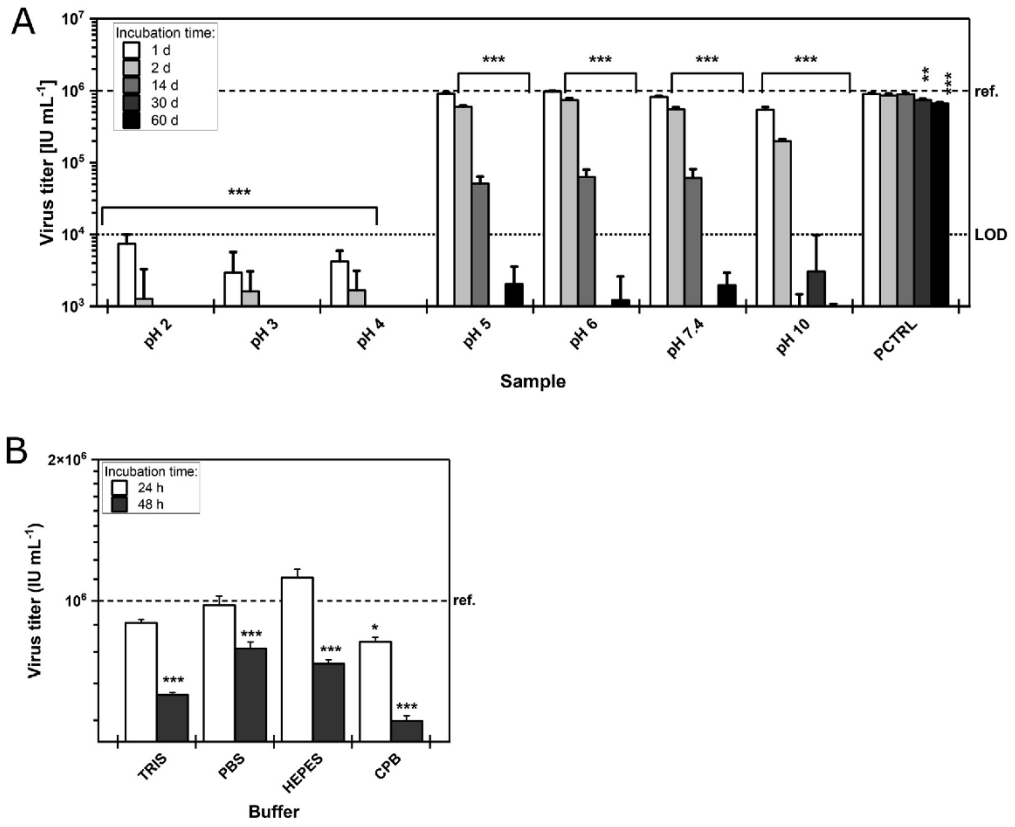

Fig. 4. pH- and buffer-dependent infectivity of the Orf virus (ORFV). (**A**) The pH-dependent infectivity was determined for pH 2–10. ORFV aliquots were diluted 1:50 in titrated 0.1 M KCl-HCL buffer (pH 2), 0.1 M citrate-phopshate buffer (pH 3–7.4), 0.1 M carbonate buffer (pH 10), or DMEM (Dulbecco's Modified Eagle's Medium) supplemented with 5 % fetal calf serum (pH 7.4), here called PCTRL (positive control). The aliquots were stored under the exclusion of light at 4 °C. Samples were taken after 1, 2, 14, 30, and 60 d. The infectivity was compared to an untreated and non-supplemtented reference value (ref.) on 0 d. An ANOVA with Tukey test was performed and significant levels are given for a comparison with the PCTRL. (**B**) represents the ORFV diluted 1:50 in different buffering systems (pH 7.4), 0.02 M TRIS PBS, 0.05 M HEPES, and 0.1 M citrate-phopshate buffer (CPB) stored for 24 or 48 h. Virus titers were compared to an untreated reference sample (ref.).LOD, Limit of detection. ANOVA, Tukey; $n = 3$; $^{*}\alpha = 0.05$; $^{**}\alpha = 0.01$; $^{***}\alpha = 0.001$. Data are mean values with standard deviations as error bars.

Table 1
Conversion of conductivity to molarity of NH_4Cl, NaCl, and $MgCl_2$. Corresponding molarities to conductivities applied for the stability study of the Orf virus (ORFV) in presence of salts.

Salt	Conductivity	Molarity
	mS cm^{-1}	M
NH_4Cl	15	0.20
	35	0.45
	45	0.60
NaCl	15	0.15
	35	0.37
	45	0.45
$MgCl_2$	15	0.09
	35	0.26
	45	0.34

the Vero cell culture was considered, which was not observed for NaCl and $MgCl_2$ (data not published). Hence, the concentration of NaCl and $MgCl_2$ (15–45 mS cm^{-1}) did not affect the ORFV titer loss for up to 7 d, whereas NH_4Cl reduced the infectivity by several log scales.

2.6. Mechanical stress

The ORFV was subjected to 60 min of cyclic pumping at a flow rate of 23.5 mL min^{-1}, using a peristaltic pump with a 1/16″ x 3/16″ tubing of 60 cm length, and samples taken after 15, 30, and 60 min. The calculated shear stress in the tubing was 999 mPas and the shear rate at 997 s^{-1}, while the volumetric power input summed up to 10^{3} W mL^{1} (see **Equation (1) and (2)**. The flow was laminar (Re = 312). Compared to an untreated sample of 1.8 × 10^{6} IU mL^{-1}, the infectious ORFV titer decreased significantly after 30 min by < 0.1 log to 1.6 × 10^{6} IU mL^{-1} ($\alpha = 0.05$) (Fig. 6**A**) and further by approximately 0.2 log to 0.9 × 10^{6} IU mL^{-1} after 60 min ($\alpha = 0.001$). Furthermore, ORFV samples with a starting titer of 6.7x 10^{6} IU mL^{-1} were stressed in an ultrasonication bath for 0.5, 1, 2, and 3 min with a 0.1 W mL^{-1} volumetric power input (Fig. 6**B**). After 2 min, a significant decrease in infectivity ($\alpha = 0.05$) by < 0.1 log to 6.0 × 10^{6} IU mL^{-1} was observed. Last, mixing by vortex was used to induce mechanical stress. The treatment of up to 3 min at 2700 min^{-1} did not result in a significant change of the ORFV initial titer of 6.7 × 10^{6} IU mL^{-1} ($\alpha = 0.05$) (Fig. 6**C**).

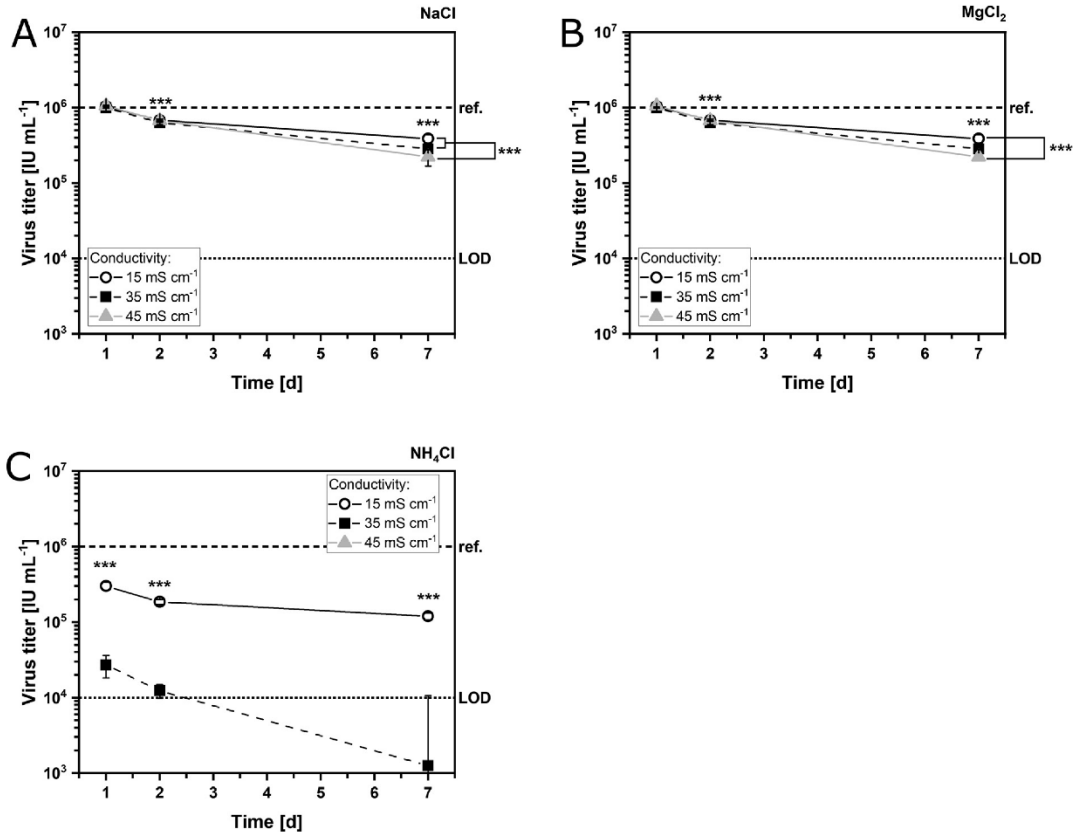

Fig. 5. Stability of the Orf virus (ORFV) in the presence of salts. The time-dependent stability of the ORFV in the presence of NaCl (**A**), $MgCl_2$ (**B**), and NH_4Cl (**C**), each adjusted to a conductivity of 15 (open circles), 35 (black squares), or 45 mS cm^{-1} (grey triangles), was recorded. ORFV aliquots were diluted 1:50 in salt-containing TRIS buffer (pH 7.4) and stored at 4 °C. Samples were taken after 1, 2, and 14 d and the virus titer compared to a reference value (ref.) on 0 d.LOD, Limit of detection. ANOVA, Tukey; $n = 3$; ***$\alpha = 0.001$. Data are mean values with standard deviations as error bars.

3. Discussion

Generally, viruses degrade over time when subjected to harsh environmental conditions of thermal stress, freeze-thawing, pH, ionic strength, or mechanical stress. Such degradation processes may be induced by aggregation, denaturation, or oxidation [31]. Forced degradation studies are a powerful tool for the identification of, firstly, critical process parameters affecting the product yield and quality of production processes; and secondly, initial indications on restrictions that need to be considered for the product formulation and analytical methods. The focus on virus infectivity as a stability factor for viral vectors is particularly relevant due to their mechanism of operation. In this study, we conducted forced degradation studies of the ORFV, a promising viral vector, based on its infectivity recovery.

3.1. Temperature-dependent infectivity

Live (attenuated) viruses are known to be heat-sensitive [38]. Although the DSP is generally done in the shortest possible timeframe, infectivity losses during production and storage are an important factor to consider. Here, the ORFV was subjected to a storage at 4 °C and 37 °C. After 14 d at 4 °C, the virus titer reduced by 0.1–0.2 log, showing a significant stabilization in the presence of at least 0.25 % rHSA. When stored at 37 °C, the ORFV titer reduced by 1 log for the non-supplemented sample, and approximately 0.3 log for the supplemented samples over the same period. As expected, the higher storage temperature destabilized the ORFV infectivity more evidently. This has previously been demonstrated by a live ORFV vaccine [5] and related vaccinia-based live vaccines, such as the Ebola vaccine MVA-BN®-Filo [39] or the smallpox vaccines ACAM2000® [40] and Dryvax® [41,42]. The titer of the non-stabilized live ORFV vaccine against the orf disease using the genotype Muk 59/05, reduced by >2 log within 14 d at 37 °C [5]. This infectivity loss is more than twice the reduction observed in our study (1 log). The Dryvax® vaccine, reconstituted in non-supplemented buffer (PBS), exhibited a 0–0.3 log virus titer reduction at 2–8 °C after 7 d of storage [42], corresponding to the titer loss of the presented results (0.1–0.2 log). Higher stabilities have been reported for vaccinia from cell cultures for unpurified virus [43]. However, it should be considered that the purified virus is generally less stable [35].

Furthermore, an increased stabilization in the presence of rHSA was observed for both tested temperatures, 4 °C and 37 °C. Stabilization by albumin is known from other viruses, such as the vaccinia virus in the ACAM2000 vaccine (2 % human serum albumin) [40], the ORFV Muk 59/05 vaccine (5 % lactalbumin) [5], the Ebola vaccinia virus vaccine (0.25 % rHSA) [39], or the M–M–R®II (mumps, measles, rubella) vaccine (rHSA in cell culture production) [44].

Considering these studies and the presented results, the temperature stability of the ORFV infectivity as well as the impact of

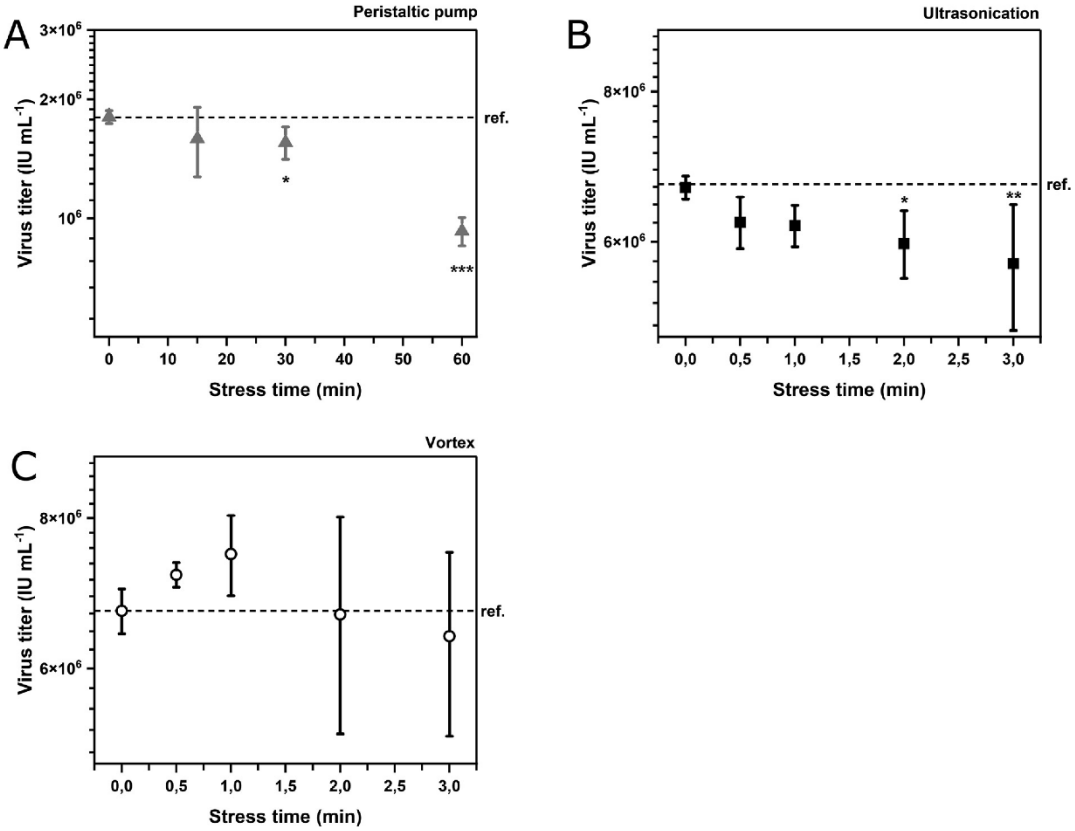

Fig. 6. Short-term mechanical stability of the Orf virus (ORFV). (**A**) 20 mL of ORFV was cycled through a persitaltic pump with 1/16″ x 3/16″ tubing (60 cm length) at 23.5 mL min^{-1}, corresponding to 10^{-3} W mL^{-1}. Samples were taken after 0, 15, 30, and 60 min. Furthermore, ORFV aliquots were subjected to (**B**) ultrasonication (0.1 W mL^{-1} and 35 kHz) and (**C**) vortexing (2,700 min^{-1}) and separate samples used for each time interval of 0, 0.5, 1, 2, and 3 min. Infectivity was compared to an untreated reference sample (ref.).ref, reference sample; ANOVA, Tukey; $n = 3$; *$\alpha = 0.05$; **$\alpha = 0.01$; ***$\alpha = 0.001$. Data are mean values with standard deviations as error bars.

stabilizing excipients were in the range of related viruses and their vaccine candidates.

3.2. Freeze-thaw-induced changes in size and infectivity

The preservation of the viral infectivity after repeated freeze-thaw cycles is an important characteristic for the production process development. First, freeze-thaw methods are often applied in small-scale applications for cell lysis to improve the recovery of a cell-associated virus, combined with a hypotonic burst and sonication [45]. Second, sample freezing allows for flexibility of any process-accompanying product analysis. Finally, the infectivity preservation throughout freeze-thawing may be an indicator for a lyophilisation process for the formulation development [46].

In this work, the ORFV was subjected to up to eight freeze-thaw cycles with and without the addition of 0.25 % or 0.5 % rHSA, which was applied as a cryoprotectant [47]. In neither of the formulations, a significant loss in infectious titer was detected. Comparing the stability of the virus titer with literature data, a recent study [27] showed no substantial reduction in the virus titer of non-supplemented samples after three freeze-thaw cycles of the same ORFV strain D1701-V. A similar result was obtained for the Modified Vaccinia Ankara (MVA) MVA-BN®-Filo Ebola vaccine, which was subjected to five freeze-thaw cycles [39]. On the contrary, Vloten *et al.* reported a 70 % loss of infectious particles of a not further specified ORFV after the first freeze-thaw cycle, however, no further inactivation for the following four cycles was observed [48]. The summarized results from this study and the literature data suggest a similar freeze-thaw infectivity stability of the ORFV strain used in this study with recent results on the ORFV and the related MVA virus, and opens the possibility for up to eight freeze-thaw cycles without a substantial titer loss, with and without an rHSA addition of 0.25 % or 0.5 %.

However, concerning the size distribution of the ORFV in the course of repeated freeze-thaw cycles in the present study, already after five freeze-thaw cycles a notable increment in size by approximately 24 % for the non-supplemented ORFV was visible, increasing to >38 % for 20 freeze-thaw cycles. This result was surprising considering the limited titer reduction and might be attributed to non-infectious ORFV particles, which are part of the aggregation process but not detected with the infectivity assay. To our knowledge, no comparable studies of the ORFV are available and little is provided in literature on related viruses throughout phase transitions. Without stating exact numbers, the assessment report for the MVA virus-based IMVANEX, a smallpox vaccine formulated in TRIS and NaCl, indicated a shift in the range of particle sizes over time following the storage at −20 °C [49]. Generally, an aggregation of viral particles caused by freeze-thawing has been observed repeatedly [50] and should be further characterised for the ORFV in the presence of stabilizing agents, to prevent the formation of (sub-)visible particles in the drug product and an impeding of the DSP and the analysis.

3.3. The pI of the ORFV

The pH-dependent charge and, accordingly the pI, the point of zero charge, highly influences the aggregation, adhesion, and adsorption behaviour of macromolecules and nanoplexes [51]. Hence, the surface charge of viruses is decisive for several DSP unit operations such as ion exchange, precipitation, or filtration. However, the determination of the pI of complex structures like viruses is relatively challenging. Accordingly, it must be understood that the pI of viruses is a point of reference rather than a fact. In the data presented here, the pI of the ORFV was determined at pH 3.5 via a charge-based method, and did not vary due to a temperature change from 6 to 22 °C, which suggests a neglectable temperature-dependency of the ORFV surface charge. The value of pH 3.5 for the pI was supported by pH-dependent size distribution measurements, showing an increase in size at pH 2, 3, and 4, but not at higher pH values. Interestingly, although pH 2 and pH 5 are equidistant from the pI at pH 3.5, a size increment at pH 2 was observable, but not at pH 5. We suspect an increased aggregation behaviour at pH 2 due to protein denaturation, which might also be the cause of the infectivity loss observed at this pH value (see **section 2.4**).

In a recent publication on the same ORFV strain D1701-V, the pI was measured to be pH 4.6 [27]. This discrepancy may be due to the different buffering system (20 mM TRIS), compared to 0.1 M CPB, or the purity of the samples. The subject is further discussed in our previous publication on the purification ORFV samples [37].

To conclude, the pI of the ORFV, strain D1707-V, was determined with pH 3.5 in 0.1 M CPB buffer, and reduced aggregation behaviour was observed for pH 5–7.4.

3.4. pH stress and buffering system

As described for the pI, the pH is an important tool to adapt and optimize DSP strategies for higher recoveries. Nevertheless, the stability, i.e., aggregation and infectivity, of the target virus must be guaranteed for pH changes and the chosen buffer. In the conducted experiments, the range of the pH stability for the ORFV infectivity was determined between pH 5 and pH 7.4. At these pH values, viral infectivity was preserved for 1 d without a notable reduction. Of the four tested buffers, only CPB showed a significant decrease in virus titer by 0.2 log after 1 d, although this buffer has been reported to increase the thermal stability of the vaccinia virus by bisecting the reaction velocity compared to distilled water [52,53]. The buffering substance with the lowest infectivity reduction after 2 d was HEPES (0.2 log), followed by PBS (0.3 log), TRIS (0.4 log) and CPB (>0.4 log). Compared to literature, a high infectivity stability across the pH range of pH 4.5 to pH 10 has been reported for poxviruses [35], and the obtained results for the ORFV (pH 5–7.4) are within these values. This also accounts for the high infectivity preservation in the presence of different buffering substances (HEPES, PBS, TRIS, CPB). In comparison with other poxviruses, the vaccinia-based vaccines are formulated in 6–8 mM HEPES at pH 6.5–7.5 (ACAM2000® [40]), in 10 mM TRIS buffer at pH 7.7 (JYNNEOS™ [54] and IMVANEX [49]). The decision for an appropriate buffering substance might depend on the virus stability, the DSP unit operation, the pharmaceutical application, and economics. Thus, the results suggested that the buffer for the ORFV DSP and formulation can be chosen from HEPES, TRIS, and PBS, titrated to pH 5–7.4, and for short-term incubation pH 10.

3.5. Influence of ionic strength and salt type

Just as the variation in pH, the salt type and concentration are utilized throughout the DSP to optimize and/or prevent adsorption processes. The salts NaCl, $MgCl_2$, and NH_4Cl were chosen due to their frequent application in DSP processes and formulations. NaCl is commonly supplemented as an additive in formulations or elution processes, e.g., for an ion exchange, while kosmotropic salts, such as NH_4Cl and $(NH_4)_2SO_4$, are frequently added for a hydrophobic interaction chromatography [55]. $MgCl_2$ is known as a stabilizer in vaccine formulations [56], as well as a supplement for different nuclease treatments [26]. The conducted experiments indicated no influence of $MgCl_2$ and NaCl up to 45 mS cm^{-1} on ORFV infectivity stability, and only after 7 d an increasing ionic strength (45 mS cm^{-1}) showed a substantial titer reduction of 0.1–0.2 log compared to lower salt concentrations (15 mS cm^{-1}). On the contrary, NH_4Cl reduced the ORFV titer significantly already for 15 mS cm^{-1}. Correlated with literature data, 15 mS cm^{-1} NaCl has been used as a formulation buffer for the vaccinia-based vaccines ACAM2000® (85–120 mM) [40] and JYNNEOS™ (140 mM) [54], indicating a high stability in the presence of this salt concentration. Furthermore, Lothert *et al.* [27] used 0.4 M NaCl (approx. 45 mS cm^{-1}) for their freeze-thaw stability studies, which were already described in **section 3.2**, indicating a tolerance of the ORFV infectivity against this salt concentration. Furthermore, the virus inactivation due to NH_4Cl has been reported in literature, e.g., for poliovirus [57], as would be expected based on its kosmotropic function. Hence, the application of NaCl and $MgCl_2$ in DSP operations can be undertaken without reservations with up to 45 mS cm^{-1}.

3.6. Mechanical stress

Mechanical stress affects viral particles throughout the biotechnological production process, i.e., liquid handling and mixing by pumps and tubing as well as in the unit operations themselves, such as during filtration [58] or chromatography [59]. To investigate the shear sensitivity of the ORFV, three different methods, pumping, ultrasonication, and mixing by vortex, exemplary for the DSP, were applied. The pumping in peristaltic pumps is ubiquitous in the DSP. The ORFV was stressed for up to 60 min by cycling in a peristaltic pump, with roughly one complete volumetric cycle per minute. The applied shear stress of 999 mPa with a volumetric power input of 10^{-3} W mL^{-1} led to a significant loss of infectivity (<0.1 log) after 30 min. A similar study conducted for the measles virus indicated a considerable degradation after 60 min with three cycles per minute, and shear stress of 295 mPa [28]. Using **Equation (1)**, the volumetric power input of this experiment with measles can be calculated to be approximately 0.07×10^{-3} W mL^{-1}. Loewe *et* al. [28] also pointed out that the applied shear rate in their experiment with measles was low compared to conventional tangential flow filtration systems, and the peristaltic pump head may therefore have induced the degradation. The comparison of our results with the described measles study [28] might indicate that the 15-times higher applied power input and three-times higher shear stress inactivated the ORFV more effectively than the cycling in the peristaltic pump itself.

As a second method, an ultrasonication of ORFV samples was conducted for up to 3 min at 0.1 W mL^{-1} and 35 kHz, showing a substantial ORFV infectivity loss (<0.1 log) after 2 min. The application of ultrasonication may be applied for a cell lysis after biotechnological production to release the viral particles, but it can also damage [60] or inactivate [61] enveloped viruses. A study for the lymphocytic choriomeningitis virus used sonication as a sample preparation method for three times 15 s [45], while 1 min at 45 kHz has been used for the MVA virus [62] with no reduction in the virus titer. An additional study used sonication (582, 862, and 1142 kHz) for 10–15 s with 0.24 W mL^{-1} to disintegrate tanapox virus aggregates without an infectious virus titer loss [61]. All three applications lie within the applied spectrum for the ORFV in

our study, although it should be noted that the samples in this experiment were not cooled.

Last, the ORFV was subjected to up to 3 min of orbital mixing by a vortex, resulting in no significant change of the virus titer. Although the exact power input by this method is hard to determine, this finding is of practical interest for the lab-scale sample handling.

In conclusion, the ORFV shows a high robustness against the applied mixing procedure, but a sensitivity towards ultrasonication and shear stress, induced by pumping in a peristaltic pump.

4. Conclusion

The development of an efficient and robust production process for the pharmaceutical industry requires an extensive knowledge of the target. In the presented work, forced degradation studies of the ORFV were applied to elucidate possible critical process parameters for the development of a large-scale DSP process, and for formulation studies focused on ORFV infectivity preservation. The investigations included thermal, freeze-thaw, chemical (salts and buffers), and mechanical stress conditions. Additionally, the pI of the ORFV was determined at pH 3.5 in 0.1 M CPB. The findings of the chemical stress studies showed a high robustness of the ORFV infectivity against a storage in pH 5 to pH 7.4, different buffers (TRIS, PBS, HEPES), and certain salts ($MgCl_2$, NaCl) up to 45 mS cm^{-1}. These results offer a degree of flexibility for the DSP and formulation, based on recovery and economic rationales. Furthermore, the applied thermal stress elucidated that an incubation of ORFV at 37 °C showed no virus titer loss up to 2 d, and rHSA supplementation increased the stability. Based on the increased infectivity preservation in presence of rHSA, this additive could be considered as a valuable excipient. The testing of the freeze-thaw stability of the ORFV revealed a complete infectivity preservation up to 20 freeze-thaw cycles (−80 °C / room temperature), but increased the aggregation of the virus. Hence, a lyophilisation of the ORFV genotype in our study might be a promising option for formulation, but needs further investigation. However, different chemical stress conditions reduced the ORFV viral titer, i.e., the addition of NH_4Cl (15–45 mS cm^{-1}), the buffering substance CPB (0.1 M), acidic pH values (up to pH 4). Additionally, the ORFV infectivity reduction only tolerated mechanical stress induced by pumping in a peristaltic pump (15 min), ultrasonication (2 min), and mixing by a vortex (3 min). Hence, the shear stress should be evaluated carefully in unit operations such as filtration. To conclude, several limitations in the application of DSP unit operations were identified by forced degradation studies, which might reduce the recovery and product quality. This knowledge will accelerate the optimisation of any ORFV DSP, or help to implement new unit operations and formulation considerations.

5. Material and methods

5.1. Orf virus (ORFV) propagation

The production of ORFV, strain D1701-V and including a green fluorescent (GFP) marker gene, in Vero cells was conducted as previously described [19]. In short, adherent Vero cells were propagated in Dulbecco's Modified Eagle's Medium (DMEM) (Gibco, Waltham, US-MA) + 5 % fetal calf serum (FCS) (Capricorn Scientific, Ebsdorfergrund, GER) in T225 CytoOne® flasks (Starlab International, Hamburg, GER) and infected at a multiplicity of infection of 0.05. To terminate virus production at 70 % cytopathic effect of the cell layer cell culture flasks were subjected to a freeze-thaw-cycle (−70 °C, 37 °C).

5.2. Virus purification

ORFV from a Vero cell culture was purified either by ultracentrifugation or by a complete DSP train. The latter was performed as described by Lothert *et al.* [26] via a two-step filtration (5 µm and 0.65 µm) or centrifugation (300 × *g* for 15 min and 4500 × *g* for 30 min), steric exclusion chromatography, and Capto Core 700. The ultracentrifugation through 36 % sucrose cushion of the ORFV was prepared according to [36] without the subsequent sucrose density gradient centrifugation. In short, 900 mL cell culture supernatant were clarified and subsequently purified via the centrifugation train (TFA20-rotor, Beckman Coulter, Krefeld, Germany). The final sample volume was 2 mL.

5.3. Analysis of infectivity

The quantification of infectious viral particles was conducted by fluorescence-activated cell counting in either a flow cytometer (Guava easyCyte HT, Merck Millipore, Burlington, US-MA) as previously described [19,63], or a real-time image-based quantification with the Incucyte life cell analysis system (Incucyte S3, Sartorius, Royston, UK) adapted from Labisch *et al.* [64]. Adaption: On day three no staining was performed, due to the use of a GFP-construct. The read-out took place 24 h post-infection. Measurements were performed at least in triplicates.

5.4. Influence of stress parameters on ORFV infectivity

5.4.1. Temperature

Purified ORFV was incubated for 24 h, 48 h, 7 d, and 14 d at 4 °C in a fridge, and at 37 °C in an incubator (HeraCell 160i, Thermo Fisher Scientific, Waltham, MA, USA). Samples were supplemented either with (0.25 % or 0.5 %) or without recombinant human serum albumin (rHSA). The rHSA, Recombumin® Prime, was kindly provided by Albumedix (Nottingham, UK). All samples were stored under the exclusion of light. After incubation, the samples were immediately prepared for an infectivity analysis. The positive control was the untreated sample on day zero.

5.4.2. Freeze-thaw cycles

The purified ORFV suspension was aliquoted in 1.5-mL tubes and frozen at −80 °C. Afterwards, the tubes were thawed by an incubation in a water bath at room temperature until no ice was visible. This procedure was repeated for 1, 2, 5, and 8 freeze-thaw cycles with and without the addition of rHSA (0.25 % or 0.5 %). The single freeze-thaw cycle served as a positive control. Additionally, non-supplemented samples were treated with the same procedure but for 1, 5, and 20 cycles and the size distribution of the thawed virus suspension was measured by dynamic light scattering (DLS) using a Zetasizer Nano ZS90 (Malvern Panalytical, Malvern, UK) and micro cuvettes DTS1070 (Sarstedt, Nuermbrecht, Germany). The data was processed with the corresponding Zetasizer software, version 7.13. The refractive index and viscosity were assumed to be equal to water.

5.4.3. Buffers and inorganic salts

Purified ORFV was diluted 1:50 in 20 mM TRIS, 50 mM HEPES, 0.1 M CPB (citrate–phosphate buffer) or PBS (phosphate buffered saline), all at pH 7.4, and adjusted to 15 mS/cm with NaCl. Ionic strength measurements were conducted with NH_4Cl, NaCl, and $MgCl_2$, at 15, 35, or 45 mS/cm, using a 1:50 dilution with ORFV suspension. All samples were stored at 4 °C under the exclusion of light, and samples were taken after 24 h and 48 h. The positive control was an ORFV suspension diluted 1:50 in DMEM (pH 7.2), supplemented with 5 % FCS.

5.4.4. pH and isoelectric point (pI)

The ORFV suspension was diluted 1:50 in 0.1 M HCl-KCl buffer (pH 2), 0.1 M CPB (pH 3–7.4), or 0.1 M carbonate buffer (pH 10), all adjusted to a constant ionic strength of 15 mS cm^{-1} with NaCl. Controls were incubated in DMEM (pH 7.2), supplemented with 5 % FCS. These were stored at 4 °C under the exclusion of light, and samples for infectivity determination were taken after 24 h, 48 h, 14 d, 30 d, and 60 d.

Measurements of the ORFV pI were undertaken via a size-based and a charge-based approach, both performed with the Zetasizer Nano ZS90 system. The size-based approach, measured by DLS (see section 5.4.2), was implemented to either determine the size distribution after 15 min of incubation, or to record a time-dependent size distribution in duplicates (n = 2), measuring every 5 min. The charge measurements were conducted via phase analysis light scattering in ZEN0118 cuvettes (Malvern Panalytical, Malvern, UK). The respective zeta potential was calculated using the Smoluchowski equation. All samples for the pI assessment were diluted 1:20 in 0.1 M HCl-KCl buffer (pH 2) or 0.1 M CPB (pH 3 7.4). Only the charge-based measurements were conducted with pre-purified ORFV, which was concentrated using spin column filters with a 30 kDa molecular weight cut-off (regenerated cellulose, Amicon® Ultra-15, Merck, Darmstadt, GER) instead of the Capto Core700 application, described in Section 5.2.

5.4.5. Mechanical stress

The influence of mechanical stress on the ORFV infectivity was investigated by cycling the purified ORFV samples through a peristaltic pump (#120U, Watson Marlow, Marlow, UK) setup at a flow rate of 23.5 mL min^{-1}. Here, a tube (ambrCF TuFLux SIL 1/16″ x 3/16″ tubing, 60 cm) was connected to the peristaltic pump and a reservoir containing 20 mL of the ORFV sample. Pumping was performed for 15, 30, and 60 min. A sample incubated for 15, 30, or 60 min at room temperature served as a negative control. Shear stress and the shear rate for a tube were calculated according to [28], assuming water at 20 °C (viscosity of 1.002 mPas and a density of 998 kg m^{-3}). The volumetric energy input induced in the tubes was calculated as follows:

$$\frac{P}{V} = \dot{\gamma}\tau = \mu\dot{\gamma}^2 \quad (1)$$

P [W] represents the power input, V [m^3] the specific volume, τ [mPa] the shear stress, and $\dot{\gamma}$ [s^{-1}] the shear rate. Shear rate and shear stress are related as:

$$\tau = \dot{\gamma}\mu \quad (2)$$

Furthermore, ultrasonication (Sonorex RK510 H, 6.6 L and 640 W, Bandelin, Berlin, GER) at 0.1 W mL^{-1} and 35 kHz, and vortexing (Genie-2 Mixer, Scientific Industries, Bohemia, NY, USA) at the highest speed (2,700 min^{-1}) were applied without cooling. For sampling, time intervals of 0.5, 1, 2, and 3 min were chosen for mixing with vortex and ultrasonication, respectively. An untreated sample stored at room temperature for the corresponding time intervals served as a negative control.

5.5. Statistical analysis

All experiments were conducted in triplicates (n = 3) unless stated otherwise, and mean values as well as standard deviations were calculated from these. An analysis of significance was performed via an appropriate ANOVA with a *Tukey* test (OriginPro 2018G, OriginLab, Northampton, MA, USA). Degrees of significance are expressed as * for α = 0.05, ** for α = 0.01, and *** for α = 0.001. Insignificant differences between samples were declared as such if tested negative for α = 0.05.

CRediT authorship contribution statement

Friederike Eilts: Conceptualization, Validation, Investigation, Visualization, Writing – original draft. **Jennifer J. Labisch:** Conceptualization, Investigation, Writing – review & editing. **Sabri Orbay:** Investigation, Writing – review & editing. **Yasmina M.J. Harsy:** Investigation, Formal analysis, Writing – review & editing. **Marleen Steger:** Investigation, Writing – review & editing. **Felix Pagallies:** Resources, Writing – review & editing. **Ralf Amann:** Writing – review & editing, Supervision, Funding acquisition. **Karl Pflanz:** Writing – review & editing, Supervision, Funding acquisition. **Michael W. Wolff:** Writing – review & editing, Supervision, Funding acquisition.

Declaration of Competing Interest

The authors declare the following financial interests/personal relationships which may be considered as potential competing interests: RA is CEO of Prime Vector Technologies, a company developing the Orf virus vector platform. FE was employed by the University of Tuebingen on an Orf virus project before the time of this study. All other authors declare no conflict of interest.

Acknowledgements

The authors would like to thank Philip Wiese for the support with the infectivity analytics as well as Keven Lothert and Catherine Meckel-Oschmann for the proofreading of the manuscript. We kindly thank Albumedix Ltd. for the provided rHSA, Recombumin Prime, used in this study. The graphical abstract was created with *biorender.com*. This work was financially supported by the Heinrich-Böll-Foundation with a doctoral scholarship to F. Eilts. Additionally, an EXIST-Forschungstransfer grant (03EFKBW171) of the German Federal Ministry for Economic Affairs and Energy was granted and the project was co-funded by the European Regional Development Fund as part of the Union's response to the COVID-19 pandemic (IGJ-ERDF-Program Hesse - React EU 20008790). The presented manuscript is part of F. Eilts' dissertation at the Graduate Centre for Engineering Sciences under the aegis of the Justus Liebig University Giessen, Germany, in cooperation with the University of Applied Sciences Mittelhessen, Giessen, Germany.

Submission declaration

All authors consent with the presented manuscript.

Data availability statement

All relevant data are within the paper.

References

[1] Nagington J, Horne RW. Morphological studies of Orf and vaccinia viruses. Virology 1962;16(3):248–60. https://doi.org/10.1016/0042-6822(62)90245-3.
[2] Nitsche A, Gelderblom HR, Eisendle K, Romani N, Pauli G. Pitfalls in diagnosing human poxvirus infections. J Clin Virol 2007;38(2):165–8. https://doi.org/10.1016/j.jcv.2006.11.013.
[3] Wang R, Luo S. Orf virus: A new class of immunotherapy drugs. In: Vlachakis D, editor. Systems Biology. London: IntechOpen; 2019.
[4] Spehner D, de Carlo S, Drillien R, Weiland F, Mildner K, Hanau D, et al. Appearance of the bona fide spiral tubule of ORF virus is dependent on an intact 10-kilodalton viral protein. J Virol 2004;78(15):8085–93. https://doi.org/10.1128/JVI.78.15.8085-8093.2004.
[5] Bora DP, Bhanupraka V, Venkatesan G, Balamuruga V, Prabhu M, Yogisharad R. Effect of stabilization and reconstitution on the stability of a novel strain of live attenuated Orf vaccine (ORFV MUK59/05). Asian J Anim Vet Adv 2015;10(8):365–75. https://doi.org/10.3923/ajava.2015.365.375.

[6] Musser JMB, Taylor CA, Guo J, Tizard IR, Walker JW. Development of a contagious ecthyma vaccine for goats. Am J Vet Res 2008;69(10):1366–70. https://doi.org/10.2460/ajvr.69.10.1366.
[7] Bala JA, Balakrishnan KN, Abdullah AA, Mohamed R, Haron AW, Jesse FFA, et al. The re-emerging of orf virus infection: A call for surveillance, vaccination and effective control measures. Microb Pathog 2018;120:55–63. https://doi.org/10.1016/j.micpath.2018.04.057#.
[8] Rziha H-J, Büttner M. Parapoxviruses. In: Reference Module in Life Sciences. Elsevier; 2020, p. 1505.
[9] Reguzova A, Ghosh M, Müller M, Rziha H-J, Amann R. Orf virus-based vaccine vector D1701-V induces strong CD8+ T cell response against the transgene but not against ORFV-derived epitopes. Vaccines 2020;8(2):. https://doi.org/10.3390/vaccines8020295295.
[10] Friebe A, Siegling A, Friederichs S, Volk H-D, Weber O. Immunomodulatory effects of inactivated parapoxvirus ovis (ORF virus) on human peripheral immune cells: induction of cytokine secretion in monocytes and Th1-like cells. J Virol 2004;78(17):9400–11. https://doi.org/10.1128/JVI.78.17.9400-9411.2004.
[11] García-Arriaza J, Esteban M. Enhancing poxvirus vectors vaccine immunogenicity. Hum Vaccin Immunother 2014;10(8):2235–44. https://doi.org/10.4161/hv.28974.
[12] Rziha H-J, Büttner M, Müller M, Salomon F, Reguzova A, Laible D, et al. Genomic characterization of Orf virus strain D1701-V (parapoxvirus) and development of novel sites for multiple transgene expression. Viruses 2019;11(2):. https://doi.org/10.3390/v11020127127.
[13] Rintoul JL, Lemay CG, Tai LH, Stanford MM, Falls TJ, de SCT, et al. ORFV: a novel oncolytic and immune stimulating parapoxvirus therapeutic. Mol Ther 2012;20(6):1148–57. https://doi.org/10.1038/mt.2011.301.
[14] Fischer T, Planz O, Stitz L, Rziha H-J. Novel recombinant parapoxvirus vectors induce protective humoral and cellular immunity against lethal herpesvirus challenge infection in mice. J Virol 2003;77(17):9312–23. https://doi.org/10.1128/jvi.77.17.9312-9323.2003.
[15] Wang R, Wang Y, Liu F, Luo S. Orf virus: A promising new therapeutic agent. Rev Med Virol 2019;29(1):e2013.
[16] O'Leary MP, Choi AH, Kim S-I, Chaurasiya S, Lu J, Park AK, et al. Novel oncolytic chimeric orthopoxvirus causes regression of pancreatic cancer xenografts and exhibits abscopal effect at a single low dose. J Transl Med 2018;16(1):. https://doi.org/10.1186/s12967-018-1483-x110.
[17] Schneider M, Müller M, Yigitliler A, Xi J, Simon C, Feger T, et al. Orf virus-based therapeutic vaccine for treatment of papillomavirus-induced tumors. J Virol 2020;94(15). https://doi.org/10.1128/JVI.00398-20.
[18] Fleming SB, Wise LM, Mercer AA. Molecular genetic analysis of orf virus: a poxvirus that has adapted to skin. Viruses 2015;7(3):1505–39. https://doi.org/10.3390/v7031505.
[19] Rziha H-J, Rohde J, Amann R. Generation and selection of Orf virus (ORFV) recombinants. Methods Mol Biol 2016;1349:177–200. https://doi.org/10.1007/978-1-4939-3008-1_12.
[20] Amann R, Rohde J, Wulle U, Conlee D, Raue R, Martinon O, et al. A new rabies vaccine based on a recombinant ORF virus (parapoxvirus) expressing the rabies virus glycoprotein. J Virol 2013;87(3):1618–30. https://doi.org/10.1128/JVI.02470-12.
[21] Friebe A, Siegling A, Weber O. Inactivated Orf-virus shows disease modifying antiviral activity in a guinea pig model of genital herpesvirus infection. J Microbiol Immunol Infect 2018;51(5):587–92. https://doi.org/10.1016/j.jmii.2017.03.002.
[22] Rohde J, Schirrmeier H, Granzow H, Rziha H-J. A new recombinant Orf virus (ORFV, Parapoxvirus) protects rabbits against lethal infection with rabbit hemorrhagic disease virus (RHDV). Vaccine 2011;29(49):9256–64. https://doi.org/10.1016/j.vaccine.2011.09.121.
[23] Rohde J, Amann R, Rziha H-J. New Orf virus (Parapoxvirus) recombinant expressing H5 hemagglutinin protects mice against H5N1 and H1N1 influenza A virus. PLoS One 2013;8(12):e83802.
[24] van Rooij E, Rijsewijk F, Moonen-Leusen HW, Bianchi A, Rziha H-J. Comparison of different prime-boost regimes with DNA and recombinant Orf virus based vaccines expressing glycoprotein D of pseudorabies virus in pigs. Vaccine 2010;28(7):1808–13. https://doi.org/10.1016/j.vaccine.2009.12.004.
[25] Cowan G, Smith P, Christofilogiannis P. Fish vaccines: The regulatory process and requirements from the laboratory bench to a final commercial product, including field trials. In: Adams A, editor. Fish Vaccines. Basel: Springer Basel; 2016. p. 105–18.
[26] Lothert K, Pagallies F, Eilts F, Sivanesapillai A, Hardt M, Moebus A, et al. A scalable downstream process for the purification of the cell culture-derived Orf virus for human or veterinary applications. J Biotechnol 2020;323:221–30. https://doi.org/10.1016/j.jbiotec.2020.08.014.
[27] Lothert K, Pagallies F, Feger T, Amann R, Wolff MW. Selection of chromatographic methods for the purification of cell culture-derived Orf virus for its application as a vaccine or viral vector. J Biotechnol 2020;323:62–72. https://doi.org/10.1016/j.jbiotec.2020.07.023.
[28] Loewe D, Häussler J, Grein TA, Dieken H, Weidner T, Salzig D, et al. Forced degradation studies to identify critical process parameters for the purification of infectious measles virus. Viruses 2019;11(8). https://doi.org/10.3390/v11080725.
[29] Schmidt AS. Forced degradation studies for biopharmaceuticals. BioPharm International 2016;29(7).
[30] Kats M. Forced degradation studies: Regulatory considerations and implementation. BioPharm International 2005;18(7):40–5.
[31] Hasija M, Li L, Rahman N, Salvador FA. Forced degradation studies: an essential tool for the formulation development of vaccines. VDT 2013;3:11–33. https://doi.org/10.2147/VDT.S41998.
[32] Evans RK, Nawrocki DK, Isopi LA, Williams DM, Casimiro DR, Chin S, et al. Development of stable liquid formulations for adenovirus-based vaccines. J Pharm Sci 2004;93(10):2458–75. https://doi.org/10.1002/jps.20157.
[33] Zhao Q, Wang Y, Abraham D, Towne V, Kennedy R, Sitrin RD. Real time monitoring of antigenicity development of HBsAg virus-like particles (VLPs) during heat- and redox-treatment. Biochem Biophys Res Commun 2011;408(3):447–53. https://doi.org/10.1016/j.bbrc.2011.04.048.
[34] Sturgess AW, Rush K, Charbonneau RJ, Lee JI, West DJ, Sitrin RD, et al. Haemophilus influenzae type b conjugate vaccine stability: catalytic depolymerization of PRP in the presence of aluminum hydroxide. Vaccine 1999;17(9–10):1169–78. https://doi.org/10.1016/S0264-410X(98)00337-5.
[35] Rheinbaben Fv, Gebel J, Exner M, Schmidt A. Environmental resistance, disinfection, and sterilization of poxviruses. In: Mercer AA, Schmidt A, Weber O, editors. Poxviruses. Basel: Birkhäuser Basel; 2007, p. 397–405.
[36] Joklik WK. The purification of four strains of poxvirus. Virology 1962;18(1):9–18. https://doi.org/10.1016/0042-6822(62)90172-1.
[37] Eilts F, Steger M, Pagallies F, Rziha H-J, Hardt M, Amann R, et al. Comparison of sample preparation techniques for the physicochemical characterization of Orf virus particles. J Virol Methods 2022;114614. https://doi.org/10.1016/j.jviromet.2022.114614.
[38] Kumru OS, Joshi SB, Smith DE, Middaugh CR, Prusik T, Volkin DB. Vaccine instability in the cold chain: Mechanisms analysis and formulation strategies. Biologicals 2014;42(5):237–59. https://doi.org/10.1016/j.biologicals.2014.05.007.
[39] Capelle MAH, Babich L, van Deventer-Troost JPE, Salerno D, Krijgsman K, Dirmeier U, et al. Stability and suitability for storage and distribution of Ad26.ZEBOV/MVA-BN®-Filo heterologous prime-boost Ebola vaccine. Eur J Pharm Biopharm 2018;129:215–21. https://doi.org/10.1016/j.ejpb.2018.06.001.
[40] Greenberg RN, Kennedy JS. ACAM2000: a newly licensed cell culture-based live vaccinia smallpox vaccine. Expert Opin Inv Drug 2008;17(4):555–64. https://doi.org/10.1517/13543784.17.4.555.
[41] Kline RL, Regnery RL, Armstrong GL, Damon IK. Stability of diluted smallpox vaccine under simulated clinical conditions. Vaccine 2005;23(41):4944–6. https://doi.org/10.1016/j.vaccine.2005.05.016.
[42] Newman FK, Frey SE, Blevins TP, Yan L, Belshe RB. Stability of undiluted and diluted vaccinia-virus vaccine. Dryvax J Infect Dis 2003;187(8):1319–22. https://doi.org/10.1086/374564.
[43] Chambers AE, Dixon MM, Harvey SP. Studies of the suitability of fowlpox as a decontamination and thermal stability simulant for variola major. Int J Microbiol 2009;2009:. https://doi.org/10.1155/2009/158749158749.
[44] Wiedmann RT, Reisinger KS, Hartzel J, Malacaman E, Senders SD, Giacoletti KED, et al. M-M-R(®)II manufactured using recombinant human albumin (rHA) and M-M-R(®)II manufactured using human serum albumin (HSA) exhibit similar safety and immunogenicity profiles when administered as a 2-dose regimen to healthy children. Vaccine 2015;33(18):2132–40. https://doi.org/10.1016/j.vaccine.2015.03.017.
[45] Laposova K, Oveckova I, Tomaskova J. A simple method for isolation of cell-associated viral particles from cell culture. J Virol Methods 2017;249:194–6. https://doi.org/10.1016/j.jviromet.2017.09.014.
[46] Amorij J-P, Huckriede A, Wilschut J, Frijlink HW, Hinrichs WLJ. Development of stable influenza vaccine powder formulations: challenges and possibilities. Pharm Res 2008;25(6):1256–73. https://doi.org/10.1007/s11095-008-9559-6.
[47] Chen D, Kristensen D. Opportunities and challenges of developing thermostable vaccines. Expert Rev Vaccines 2009;8(5):547–57. https://doi.org/10.1586/erv.09.20.
[48] van Vloten JP, Minott JA, McAusland TM, Ingrao JC, Santry LA, McFadden G, et al. Production and purification of high-titer OrfV for preclinical studies in vaccinology and cancer therapy. Mol Ther Methods Clin Dev 2021;23:434–47. https://doi.org/10.1016/j.omtm.2021.08.004.
[49] European Medicines Agency. Assessment report IMVANEX. [August 04, 2021]; Available from: https://www.ema.europa.eu/en/documents/assessment-report/imvanex-epar-public-assessment-report_en.pdf.
[50] Gerba CP, Betancourt WQ. Viral aggregation: Impact on virus behavior in the environment. Environ Sci Technol 2017;51(13):7318–25. https://doi.org/10.1021/acs.est.6b05835.
[51] Taylor DH, Bosmann H. Measurement of the electrokinetic properties of vaccinia and reovirus by laser-illuminated whole-particle microelectrophoresis. J Virol Methods 1981;2(5):251–60. https://doi.org/10.1016/0166-0934(81)90023-9.
[52] Kaplan C. The influence of some metal ions and pH on the inactivation of vaccinia virus by heat. J Gen Microbiol 1963;31(2):311–4.
[53] Kaplan C. The heat inactivation of vaccinia virus. J Gen Microbiol 1958;18(1):58–63. https://doi.org/10.1099/00221287-18-1-58.
[54] Bavarian Nordic A/S. Package insert JYNNEOS. [August 05, 2021]; Available from: https://www.fda.gov/media/131078/download.
[55] Wolff MW, Reichl U. Downstream processing of cell culture-derived virus particles. Expert Rev Vaccines 2011;10(10):1451–75. https://doi.org/10.1586/erv.11.111.
[56] Selvaraj J, Formulation RV. Efficacy and immunogenicity studies of a liquid state rabies vaccine with magnesium chloride as stabilizer. J Vaccines Vaccin 2015;06(05). https://doi.org/10.4172/2157-7560.1000292.

[57] Cramer WN, Burge WD, Kawata K. Kinetics of virus inactivation by ammonia. Appl Environ Microb 1983;45(3):760–5. https://doi.org/10.1128/aem.45.3.760-765.1983.
[58] Eilts F, Harnischfeger J, Loewe D, Wolff MW, Salzig D, Czermak P. Production of baculovirus and stem cells for baculovirus-mediated gene transfer into human mesenchymal stem cells. In: Pfeifer BA, Hill A, editors. Vaccine Delivery Technology. Springer, US: New York, NY; 2021. p. 367–90.
[59] Hoffmann D, Leber J, Loewe D, Lothert K, Oppermann T, Zitzmann J, et al. Purification of new biologicals using membrane-based processes. In: Basile AB, Charcosset C, editors. Current trends and future developments on (bio-) membranes: Membrane processes in the pharmaceutical and biotechnological field. Amsterdam: Elsevier; 2019. p. 123–50.
[60] Haywood AM. Membrane uncoating of intact enveloped viruses. J Virol 2010;84(21):10946–55. https://doi.org/10.1128/JVI.00229-10.
[61] Chrysikopoulos CV, Manariotis ID, Syngouna VI. Virus inactivation by high frequency ultrasound in combination with visible light. Colloid Surface B 2013;107:174–9. https://doi.org/10.1016/j.colsurfb.2013.01.038.
[62] Vázquez-Ramírez D, Genzel Y, Jordan I, Sandig V, Reichl U. High-cell-density cultivations to increase MVA virus production. Vaccine 2018;36(22):3124–33. https://doi.org/10.1016/j.vaccine.2017.10.112.
[63] Lothert K, Dekevic G, Loewe D, Salzig D, Czermak P, Wolff MW. Upstream and downstream processes for viral nanoplexes as vaccines. In: Pfeifer BA, Hill A, editors. Vaccine Delivery Technology. Springer, US: New York, NY; 2021. p. 217–48.
[64] Labisch JJ, Wiese GP, Barnes K, Bollmann F, Pflanz K. Infectious titer determination of lentiviral vectors using a temporal immunological real-time imaging approach. PLoS One 2021;16(7):e0254739.

Part C: Stable formulations for Orf virus storage and processing

Eilts, F.; Harsy, Y. M. J.; Lothert, K.; Pagallies, F.; Dalby, P.; Amann, R.; Wolff, M. W. (2023, submitted). Investigation of excipients for a stable Orf viral vector formulation. Journal of Virus Research, VIRUS-D-23-00288.

Virus Research 336 (2023) 199213

Contents lists available at ScienceDirect

Virus Research

journal homepage: www.elsevier.com/locate/virusres

An investigation of excipients for a stable Orf viral vector formulation

Friederike Eilts [a,1], Yasmina M.J. Harsy [a], Keven Lothert [a], Felix Pagallies [b], Ralf Amann [b,c], Michael W. Wolff [a,*]

[a] Institute of Bioprocess Engineering and Pharmaceutical Technology, University of Applied Sciences Mittelhessen (THM), Wiesenstr.14, Giessen 35390, Germany
[b] Department of Immunology, University of Tuebingen, Auf der Morgenstelle 15, Tuebingen 72076, Germany
[c] PRiME Vector Technologies, Herrenberger Straße 24, Tuebingen 72070, Germany

ARTICLE INFO

Keywords:
Formulation
Poxvirus
Recombinant human serum albumin
SARS-CoV-2 vaccine
Thermo-stability
Vector vaccines
viral vectors

ABSTRACT

The Orf virus (ORFV) is a promising candidate for vector vaccines as well as for immunomodulatory and oncolytic therapies. However, few publications are available on its infectivity degradation or on suitable additives for prolonging its viral stability. In this study, the non-supplemented ORFV itself showed a very high stability at storage temperatures up to 28 °C, with a linear titer loss of 0.10 log infectious particles per day at 4 °C over a period of five weeks. To prolong this inherent stability, thirty additives, i.e., detergents, sugars, proteins, salts, and buffers as well as amino acids, were tested for their time- and temperature-dependent influence on the ORFV infectivity. A stabilizing effect on the infectivity was identified for the addition of all tested proteins, i.e., gelatine, bovine serum albumin, and recombinant human serum albumin (rHSA), of several sugars, i.e., mannitol, galactose, sucrose, and trehalose, of amino acids, i.e., arginine and proline, of the detergent Pluronic F68, and of the salt Na_2SO_4. The infectivity preservation was especially pronounced for proteins in liquid and frozen formulations, sugars in frozen state, and arginine und Pluronic in liquid formulations at high storage temperatures (37 °C). The addition of 1% rHSA with and without 5% sucrose was evaluated as a very stable formulation with a high safety profile and economic validity at storage temperatures up to 28 °C. At increased temperatures, the supplementation with 200 mM arginine performed better than with rHSA. In summary, this comprehensive data provides different options for a stable ORFV formulation, considering temperature, storage time, economic aspects, and downstream processing integrity.

1. Introduction

More recently, the Orf virus (ORFV), *Parapoxvirus ovis*, has gained attention as a viral vector and has been tested as an immunomodulatory (Fleming et al., 2015) and oncolytic agent (2018; Rintoul et al., 2012; Schneider et al., 2020) as well as a vector vaccine (Amann et al., 2013; Friebe et al., 2018; Rohde et al., 2011, 2013; Rziha et al., 2016, 2019; van Rooij et al., 2010), among these as anti-SARS-CoV-2 vaccine (Reguzova et al., 2023). The ovoid virus is roughly 140×300 nm in size (Nagington and Horne, 1962; Nitsche et al., 2007; Wang and Luo, 2019) and covered by a tubule-like structure (Spehner et al., 2004), resembling a ball of wool. Recombinant ORFV like the D1701-V vector possess several beneficial characteristics for pharmaceutical application (Müller et al., 2022), i.e., for (i) the mediation of a strong humoral and cellular immune response,(ii) a long-term protective immunity against the target antigens without attacking the ORFV vector (Rziha and Büttner, 2020), (iii) a short-lived duration of the ORFV-specific immunity, which allows for re-immunization (Fischer et al., 2003; Reguzova et al., 2020; Rintoul et al., 2012; Rziha and Büttner, 2020), (iv) a restricted host range, and (v) the lack of systemic spread (Fischer et al., 2003; Reguzova et al., 2020; Rziha et al., 2019).

The potency of the live ORFV as a pharmaceutical product is determined by its infectivity, which must be monitored for an effective application. This accounts for the extensive production process, including the virus propagation, the purification, the formulation, as well as the storage and the distribution until the application. Concerning the ORFV, a recent work from our group tested process-related parameters such as the shear force, the heat- and freeze-thaw stress, the pH,

Abbreviations: DOE, design of experiments; FCS, fetal calf serum; IU, infectious units; MVA virus, modified vaccinia Ankara virus; NCTRL, negative control; ORFV, Orf virus; PCTRL, positive control; rHSA, recombinant human serum albumin (-E, Exbumin; -R, Recombumin Prime); TRIS, tris(hydroxymethyl)aminomethane.

* Corresponding author at: Wiesenstr.14, Giessen 35390, Germany.
E-mail address: michael.wolff@lse.thm.de (M.W. Wolff).
[1] Present address: Chair of Bioseparation Engineering, Technical University Munich, Boltzmannstraße 15, 85748 Garching, Germany.

https://doi.org/10.1016/j.virusres.2023.199213
Received 12 June 2023; Received in revised form 27 August 2023; Accepted 29 August 2023
0168-1702/© 2023 The Authors. Published by Elsevier B.V. This is an open access article under the CC BY license (http://creativecommons.org/licenses/by/4.0/).

and the ionic strength (Eilts et al., 2023). All tests indicated that the ORFV, like other poxviruses, is very robust against changes in environmental conditions. Next to applying this knowledge on environmental factors, the implementation of a stable formulation can reduce infectivity losses, especially throughout distribution and long-term storage. Potential excipients are evaluated with regard to the potency of the active pharmaceutical ingredient in terms of its infectivity preservation, the simplicity of the formulation composition as well as economic considerations for the formulation by reducing unit operations, material, and energy input (Cardoso et al., 2017), e.g., due to lyophilization (Kumru et al., 2018. Data on the composition of formulations for the ORFV is scarce. A report studies suitable formulations for an lyophilized ORFV vaccine against the natural Orf disease itself (Bora et al., 2015). Here, the addition of the protein lactalbumin, combined with the sugars sucrose or trehalose, revealed the best stabilizing effects even at elevated temperatures. Further conclusions may be drawn from formulations for the closely related modified vaccinia Ankara (MVA) virus, which has been traditionally used as a smallpox vaccine (Volz and Sutter, 2017) and found further application as a viral vector against other infectious diseases such as influenza (Rimmelzwaan and Sutter, 2009), Ebola (Capelle et al., 2018) or COVID-19 (García-Arriaza and Esteban, 2014). Selected marketed MVA-virus-based vaccines targeting smallpox are ACAM2000, JYNNEOS, and Imvanex. All three candidates are lyophilized, and a stable storage is possible for several years. The infectivity stabilization is conveyed by the addition of proteins (ACAM2000 (FDA, 2022a; Kumru et al. 2014)), sugars (ACAM2000 (FDA, 2022a; Kumru et al. 2014)), salts, and a suitable buffering system (Bavarian Nordic A/S, 2021; European Medicines Agency, 2013; FDA, 2022a; Greenberg and Kennedy, 2008; Kumru et al., 2014).

Based on the existing knowledge of the ORFV und MVA virus stability, we investigated the infectivity preservation of the ORFV in the presence of different liquid formulation buffers and additives, i.e., salts, amino acids, osmolytes, sugars, proteins, and surfactants. Additionally, the heat stability of the ORFV was analyzed, and the applicability of accelerated stability studies at elevated temperatures was evaluated. Finally, combinations of several excipients were used to propose options for ORFV formulations with an increased infectivity stability, considering potency and economics.

2. Materials and methods

Relative concentrations were provided in v/v for the liquid starting material, i.e., fetal calf serum (FCS), Pluronic, and Tween, and in w/v for the other substances.

2.1. Propagation and purification of the ORFV

For all experiments, the ORFV genotype D1701-V was used, expressing the green fluorescent protein AcGFP (D1701-V-GFP) (Rziha et al., 2019). The amplification of the virus in Vero cells, using DMEM (Gibco) with 5% FCS (Capricorn), was executed as previously reported by Rziha et al. (2016). After successful infection, the cell-culture was subjected to one freeze-thaw cycle (−80 °) and cell debris was removed by centrifugation (clarification) as previously described (Eilts et al., 2022b). For each set of experiments, several batches from this procedure were pooled to generate one stock. After the initial centrifugal clarification, the propagated ORFV was concentrated and purified, using a 37% sucrose cushion ultracentrifugation as described by Rziha et al. (2016). The infectious titer of the purified ORFV solution was $> 5 \times 10^8$ IU mL^{-1} (infectious units per mL). For one set of comparative studies (Section 3.1.2, **rHSA**), the ORFV was not prepared by ultracentrifugation, but by steric exclusion chromatography and Capto Core 700 chromatography, as reported by Lothert et al. (2020a). The latter preparation reached an infectious titer of 8×10^6 IU mL^{-1}. The methods were studied recently to generate comparable ORFV starting material (Eilts et al., 2022c). The ORFV titer was quantified by a flow cytometric assay described in Section 2.4.1 if not stated otherwise. All dilutions of the concentrated ORFV preparations were performed in the intended formulation buffer.

2.2. Stability studies of the candidate formulations

All substances were at least of analytical grade and their suppliers are listed in the **Supplementary Material S1**. The excipients were prepared in a concentrated manner in the intended buffer, i.e., 20 mM TRIS with either 20 or 180 mM NaCl or PBS, prior to their use. If not stated otherwise, the 20 mM TRIS buffer with 180 mM NaCl was applied. Each excipient (Table 1) solution was titrated to a neutral pH using HCl, 0.2 µm sterile filtered, and stored at 4 °C. Next, the concentrated excipients were combined according to their intended final concentration, again in the respective buffer. If not indicated otherwise, samples were supplemented with 1% penicillin/streptomycin (Sigma Aldrich). Last, the concentrated ORFV was added to achieve a final concentration of approximately 1×10^7 IU mL^{-1}. This time point was labeled as the start of the experimental kinetics t_0. Throughout the studies on ORFV titer reduction, the influence of the initial titer was decisive. We observed that a higher titer reduces the relative ORFV degradation compared to lower initial titer, which might be due to, e.g., adsorption of the ORFV to the storage containers or initial aggregation (Kline et al., 2005). Thus, the experiments were conducted with the same starting titer, if possible.

All formulated ORFV samples were stored either in 1.5 mL plastic tubes (crimp vial, VWR) or in 96-deepwell plates (1000 µL protein LoBind, Eppendorf). In the deep well plates, the surrounding wells were filled with 800 µL sterile PBS to reduce evaporation and sample volume reduction effects. The storage was done under the exclusion of light either in a freezer (−20 and −80 °C), in a fridge (4 °C), at controlled room temperature (22 °C), or in an incubator (28 and 37 °C). Samples

Table 1
Overview of single additives for the ORFV infectivity stability study.
All listed substances were applied as described in the main text. The supplementation was performed without other excipients, using the concentration ranges stated in the table. BSA, bovine serum albumin; EDTA, ethylenediaminetetraacetic acid; PBS, phosphate buffered saline; rHSA, recombinant human serum albumin; TRIS, tris(hydroxymethyl)aminomethane.

Section	Substance (Product name)	Concentration
3.1.1	Arginine	0 – 300 mM
3.1.2	BSA	2%
3.1.1	$CaCl_2$	2 – 150 mM
3.1.3	Dextran 40	0.5%
3.1.3	Galactose	2.5 – 10%
3.1.2	Gelatine type A, hydrolized	0.5%
3.1.3	Glucose	2.5 – 10%
3.1.1	Glutamine	50 mM
3.1.1	Glycine	50 mM
3.1.1	Histidine	50 mM
3.1.1	KCl	0 – 200 mM
3.1.3	Lactose	10%
3.1.3	Mannitol	0 – 10%
3.1.1	Methionine	50 mM
3.1.1	$MgCl_2$	0 – 150 mM
3.1.1	$MgSO_4$	0 – 200 mM
3.1.1	NaCl	0 – 200 mM
3.1.1	$NaNO_3$	0 – 200 mM
3.1.1	Na_2SO_4	0 – 200 mM
3.2.7	PBS	Pure
3.1.1	Poloxamere 188 (Pluronic F68)	0.05%
3.2.1	Proline	0 – 150 mM
3.1.2	rHSA-R (*Recombumin Prime*)	0 – 2%
3.1.2	rHSA-E (*Exbumin*)	0 – 2%
3.1.3	Sucrose	0 – 20%
3.1.3	Trehalose	0 – 20%
3.2.7	TRIS	20 mM
3.1.1	Tryptophane	50 mM
3.1.1	Tween 20	0.05%
3.1.1	Tween 80	0.05%

were frozen directly in the mentioned 96-well plates without further temperature control. The plates were filled to at least 80% of the wells, starting with 800 µL each, while the surrounding wells were filled with PBS to weaken the volumetric effect of sampling. Thawing was conducted at room temperature without temperature control if not stated otherwise. After sampling, the plates were directly frozen again. A control with non-supplemented ORFV material, only diluted in the intended buffer, was used to monitor any material-specific changes (negative control, NCTRL). Additionally, respective positive controls (PCTRL) were implemented, with ORFV in DMEM + 5% FCS as a standard with a high infectivity stability (Eilts et al., 2023).

2.2.1. Single component stability studies

For the infectivity stability studies of the ORFV, several excipients were tested in pure state (Table 1) as well as combined with others (Table 2).

The samples for studies with inorganic salts (KCl, NaCl, $NaNO_3$, $MgCl_2$, $(NH_4)_2SO_4$, Na_2SO_4, and $MgSO_4$) were prepared in a 20 mM TRIS-HCl buffer, pH 7.4, without any further NaCl supplementation, to study the influence of the individual salts. Furthermore, no antibiotics were added for these experiments.

2.2.2. Multi-component stability studies

For the studies with combined excipients, several different salts, sugars, amino acids, and proteins were mixed Table 2). Furthermore, two different experimental sets were planned and evaluated, using a design of experiments (DOE)-based approach, which is further described in Section 2.3: ((1) the amino acids arginine and proline, combined with $MgCl_2$, and (2) sucrose, rHSA-E, i.e., (recombinant human serum albumin *Exbumin*), and arginine.

2.3. Statistical evaluation

Two sets of experiments with combined additives were planned and statistically evaluated via a DOE-based approach (Design Expert 12, Stat-Ease), which were the interaction of $MgCl_2$, arginine, and proline (Section 3.2.1) on the one hand, and the interaction of sucrose, rHSA-E, and arginine (Section 3.2.6) on the other hand. The designs and their respective analysis can be found in the **Supplementary Material S3 to S4**. All other experiments were analyzed via ANOVA with *Tukey* test or Student *t*-test, as was appropriate (OriginPro 2021b, OriginLab Corporation).

Table 2
Overview of studies with combined additives for ORFV infectivity stability. The combination of additives was chosen according to previous findings, explained in the results and discussion section. The experiments were performed as described in the main text. PBS, phosphate buffered saline; rHSA-E, recombinant human serum albumin purchased from Invitria (Exbumin); TRIS, tris (hydroxymethyl)aminomethane.

Section	Excipient	Concentration	Buffer
3.2.2	$CaCl_2$	0 – 5 mM	20 mM TRIS + 180 mM NaCl
	$MgCl_2$	0 – 5 mM	
3.2.2	$MgCl_2$	0 – 2 mM	20 mM TRIS
	NaCl	20 – 180 mM	
3.2.1	Arginine	30 – 120 mM	20 mM TRIS + 180 mM NaCl
	Proline	30 – 120 mM	
	$MgCl_2$	2 – 8 mM	
3.2.3	Sucrose	0 – 20%	20 mM TRIS + 180 mM NaCl + 2 mM $MgCl_2$
	Trehalose	0 – 20%	
3.2.5	Sucrose	0 – 5%	20 mM TRIS + 180 mM NaCl
	rHSA-E	0 – 2%	
	$MgCl_2$	0 – 2 mM	
3.2.6	Arginine	0 – 300 mM	20 mM TRIS + 180 mM NaCl
	rHSA-E	0 – 2%	
	Sucrose	0 – 25%	
3.2.7	rHSA-E	0 – 1%	PBS or 20 mM TRIS + 20/180 mM NaCl
	Sucrose	0 –5%	

2.4. Analytics of formulated samples

2.4.1. ORFV infectivity titration

The quantification of infectious ORFV particles was performed by a flow cytometric assay, using fluorescence-activated cell counting (Guava easyCyte HT, Merck Millipore), adapted without viability staining from (2019). After sample fixation with 1% paraformaldehyde, 2% FCS, and 2 mM EDTA (VWR International) in PBS, the read-out was conducted within 48 h. The quantification was based on the ratio of fluorescent (infected) to non-fluorescent cells, which was standardized by virus plaque titration in triplicates. Each sample was prepared at least in two different dilutions, and each dilution was titrated at least in duplicates. The standard deviation of the ORFV infectivity within one measurement set was determined below 10%, and increased up to 20% between different sampling points, i.e., days.

2.4.2. Size measurements

Particle size distribution measurements were conducted using a Zetasizer Nano ZS90 (Malvern Panalytical), as previously described (Lothert et al., 2020c). The refractive index and viscosity of the samples were adjusted accordingly.

2.4.3. Solvent characterization

The formulated solvents were characterized concerning their pH (InLab Micro-Pro-ISM, FiveEasy, Mettler Toledo), viscosity (MCR 102, Anton Paar), osmolality (OM806, Löser), conductivity (InLab Expert-Pro-ISM, SG78, Mettler Toledo), and refractive index (AR-4, Abbe).

3. Results

3.1. Impact of single additives on ORFV infectivity

3.1.1. Detergents, amino acids, and inorganic salts

First, a screening of the stabilizing effect on the ORFV infectivity of different detergents, amino acids, and inorganic salts as single additives was performed (Table 3). Out of the fifteen substances tested, Pluronic F68 (0.5%), arginine (100 and 200 mM), and Na_2SO_4 (20 mM) reduced

Table 3
Effect of single additives on ORFV infectivity stability at 4 °C and up to 14 d storage. Non-supplemented samples showed an infectious ORFV titer reduction of nearly 3 log IU mL^{-1}, compared to the initial sample (1×10^6 IU mL^{-1}). For substances with a significantly stabilizing effect, the titer compared to the starting titer of 1×10^7 IU mL^{-1} is listed.

Type	Substance	Concentration	Stabilizing effect	Titer
Detergent	Tween 20	0.5%	no effect	
	Tween 80	0.5%	no effect	
	Pluronic F68	0.5%	stabilizing	4×10^5 IU $mL^{-1} \pm 1 \times 10^5$ IU mL^{-1}
Amino acids	arginine	50 – 300 mM	slight stabilization at 100 and 200 mM	2×10^5 IU $mL^{-1} \pm 2 \times 10^5$ IU mL^{-1}
	glutamine	50 mM	no effect	
	glycine	50 mM	no effect	
	histidine	50 mM	no effect	
	methionine	50 mM	no effect	
	tryptophane	50 mM	no effect	
Inorganic salts	KCl	20 – 200 mM	no effect	
	NaCl	20 – 200 mM	no effect	
	$NaNO_3$	20 – 200 mM	no effect	
	$MgCl_2$,	20 – 200 mM	no effect	
	Na_2SO_4	20 – 200 mM	slight stabilization at 20 mM	3×10^6 IU $mL^{-1} \pm 1 \times 10^5$ IU mL^{-1}
	$MgSO_4$,	20 – 200 mM	no effect	

the infectivity loss of the infectious virus over a period of 14 d at 4 °C. A non-supplemented control revealed an infectious ORFV loss of nearly 3 log IU mL^{-1} (from 1×10^6 IU mL^{-1} to 3.7×10^4 IU $mL^{-1} \pm 5 \times 10^3$ IU mL^{-1}). Furthermore, the supplementation of Pluronic F68 increased the cryostability of the ORFV significantly. The formulation was subjected to up to 20 freeze-thaw cycles (−80 °C - 37 °C), and the infectious titer was reduced by roughly 0.5 log IU mL^{-1} (from 1×10^7 IU mL^{-1} to 5×10^4 IU $mL^{-1} \pm 2 \times 10^4$ IU mL^{-1}), compared with non-supplemented samples, which lost 3 log IU mL^{-1} (from 1×10^6 IU mL^{-1} to 5×10^4 IU $mL^{-1} \pm 2 \times 10^4$ IU mL^{-1}). Another observation was that the stabilizing effect of arginine on the ORFV infectivity was more pronounced at elevated temperatures (37 °C). The effect of arginine is further explored in Sections 3.2.1, 3.2.3, **and** 3.2.6.

3.1.2. Proteins

From our previous study, the stabilizing effect of proteins on the ORFV infectivity was known (Eilts et al., 2023). Thus, we evaluated the addition of two animal-derived proteins as stabilizing agents, i.e., bovine serum albumin (BSA), 2%, and gelatine type A, 0.5% (Table 4). Both additives acted as potent cryoprotectants, causing little ORFV titer reduction from 1×10^7 IU mL^{-1} in up to 20 freeze-thaw cycles (< 0.5 log IU mL^{-1}) compared with a non-supplemented control (titer loss of 3 log IU mL^{-1}) (see Section 3.1.1). Additionally, a similarly strong stabilization of the ORFV infectivity was observed in a liquid state for both proteins at all tested temperatures between 4 °C and 37 °C.

Next, recombinant human serum albumin (rHSA) procured from two different manufacturing companies, i.e., InVitria (*Exbumin*, rHSA-E) and Albumedix Ltd. (*Recombumin Prime*, rHSA-R), was tested (Table 4). rHSA is free of compounds of animal or human origin. Both proteins stabilized the Orf virus less effectively than the animal-derived BSA and gelatine. After 14 d of incubation, a temperature-dependent stabilizing effect on the ORFV infectious titer was visible with increasing titer reduction with elevated temperatures (Fig. 1). At all tested temperatures up to 28 °C, the supplementation with one of the proteins, rHSA-E, maintained the initial infectious titer to a higher degree than its omission by approximately 0.1 – 0.3 log IU mL^{-1} (Fig. 1A). At 37 °C, on the contrary, the two rHSA variants revealed differences in their effect on the ORFV stability. On the one hand, the application of 2% rHSA-E caused significantly higher infectious titers than the NCTRL ($\Delta = 0.3$ log IU mL^{-1}), whereas the addition of 1% rHSA-E caused increased ORFV inactivation by roughly 0.5 log IU mL^{-1} (Fig. 1A). On the other hand, all rHSA-R-supplemented samples (1% and 2%) revealed an increased infectivity stability of the ORFV (Fig. 1B).

3.1.3. Sugars

We tested galactose, glucose, lactose, mannitol, sucrose, and trehalose, each at a concentration of 10%, for their stabilizing effect on the ORFV at −80, 4, 22, and 37 °C (Table 4). The addition of any sugar, except glucose, preserved the ORFV infectivity in up to 20 freeze-thaw cycles. Especially mannitol, sucrose, and lactose acted as potent cryoprotectants, i.e., the reduction from the starting titer was less than 0.5 log IU mL^{-1} compared to nearly 3 log IU mL^{-1} for a non-supplemented control. At 4 °C, all supplemented sugars, apart from lactose and glucose, showed a titer loss of less than 0.5 log IU mL^{-1}, indicating the stabilizing properties of sugars. At 22 °C, trehalose and galactose stabilized the best. Incubation at 37 °C, reduced the ORFV titer significantly for all sugar supplementations, and only trehalose and sucrose compositions maintained an infectious titer with a loss less than 1.5 log IU mL^{-1}. Furthermore, concentration-dependent studies of galactose, sucrose, trehalose, and glucose indicated an increased ORFV stability with an increased carbohydrate concentration (2.5 – 10%) at all temperatures.

3.2. Infectivity stability of ORFV in the presence of combined additives

3.2.1. $MgCl_2$, arginine, and proline

Based on the potential stabilizing effect of arginine (Section 3.1) on the ORFV infectivity, the amino acid was combined with $MgCl_2$ and a second amino acid, proline. The formulation experiments were planned using a DOE-based approach (**Supplementary Material S3**), and evaluated for 2 – 8 mM $MgCl_2$ as well as 30 – 120 mM arginine and proline. The storage was performed at 4 °C and at 37 °C.

First, the model at 4 °C is presented. According to the statistical model, all three components themselves had a significant influence on the ORFV infectivity. A relatively constant ORFV recovery (< 0.7 log IU mL^{-1} loss, equals 50%) was maintained for all combinations over the full period of 35 d (Fig. 2A). The optimum formulation was predicted for 90 – 120 mM arginine for all $MgCl_2$ concentrations. Concerning proline, the infectious ORFV recovery increased in a linear manner towards 120 mM. Thus, the concentration for a maximum stabilization was not covered by this design. However, the impact of proline on the ORFV titer stability was less pronounced than for arginine with roughly 10% between the optimum and minimum. Last, $MgCl_2$, like proline, showed a linear relationship with the infectious titer, and an optimum at 2 mM $MgCl_2$. An increase to 10 mM caused a decrease of infectivity by 10 – 15% (~ 0.2 log IU mL^{-1}).

At 37 °C, the statistical model predicted a linear influence of arginine and $MgCl_2$ on the infectivity of the ORFV. The addition of proline was not significant and set to 0 mM in Fig. 2B. The incubation of the samples at 37 °C caused a considerable decrease of infectivity after 7 d of roughly 50% (0.7 log IU mL^{-1}). Furthermore, the influence of the additives, $MgCl_2$ and arginine, on each sampling point was less pronounced at 37 °C compared to 4 °C. Compared with the optimum, the ORFV recovery varied by < 15% at 37 °C, however, by 15 – 30% at 4 °C. Like at 4 °C, the addition of $MgCl_2$ caused the highest ORFV titer at 2 mM. Yet, arginine had an optimum concentration at 120 mM at 37 °C.

Next to the analysis of the infectious titer, the size distribution of each sample was assessed. During the storage time, we observed a slight

Table 4
Effect of single additives on ORFV infectivity stability for up to 14 d storage time. Non-supplemented samples showed an infectious ORFV titer reduction of nearly 3 log IU mL^{-1}, compared to the initial sample. The (-) destabilizing or (++) stabilizing effect was rated according to a significant difference compared with non-supplemented controls. The rating slightly stabilizing (+) was attributed if significance was not observed in every batch. Values for the titers can be found in the Supplementary Material S2. N/A, not assessed.

Type	Substance	Concentration	Stabilizing effect at				Comment
			−80 °C	4 °C	22 °C	37 °C	
Protein	gelatine	0.5%	++	++	++	++	
	BSA	2%	++	++	++	++	
	rHSA-R	1 – 2%	++	++	N/A	++	
	rHSA-E	1 – 2%	++	++	++	+	At 37 °C stabilization only with 2%, and not 1%
Sugar	galactose	2.5 - 10%	++	++	++	–	increasing stabilization with increasing concentration
	glucose	2.5 - 10%	+	+	++	–	increasing stabilization with increasing concentration
	lactose	10%	++	+	+	–	
	mannitol	10%	++	++	++	–	
	sucrose	2.5 - 10%	++	++	+	+	increasing stabilization with increasing concentration
	trehalose	2.5 - 10%	++	++	++	+	increasing stabilization with increasing concentration

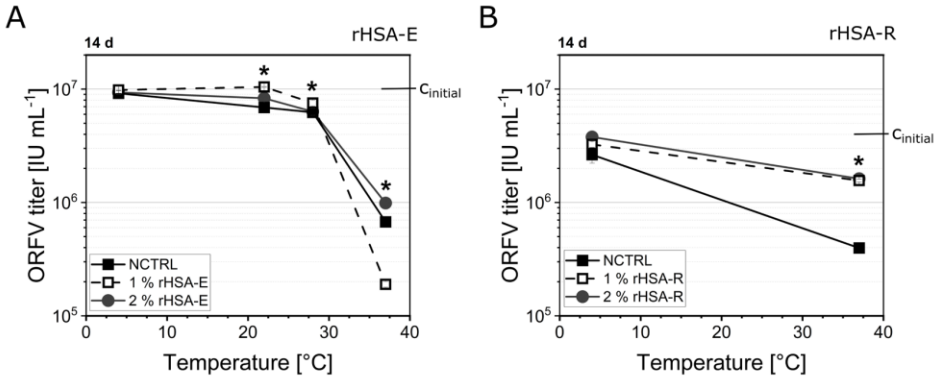

Fig. 1. Comparison of rHSA addition of two different origins.
rHSA from two different companies, Exbumin (rHSA-E, **A**) and Recombumin Prime (rHSA-R, **B**), was tested for its effect on the ORFV infectivity over time. The samples were stored at temperature between 4 °C and 37 °C. The ORFV was supplemented with 0% (NCTRL) to 2% rHSA. The initial infectious ORFV concentration (c_{intial}) was 1.1 x E7 IU mL^{-1} (**A**) and 4.0 x E6 IU mL^{-1} (**B**). Lines are only guide to the eye. The samples were statistically compared by ANOVA with Tukey test (α = 0.05). Asterisks indicate significant differences compared to the negative control (NCTRL). $n = 4$.

reduction of particle aggregations in samples with increased arginine concentrations (data not shown). This effect was especially visible for elevated temperatures, where aggregation in the presence of albumin was detected, correlating with a decrease of infectivity for these conditions.

The infectivity of the ORFV was evaluated at 4 °C (**A**) and at 37 °C (**B**), depending on the arginine, proline, and $MgCl_2$ concentrations using a DOE-based approach (**Supplementary Material S3**). In the contour plots, the infectivity recovery of the ORFV at each sampling time (7, 14, 21, or 35 d) is reported relative to the initial concentration of 1.1 × 10^7 IU mL^{-1}. Blue coloring indicates the lowest ORFV infectivity recovery, followed by green and yellow, while red represents the highest.

3.2.2. *NaCl, $MgCl_2$, and $CaCl_2$*

The influence of NaCl (20 and 180 mM) combined with $MgCl_2$ and $CaCl_2$ (0.5 – 5 mM) on the ORFV infectivity was tested as formulations in 20 mM TRIS buffer. First, an initial reduction of titer was observed for all samples apart from the protein-supplemented ones (PCTRL) (Fig. 3A). We attributed this to the adsorption of the ORFV to the storage container, which was prevented in the presence of FCS. Concerning NaCl. For an addition of either 20 or 180 mM NaCl, no difference in the ORFV titer was observed for any combination at 4 or 22 °C. $MgCl_2$ and $CaCl_2$, on the contrary, slightly reduced the ORFV titer (10 – 20%, equals up to 0.3 log IU mL^{-1}) with increasing storage time compared with a non-supplemented NCTRL at 4 °C (Fig. 3A). Additionally, we observed that the addition of 150 mM $CaCl_2$ caused ORFV titer reduction at different temperatures (−20, 4, 22, 37 °C) (data not shown).

Concerning a temperature-dependent study for the addition of 2 mM $MgCl_2$, the $MgCl_2$-supplementation significantly improved the stability of the infectious ORFV by 0.4 log IU mL^{-1} at 37 °C (Fig. 3B).

The ORFV was prepared in the intended formulations and stored over a period of up to 21 d The incubation time and temperatures are indicated in the respective graphs.

(**A**) The impact of combined $MgCl_2$ and $CaCl_2$ on the ORFV infectivity at 4 °C was assessed over time. Samples containing 0 mM additional salts were of either pure buffer (NCTRL) or contained DMEM + 5% FCS as positive control (PCTRL). Significant deviations from the initial ORFV concentration are marked by an asterisk.

(**B**) The temperature-dependent influence of 2 mM $MgCl_2$ on the ORFV infectivity, compared to the omission of $MgCl_2$, was assessed. The initial infectious titer (c_{intial}) was 1.1 x E7 IU mL^{-1}. Asterisks indicate significant difference between the two set-ups at each temperature. n = 4.

(**C**) Over the period of 21 d, the influence of 0 – 300 mM arginine and 1% rHSA-E (PCTRL) on the ORFV infectivity was assessed. 0 mM arginine represents a non-supplemented control (NCTRL). The ORFV infectious titer was normalized to the initial concentration (100%) of 1.1 × 10^7 IU mL^{-1}. An asterisk indicates a significant difference between 0, 100, 200, and 300 mM arginine in each temperature group (4, 22, 28 or 27 °C), while crosses show a significant difference between the sample with and without 1% rHSA-E addition (0 and 200 mM arginine), as well in the respective temperature group. $n = 4$.

(**D**) Sucrose and trehalose were applied at a concentration of 20%, either single or combined, at 20% each. A negative control (NCTRL) consisted of pure buffer. The samples were stored at 4, 22, 28, and 37 °C, and analyzed for their infectious ORFV titer after 14 d incubation time. The initial titer was 1.1 × 10^7 IU mL^{-1}. $n = 4$.

(**E**) rHSA-E (0% squares, 1% triangles, 2% circles), sucrose, and $MgCl_2$ (0 mM gray, 2 mM black) were tested in different combinations, shown in the table next to the plot, which is ordered according to the data points next to it. The samples were stored at 4, 22, 28, and 37 °C, and analyzed for their infectious ORFV titer after 14 d incubation time. The initial titer was 1.1 × 10^7 IU mL^{-1}. $n = 4$. The data from (**B**) is replicated in this figure.

Statistical analysis was done by ANOVA with a Tukey test, *, α = 0.05;***, $\alpha = 0.001$. $n = 3$ if not stated otherwise. The full Tukey test results of graph (**C**) may be found in the **Supplementary Material S5**.

3.2.3. *rHSA and arginine*

To analyze the interaction of rHSA and arginine in stabilizing the ORFV, 1% rHSA-E was combined with 200 mM arginine (Fig. 3C**)**. At 4 and 22 °C, the addition of 1% rHSA-E caused significantly higher ORFV titers of up to 0.3 log IU mL^{-1} compared with the addition of 0 – 300 mM arginine without albumin, conforming with the results from the previous sections. Only a slight increase in infectious titer of less than 0.5 log IU mL^{-1} was observed by combining 1% rHSA-E with 200 mM arginine at 22 °C. Additionally, this stabilizing effect was less pronounced with increasing storage time (data not shown). By increasing the temperature to 28 or 37 °C, a supplementation with 100 or 200 mM arginine without albumin revealed a significantly higher infectivity preservation than only rHSA-E or no supplementation.

3.2.4. *Sugar combination: sucrose, trehalose*

Two of the most stabilizing carbohydrates, trehalose and sucrose (Section 3.1.3), were additionally tested at a concentration of 20% as single and combined supplements with 20% each, 40% in total (Fig. 3D). The high concentrations were chosen the cover the experimental design space for a DOE-application. Both additives had a comparable

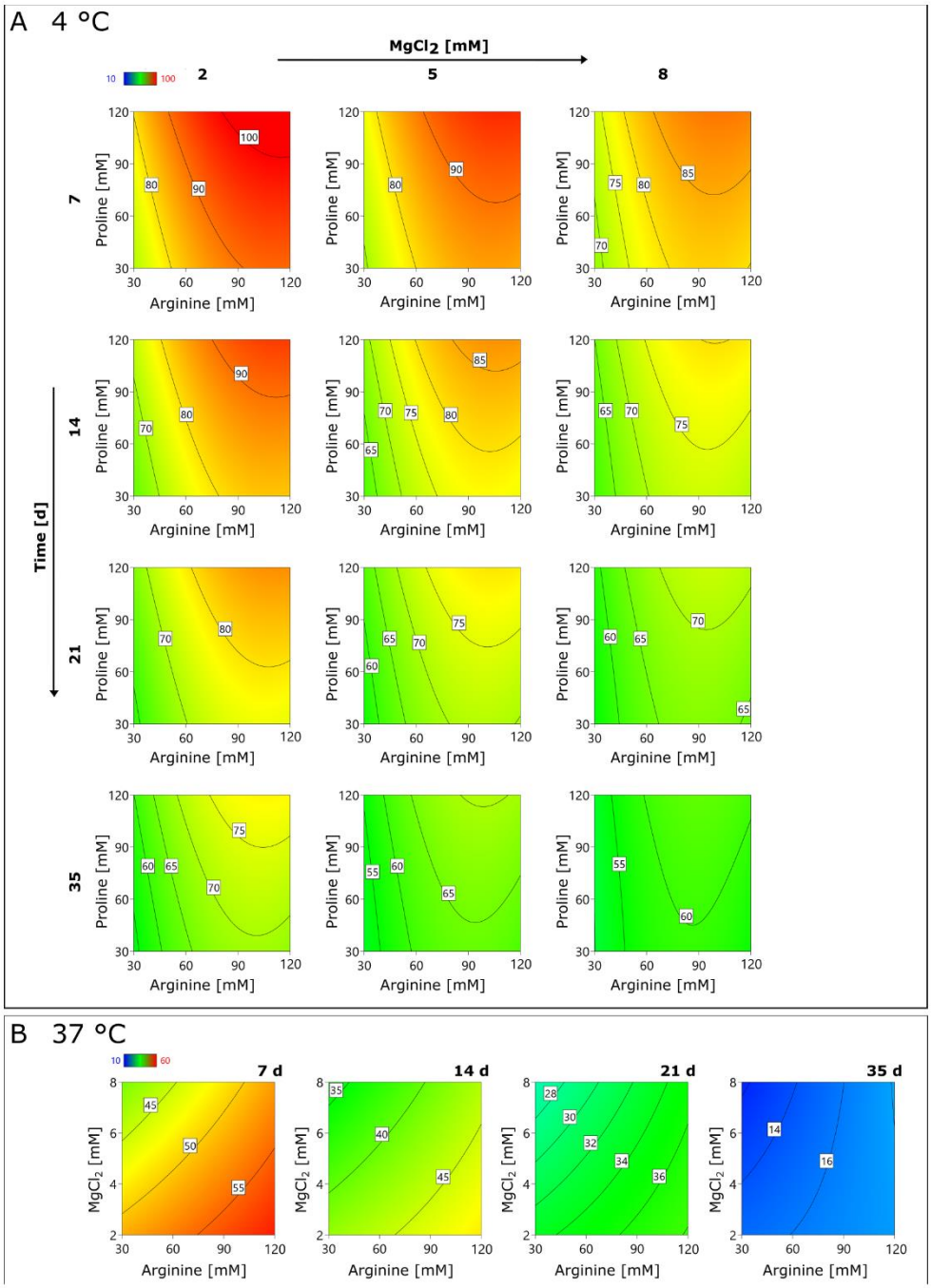

Fig. 2. Infectivity recovery of ORFV in the presence of arginine, proline, and $MgCl_2$.

stabilizing effect on the ORFV infectious titer at all tested temperatures, i.e., after 14 d incubation time no infectivity loss at 4 °C, 0.3 – 0.4 log IU mL^{-1} at 22 °C, and 0.4 – 0.5 log IU mL^{-1} at 28 °C. At these three temperatures, the combination of both sugars, with 40% in total, caused significantly lower ORFV titers of 0.2 – 0.3 log IU mL^{-1}. Only at 37 °C, this formulation stabilized the ORFV comparable to their single supplementation.

3.2.5. *Sucrose, rHSA-E, $MgCl_2$*

Next, the temperature-dependent storage of the ORFV in formulations combined with sucrose (0% or 5%), rHSA-E (0%, 1%, or 2%), and $MgCl_2$ (0 or 2 mM) was evaluated. After 14 d storage, the ORFV infectious titer was assessed, revealing significant differences between the formulation composition (Fig. 3E). At 4 and 22 °C, the addition of any additive combination reduced the ORFV infectivity losses. A notable preservation of the ORFV infectivity was achieved with 1% rHSA-E

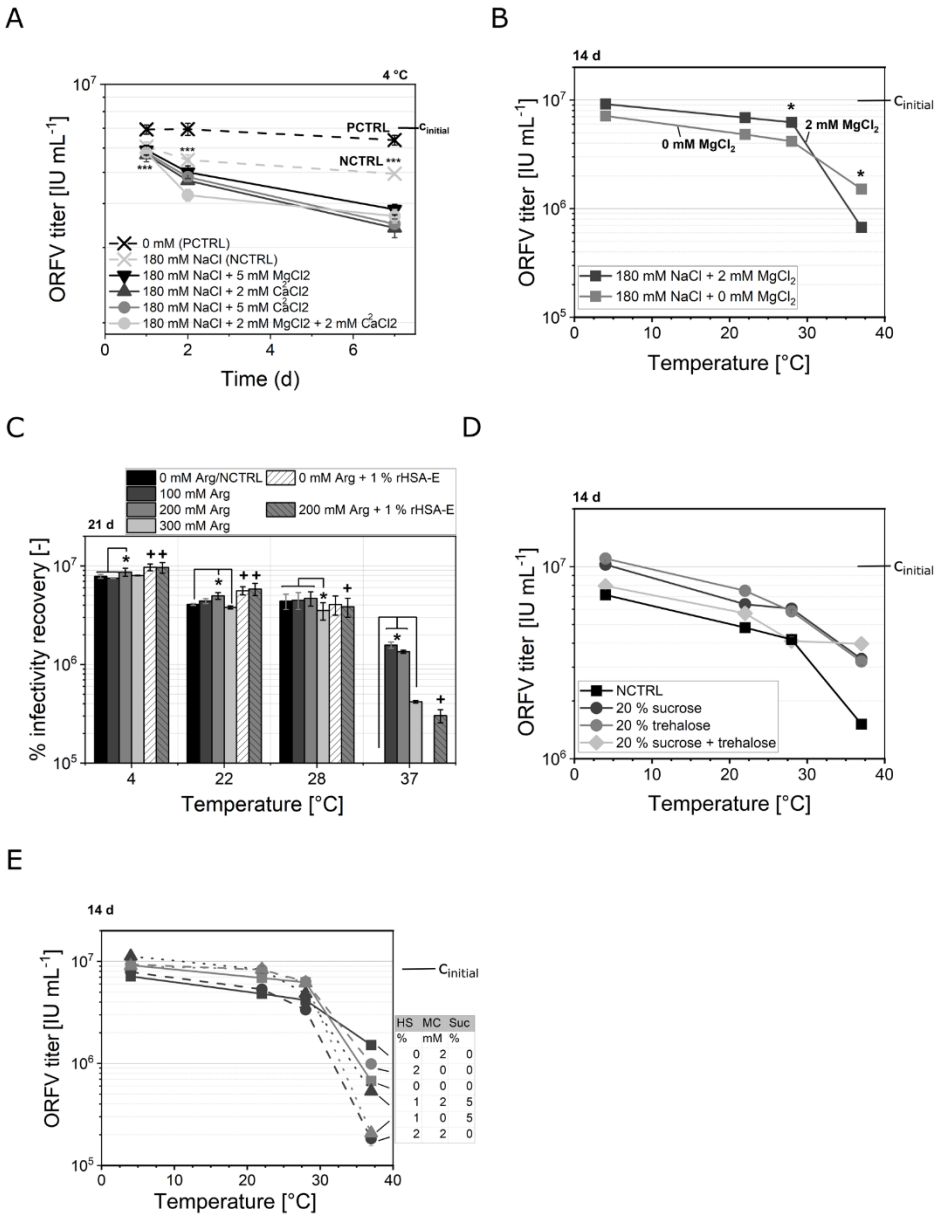

Fig. 3. ORFV infectivity stability in the presence of different additives.

combined with 5% sucrose (2 and 0 mM MgCl), 2% rHSA-E, and 2 mM $MgCl_2$, in this order, with less than 0.2 log IU mL^{-1} infectivity loss at 4 °C and 0.3 log IU mL^{-1} at 22 °C. Additionally, 2% rHSA-E combined with 2 mM $MgCl_2$ (black circles) did not improve the stability compared with the non-supplemented buffer (gray squares), i.e., both showing approximately 0.3 log IU mL^{-1} loss at 4 °C, 0.6 log IU mL^{-1} loss at 22 °C, and 0.7 log IU mL^{-1} loss at 28 °C. At 37 °C, a supplementation with 2 mM $MgCl_2$ generally reduced the ORFV infectivity (black symbols). The same accounted for 5% sucrose and rHSA-E, which was even more pronounced in combination with $MgCl_2$. The most stabilizing formulation at this temperature was the non-supplemented buffer (gray square), followed by 2% rHSA-E (gray circle), both with roughly 1 log IU mL^{-1} ORFV infectivity loss.

3.2.6. *Sucrose, rHSA-E, arginine*

In a final experimental set-up, sucrose (0 – 25%), arginine (0 – 300 mM), and rHSA-E (0 – 2%) were tested in a DOE-based approach (**Supplementary Material S4**). Comparing the samples without a rHSA-E addition, sucrose and arginine significantly increased the ORFV stability (Fig. 4A). At 4 °C, sucrose and arginine stabilized the ORFV in a comparable manner, while preservation with sucrose was better at higher concentrations (15 – 20%), whereas arginine stabilized at medium to high concentrations (100 – 300 mM). At 22 °C, on the other hand, sucrose had a minor stabilizing influence, and its omission was possible without ORFV titer losses. At this temperature, 22 °C, arginine improved the infectivity stability at its highest concentration of 300 mM up to 15% (0.2 log IU mL^{-1}) after 35 d incubation. In solid state at

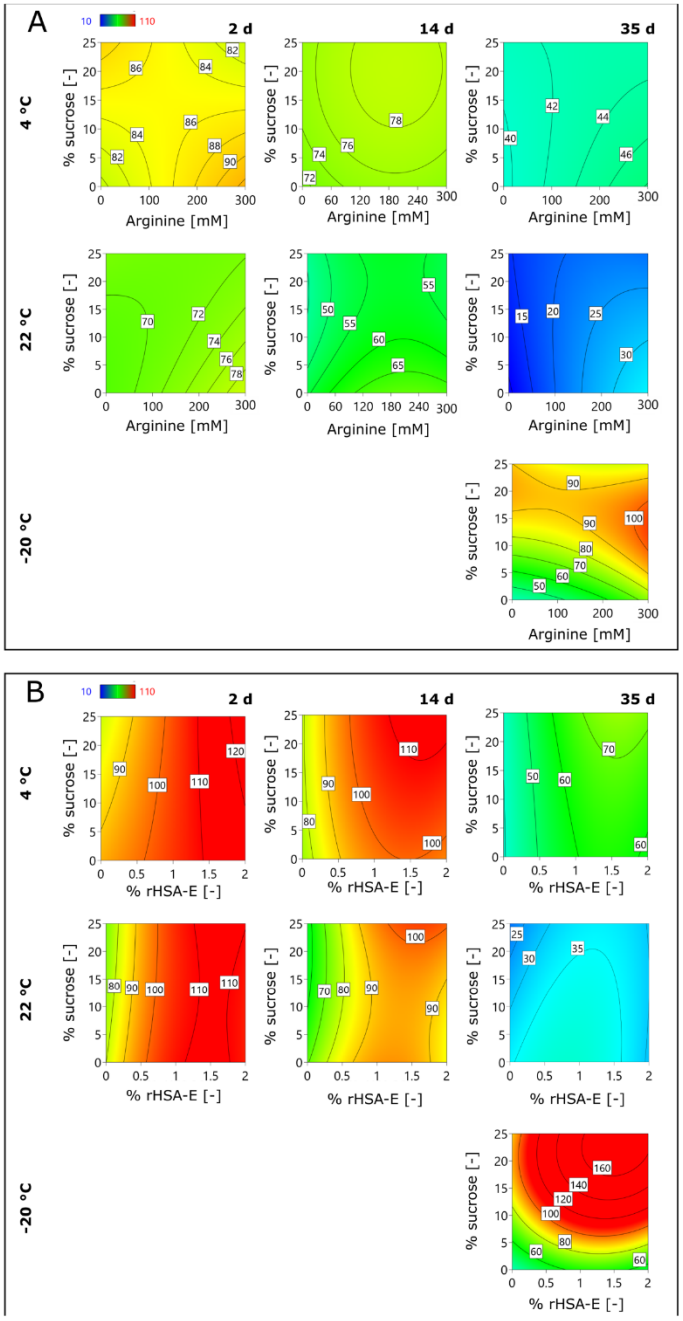

Fig. 4. Infectivity recovery of ORFV in presence of arginine and sucrose.

−20 °C, the ORFV was best stabilized by roughly 15% sucrose with nearly full recovery.

The ORFV was combined with sucrose and arginine to evaluate formulations without rHSA-E addition (0%) (**A**) compared with formulations with rHSA-E (**B**). The samples were stored at −20, 4 and 22 °C and samples were taken after 2, 14, and 22 d In the contour plots, the infectivity recovery of the ORFV is reported a percentage relative to the initial concentration of 1.1×10^7 IU mL^{-1}.

Blue coloring indicates the lowest ORFV infectivity recovery, followed by green and yellow, while red represents the highest.

The addition of rHSA-E increased the infectivity recovery of the ORFV effectively, i.e., the infectious titer was increased by roughly 30% (0.5 log IU mL^{-1}) for all tested temperatures and sampling times compared to non-supplemented samples (Fig. 4B). However, the statistical analysis suggested no significant influence of sucrose and/or arginine in the presence of rHSA at both tested temperatures, 4 and 22 °C. This suggests the dominant character of the stabilization by proteins.

For all tested temperatures and incubation times, the optimal rHSA-E

concentration was at least 1%, while most models predict 1.5 – 1.7%. Additionally, the recovery of the ORFV was increased by the addition of sucrose, which was optimal at a concentration of 23 – 25%, except for 22 °C after 35 d, where the concentration was predicted at low sucrose concentrations. Last, arginine stabilized the ORFV at high concentrations of 200 – 300 mM in all liquid formulations combined with rHSA-E. However, at −20 °C, arginine had no effect on the ORFV infectious titer (data not shown).

3.2.7. Buffers

To investigate the influence of the buffering system for one of the best suited excipient combinations from this study (1% rHSA-E and 5% sucrose), the ORFV was prepared in three different buffers: (1) PBS, (2) 20 mM TRIS with 20 mM NaCl, and (3) 20 mM TRIS with 180 mM NaCl. Half of the samples were supplemented with the respective formulation of 1% rHSA-E and 5% sucrose (PCTRL). The relative infectivity recovery was assessed in a temperature-dependent manner, and samples were taken after 2, 14, and 21 d (Fig. 5). Without the supplementation of stabilizers, the choice of the buffering substance indicates a minor influence on the infectivity recovery ($\Delta < 15\%$, equals 0.2 log IU mL^{-1}). Additionally, at 4 °C, PBS seems to have a reinforcing stabilizing effect on the ORFV combined with 1% rHSA-E and 5% sucrose (PCTRL) compared with TRIS. In other words, the PBS PCTRL had the highest titers, while the PBS NCTRL had the lowest. The influence of the NaCl concentration (20 or 180 mM) in the TRIS buffer was neglectable as already described in the previous sections.

Three different buffers, PBS, 20 mM TRIS with 20 mM NaCl and with 180 mM NaCl, were tested as diluent for the ORFV. The buffers were either pure (NCTRL) or supplemented with 1% rHSA-E and 5% sucrose (PCTRL). All combinations were stored at 4 – 37 °C, except 20 mM TRIS with 20 mM NaCl, which was stored at 4 and 22 °C. Samples were taken after 2 (**A**), 14 (**B**), and 21 d (**C**), and the initial concentration was 1.1×10^7 IU mL^{-1}. $n = 4$.

3.3. Summary of the excipient's effects on the ORFV infectivity stability

Last, a summary of the stabilizing effect of all tested substances is given in this section to facilitate a quick overview of the results (Table 5).

3.4. Modeling the degradation kinetics of ORFV

The reaction rates of the ORFV infectivity degradation can be valuable for an extrapolation of the infectivity loss under prolonged storage. Although, for approval of pharmaceuticals, such estimates need experimental verification, these models can be useful tools. Thus, the reaction rate constant k was determined for the most promising ORFV formulations 1 or 2% rHSA-E, as well as 1% rHSA-E with 5% sucrose, and non-supplemented samples. Considering the degradation kinetics of the ORFV infectivity, the non-supplemented virus was destabilized with increasing time and temperature. The data for the tested temperatures, 4, 22, 28, and 37 °C, could be described by an exponential regression of

Table 5
Overview of stabilizing effects of additives on ORFV infectivity stability.
The stabilizing effect of the substances was rated as (-) destabilizing or (+) stabilizing, depending on their statistically significant impact on the ORFV preservation compared to non-supplemented controls. The rating between slightly stabilizing (+) and strongly stabilizing (+++) was performed as internal comparison of all stabilizing components, while (+++) was attributed to the highest stabilizing effects observed. All listed substances were applied as described in the main text. BSA, bovine serum albumin; EDTA, ethylenediaminetetraacetic acid; PBS, phosphate buffered saline; rHSA, recombinant human serum albumin; TRIS, tris(hydroxymethyl)aminomethane.

Stabilizing effect	Substance (Product name)	Concentration	Comment
+++	BSA	2%	at all conditions
	Gelatine type A	0.5%	at all conditions
++	Mannitol	0 – 10%	++ at all conditions +++ at −20 °C only alone without trehalose and sucrose
	Sucrose	0 – 20%	++ at all conditions +++ at −20 °C
	Galactose	2.5 – 10%	++ at all conditions except at 37 °C +++ at −20 °C
	Trehalose	0 – 20%	++ at all conditions +++ at −20 °C
	Poloxamere 188 (Pluronic F68)	0.05%	++ at all conditions
	Arginine	0 – 300 mM	++ at 37 °C
	Dextran 40	0.5%	++ at 4 °C
+	Glucose	2.5 – 10%	+ at all conditions +++ at −20 °C
	Lactose	10%	+ at all conditions except at 37 °C +++ at −20 °C
	Glutamine	50 mM	+ at 4 °C
	Glycine	50 mM	+ at 4 °C
	Histidine	50 mM	+ at 4 °C
	Methionine	50 mM	+ at 4 °C
	Proline	0 – 150 mM	+ in combination with 120 mM arginine
	rHSA-R (Recombumin Prime)	0 – 2%	+ at all conditions except at 37 °C
	rHSA-E (Exbumin)	0 – 2%	+ at all conditions except at 37 °C
	Tryptophane	50 mM	+ at 4 °C
	Tween 80	0.05%	+ at 22 °C
	$MgCl_2$	0 – 150 mM	No effect + in combination with sucrose and rHSA + except at 37 °C
/	KCl	0 – 200 mM	no effect
	$MgSO_4$	0 – 200 mM	no effect
	NaCl	0 – 200 mM	no effect
	$NaNO_3$	0 – 200 mM	no effect
	Na_2SO_4	0 – 200 mM	no effect
	TRIS	20 mM	no effect
	Tween 20	0.05%	no effect
-	PBS	pure	at all conditions
	$CaCl_2$	2 – 150 mM	at all conditions

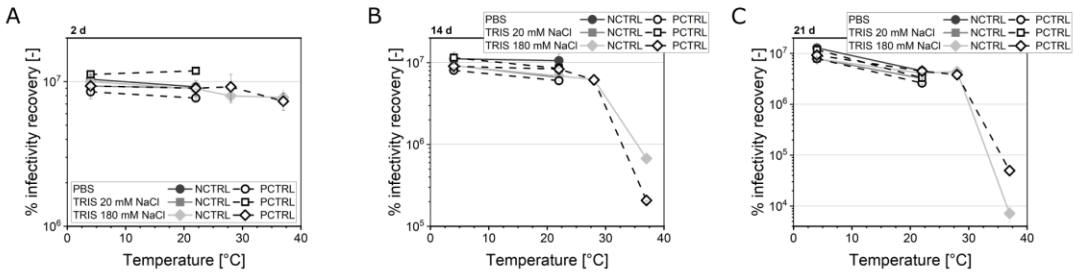

Fig. 5. Testing different buffering systems for an ORFV formulation.

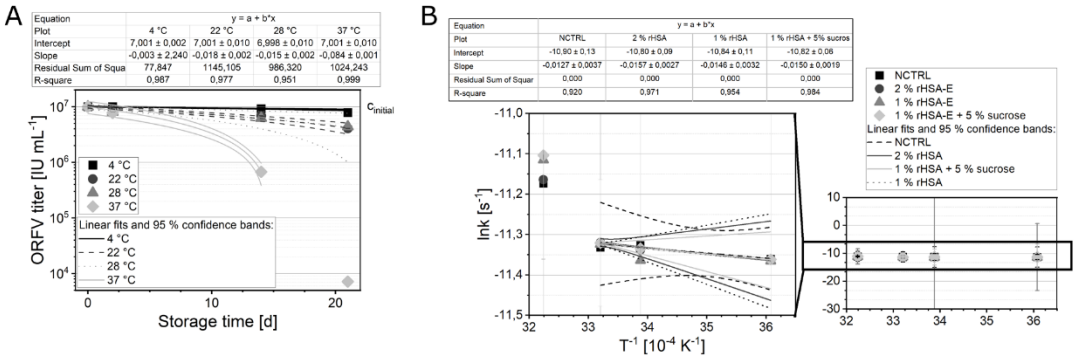

Fig. 6. Degradation kinetics of the ORFV.

first order decay (Fig. 6A). A similar behavior was observed for the supplementation with 1% or 2% rHSA-E as well as 1% rHSA-E with 5% sucrose (Fig. 7).

Using this data, the reaction rate as a function of temperature T and the related thermodynamic parameters was estimated according to (Hahon and Kozikowski, 1961) with

$$k = \frac{k_B T}{h} e^{\frac{-\Delta H}{RT} + \frac{\Delta S}{R}} \quad (1)$$

where

k reaction rate constant [s^{-1}]
k_B Boltzmann's constant [J K^{-1}]
h Planck's constant [J s]
H enthalpy of activation [J mol^{-1}]
R gas constant [J mol^{-1} K^{-1}]
S entropy of activation [J mol^{-1} K^{-1}].

Furthermore, the reaction rate constant k can be defined as

$$k = A\, e^{\frac{E_A}{RT}} \quad (2)$$

Where

A pre-exponential Arrhenius factor [s^{-1}]
E_A activation energy [J mol^{-1}].

The reaction rate constant k (ln$k$) was derived from the slope of Figs. 6A and 7, and plotted against the reciprocal of the absolute temperature (T^{-1}) according to an Arrhenius plot (Fig. 6B). In an Arrhenius plot, for linear relationships, degradation follows the same thermodynamic principles, defined by enthalpy and entropy of activation. Thus, temperatures within may be varied for the accelerated degradation studies.

The relation of the specific reaction rate for the inactivation of the ORFV and the absolute temperature was not linear for the full tested temperature range from 4 to 37 °C. Hence, enthalpy and entropy of activation were not determined from this data set. However, storage at the temperatures 4, 22, 28 °C revealed a linear relationship with little variation of the reaction rate (Fig. 6B). The highest value of the reaction rate was determined for both formulations with 1% rHSA, corresponding to the slowest degradation.

(**A**) The ORFV, with an initial concentration ($c_{initial}$) of 1×10^7 IU mL^{-1}, was stored in 20 mM TRIS with 180 mM NaCl without other supplements at four different temperatures. A linear regression was fitted to the half-logarithmic data set ($n = 3$). The fit data is displayed in the table. (**B**) The specific reaction rate constants k, according to Eqs.

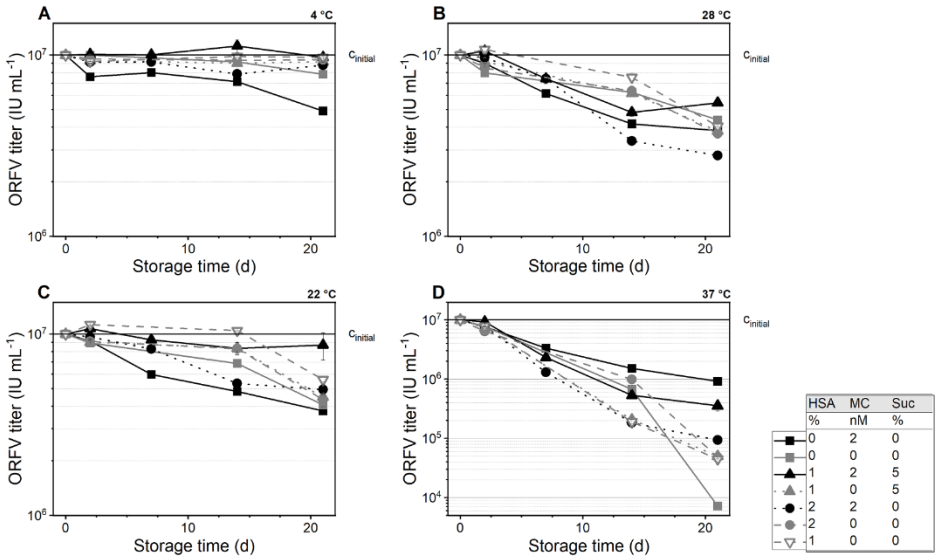

Fig. 7. Time-dependent storage of the ORFV.

(1)-2, were derived from (**A**) and Fig. 7. The relationship of k and the absolute temperature is shown according to the Arrhenius plot.

The ORFV, with an initial concentration ($c_{initial}$) of 1×10^7 IU mL^{-1}, was supplemented with rHSA-E (HSA), $MgCl_2$ (MC), Sucrose (Suc) according to the presented table. The formulations were stored at 4 °C (**A**), 22 °C (**B**), 28 °C (**C**), 37 °C (**D**). $n = 3$. The data presented is in part shown in figure Fig. 3E, and replicated here to facilitate comparison.

4. Discussion

Few studies concerning the infectivity stability of the ORFV have been published by now. A recent study from our group identified calf serum and recombinant albumin, rHSA, as stabilizing agents in liquid ORFV formulations, while phosphate and citrate buffers as well as ammonium salts reduced the infectivity (Eilts et al., 2023). Other publications on lyophilized vaccines of the ORFV and the closely related MVA virus reported an increased stability in formulations supplemented with different proteins, e.g., lactalbumin (Bora et al., 2015) and human albumin (FDA, 2022a), and sugars, e.g., sucrose (Bora et al., 2015), trehalose (Bora et al., 2015), and mannitol (FDA, 2022a). In this study, we could confirm the findings of these previous publications, and additionally tested a wide range of detergents, salts and buffers, sugars, proteins as well as amino acids as excipients to propose suitable stable formulation options for an ORFV vector vaccine.

First, it should be noted that the ORFV, comparable to other viruses of the family *Poxviridae* such as the MVA virus (Kaplan, 1958) or the variola (smallpox) virus (Hahon and Kozikowski, 1961), has an extremely high infectivity conservation over a long period of time. Thus, significant differences in the infectious titer were often first detected after days of storage, or at elevated temperatures, e.g., at 37 °C, where degradation was significantly different from temperatures of 28 °C or lower (Fig. 6B). This effect is reinforced by the small standard deviation in the infectivity assay within one set of measurements (< 10%), however, a pronounced effect between different days, i.e., sampling points, of measurements (up to 20%), which is visible, e.g., in Figs. 3D and 5. Thus, for an evaluation of significant differences, this should be kept in mind. Nevertheless, throughout the studies on a liquid formulation for an ORFV vector vaccine, stabilizing effects were identified for different excipients from the groups, detergents, salts and buffers, sugars, proteins, and amino acids.

For comparative reasons, the initial ORFV titer had a constant concentration. This approach was chosen, as a higher relative titer reduction was observed for samples with a lower initial titer, especially without protein supplementation. One explanation for this behavior was virus adsorption to the storage container.

Initially, an appropriate buffering system needed to be defined for a liquid formulation, as well as a possible reconstitution buffer, if lyophilization is applied. We hereby considered the stability of the ORFV, a possible adaption in the downstream process, and the interference with unit operations as well as the economics of the substances. In our recent work, the TRIS and PBS buffering systems were among the ones with the highest infectivity recovery at 4 °C (Eilts et al., 2023). We extended the experiments for these two buffers over a wider temperature range and found that PBS reduced the ORFV infectivity compared with TRIS by 0.1 – 0.2 log at 4 °C to 28 °C without the addition of other excipients (Fig. 5). Thus, a 20 mM TRIS buffer with either 20 or 180 mM NaCl was identified as the buffer of choice, conforming with the buffering system of a proposed production process (Lothert et al., 2020a, 2020b) as well as of several MVA virus vaccine formulations (Bavarian Nordic A/S, 2021; European Medicines Agency, 2013; FDA, 2022a; Greenberg and Kennedy, 2008; Kumru et al., 2014). With this knowledge, suitable salts were tested, keeping a parental application as a vaccine in mind. Salts mainly influence the tonicity and osmolarity as well as the viscosity of the formulation. A typical range for injections is around 300 mOsmol kg^{-1}, which corresponds to an isotonic solution. Furthermore, salts can inhibit aggregation and adhesion processes of viruses, improving the storage stability of pharmaceuticals (Tlaxca et al., 2015). Last, different salts are applied in the virus purification process, and may persist as residues, if not removed by consecutive unit operations. Thus, their presence should be evaluated concerning beneficial or disadvantageous effects on the virus stability. The salts KCl, NaCl, $NaNO_3$, and $MgSO_4$ had no effect on the ORFV infectivity at 4 °C, $CaCl_2$ reduced the virus titer by roughly 0.2 log (Fig. 3A), and Na_2SO_4 stabilized the virus slightly by 0.2 log at 20 mM (Table 3). Thus, the addition of $CaCl_2$ is not recommended for an ORFV formulation. The findings on $MgSO_4$ conform with earlier studies on the ORFV infectivity stability by (Bora et al., 2015). Additionally, $MgCl_2$, in the range of 0.5 – 2 mM, increased the ORFV stability most significantly at 37 °C, which was especially pronounced with 2 log of infectious titer after three weeks of storage for otherwise non-supplemented samples (Fig. 7). Thus, its addition might be reconsidered if a high storage temperature might be expected, e.g., in tropical regions. However, a $MgCl_2$ supplementation is not recommended for liquid long-term storage under cooled conditions. As $MgCl_2$ is frequently added in viral pharmaceutical production processes throughout the nuclease treatment (Lothert et al., 2020a), this information directs towards a timely rebuffering of the drug substance.

Next, several detergents were assessed as additives. Apart from the infectivity preservation, this group of chemicals can prevent an aggregation of the ORFV and adsorption to storage containers, which was assumed throughout the degradation experiments on different salts (Section 3.1.1). From the tested detergents, Tween20, Tween80, and Pluronic F68, only 0.5% Pluronic F68 had a slightly stabilizing effect on the liquid ORFV formulation with approximately 0.5 log IU mL^{-1} (Table 3). This result can be explained by the degrading effect on the lipids of the budded poxvirus (Feroz et al., 2022). Thus, no further experiments with detergents as excipients were conducted.

In general, amino acids are supplemented for their stabilizing and bulking properties as well as their influence on tonicity, pH, and viscosity. In this study, glutamine, glycine, histidine, methionine, and tryptophane had no effect on the virus titer (Table 3). But arginine was found to stabilize the ORFV by 0.1 – 0.2 log IU mL^{-1} (Fig. 2), especially at concentrations of 100 – 200 mM, and proline to a lesser extent (0.1 log IU mL^{-1}) and only at 4 °C in combination with arginine at concentrations of approximately 120 mM (Fig. 2). The amino acids arginine (Arakawa et al., 2007; Kim et al., 2016; Miyatake et al., 2016; Ohtake et al., 2011) and proline (Bolli et al., 2010; Jensen et al., 2014) are often applied in pharmaceutical formulations to prevent protein aggregation by increasing the protein solubility. Furthermore, both are safe to use in humans and have been applied in different vaccines, e.g., arginine in the Dengue virus-based *Dengvaxia* (EMA, 2022a) and the influenza vaccine *FluMist* (FDA, 2022b). However, arginine can reduce the transition melting temperature of proteins, which could lead to denaturation (Kim et al., 2016). In this study, on the contrary, arginine was found to stabilize the ORFV infectivity at temperatures of 37 °C by 0.1 – 0.2 log (Fig. 3C**)**. Additionally, a slight reduction of aggregation in arginine-supplemented samples was observed. Thus, 100 – 200 mM arginine might be a valid liquid formulation option, especially for increased storage temperatures, however, arginine should be omitted for frozen formulations. Additionally, the supplementation with proline might be an option for further studies.

The addition of different proteins for the stabilization of viruses in vaccines has been applied in the past for multiple vaccines. Proteins are especially supplemented to thermo-stabilize viruses by steric hindrance via protein-protein interaction (Chen and Kristensen, 2009). Among these are gelatine, supplemented in the varicella zoster-based *Varivax* (MSD Sharp & Dohme GmBH, 2022) and the influenza vaccine *FluMist* (FDA, 2022b), HSA, applied in the modified vaccinia Ankara-based *ACAM2000* vaccine (FDA, 2022a), and recombinant albumin (rHSA), supplemented in the mumps-measles-rubella vaccine MMRII (Wiedmann et al., 2015) and in the Vesicular stomatitis virus-based Ebola vaccine *Ervebo* (EMA, 2022b). Concerning the ORFV, BSA and gelatine type A were found to be potent cryoprotectants ($\Delta = 2.5$ log IU mL^{-1}

after 20 freeze thaw cycles) as well as strong stabilizers in liquid formulations. However, considering current trends in the safety of pharmaceutical products and in the short time frames for approval, it is preferable to use alternatives like rHSA, which avoid extensive testing for donor-derived pathogens, facilitating manufacturing and admission processes as well as a market-release (Bosse et al., 2005; Wiedmann et al., 2015). Thus, in this study, only recombinant rHSA forms were used for further formulation characterizations, which were *Recombumin Prime* (rHSA-E) and *Exbumin* (rHSA-E). We observed a higher infectivity stability with the supplementation of both rHSA forms by 0.1 – 0.3 log IU mL^{-1} (

Fig. 1), while 1% rHSA-R might stabilize the virus more efficiently than rHSA-E. However, more experiments need to be conducted on this question. Interestingly, at elevated temperatures of 37 °C, the addition of rHSA-E, especially 2%, caused a decrease of the ORFV infectivity compared with non-supplemented samples (Fig. 7D). Here, the addition of arginine was able to increase the virus stability (Fig. 3C). This is further supported by the observation that arginine prevented an ORFV aggregation at elevated temperatures compared with the addition of rHSA-E.

Another additive, frequently applied in poxvirus vaccines (Bora et al., 2015; FDA, 2022a), are sugars. They act as stabilizers, cryo- and lyoprotectants, as bulking agents, and improve reconstitution. Furthermore, sugars influence the tonicity of the formulation, without increasing the ionic strength, and increase the viscosity. However, especially for long-term storage or lyophilization, attention should be paid to the potentially reactive effect of reducing sugars, e.g., glucose, fructose, or lactose, with proteins (Li et al., 1996). Such effects were not investigated in this study but are crucial for understanding modifications in protein structure of formulated products. Out of the tested carbohydrates, sucrose and trehalose acted beneficial on the ORFV infectivity recovery at all tested temperatures with at least 0.3 log higher titers compared with no supplementation (−80 – 37 °C), and, additionally, galactose, lactose, and mannitol were potent cryoprotectants (Δ 2 log IU mL^{-1}) (Table 4**)**. All sugars were more potent with increasing concentrations (up to 20%). However, the high osmolarity (1000 – 1200 mOsm $kg_{H_2O}^{-1}$) and viscosity (2 mPas) with a 20% sugar supplementation should be considered as impracticable for parenteral application. Additionally, further problems arise with high viscosities: processability, homogeneity and stability of formulation, and temperature sensitivity due to reduced mixing.

Overall, the combination of 5% sucrose and 1% rHSA-E proved to be an efficient stabilizing agent for liquid and frozen formulations (Fig. 4). This combination is currently being used in clinical trials for a SARS-CoV-2 vaccine candidate based on the ORFV vector (ClinicalTrials.gov identifier: NCT05389319 and NCT05367843). For future formulations, the addition of arginine might be a suitable alternative for the storage at elevated temperatures.

Considering the storage temperature for the ORFV, the lowest tested temperature for liquid formulations, 4 °C, proved to have the least degrading effects on the virus. Interestingly, a storage at 22 or 28 °C did not result in a difference in their reaction constant and thus degradation kinetics (Fig. 6A). Furthermore, for accelerated degradation studies at increased temperatures, 28 °C was tested as the maximum temperature, as a presumably linear relationship was not given for the next higher temperature 37 °C (Fig. 6A).

5. Conclusion

This study presents a comprehensive overview of the infectivity stability of the ORFV in the presence of several additives, i.e., detergents, salts and buffers, sugars, proteins as well as amino acids. The presented data indicates a high stability of the ORFV virus over several weeks of storage, and at temperatures up to 28 °C (Fig. 6B). For non-supplemented formulations, a loss of 0.10 log infectious particles per day at 4 °C ($10^{-0,003}$) and 0.12 log infectious particles per day at 37 °C ($10^{-0,084}$), can be expected (Fig. 6A). The degradation process was reduced by supplementation with different additives, while proteins showed the best results in a liquid state and sugars, especially mannitol, galactose, sucrose, and trehalose, as well as proteins in a frozen state. The supplementation with proteins in a liquid state was especially beneficial at 4 °C, where the degradation kinetics revealed a significantly higher ORFV stability for the supplementation with 1% rHSA, a recombinant albumin, with and without 5% sucrose (Fig. 6B). However, at temperatures of 37 °C, the degradation reaction rates were non-linear and different mechanisms of degradation are present compared with lower temperatures. On the contrary to rHSA, arginine at approximately 200 mM reduced the loss of infectious viruses at elevated temperatures, e.g., 37 °C, however, not in a frozen state. Thus, for the storage of the ORFV in liquid formulations at room temperature or higher temperatures, a formulation with an arginine addition is recommended, whereas for the storage at 4 °C or in a solid state, rHSA and sucrose should be added as stabilizers. In a next step, ORFV lyophilization studies should be conducted to take advantage of the presented results on cryopreservatives and possible reconstitution buffers for an ORFV vector vaccine application. Additionally, data on long-term preservation of the ORFV with the suggested formulations will be essential for pharmaceutical approval.

Submission declaration

All authors consent with the presented manuscript.

Data availability statement

All relevant data are within the paper.

Author statement

We will gladly submit the form as soon as it is available, as I am not able to locate it on your homepage under the corresponding keyword.
Best regards, Michael Wolff

CRediT authorship contribution statement

Friederike Eilts: Conceptualization, Validation, Investigation, Visualization, Writing – original draft. **Yasmina M.J. Harsy:** Conceptualization, Investigation, Visualization. **Keven Lothert:** Conceptualization, Investigation. **Felix Pagallies:** Conceptualization, Investigation, Resources. **Ralf Amann:** Writing – review & editing, Funding acquisition, Project administration. **Michael W. Wolff:** Writing – review & editing, Funding acquisition, Supervision, Project administration.

Declaration of Competing Interest

The authors declare that they have no known competing financial interests or personal relationships that could have appeared to influence the work reported in this paper.

Data availability

Data will be made available on request.

Acknowledgments

The authors greatly thank Sabri Orbay for his diligent support characterizing the influence of salts on the ORFV infectivity, and Catharine Meckel-Oschmann for her thorough proofreading of the manuscript. Furthermore, we want to thank Paul Dalby, University College London, for his scientific support in this project. This work was

financially supported by the Heinrich Böll Foundation with a doctoral scholarship to F Eilts and the University of Applied Sciences Mittelhessen, Giessen, Germany. Additionally, an EXIST-Forschungstransfer grant (03EFKBW171) of the German Federal Ministry for Economic Affairs and Energy was granted and the project was co-funded by the European Regional Development Fund as part of the Union's response to the COVID-19 pandemic (IGJ-ERDF-Program Hesse - React EU 20008790). The presented manuscript is part of F Eilts' dissertation at the Graduate centre for Engineering Sciences under the aegis of the Justus-Liebig University Giessen, Germany, in cooperation with the University of Applied Sciences Mittelhessen, Giessen, Germany.

Supplementary materials

Supplementary material associated with this article can be found, in the online version, at doi:10.1016/j.virusres.2023.199213.

References

Amann, R., Rohde, J., Wulle, U., Conlee, D., Raue, R., Martinon, O., Rziha, H.J., 2013. A new rabies vaccine based on a recombinant ORF virus (parapoxvirus) expressing the rabies virus glycoprotein. J. Virol. 87 (3), 1618–1630.

Arakawa, T., Ejima, D., Tsumoto, K., Obeyama, N., Tanaka, Y., Kita, Y., Timasheff, S.N., 2007. Suppression of protein interactions by arginine: a proposed mechanism of the arginine effects. Biophys. Chem. 127 (1–2), 1–8.

Bavarian Nordic A/S, 2021. Package insert JYNNEOS. https://www.fda.gov/media/131078/download. Accessed 5 August 2021.

Bolli, R., Woodtli, K., Bärtschi, M., Höfferer, L., Lerch, P., 2010. L-Proline reduces IgG dimer content and enhances the stability of intravenous immunoglobulin (IVIG) solutions. Biologicals 38 (1), 150–157.

Bora, D.P., Bhanupraka, V., Venkatesan, G., Balamuruga, V., Prabhu, M., Yogisharad, R., 2015. Effect of stabilization and reconstitution on the stability of a novel strain of live attenuated Orf vaccine (ORFV MUK59/05). Asian J. Anim. Vet. Adv. 10 (8), 365–375.

Bosse, D., Praus, M., Kiessling, P., Nyman, L., Andresen, C., Waters, J., Schindel, F., 2005. Phase I comparability of recombinant human albumin and human serum albumin. J. Clin. Pharmacol. 45 (1), 57–67.

Capelle, M.A.H., Babich, L., van Deventer-Troost, J.P.E., Salerno, D., Krijgsman, K., Dirmeier, U., Raaby, B., Adriaansen, J., 2018. Stability and suitability for storage and distribution of Ad26.ZEBOV/MVA-BN®-Filo heterologous prime-boost Ebola vaccine. Eur. J. Pharm. Biopharm. 129, 215–221.

Cardoso, F.M.C., Petrovajová, D., Horňáková, T., 2017. Viral vaccine stabilizers: status and trends. Acta Virol. 61 (3), 231–239.

Chen, D., Kristensen, D., 2009. Opportunities and challenges of developing thermostable vaccines. Expert Rev. Vaccines 8 (5), 547–557.

Eilts, F., Labisch, J.J., Orbay, S., Harsy, Y.M.J., Steger, M., Pagallies, F., Amann, R., Pflanz, K., Wolff, M.W., 2023. Stability studies for the identification of critical process parameters for a pharmaceutical production of the Orf virus. Vaccine 41 32, 4731–4742.

Eilts, F., Lothert, K., Orbay, S., Pagallies, F., Amann, R., Wolff, M.W., 2022b. A Summary of practical considerations for the application of the steric exclusion chromatography for the purification of the Orf viral vector. Membranes 12 (11), 1070.

Eilts, F., Steger, M., Pagallies, F., Rziha, H.J., Hardt, M., Amann, R., Wolff, M.W., 2022c. Comparison of sample preparation techniques for the physicochemical characterization of Orf virus particles. J. Virol. Methods, 114614.

EMA. Product information dengvaxia. https://www.ema.europa.eu/en/documents/product-information/dengvaxia-epar-product-information_en.pdf. Accessed 29 April 2022.

EMA. Produkt information ERVEBO. https://www.ema.europa.eu/en/documents/product-information/ervebo-epar-product-information_de.pdf. Accessed 29 April 2022.

European Medicines Agency, 2013. Assessment report IMVANEX. https://www.ema.europa.eu/en/documents/assessment-report/imvanex-epar-public-assessment-report_en.pdf. Accessed 4 August 2021.

FDA. Product Information ACAM2000. https://www.fda.gov/media/75792/download. Accessed 29 April 2022.

FDA. Product information FluMist quadrivalent. https://www.fda.gov/media/83072/download. Accessed 29 April 2022.

Feroz, H., Chennamsetty, N., Byers, S., Holstein, M., Li, Z.J., Ghose, S., 2022. Assessing detergent-mediated virus inactivation, protein stability, and impurity clearance in biologics downstream processes. Biotechnol. Bioeng. 119 (4), 1091–1104.

Fischer, T., Planz, O., Stitz, L., Rziha, H.J., 2003. Novel recombinant parapoxvirus vectors induce protective humoral and cellular immunity against lethal herpesvirus challenge infection in mice. J. Virol. 77 (17), 9312–9323.

Fleming, S.B., Wise, L.M., Mercer, A.A., 2015. Molecular genetic analysis of orf virus: a poxvirus that has adapted to skin. Viruses 7 (3), 1505–1539.

Friebe, A., Siegling, A., Weber, O., 2018. Inactivated Orf virus shows disease modifying antiviral activity in a guinea pig model of genital herpesvirus infection. J. Microbiol. Immunol. Infect. 51 (5), 587–592.

García-Arriaza, J., Esteban, M., 2014. Enhancing poxvirus vectors vaccine immunogenicity. Hum. Vaccin. Immunother. 10 (8), 2235–2244.

Greenberg, R.N., Kennedy, J.S., 2008. ACAM2000: a newly licensed cell culture-based live vaccinia smallpox vaccine. Expert Opin. Inv. Drug 17 (4), 555–564.

Hahon, N., Kozikowski, E., 1961. Thermal inactivation studies with variola virus. J. Bacteriol. 81, 609–613.

Jensen, K.T., Löbmann, K., Rades, T., Grohganz, H., 2014. Improving co-amorphous drug formulations by the addition of the highly water soluble amino Acid, proline. Pharmaceutics 6 (3), 416–435.

Kaplan, C., 1958. The heat inactivation of vaccinia virus. J. Gen. Microbiol. 18 (1), 58–63.

Kim, N.A., Hada, S., Thapa, R., Jeong, S.H., 2016. Arginine as a protein stabilizer and destabilizer in liquid formulations. Int. J. Pharm. 513 (1–2), 26–37.

Kline, R.L., Regnery, R.L., Armstrong, G.L., Damon, I.K., 2005. Stability of diluted smallpox vaccine under simulated clinical conditions. Vaccine 23 (41), 4944–4946.

Kumru, O.S., Joshi, S.B., Smith, D.E., Middaugh, C.R., Prusik, T., Volkin, D.B., 2014. Vaccine instability in the cold chain: mechanisms, analysis and formulation strategies. Biologicals 42 (5), 237–259.

Kumru, O.S., Wang, Y., Gombotz, C.W.R., Kelley-Clarke, B., Cieplak, W., Kim, T., Joshi, S.B., Volkin, D.B., 2018. Physical characterization and stabilization of a lentiviral vector against adsorption and freeze-thaw. J. Pharm. Sci. 107 (11), 2764–2774.

Li, S., Patapoff, T.W., Overcashier, D., Hsu, C., Nguyen, T.H., Borchardt, R.T., 1996. Effects of reducing sugars on the chemical stability of human relaxin in the lyophilized state. J. Pharm. Sci. 85 (8), 873–877.

Lothert, K., Pagallies, F., Eilts, F., Sivanesapillai, A., Hardt, M., Moebus, A., Feger, T., Amann, R., Wolff, M.W., 2020a. A scalable downstream process for the purification of the cell culture-derived Orf virus for human or veterinary applications. J. Biotechnol. 323, 221–230.

Lothert, K., Pagallies, F., Feger, T., Amann, R., Wolff, M.W., 2020b. Selection of chromatographic methods for the purification of cell culture-derived Orf virus for its application as a vaccine or viral vector. J. Biotechnol. 323, 62–72.

Lothert, K., Sprick, G., Beyer, F., Lauria, G., Czermak, P., Wolff, M.W., 2020c. Membrane-based steric exclusion chromatography for the purification of a recombinant baculovirus and its application for cell therapy. J. Virol. Methods 275, 113756.

Miyatake, T., Yoshizawa, S., Arakawa, T., Shiraki, K., 2016. Charge state of arginine as an additive on heat-induced protein aggregation. Int. J. Biol. Macromol. 87, 563–569.

MSD Sharp & Dohme GmBH. Fachinformationen VARIVAX. https://www.msd.de/fileadmin/files/fachinformationen/varivax.pdf. Accessed 29 April 2022.

Müller, M., Reguzova, A., Löffler, M.W., Amann, R., 2022. Orf virus-based vectors preferentially target professional antigen-presenting cells, activate the STING Pathway and induce strong antigen-specific T cell responses. Front. Immunol. 13, 873351.

Nagington, J., Horne, R.W., 1962. Morphological studies of Orf and vaccinia viruses. Virology 16 (3), 248–260.

Nitsche, A., Gelderblom, H.R., Eisendle, K., Romani, N., Pauli, G., 2007. Pitfalls in diagnosing human poxvirus infections. J. Clin. Virol. 38 (2), 165–168.

Ohtake, S., Kita, Y., Arakawa, T., 2011. Interactions of formulation excipients with proteins in solution and in the dried state. Adv. Drug Deliv. Rev. 63 (13), 1053–1073.

Reguzova, A., Ghosh, M., Müller, M., Rziha, HJ., Amann, R., 2020. Orf virus-based vaccine vector D1701-V induces strong CD8+ T cell response against the transgene but not against ORFV-derived epitopes. Vaccines 8 (2), 295 (Basel).

Reguzova A., Sigle M., Pagallies F., Salomon F., Rziha HJ., Bittner-Schrader Z., Verstrepen B., Böszörményi K., Verschoor E., Elbers K., Esen M., Manenti A., Monti M., Derouazi M., Rammensee HG., Löffler M., Amann R., 2023. A novel multi-antigenic parapoxvirus-based vaccine demonstrates efficacy in protecting hamsters and non-human primates against SARS-CoV-2 challenge. ResearchSquare preprint.

Rimmelzwaan, G.F., Sutter, G., 2009. Candidate influenza vaccines based on recombinant modified vaccinia virus Ankara. Expert Rev. Vaccines 8 (4), 447–454.

Rintoul, J.L., Lemay, C.G., Tai, L.H., Stanford, M.M., Falls, T.J., de, S.C.T., Bridle, B.W., Daneshmand, M., Ohashi, P.S., Wan, Y., Lichty, B.D., Mercer, A.A., Auer, R.C., Atkins, H.L., Bell, J.C., 2012. ORFV: a novel oncolytic and immune stimulating parapoxvirus therapeutic. Mol. Ther. 20 (6), 1148–1157.

Rohde, J., Amann, R., Rziha, H.J., 2013. New Orf virus (Parapoxvirus) recombinant expressing H5 hemagglutinin protects mice against H5N1 and H1N1 influenza a virus. PLoS One 8 (12), e83802.

Rohde, J., Schirrmeier, H., Granzow, H., Rziha, H.J., 2011. A new recombinant Orf virus (ORFV, Parapoxvirus) protects rabbits against lethal infection with rabbit hemorrhagic disease virus (RHDV). Vaccine 29 (49), 9256–9264.

Rziha, HJ., Büttner, M., 2020. Parapoxviruses. In: Reference Module in Life Sciences, 7. Elsevier, p. 1505.

Rziha, HJ., Büttner, M., Müller, M., Salomon, F., Reguzova, A., Laible, D., Amann, R., 2019. Genomic characterization of Orf virus strain D1701-V (Parapoxvirus) and development of novel sites for multiple transgene expression. Viruses 11 (2), 127.

Rziha, HJ., Rohde, J., Amann, R., 2016. Generation and selection of Orf virus (ORFV) recombinants. Methods Mol. Biol. 1349, 177–200.

Schneider, M., Müller, M., Yigitliler, A., Xi, J., Simon, C., Feger, T., Rziha, H.J., Stubenrauch, F., Rammensee, H.G., Iftner, T., Amann, R., 2020. Orf virus-based therapeutic vaccine for treatment of papillomavirus-induced tumors. J. Virol. 94 (15).

Spehner, D., Carlo, S., Drillien, R., Weiland, F., Mildner, K., Hanau, D., Rziha, H.J., 2004. Appearance of the bona fide spiral tubule of ORF virus is dependent on an intact 10-kilodalton viral protein. J. Virol. 78 (15), 8085–8093.

Tlaxca, J.L., Ellis, S., Remmele, R.L., 2015. Live attenuated and inactivated viral vaccine formulation and nasal delivery: potential and challenges. Adv. Drug Deliv. Rev. 93, 56–78.

van Rooij, E., Rijsewijk, F., Moonen-Leusen, H.W., Bianchi, A., Rziha, H.J., 2010. Comparison of different prime-boost regimes with DNA and recombinant Orf virus based vaccines expressing glycoprotein D of pseudorabies virus in pigs. Vaccine 28 (7), 1808–1813.

Volz, A., Sutter, G., 2017. Modified vaccinia virus ankara: history, value in basic research, and current perspectives for vaccine development. Adv. Virus Res. 97, 187–243.

Wang, R., Luo, S., Vlachakis, D., 2019. Orf virus: a new class of immunotherapy drugs. Systems Biology. IntechOpen, London.

Wiedmann, R.T., Reisinger, K.S., Hartzel, J., Malacaman, E., Senders, S.D., Giacoletti, K. E.D., Shaw, E., Kuter, B.J., Schödel, F., Musey, L.K., 2015. M-M-R(®)II manufactured using recombinant human albumin (rHA) and M-M-R(®)II manufactured using human serum albumin (HSA) exhibit similar safety and immunogenicity profiles when administered as a 2-dose regimen to healthy children. Vaccine 33 (18), 2132–2140.

An investigation of excipients for a stable Orf viral vector formulation

Supplementary Material

Friederike Eilts[a]

Yasmina M. J Harsy[a]

Keven Lothert[a]

Felix Pagallies[b]

Ralf Amann[b,c]

Michael W. Wolff[a,d,] (michael.wolff@lse.thm.de)

[a] Institute of Bioprocess Engineering and Pharmaceutical Technology, University of Applied Sciences Mittelhessen (THM), Wiesenstr.14, 35390 Giessen, Germany

[b] Department of Immunology, University of Tuebingen, Auf der Morgenstelle 15/3.008, 72076 Tuebingen, Germany

[c] PRiME Vector Technologies, Herrenberger Straße 24, 72070 Tuebingen, Germany

[d] Fraunhofer Institute for Molecular Biology and Applied Ecology (IME), Ohlebergsweg 12, 35392 Giessen, Germany

S1: List of excipients for ORFV infectivity stability studies

Table S1.1: List of excipients

Substance (Product name)	Concentration	Manufacturer
Arginine	0 – 300 mM	Carl Roth
BSA	2 %	Carl Roth
$CaCl_2$	2 – 150 mM	Sigma Aldrich
Dextran 40	0.5 %	Sigma Aldrich
Galactose	2.5 – 10 %	Sigma Aldrich
Gelatine type A	0.5 %	Sigma Aldrich
Glucose	2.5 – 10 %	Carl Roth
Glutamine	50 mM	Carl Roth
Glycine	50 mM	Sigma Aldrich
Histidine	50 mM	Carl Roth
KCl	0 – 200 mM	Carl Roth
Lactose	10 %	Sigma Aldrich
Mannitol	0 – 10 %	VWR
Methionine	50 mM	Sigma Aldrich
$MgCl_2$	0 – 150 mM	Sigma Aldrich
$MgSO_4$	0 – 200 mM	Sigma Aldrich
NaCl	0 – 200 mM	VWR
$NaNO_3$	0 – 200 mM	Sigma Aldrich
Na_2SO_4	0 – 200 mM	AppliChem
PBS	pure	Biochrom
Poloxamere 188 (Pluronic F68)	0.05 %	Gibco
Proline	0 – 150 mM	Alfa Aesar
rHSA-R (Recombumin Prime)	0 – 2 %	Albumedix
rHSA-E (Exbumin)	0 – 2 %	InVitria
Sucrose	0 – 20 %	Sigma Aldrich
Trehalose	0 – 20 %	AppliChem
TRIS	20 mM	Carl Roth
Tryptophane	50 mM	Sigma Aldrich
Tween 20	0.05 %	Sigma Aldrich
Tween 80	0.05 %	Carl Roth

S2: Metrix of DOE-based evaluation of $MgCl_2$, arginine, and proline

The DOE was built with the Design Expert Software (DX11, Stat-Ease Inc.). The components are coded as **A** arginine, **B** proline, and **C** $MgCl_2$. The separate sampling times are generated with the same samples from the same design set-up. They were planned by a central-composite response surface design and were evaluated via the historical data option.

Table S2.1: Experiment design

File Version	12.0.12.0		
Study Type	Response Surface	**Subtype**	Split-plot
Design Type	Historical Data	**Runs**	120.00
Design Model	Quadratic	**Blocks**	No Blocks
Groups	3.00	**Build Time (ms)**	1.0000

Table S2.2: ANOVA (REML) for historical data evaluation at 4 °C

Source	Term df	Error df	F-value	p-value	
Whole-plot	2	Not defined[1]			
d-Time	1	Not defined[1]			
d^2	1	Not defined[1]			
Subplot	12	105.09	14.05	< 0.0001	significant
A-Arginine	1	105.00	60.81	< 0.0001	significant
B-Proline	1	105.00	15.30	0.0002	significant
C-MgCl2	1	105.00	25.90	< 0.0001	significant
AB	1	105.00	0.5257	0.4700	
AC	1	105.00	2.89	0.0918	
Ad	1	105.00	1.79	0.1840	
BC	1	105.00	0.8596	0.3560	
Bd	1	105.00	0.6481	0.4226	
Cd	1	105.00	0.0882	0.7671	
A^2	1	105.36	48.09	< 0.0001	significant
B^2	1	105.18	0.1217	0.7279	
C^2	1	105.34	0.0451	0.8322	

Table S2.3: ANOVA (REML) for historical data evaluation at 37 °C

Source	Term df	Error df	F-value	p-value	
Whole-plot	1	109.00	327.14	< 0.0001	significant
d-Time	1	109.00	327.14	< 0.0001	
Subplot	9	109.00	2.86	0.0046	significant
A-Arginine	1	109.00	8.96	0.0034	significant
B-Proline	1	109.00	0.1491	0.7002	

C-MgCl2	1	109.00	8.72	0.0039 significant
AB	1	109.00	0.0843	0.7721
AC	1	109.00	0.5947	0.4423
Ad	1	109.00	1.04	0.3096
BC	1	109.00	0.1346	0.7144
Bd	1	109.00	0.0730	0.7876
Cd	1	109.00	2.18	0.1425

S3: Metrix of DOE-based evaluation of sucrose, arginine, and rHSA

The DOE was built with the Design Expert Software (DX11, Stat-Ease Inc.). The components are coded as **A** arginine, **B** rHSA, and **C** sucrose. The separate sampling times are generated with the same samples from the same design set-up but evaluated separately.

Table S3.1: Experiment design

File Version	12.0.12.0			
Study Type	Response Surface		**Subtype**	Randomized
Design Type	I-optimal	Coordinate Exchange	**Runs**	23.00
Design Model	Quadratic		**Blocks**	No Blocks
Build Time (ms)	40.00			

Table S3.2: ANOVA 2 d incubation at 4 °C

Source	Sum of Squares	df	Mean Square	F-value	p-value	
Model	6266.94	6	1044.49	9.43	< 0.0001	significant
A-Arginine	276.49	1	276.49	2.50	0.1231	
B-rHSA	4564.00	1	4564.00	41.20	< 0.0001	significant
C-Sucrose	290.70	1	290.70	2.62	0.1142	
AB	119.61	1	119.61	1.08	0.3059	
AC	332.57	1	332.57	3.00	0.0919	significant
BC	292.02	1	292.02	2.64	0.1134	
Residual	3876.98	35	110.77			
Lack of Fit	2300.58	21	109.55	0.9729	0.5352	not significant
Pure Error	1576.40	14	112.60			
Cor Total	10143.91	41				

Table S3.3: ANOVA 2 d incubation at 22 °C

Source	Sum of Squares	df	Mean Square	F-value	p-value	
Model	9658.99	9	1073.22	17.20	< 0.0001	significant
A-Arginine	189.82	1	189.82	3.04	0.0907	significant
B-rHSA	5209.02	1	5209.02	83.48	< 0.0001	significant
C-Sucrose	42.08	1	42.08	0.6743	0.4176	
AB	6.15	1	6.15	0.0985	0.7556	
AC	85.83	1	85.83	1.38	0.2495	
BC	90.35	1	90.35	1.45	0.2377	
A^2	5.01	1	5.01	0.0803	0.7787	
B^2	1623.27	1	1623.27	26.02	< 0.0001	significant
C^2	6.62	1	6.62	0.1061	0.7467	
Residual	1996.69	32	62.40			

Lack of Fit	1330.49	18	73.92	1.55	0.2038 not significant
Pure Error	666.20	14	47.59		
Cor Total	11655.69	41			

Table S3.4: ANOVA 14 d incubation at 4 °C

Source	Sum of Squares	df	Mean Square	F-value	p-value	
Model	7474.05	9	830.45	20.98	< 0.0001	significant
A-Arginine	41.91	1	41.91	1.06	0.3112	
B-rHSA	3944.13	1	3944.13	99.64	< 0.0001	significant
C-Sucrose	308.91	1	308.91	7.80	0.0087	significant
AB	1.05	1	1.05	0.0265	0.8716	
AC	0.0281	1	0.0281	0.0007	0.9789	
BC	99.21	1	99.21	2.51	0.1232	
A^2	31.60	1	31.60	0.7983	0.3783	
B^2	991.40	1	991.40	25.05	< 0.0001	significant
C^2	10.99	1	10.99	0.2778	0.6018	
Residual	1266.63	32	39.58			
Lack of Fit	616.86	18	34.27	0.7384	0.7311	not significant
Pure Error	649.77	14	46.41			
Cor Total	8740.68	41				

Table S3.5: ANOVA 14 d incubation at 22 °C

Source	Sum of Squares	df	Mean Square	F-value	p-value	
Model	11610.79	9	1290.09	17.01	< 0.0001	significant
A-Arginine	546.49	1	546.49	7.21	0.0114	
B-rHSA	4523.09	1	4523.09	59.64	< 0.0001	significant
C-Sucrose	32.40	1	32.40	0.4272	0.5180	
AB	17.25	1	17.25	0.2274	0.6367	
AC	29.07	1	29.07	0.3833	0.5402	
BC	607.82	1	607.82	8.02	0.0080	significant
A^2	287.22	1	287.22	3.79	0.0605	
B^2	2395.56	1	2395.56	31.59	< 0.0001	significant
C^2	126.44	1	126.44	1.67	0.2059	
Residual	2426.73	32	75.84			
Lack of Fit	2190.73	18	121.71	7.22	0.0003	significant
Pure Error	236.00	14	16.86			
Cor Total	14037.52	41				

Table S3.6: ANOVA 35 d incubation at 4 °C

Source	Sum of Squares	df	Mean Square	F-value	p-value	
Model	0.0060	9	0.0007	31.62	< 0.0001	significant
A-Arginine	4.831E-07	1	4.831E-07	0.0230	0.8807	

B-rHSA	0.0024	1	0.0024	113.51	< 0.0001	significant
C-Sucrose	0.0000	1	0.0000	0.8846	0.3553	
AB	0.0002	1	0.0002	8.18	0.0081	significant
AC	0.0001	1	0.0001	2.76	0.1084	
BC	0.0001	1	0.0001	2.76	0.1085	
A^2	3.972E-06	1	3.972E-06	0.1889	0.6673	
B^2	0.0015	1	0.0015	71.24	< 0.0001	significant
C^2	2.215E-06	1	2.215E-06	0.1053	0.7480	
Residual	0.0006	27	0.0000			
Lack of Fit	0.0004	16	0.0000	2.08	0.1106	not significant
Pure Error	0.0001	11	0.0000			
Cor Total	0.0066	36				

Table S3.7: ANOVA 35 d incubation at 22 °C

Source	Sum of Squares	df	Mean Square	F-value	p-value	
Model	1882.14	9	209.13	25.52	< 0.0001	significant
A-Arginine	286.89	1	286.89	35.01	< 0.0001	significant
B-rHSA	234.25	1	234.25	28.59	< 0.0001	significant
C-Sucrose	26.76	1	26.76	3.27	0.0819	
AB	79.41	1	79.41	9.69	0.0043	significant
AC	143.46	1	143.46	17.51	0.0003	significant
BC	105.85	1	105.85	12.92	0.0013	significant
A^2	40.52	1	40.52	4.95	0.0347	
B^2	373.94	1	373.94	45.63	< 0.0001	significant
C^2	2.75	1	2.75	0.3354	0.5673	
Residual	221.25	27	8.19			
Lack of Fit	162.42	16	10.15	1.90	0.1421	not significant
Pure Error	58.83	11	5.35			
Cor Total	2103.39	36				

Table S3.8: ANOVA 35 d incubation at -20 °C

Source	Sum of Squares	df	Mean Square	F-value	p-value	
Model	4.24	9	0.4715	18.90	< 0.0001	significant
A-Arginine	0.0044	1	0.0044	0.1751	0.6783	
B-rHSA	0.2861	1	0.2861	11.47	0.0018	significant
C-Sucrose	1.24	1	1.24	49.79	< 0.0001	significant
AB	0.1046	1	0.1046	4.19	0.0486	
AC	0.2633	1	0.2633	10.56	0.0027	significant
BC	0.0781	1	0.0781	3.13	0.0861	
A^2	0.0133	1	0.0133	0.5315	0.4711	
B^2	0.5076	1	0.5076	20.35	< 0.0001	significant
C^2	0.5035	1	0.5035	20.19	< 0.0001	significant
Residual	0.8230	33	0.0249			

Lack of Fit	0.3388 18	0.0188	0.5832	0.8625 not significant
Pure Error	0.4842 15	0.0323		
Cor Total	5.07 42			

8

S4: Tukey test results for rHSA-E, sucrose and $MgCl_2$

Table S4.1: Tukey test results of Orf virus infectivity recovery in presence of arginine. Three-way ANOVA with Tukey test was performed ($\alpha = 0.05$). All factors, sample type, temperature, and time, were significant as well as their respective interactions. The same letter indicates no significant difference between the individual combinations. Part of the results are visualized in **section** Fehler! Verweisquelle konnte nicht gefunden werden..

Sample	Temperature	Time	Mean Value	Groups
-	°C	d	% inf. rec.	
A-200-PCTRL	28	2	103.62	A B C D
A-200-PCTRL	22	2	107.47	A B C
A-200-PCTRL	4	2	109.40	A B
A-200-PCTRL	4	14	110.24	A
A-0-PCTRL	22	2	102.27	B C D E
A-100	4	2	99.24	C D E F
A-0-PCTRL	28	2	97.30	D E F
A-200	4	14	95.63	E F G
A-0	4	2	90.57	F G H I J K
A-200-PCTRL	22	14	91.00	F G H I J
A-200	4	2	94.02	F G H I
A-200-PCTRL	37	2	92.70	F G H I
A-300	4	2	92.48	F G H I
A-0-PCTRL	22	14	94.66	F G H
A-0-PCTRL	4	14	89.10	G H I J K L
A-0-PCTRL	4	21	87.95	H I J K L M
A-200-PCTRL	4	21	87.22	I J K L M N
A-300	22	2	86.84	I J K L M N
A-0-PCTRL	4	2	83.58	J K L M N O
A-200	22	2	84.50	J K L M N O
A-200	28	2	84.57	J K L M N O
A-0	4	14	83.20	K L M N O
A-100	22	2	83.26	K L M N O
A-100	4	14	81.99	L M N O
A-0	22	2	80.97	M N O
A-300	4	14	80.08	N O P
A-200	4	21	78.48	O P Q
A-100	28	2	73.40	P Q R
A-100	37	2	73.30	P Q R
A-0	28	2	72.24	Q R S
A-300	28	2	71.56	Q R S
A-300	4	21	72.34	Q R
A-0-PCTRL	28	14	68.33	R S T U
A-100	4	21	68.17	R S T U
A-200	22	14	66.77	R S T U
A-0	37	2	70.44	R S T
A-0-PCTRL	37	2	70.67	R S T
A-0	4	21	71.01	R S
A-200	37	2	70.73	R S
A-200-PCTRL	28	14	64.86	S T U V
A-100	22	14	63.29	T U V W
A-0	22	14	62.40	U V W X
A-200	28	14	57.59	V W X Y Z
A-300	22	14	58.76	V W X Y
A-0	28	14	56.55	W X Y Z
A-300	37	2	55.81	X Y Z
A-100	28	14	52.28	Y Z A1
A-200-PCTRL	22	21	52.86	Y Z
A-0-PCTRL	22	21	50.82	Z A1 B1
A-200	22	21	45.09	A1 B1 C1
A-300	28	14	44.25	B1 C1 D1
A-0	28	21	39.82	C1 D1 E1 F1
A-100	22	21	39.87	C1 D1 E1 F1
A-100	28	21	40.66	C1 D1 E1 F1
A-200	28	21	42.47	C1 D1 E1
A-0	22	21	36.86	D1 E1 F1 G1
A-0-PCTRL	28	21	36.78	E1 F1 G1
A-200-PCTRL	28	21	34.91	F1 G1
A-300	22	21	34.35	F1 G1
A-300	28	21	31.93	G1 H1
A-100	37	14	26.73	H1
A-200	37	14	25.90	H1
A-300	37	14	9.28	I1 J1 K1 L1
A-200-PCTRL	37	14	11.17	I1 J1 K1
A-200	37	21	12.22	I1 J1
A-100	37	21	14.27	I1
A-0	37	14	6.11	J1 K1 L1 M1
A-300	37	21	3.80	K1 L1 M1
A-200-PCTRL	37	21	2.74	L1 M1
A-0	37	21	0.07	M1
A-0-PCTRL	37	14	1.72	M1
A-0-PCTRL	37	21	0.41	M1

CHAPTER 3: Applying the steric exclusion chromatography for Orf virus downstream processing

To transfer biopharmaceutical production processes from lab to production scale, possible limitations need to be identified. Acquiring the knowledge of degrading conditions for the ORFV was the first step in the process (**Chapter 2**). Next, the implemented purification methods must be characterized. In previous studies the SXC was identified as suitable chromatographic purification step as part of a purification train to process the ORFV from cell culture broth to formulation. High yields of infectious virus with impurity removal sufficient to conform with regulatory limitations were reported for this set-up [127]. However, the yields of the SXC varied depending on the feed material [127,128], indicating unidentified variables, which need to be addressed for scale-up procedures.

In this chapter, the identification of critical process parameters for the processing of the ORFV using the SXC is presented. In **part A**, a model system with nanometer-sized latex particles, which corresponds to the ORFV in size and charge, was tested. However, a comparison with the virus itself revealed the need for further adaptation of a model process. Nevertheless, the nanoparticles were used to improve the understanding of target precipitation throughout the SXC. These studies were extended to the ORFV in **part B**. Here, the virus was processed in the SXC by changing the PEG concentration, the incubation time before column loading, the composition of the added salts and their ionic strength, the elution conditions as well as the membrane pore size. All aforementioned parameters were identified as critical, while the salt composition and concentration were the most complex variables. The latter might even offer the option to reduce the PEG concentration while maintaining high yields. This option could help to counteract pressure problems throughout processing.

In conclusion, the characterization of the SXC with a model is a valuable tool for understanding the methods working principle and limitations more deeply. However, such a system needs individual optimization to represent the target of interest. Concerning the ORFV, unexplored critical process parameters were characterized, which equip the reader with a deeper understanding of the SXCs limitation due to excess precipitation and filtration effects. These parameters should be addressed throughout scale-up or adaption to other genotypes.

Part A: Evaluation of a model system for the steric exclusion chromatography

Eilts, F.; Steger, M.; Lothert, K.; Wolff, M. W. (2022). The suitability of latex particles to evaluate critical process parameters in steric exclusion chromatography. Membranes 12 (5), 488. doi: 10.3390/membranes12050488

membranes

MDPI

Communication

The Suitability of Latex Particles to Evaluate Critical Process Parameters in Steric Exclusion Chromatography

Friederike Eilts [1], Marleen Steger [1], Keven Lothert [1] and Michael W. Wolff [1,2,*]

[1] Institute of Bioprocess Engineering and Pharmaceutical Technology, University of Applied Sciences Mittelhessen (THM), Wiesenstr. 14, 35390 Giessen, Germany; friederike.eilts@lse.thm.de (F.E.); anna.marleen.steger@lse.thm.de (M.S.); keven.lothert@lse.thm.de (K.L.)
[2] Fraunhofer Institute for Molecular Biology and Applied Ecology (IME), Ohlebergsweg 12, 35392 Giessen, Germany
* Correspondence: michael.wolff@lse.thm.de; Tel.: +49-641-309-2608

Abstract: The steric exclusion chromatography (SXC) is a rather new method for the purification of large biomolecules and biological nanoparticles based on the principles of precipitation. The mutual steric exclusion of a nonionic organic polymer, i.e., polyethylene glycol (PEG), induces target precipitation and leads to their retention on the chromatographic stationary phase. In this work, we investigated the application of latex particles in the SXC by altering the particle's surface charge as well as the PEG concentration and correlated both with their aggregation behavior. The parameters of interest were offline precipitation kinetics, the product recovery and yield, and the chromatographic column blockage. Sulfated and hydroxylated polystyrene particles were first characterized concerning their aggregation behavior and charge in the presence of PEG and different pH conditions. Subsequently, the SXC performance was evaluated based on the preliminary tests. The studies showed (1) that the SXC process with latex particles was limited by aggregation and pore blockage, while (2) not the aggregate size itself, but rather the aggregation kinetics dominated the recoveries, and (3) functionalized polystyrene particles were only suitable to a limited extent to represent biological nanoparticles of comparable size and charge.

Keywords: aggregation; crowding out; downstream processing; pH; polyethylene glycol; SXC; precipitation

check for updates

Citation: Eilts, F.; Steger, M.; Lothert, K.; Wolff, M.W. The Suitability of Latex Particles to Evaluate Critical Process Parameters in Steric Exclusion Chromatography. *Membranes* **2022**, *12*, 488. https://doi.org/10.3390/membranes12050488

Academic Editor: Marília Mateus

Received: 5 April 2022
Accepted: 28 April 2022
Published: 30 April 2022

Publisher's Note: MDPI stays neutral with regard to jurisdictional claims in published maps and institutional affiliations.

Copyright: © 2022 by the authors. Licensee MDPI, Basel, Switzerland. This article is an open access article distributed under the terms and conditions of the Creative Commons Attribution (CC BY) license (https://creativecommons.org/licenses/by/4.0/).

1. Introduction

The steric exclusion chromatography (SXC), as an upcoming purification technique for biological macromolecules and viruses, was first introduced by the work of Lee et al. [1] in 2012. The authors described the method to be based on the molecule capture at a hydrophilic surface without direct chemical interactions, but induced by mutual steric exclusion. The working principle of the SXC is closely related to precipitation, and extensively described elsewhere [1,2]. Here, only a summary of the core concepts relevant for this work is presented, and their impact on the SXC operation. This is visualized schematically in Figure 1. First, the SXC is often operated with polyethylene glycol (PEG), which serves as the driving force for strong mutual steric exclusion of chemically non-reactive solutes from one another [3,4]. This process leads to a deficient zone around given solute molecules, e.g., virus particles. Here, the concentration of the crowding solutes, in this case PEG, is lower than in the bulk solution [5,6]. The deficiency is caused by two phenomena [2]: On the one hand, the deficient zone is incompletely filled by the PEG spheres due to the fact that two solid objects cannot exist in the same place at the same time. On the other hand, the water molecules, which are smaller in size than the PEG, occupy the free space by preferential inclusion, consequently, leading to a lower PEG concentration in the PEG-deficient zone. The presence of the PEG-deficient (around virus particles and the stationary chromatographic phase) and PEG-concentrated (bulk solution) zones causes an unfavorable increase

in free energy (Figure 1A, Load). Hence, the system strives for a thermodynamic stability, realized by depletion effects [7], which are defined by the solubility of the solutes [8]. This implies that solvent (water molecules) from the PEG-deficient zones is released by the association of the virus particles and their accretion at a surface, e.g., the stationary phase. Hence, the target viruses arrange themselves on the chromatographic material, while contaminants may be washed out (Figure 1A, Wash). To reverse the binding, the PEG content is reduced, or omitted, and the virus particles are eluted in a concentrated, purified state (Figure 1A, Elute).

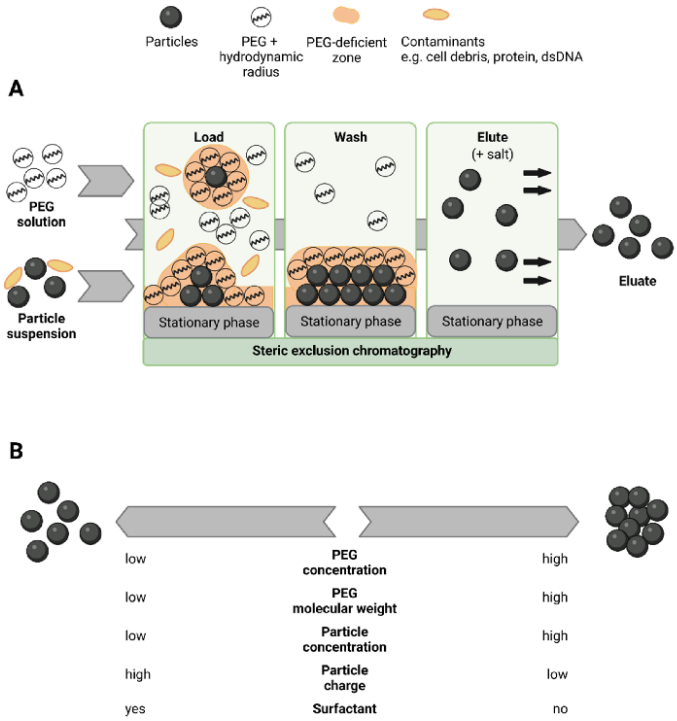

Figure 1. Theory of working principle and influencing factors of the steric exclusion chromatography (SXC). The SXC is a chromatographic method based on the core-concepts of polyethylene glycol (PEG) precipitation: (**A**) represents the steps of the method's application as a chromatographic purification technique. (**B**) depicts a selection of parameters influencing the target aggregation and accretion behavior, which were found to be critical for the SXC. Created with bioRender.com.

The selective interaction of virus particles depends on several factors related to their characteristics and the solution composition. The two most important ones for this work are (1) the size and concentration of the solutes, which determine the extent of the mutual steric exclusion. Thus, the smaller and the lower concentrated the virus particles are, the higher concentrated and the higher the molecular weight of the PEG must be, and vice versa [4,5,9]. (2) Accordingly, the chemical surface characteristics of the virus particles determine repulsive and attractive forces and can therefore prevent accretion [6,10,11]. This effect may be augmented by changes in pH, temperature, and salt composition, all having a direct impact on the electrostatic behavior and solubility [1,2,12].

For the operation of the SXC, considerations of practical relevance include the use of a liquid chromatographic (LC) system. As explained, the SXC is based on precipitation of the targets with retention at the stationary phase. Thus, the process is also limited by the target association itself, which can cause pore blockage of the adsorbent, if either the capacity of the column is reached, or bigger precipitates are formed throughout loading. Therefore,

pressure limits are of utmost importance for the stationary phase as well as for the LC system. In the past, convective media, such as monoliths [1,2,13,14] and membranes [15–19], were applied to counteract diffusion limitations and clogging caused by the virus particles' large size. As a secondary effect, the high viscosity of the PEG solutions was easier to handle with these stationary phases. Last, in-line mixing, representing the blending in the mixer and tubes of the LC immediately before loading onto the stationary phase, was proposed to reduce a possible pressure increase [1,18], but several authors worked on a laboratory scale with off-line mixing without describing such limitations [10,15–18].

As concluded from these concepts, the role of charge-induced and pre-column aggregation has not yet been discussed. We aimed to tackle this question with an artificial particle system. Certainly, the latter remains to be validated with corresponding biological nanoparticles, e.g., viruses; nevertheless, the advantages concerning the continuity of the system prevailed. More precisely, viruses are heterogeneous particles with batch-to-batch variances. Additionally, virus inactivation may impede quantification. Therefore, in this work, polystyrene calibration particles (CP) were selected, as they are stable in harsh environmental conditions, i.e., degradation was unexpected, and recovery losses may be attributed to retention on the stationary phase. Furthermore, CP of varying sizes are easily available with different functionalization and have previously been used for chromatographic modeling [20,21]. This article reports first results from the experimental evaluation of the suitability of latex particles to identify critical process parameters of SXC applications, and the role of target aggregation in the process.

2. Materials and Methods

All chemicals were purchased from Carl Roth (Karlsruhe, Germany) if not indicated otherwise.

2.1. Polystyrene Calibration Particles Characterization

CP particles with 190 nm mean diameter, were purchased with two types of surface functionalization, either sulfate-or hydroxyl-groups, CPS and CPH, respectively (Polybead, Polysciences Europe, Hirschberg a. d. Bergstrasse, Germany). Size distribution and charge measurements were performed with a Zetasizer Nano ZS90 and the corresponding Zetasizer software (version 7.13) (both Malvern Panalytical, Malvern, UK) according to Lothert et al. [16] with the deviation of the pre-set "polystyrene latex". CP with a final concentration of 10^{10} particles mL^{-1} were prepared in 0.1 M citrate phosphate buffer (CPB), the conductivity (15 mS cm^{-1}) adjusted with NaCl. Depending on the experiment, the CPB was of varying pH (3.0–7.4), PEG_{8000} concentration (0–10% (w/v)), 8000 Da molecular weight, and polysorbate 20 (Tween 20) addition (0% or 0.03%). Every sample preparation was carried out directly before analysis, including 2 min ultrasonication and 30 s mixing by vortex. Kinetics were recorded automatically with a measurement every 5 min.

2.2. Steric Exclusion Chromatography

All SXC experiments were conducted on an Äkta Pure 25 (Cytiva, Marlborough, MA, USA) with online UV (260 nm), pre-column pressure, and dynamic light scattering (DLS) (Nano DLS Particle Size Analyzer, Brookhaven Instruments, Holtsville, NY, USA) monitoring, controlled via the Unicorn 7.1 software (Cytiva, Marlborough, MA, USA). The execution of the SXC runs was adapted from Lothert et al. [17] with minor adjustments. In short, the single-use adsorbent was a stack of ten layers of regenerated cellulose membranes (Whatman, Maidstone, UK), 13 mm in diameter and 1 µm nominal pore size, inserted into a stainless-steel filter holder (Pall Life Sciences, Port Washington, NY, USA). Before assembly, the membranes were left for swelling in PBS overnight. The volume of the stationary phase was 0.1 mL. However, the effective column volume was 1.2 mL, including connectors and fittings. The prepared membranes were equilibrated with 10 mL CPB of the desired pH and PEG_{8000} concentration. For the batch loading (10 mL), the CP were diluted in the respective equilibration buffer aiming for a concentration of 10^{10} particles mL^{-1}, filled

into a 10 mL superloop, and loaded onto the column. Afterwards, no washing step was performed as no contaminants were present, but the CP were eluted with 20 mL CPB, always at pH 7.4, without PEG_{8000}, but supplemented with 0.03% polysorbate 20. The flow rate for all steps was set to 0.5 mL min^{-1}. The quantification of the CP was performed indirectly via measurement of the optical density at 260 nm. The relative recoveries were determined based on the concentration of the initial load sample. All experiments were carried out in triplicates.

3. Results

3.1. Polystyrene Particle Characterization

For comparative reasons, the CP were chosen to be spherical and of an average size (190 nm) of viruses, which were successfully purified by the SXC in previous studies [15,17,19]. In order to characterize the CP aggregation behavior, the pH-and PEG_{8000}-dependent size and charge distributions were assessed. Their concentration was chosen according to previous size and charge measurements, indicating a concentration-independent plateau for 10^9–10^{11} particles mL^{-1} (data not shown). Firstly, CPH and CPS samples were titrated to pH 3.0–7.4 without the addition of PEG_{8000} (Figure 2A,B). Concerning the pH-dependent size (Figure 2A), CPS revealed constant values of 231 ± 3 nm, also in the presence of polysorbate 20 (0.03%). Likewise, the obtained size of CPH behaved independently of the pH. However, the mean value of 721 ± 105 nm without polysorbate 20 addition, and 300 nm in its presence (0.03%), was larger than the diameter stated by the manufacturer in PBS at pH 7.4 (190 nm) as well as the diameter of the CPS. It should be noted that the diameters for CPS and CPH in a second phosphate buffer, PBS, with and without polysorbate 20, was around 200 nm (data not shown). Next, the CP charge varied in a pH-dependent manner (Figure 2B). The zeta potential of CPS and CPH similarly increased with reduced pH values, but CPH revealed higher zeta potentials. CPS samples exhibited the lowest charge (−34 mV) at pH 7.4, and the highest (−13 mV) at pH 3.0. For CPH, −19 mV was measured at pH 7.4, and −6 mV at pH 3.0. Additionally, only negative charges were obtained for the tested pH range. Hence, no isoelectric point (pI) could be determined. Last, polysorbate 20 increased the zeta potential at pH 3.0 and pH 7.4 to −3–−7 mV, respectively.

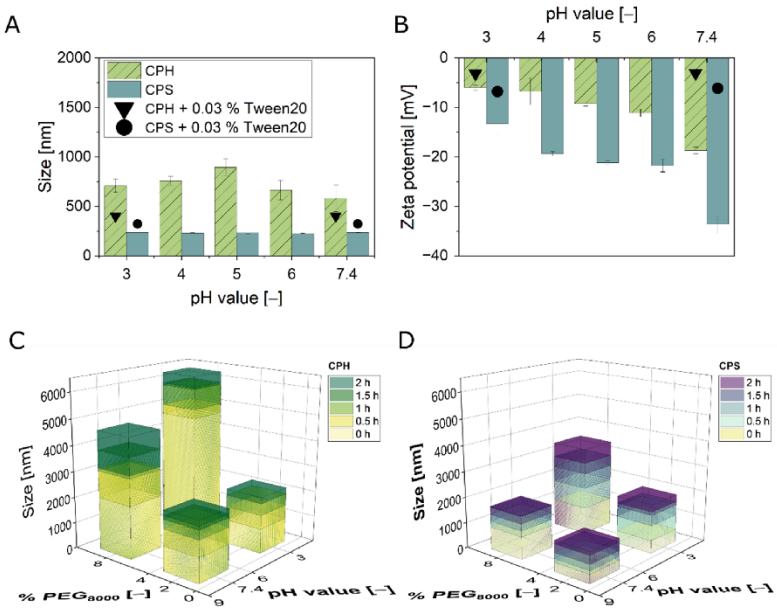

Figure 2. *Cont.*

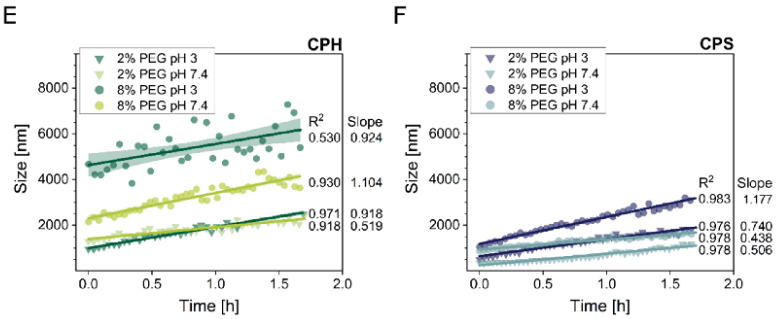

Figure 2. Polystyrene particle characterization. The functionalized polystyrene particles, sulfated (CPS) and hydroxylated (CPH), were characterized prior to the chromatographic experiments. (**A**,**B**) show the size distribution and electrophoretic mobility, expressed as zeta potential, of CPH (green, striped) and CPS (blue) at varying pH (and 0% PEG_{8000}). Additionally, the particles were supplemented with 0.03% polysorbate 20 (Tween 20) (black triangle and circle, respectively). Visualized are the measurements directly after the sample preparation at t = 0 min. The data shows the mean of n = 3 and standard deviations as error bars. (**C**–**F**) present the size distribution kinetics of the pH- and PEG_{8000}-dependent particle aggregation behavior analyzed over a period of 2 h. The data shows the means of n = 2. (**E**,**F**) depict linear fits for the presented kinetics, including all generated data points, with the respective R^2 and slopes. The lines represent the fits, while the hatched areas indicate the 95% confidence intervals. Data in (**E**,**F**) partly overlaps with the data shown in (**C**,**D**), but is included to facilitate the overview.

Secondly, aggregation kinetics were performed to clarify possible interactions of the two parameters, pH and PEG_{8000} concentration. Four selected pH/PEG combinations were chosen, to match conditions applied for similar-sized viruses [15,17], and to represent extremes for more pronounced results. The obtained kinetics showed positive linear trends with mostly steeper slopes (a) for bigger initial precipitate sizes (Figure 2E,F). The only exceptions were CPS with the conditions 8% PEG_{8000} at pH 7.4, and CPH with 2% PEG_{8000} at pH 7.4. The R^2 for the fits were above 0.91 for all data sets, apart from the recording of CPH with 8% PEG_{8000}, pH 3.0 (0.53), which also had a reduced a-value for the slope. In comparison, all tested conditions indicated bigger sizes for CPH than for CPS at t = 0 min as well as after 2 h of incubation time, except for pH 3.0 with 2% PEG_{8000}. The latter showed similar end values of roughly 2000 nm. The biggest sizes were reached at pH 3.0 (8% PEG_{8000}), 3000 nm (CPS) and 6000 nm (CPH). In detail, the aggregation kinetics of CPH were controlled by the PEG_{8000} concentration. At 2%, similar size distributions were measured for both pH values, but the slope was steeper for pH 3.0 (a = 0.918) as compared to pH 7.4 (a = 0.519) (Figure 2E). An increase to 8% PEG_{8000} led to significantly elevated mean sizes of 4000 nm and 6000 nm after 2 h for pH 7.4 and pH 3.0, respectively, but with comparable slopes of the fits of 1.104 and 0.924 (Figure 2C,E). Next, the size measurements of CPS revealed a pH-dominant distribution (Figure 2D,F). After the full incubation time, 1000 nm were measured for pH 7.4 with 2% PEG_{8000}, followed by similar trends for pH 7.4 combined with 8% and pH 3.0 with 2% PEG_{8000} (1500 nm). Concerning the latter two combinations, the slope was flatter for pH 7.4 (a = 0.438) compared to pH 3.0 (a = 0.740).

3.2. Steric Exclusion Chromatography with Polystyrene Particles

To evaluate the role of CP aggregation for the SXC, the parameters were chosen to correspond to the particle aggregation kinetics (Figure 2C–F). First focusing on the CPH, processing by SXC revealed 15% or less recovery of particles in the two fractions, flow-through and elution combined, for all combinations tested (Figure 3A). More specifically, only for the loading conditions pH 7.4 with 2% PEG_{8000}, CPH were recovered in the elution fraction with approximately 8% of the total load. Concerning the flow-through, both applications of pH 7.4 resulted in the detection of 7%, and the pH 3.0 runs in 2%

of the initial particle load. These observations were supported by the chromatograms (Figure 4A–D). No changes in the UV signal were recorded over the full process length, except for pH 7.4 with 2% PEG_{8000} (400 mAU in the elution peak) (Figure 4A).

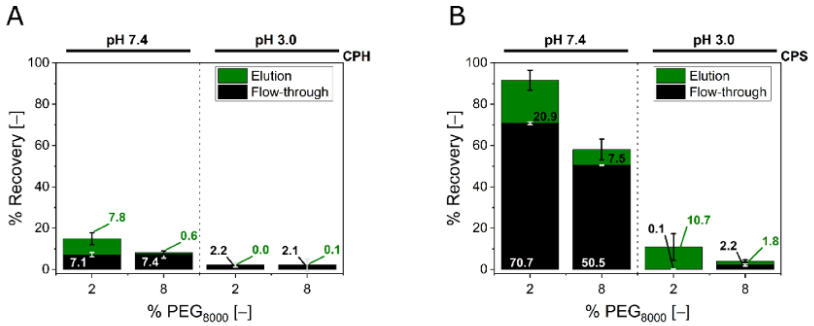

Figure 3. Recoveries of steric exclusion chromatography (SXC) runs. (**A**) represents the particle recoveries of SXC runs with the hydroxylated particles (CPH), chromatograms visualized in Figure 4A–D, while (**B**) accounts for sulfated beads (CPS) from Figure 4E–H. The recoveries of the different fractions were normalized to the respective initial load sample, accounting for volumetric ratios. Hence, the cumulative load is 100%, while elution (black), flow-through (green), and losses (not depicted) sum-up to this number. The CP concentration was indirectly determined by optical density at 260 nm. The bars represent means of triplicate runs and their respective standard deviations.

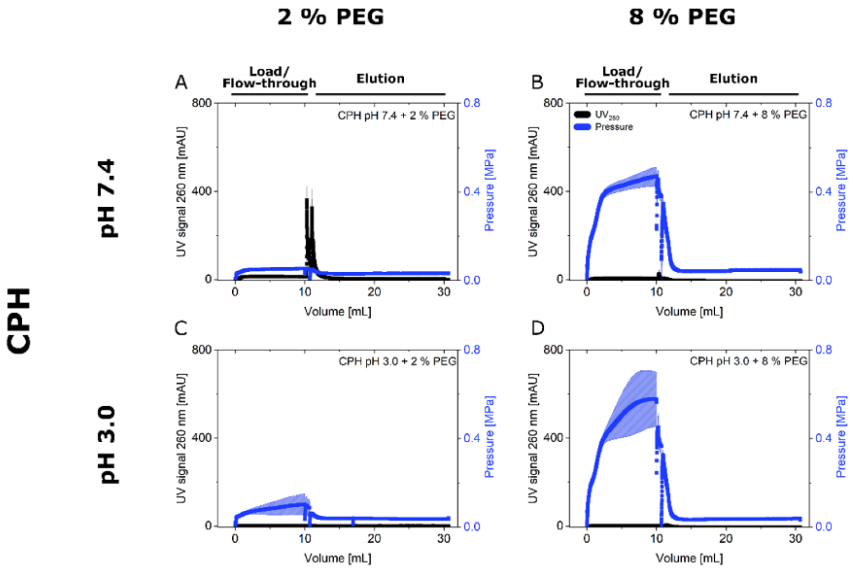

Figure 4. *Cont.*

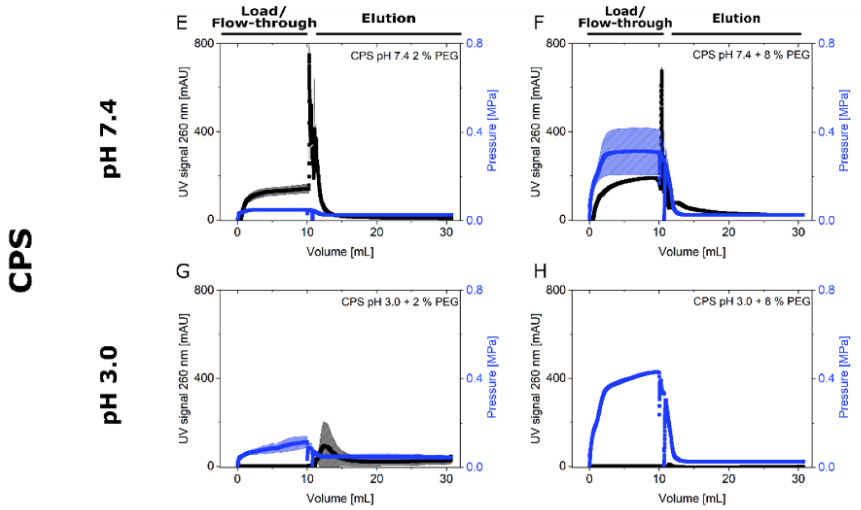

Figure 4. Chromatograms of steric exclusion chromatography (SXC) application. Hydroxylated (CPH) and sulfated (CPS) polystyrene particles were processed via SXC. For each experiment, 10 mL of the pre-mixed suspension were loaded onto the column. Elution (20 mL) was performed at neutral pH 7.4 (0% PEG_{8000} and 0.03% polysorbate 20). The UV signal at 260 nm (black) and the pre-column pressure (blue) were recorded online. The solid lines represent the means of t $n = 3$ runs, whereas the hatched areas indicate the standard deviations. The load of the experiments with CPH (**A**–**D**) was modified with 2% (**A**,**C**) or 8% (**B**,**D**) PEG_{8000}. Additionally, the pH was varied between 7.4 (**A**,**B**) and 3.0 (**C**,**D**). Like the CPH experiments, CPS (**E**–**H**) loads contained 2% (**E**,**G**) or 8% (**F**,**H**) PEG_{8000} and the pH was varied between 7.4 (**E**,**F**) and 3.0 (**G**,**H**).

A similar behavior was obtained for the CPS applications at pH 3.0, where the lower PEG_{8000} concentration (2%) led to a small CPS yield in the elution fraction (11%), while 8% PEG_{8000} inhibited the particle passage in flow-through and elution. The application of pH 7.4 revealed approximately 90% and 60% of total recovery for 2% and 8% PEG_{8000}, respectively. Here, the lower PEG_{8000} concentration of 2% resulted in a yield of 21% CPS in the elution fraction, and the higher concentration showed 8% yield (Figure 3B). Again, the results were supported by the UV signals (Figure 4E–H), indicating elution peaks, 100 (G), 700 (F), and 800 mAU (E) corresponding to increasing yields and recoveries. Additionally, the presence of CPS in the flow-through fractions (51% and 71%) at pH 7.4 were suggested by break-through UV signals of 150–200 mAU (Figure 4E,F).

Lastly, the pre-column pressure was monitored online to examine putative particle adhesion to the chromatographic membranes and pore blockage of the same. The pressure was increased for all runs throughout the loading process (Figure 4). Here, the initial pressure and the pressure increase were higher for elevated PEG_{8000} concentrations as well as for reduced pH values. Furthermore, CPH runs revealed higher final pressures than CPS ones.

4. Discussion

This study aimed to investigate whether functionalized CP, CPS and CPH, are a potential option to analyze critical process parameters of the SXC. Additionally, correlations of their pH- and PEG-dependent precipitation behavior and the SXC yields and recoveries were intended to elucidate pore blockage events and retention patterns. Therefore, the particles were characterized, and the precipitation kinetics recorded. The applied parameters were used in the SXC process afterwards.

4.1. Particle Characterization

Firstly, the pH-dependent size measurements showed constant values for CPS (230 nm) and CPH (720 nm) in CPB. The addition of polysorbate 20 revealed mean values of 300 nm for CPH. Presumably, the addition of polysorbate 20 helped to reduce spontaneous aggregation of CPH in the presence of CPB. Interestingly, the values in PBS for CPS were around 200 nm, comparable to the manufacturer specifications (190 nm) (Figure 2A). All measurements were done using a dynamic light scattering system. Thus, we attributed the deviations, to differences in the hydration shell in the presence of CPB and polysorbate 20, which influenced the Brownian motion, i.e., the recorded parameter in DLS measurements. Kinetic studies with different buffers and 0% PEG could clarify this observation. However, we decided to use CPB as buffering substance nevertheless, although PBS seemed to increase particle stability on solution. The main reason for this decision was that PBS has no buffering capacity over the full range of the conducted experiments, whereas CPB covers pH 2.5–7.5. Secondly, no pI was observed for CPH or CPS (Figure 2A,B) in the pH range 3.0–7.4. According to the functional groups, the pI was expected at pH 1–2 for particles functionalized with sulfate groups [22] and pH 6–7 for hydroxy groups [23]. However, here, a decreasing pH, accompanied by a zeta potential increase, showed a comparable function for both, CPH and CPS. Accordingly, the exhibited charge could be attributed to the core latex material, which contained sulfate groups from manufacturing (communication with Polysciences Europe, Hirschberg a. d. Bergstrasse, Germany). Furthermore, the association of anions to the spheres themselves should contribute to the observed negative zeta potential values in the range down to pH 3. Anions have been reported to adsorb to hydrophobic surfaces and to deprotonate counterions, like carboxyl groups [24]. Thus, measurements of the zeta potential might not reflect the neutral state of a surface that is in interaction with an anion-containing solution. Nevertheless, the additional sulfate functionalization of the CPS led to an increased electrostatic repulsion compared to the CPH, indicated by the lower sizes and zeta potential values. The lower zeta potential of CPS than CPH in the presence of 0.03% polysorbate 20 supports this assumption. The exhibited surface charge of CPS was putatively less effectively shielded than that of CPH. We also assume that these differences in the electrostatic repulsion were the main influencing factor in the aggregation kinetics (Figure 2C–F). While the aggregation of CPH was enhanced by the addition of PEG_{8000}, the CPS samples indicated the need for a reduction of the repulsion (by lowering the pH) to enable aggregation. This could be further investigated by the addition of high concentrated salts, which largely eliminates electrostatic interactions. Additionally, the use of different-sized CP and PEG could help to understand the role of their solubility in the system.

Last, the low value of the R^2 for the fit of CPH with 8% PEG_{8000} at pH 3.0 (0.53) was presumably caused by sedimenting aggregates, due to the lack of agitation. This phenomenon was observed for the latex particles as well as different viruses, but not quantitatively recorded. Additionally, we assume that the non-spherical form of the aggregates caused deviating results, depending on the measured orientation, and this was more pronounced for the bigger sizes. The application of DLS for the recording of aggregation kinetics has its limitations, especially in a static particulate system, where sedimentation can alter the results. However, we expected to derive indications concerning the influence of pH and PEG_{8000} concentration from the kinetics, rather than the knowledge of the finite size. This point should be especially stressed as the SXC operation introduces shear forces, which might break-up aggregates [25] and cannot be reflected by the kinetics presented in this work.

4.2. Steric Exclusion Chromatography

Next, the four different conditions of PEG/pH-combinations, which were used for the aggregation kinetics, were now applied in the SXC. Both particle types revealed very low yields in the elution fractions of $\leq$21% for CPS and $\leq$7% for CPH, either due to low total recoveries, or due to a breakthrough during loading (Figure 3). None of the tested

conditions were appropriate to cause particle retention throughout loading and allow for a full elution at the same time. These results were contradictory to previous applications of the SXC with 8% PEG_{8000} (pH 7.4) for a similar-sized virus, the Orf virus, which revealed >90% yield [17]. A similar zeta potential of 15 mV with the same PEG_{8000} concentration showed virtually no recovery of the CP. Thus, we assumed the recovery losses were caused by dense particle aggregates, which remained on the stationary phase and induced filtration effects. This aspect will be discussed later in more detail. Additionally, an incubation of the loaded column, with salt- or surfactant-containing buffer throughout the elution [15], could improve the elution conditions and would help to understand the incomplete mass balances. Another explanation for the low recoveries could be (un-)specific binding to the membranes. However, we excluded this hypothesis at least for the CPS at neutral process conditions, as substantial amounts of the beads were obtained in the flow-through fractions.

The occurrence of CPS in the flow-through fraction was diminished by increased PEG_{8000} concentrations and reduced pH values. For these conditions, the slope of the pressure increase was considerably steeper than reported for biological nanoparticles using the SXC [1,10,16,17]. We propose two reasons for this behavior: (1) the approximated two-dimensional surface charge distribution of the hard latex spheres is less complex than the three-dimensional characteristics of so-called soft particles, e.g., viruses [26–30], which additionally have an amphoteric character. Furthermore, the distribution of the functional groups is assumed to be more homogenous on chemically defined hard particles. These characteristics cause more compact aggregates with reduced permeability [11]. Further investigations might focus on the addition of salts to investigate the reduction of electrostatic attraction [1], and the impact of the functionalization on the precipitation. (2) The high concentration and purity of the latex suspensions led to increased crowding-out effects as no other solutes interfered with the osmotic force induced by the PEG_{8000} [1]. Lowering the particle concentration (Figure 1B) was no option, as unstable size and charge measurements were obtained in the pre-experiments. Therefore, reduced PEG concentrations might improve a comparison of the latex particle system with the biological counterparts. We would further like to point out that latex particles are presumably more hydrophobic [31] than viruses [32]. This characteristic should lead to reduced SXC efficiencies. On the one hand, the binding to the hydrophilic cellulose membranes is expected to be reduced, and on the other hand, PEG is less effectively excluded from hydrophobic surfaces, having a slightly hydrophobic character itself [1].

It should be mentioned that, although the exact values, i.e., the charge of similar-sized particles, may not be appropriate to compare the SXC applications, general core concepts could be extracted, e.g., the pre-column pressure behavior throughout loading. The initial pressure was dominated by the PEG_{8000} concentration, drastically increasing for loading conditions with reduced pH values. As mentioned, we attributed this to the formation of big aggregates causing pore blockage. As a secondary effect, increased PEG_{8000} concentrations cause higher viscosities, reinforcing the behavior. For the purification of a hepatitis C virus by SXC, a similar trend was reported [10]. Here, the approximation of the pH to the pI caused increased yields and higher pre-column pressures throughout loading, i.e., the reduced repulsion caused stronger accretion. However, the limitations of this concept, and the impact of the aggregate size and aggregation kinetics on the SXC, have not yet been evaluated. Presumably, the identification of an operation window allows for a stable SXC operation without pore blockage events. Thus, the optimization of the SXC operation itself is more complex than traditional PEG precipitation, as concerns of elevated precipitation are not existent for the latter. Thus, optima for a sufficient target association without instant pore blockage should be investigated.

For the time-interval of loading (20 min), only the aggregate sizes equaling the pore diameter of the stationary phase (1 µm) (Figure 2E,F) revealed recoveries in the elution fraction (Figure 3). Presumably, stationary phases with bigger pore sizes might help to overcome the observed limitations. Future experiments with different pore structures will give valuable insights into the correlation between target precipitation, target retention,

and pore blockage. However, it should be noted again, that the aggregation kinetics in this study were of a static character. Thus, they were not representative for the true precipitate size that was loaded onto the stationary phase, but rather an indication of the aggregation behavior. For predicting the particle retention, these statically measured aggregate sizes did not correlate with the recovery in the flow-through fraction. This was especially visible for the CPS (Figures 2F and 4B). In more detail, the aggregate size and therefore the retention, due to filtration effects, can explain the higher total recoveries of CPS for 2% PEG_{8000} compared to 8% at pH 7.4, but not the zero breakthrough for 2% PEG_{8000} at pH 3.0. In this case, the steeper slope of the aggregation kinetics of the latter might explain the increased retention. The steepness represents the likelihood of bead association and retention. For all observed cases, the particle breakthrough was reduced with an increasing slope of the kinetics. However, the effects were not transferable between the two different latex particle types by sheer number.

We further concluded that the leveling pre-column pressure, following particle breakthrough of the CPS during loading at pH 7.4 (Figure 4E,F), was caused by repulsion, impeding a stable adherence to layers of particles inside the chromatographic membrane. More precisely, the CPS accreted to the hydrophilic stationary phase throughout loading due to crowding-out effects. At a certain point, the membrane pores were covered with CPS, which exhibited a high charge repulsion at this pH (−34 mV). This prevented further layering. A similar effect was observed for the phage M13K07 [1], a linear, uniformly negative-charged nanoparticle. Thus, the charge distribution on the latex particle surface could be the cause of this behavior. As already suggested, the addition of high salt concentrations would help to differentiate between the effects of the electrostatic interaction and the solubility of the beads throughout this process.

In summary, next to the already stated open questions, a study of PEG concentrations and pH values between the tested ranges would result in a further understanding of the retention mechanisms throughout the SXC process with CP. Nevertheless, we propose a general suitability of CPS for SXC description in the context of the tested conditions, as both extrema of full retention and complete breakthrough were observed for the CPS. Concerning an imitation of virus processing by SXC, we assume that further experiments with protein-functionalized CP in a wide pH and salt concentration range would be required. Such a study could be augmented by the inclusion of varying column-loading concepts. In our study, bulk loading was performed, but continuous in-line mixing could reduce variations of the holding time in the superloop, and improve column characterization.

5. Conclusions

In the present study, the suitability of polystyrene particles, CPH and CPS, to determine critical process parameters for the SXC process, was investigated. We assume that the recoveries and yields were controlled by the attractive and repulsive forces of the particles, determining their aggregation kinetics, i.e., size distribution and slope. However, the role of solubility, in contrast to electrostatic interaction, was not investigated. More precisely, the aggregate size served as an indicator for the total recovery in most cases, which was reduced with increasing size. Additionally, for similar sizes, an increase of the kinetics' slopes also indicated reduced total recoveries. Especially for CPS, the slope as well as the mean aggregate size predicted relative total recoveries and yields. Overall, the highest yields were achieved for the lowest slope values for both particle types. This observation served as a general concept, but the exact numbers were not transferable between the CP. In conclusion, the determination of aggregation kinetics were helpful for understanding losses throughout the SXC process, describing relative yields and recoveries. We propose this first description of the SXC by the target aggregation behavior as helpful for future investigations of the fundamentals of this method.

Author Contributions: Conceptualization, F.E., M.S., K.L.; validation, F.E.; investigation, F.E., M.S.; resources, M.W.W.; data curation, F.E., M.S.; writing—original draft preparation, F.E.; writing—review and editing, M.S., K.L., M.W.W.; visualization, F.E., M.S.; supervision, M.W.W.; project administration, M.W.W.; funding acquisition, M.W.W. All authors have read and agreed to the published version of the manuscript.

Funding: This work was financially supported by the Heinrich Boell Foundation with a doctoral scholarship to F.E. and the University of Applied Sciences Mittelhessen, Giessen, Germany.

Institutional Review Board Statement: Not applicable.

Informed Consent Statement: Not applicable.

Data Availability Statement: All relevant data are within the paper.

Acknowledgments: We thank Jonas S. Schmidt for his diligent support with the particle characterization, and Catherine Meckel-Oschmann for the thorough proofreading of the manuscript. The presented manuscript is part of F.E.'s dissertation at the Graduate Centre for Engineering Sciences under the aegis of the Justus Liebig University Giessen, Germany, in cooperation with the University of Applied Sciences Mittelhessen, Giessen, Germany.

Conflicts of Interest: The authors declare no conflict of interest.

References

1. Lee, J.; Gan, H.T.; Latiff, S.M.A.; Chuah, C.; Lee, W.Y.; Yang, Y.-S.; Loo, B.; Ng, S.K.; Gagnon, P. Principles and Applications of Steric Exclusion Chromatography. *J. Chromatogr. A* **2012**, *1270*, 162–170. [CrossRef] [PubMed]
2. Gagnon, P.; Toh, P.; Lee, J. High Productivity Purification of Immunoglobulin G Monoclonal Antibodies on Starch-Coated Magnetic Nanoparticles by Steric Exclusion of Polyethylene Glycol. *J. Chromatogr. A* **2014**, *1324*, 171–180. [CrossRef] [PubMed]
3. Minton, A.P. Molecular crowding: Analysis of effects of high concentrations of inert cosolutes on biochemical equilibria and rates in terms of volume exclusion. In *Energetics of Biological Macromolecules Part B*; Ackers, G.K., Johnson, M.L., Eds.; Elsevier: Amsterdam, The Netherlands, 1998; pp. 127–149. ISBN 9780121821968.
4. Arakawa, T.; Timasheff, S.N. Mechanism of poly(ethylene glycol) interaction with proteins. *Biochemistry* **1985**, *24*, 6756–6762. [CrossRef]
5. Lee, J.C.; Lee, L.L. Preferential Solvent Interactions Between Proteins and Polyethylene Glycols. *J. Biol. Chem.* **1981**, *256*, 625–631. [CrossRef]
6. Großhans, S.; Wang, G.; Hubbuch, J. Water on Hydrophobic Surfaces: Mechanistic Modeling of Polyethylene Glycol-Induced Protein Precipitation. *Bioprocess Biosyst. Eng.* **2019**, *42*, 513–520. [CrossRef]
7. Sukenik, S.; Sapir, L.; Harries, D. Balance of enthalpy and entropy in depletion forces. *Curr. Opin. Colloid Interface Sci.* **2013**, *18*, 495–501. [CrossRef]
8. Arakawa, T.; Gagnon, P. Excluded Cosolvent in Chromatography. *J. Pharm. Sci.* **2018**, *107*, 2297–2305. [CrossRef]
9. Kuznetsova, I.M.; Turoverov, K.K.; Uversky, V.N. What macromolecular crowding can do to a protein. *Int. J. Mol. Sci.* **2014**, *15*, 23090–23140. [CrossRef] [PubMed]
10. Lothert, K.; Offersgaard, A.F.; Pihl, A.F.; Mathiesen, C.K.; Jensen, T.B.; Alzua, G.P.; Fahnøe, U.; Bukh, J.; Gottwein, J.M.; Wolff, M.W. Development of a downstream process for the production of an inactivated whole hepatitis C virus vaccine. *Sci. Rep.* **2020**, *10*, 3018. [CrossRef]
11. Zemb, T.; Leontidis, E. Equilibrium in soft-matter systems under the influence of competing forces. *Curr. Opin. Colloid Interface Sci.* **2013**, *18*, 493–494. [CrossRef]
12. Arakawa, T.; Timasheff, S.N. Preferential interactions of proteins with salts in concentrated solutions. *Biochemistry* **1982**, *21*, 6545–6552. [CrossRef] [PubMed]
13. Levanova, A.; Poranen, M.M. Application of Steric Exclusion Chromatography on Monoliths for Separation and Purification of RNA Molecules. *J. Chromatogr. A* **2018**, *1574*, 50–59. [CrossRef] [PubMed]
14. Wang, C.; Bai, S.; Tao, S.-P.; Sun, Y. Evaluation of Steric Exclusion Chromatography on Cryogel Column for the Separation of Serum Proteins. *J. Chromatogr. A* **2014**, *1333*, 54–59. [CrossRef] [PubMed]
15. Lothert, K.; Sprick, G.; Beyer, F.; Lauria, G.; Czermak, P.; Wolff, M.W. Membrane-Based Steric Exclusion Chromatography for the Purification of a Recombinant Baculovirus and its Application for Cell Therapy. *J. Virol. Methods* **2020**, *275*, 113756. [CrossRef]
16. Lothert, K.; Pagallies, F.; Eilts, F.; Sivanesapillai, A.; Hardt, M.; Moebus, A.; Feger, T.; Amann, R.; Wolff, M.W. A scalable downstream process for the purification of the cell culture-derived Orf virus for human or veterinary applications. *J. Biotechnol.* **2020**, *323*, 221–230. [CrossRef]
17. Lothert, K.; Pagallies, F.; Feger, T.; Amann, R.; Wolff, M.W. Selection of chromatographic methods for the purification of cell culture-derived Orf virus for its application as a vaccine or viral vector. *J. Biotechnol.* **2020**, *323*, 62–72. [CrossRef]

18. Marichal-Gallardo, P.; Börner, K.; Pieler, M.M.; Sonntag-Buck, V.; Obr, M.; Bejarano, D.; Wolff, M.W.; Kräusslich, H.-G.; Reichl, U.; Grimm, D. Single-use capture purification of adeno-associated viral gene transfer vectors by membrane-based steric exclusion chromatography. *Hum. Gene Ther.* **2021**, *32*, 959–974. [CrossRef]
19. Marichal-Gallardo, P.; Pieler, M.M.; Wolff, M.W.; Reichl, U. Steric Exclusion Chromatography for Purification of Cell Culture-Derived Influenza A Virus Using Regenerated Cellulose Membranes and Polyethylene Glycol. *J. Chromatogr. A* **2017**, *1483*, 110–119. [CrossRef]
20. Giesler, J.; Weirauch, L.; Thöming, J.; Baune, M.; Pesch, G.R. Separating microparticles by material and size using dielectrophoretic chromatography with frequency modulation. *Sci. Rep.* **2021**, *11*, 16861. [CrossRef]
21. de Beeck, J.O.; de Malsche, W.; Vangelooven, J.; Gardeniers, H.; Desmet, G. Hydrodynamic chromatography of polystyrene microparticles in micropillar array columns. *J. Chromatogr. A* **2010**, *1217*, 6077–6084. [CrossRef]
22. Meder, F.; Daberkow, T.; Treccani, L.; Wilhelm, M.; Schowalter, M.; Rosenauer, A.; Mädler, L.; Rezwan, K. Protein adsorption on colloidal alumina particles functionalized with amino, carboxyl, sulfonate and phosphate groups. *Acta Biomater.* **2012**, *8*, 1221–1229. [CrossRef] [PubMed]
23. Wu, C.-Y.; Tu, K.-J.; Deng, J.-P.; Lo, Y.-S.; Wu, C.-H. Markedly Enhanced Surface Hydroxyl Groups of TiO_2 Nanoparticles with Superior Water-Dispersibility for Photocatalysis. *Materials* **2017**, *10*, 566. [CrossRef] [PubMed]
24. Sthoer, A.P.A.; Tyrode, E.C. Anion Specific Effects at Negatively Charged Interfaces: Influence of Cl-, Br-, I-, and SCN- on the Interactions of Na+ with the Carboxylic Acid Moiety. *J. Phys. Chem. B* **2021**, *125*, 12384–12391. [CrossRef] [PubMed]
25. Del Pons Royo, M.C.; Beulay, J.-L.; Valery, E.; Jungbauer, A.; Satzer, P. Mode and dosage time in polyethylene glycol precipitation process influences protein precipitate size and filterability. *Process BioChem.* **2022**, *114*, 77–85. [CrossRef]
26. Duval, J.F.L.; Merlin, J.; Narayana, P.A.L. Electrostatic Interactions Between Diffuse Soft Multi-layered (Bio)Particles: Beyond Debye–Hückel Approximation and Deryagin Formulation. *Phys. Chem. Chem. Phys.* **2011**, *13*, 1037–1053. [CrossRef]
27. Duval, J.F.; Gaboriaud, F. Progress in electrohydrodynamics of soft microbial particle interphases. *Curr. Opin. Colloid Interface Sci.* **2010**, *15*, 184–195. [CrossRef]
28. Dika, C.; Duval, J.F.L.; Francius, G.; Perrin, A.; Gantzer, C. Isoelectric Po*Int.* is an Inadequate Descriptor of MS2, Phi X 174 and PRD1 Phages Adhesion on Abiotic Surfaces. *J. Colloid Interface Sci.* **2015**, *446*, 327–334. [CrossRef]
29. Langlet, J.; Gaboriaud, F.; Gantzer, C.; Duval, J.F.L. Impact of Chemical and Structural Anisotropy on the Electrophoretic Mobility of Spherical Soft Multilayer Particles: The Case of Bacteriophage MS2. *Biophys. J.* **2008**, *94*, 3293–3312. [CrossRef]
30. Dika, C.; Ly-Chatain, M.H.; Francius, G.; Duval, J.; Gantzer, C. Non-DLVO Adhesion of F-Specific RNA Bacteriophages to Abiotic Surfaces: Importance of Surface Roughness, Hydrophobic and Electrostatic Interactions. *Colloid Surf. A* **2013**, *435*, 178–187. [CrossRef]
31. Faille, C.; Lemy, C.; Allion-Maurer, A.; Zoueshtiagh, F. Evaluation of the hydrophobic properties of latex microspheres and Bacillus spores. Influence of the particle size on the data obtained by the MATH method (microbial adhesion to hydrocarbons). *Colloid Surf. B* **2019**, *182*, 110398. [CrossRef]
32. Shi, H.; Tarabara, V.V. Charge, size distribution and hydrophobicity of viruses: Effect of propagation and purification methods. *J. Virol. Methods* **2018**, *256*, 123–132. [CrossRef] [PubMed]

Part B: Identification of critical process parameters for the Orf virus

Eilts, F.; Lothert, K.; Orbay, S.; Pagallies, F.; Amann, R.; Wolff, M. W. (2022). A summary of practical considerations for the application of the steric exclusion chromatography for the purification of the Orf viral vector. Membranes 12 (11), 1070. doi: 10.3390/membranes12111070

membranes

MDPI

Article

A Summary of Practical Considerations for the Application of the Steric Exclusion Chromatography for the Purification of the Orf Viral Vector

Friederike Eilts [1], Keven Lothert [1], Sabri Orbay [1], Felix Pagallies [2], Ralf Amann [2,3] and Michael W. Wolff [1,4,*]

[1] Institute of Bioprocess Engineering and Pharmaceutical Technology, University of Applied Sciences Mittelhessen (THM), Wiesenstr.14, 35390 Giessen, Germany
[2] Department of Immunology, University of Tuebingen, Auf der Morgenstelle 15, 72076 Tuebingen, Germany
[3] PRiME Vector Technologies, Herrenberger Straße 24, 72070 Tuebingen, Germany
[4] Fraunhofer Institute for Molecular Biology and Applied Ecology (IME), Ohlebergsweg 12, 35392 Giessen, Germany
* Correspondence: michael.wolff@lse.thm.de

Abstract: Steric exclusion chromatography (SXC) is a promising purification method for biological macromolecules such as the Orf virus (ORFV) vector. The method's principle is closely related to conventional polyethylene glycol (PEG) precipitation, repeatedly implementing membranes as porous chromatographic media. In the past decade, several purification tasks with SXC showed exceptionally high yields and a high impurity removal. However, the effect of varying process parameters, on the precipitation success and its limitations to SXC, is not yet well understood. For this reason, the precipitation behavior and SXC adaptation for ORFV were investigated for the PEG/ORFV contact time, the membranes pore size, and the type and concentration of ions. All three parameters influenced the ORFV recoveries significantly. A small pore size and a long contact time induced filtration effects and inhibited a full virus recovery. The application of salts had complex concentration-dependent effects on precipitation and SXC yields, and ranged from a complete prevention of precipitation in the presence of kosmotropic substances to increased efficiencies with Mg^{2+} ions. The latter finding might be useful to reduce PEG concentrations while maintaining high yields. With this knowledge, we hope to clarify several limitations of SXC operations and improve the tool-set for a successful process adaptation.

Keywords: hofmeister series; membrane chromatography; polyethylene glycol precipitation; pore size; regenerated cellulose; steric exclusion

check for updates

Citation: Eilts, F.; Lothert, K.; Orbay, S.; Pagallies, F.; Amann, R.; Wolff, M.W. A Summary of Practical Considerations for the Application of the Steric Exclusion Chromatography for the Purification of the Orf Viral Vector. *Membranes* **2022**, *12*, 1070. https://doi.org/10.3390/membranes12111070

Academic Editor: Scott M. Husson

Received: 29 August 2022
Accepted: 26 October 2022
Published: 29 October 2022

Publisher's Note: MDPI stays neutral with regard to jurisdictional claims in published maps and institutional affiliations.

Copyright: © 2022 by the authors. Licensee MDPI, Basel, Switzerland. This article is an open access article distributed under the terms and conditions of the Creative Commons Attribution (CC BY) license (https://creativecommons.org/licenses/by/4.0/).

1. Introduction

The application of biological nanoparticles, such as viruses, is increasingly in the focus of the biopharmaceutical industry. Compared to proteins as active pharmaceutical ingredients, new challenges have been encountered in the production processes of viruses, especially in downstream processing. This is mainly due to the different composition and size of virions. Thus, the unit operations in downstream processing need reconsideration. For chromatographic purification tasks, convective mass transport, e.g., in membranes or monoliths, is often preferred over resin-based applications, offering primarily diffusion [1,2]. A rather new chromatographic method, which frequently implements membranes for virus purification, is the steric exclusion chromatography (SXC). The SXC is closely related to precipitation [3], which is intrinsically described by the theories of attractive depletion and excluded volumes [4]. Precipitation is strongly dependent on self-association effects [5], which alter the interaction of the solvents (including the targets) among each other [6]. Additionally, precipitation is adaptable to nearly all biological nanoparticles and large proteins, by varying the process parameters, e.g., solvent concentrations, incubation time, or

ionic strength [7]. However, the impurity removal in precipitation is often insufficient and a solid-liquid separation needs to be performed subsequently [8]. For this reason, chromatographic processes are preferred over precipitation in modern pharmaceutical production, due to their selectivity and scalable throughput [3]. Steric exclusion chromatography (SXC) combines the approaches of precipitation and chromatography and several advantages are offered: the flow rates and, therefore, throughput are adjustable, continuous processing is possible, and a secondary step for the separation of the precipitates from the supernatant is omitted [3,8]. SXC was first described by Lee et al. [9]. Since then, applications with various biological macromolecules and nanoparticles, such as immunoglobulins [8–11], viruses [9,12–20], virus-like particles [21], latex particles [22], and nucleic acids [23] were published. Excellent introductions into the working principles of SXC were published by Lee et al. [9] and Gagnon et al. [10], which we encourage to consult.

As the name suggests, SXC is based on exclusion effects. In most applications, polyethylene glycol (PEG) is utilized as the precipitating agent. Just as in conventional PEG precipitation, by using PEG of an appropriate size, i.e., hydrodynamic radius [7,24], and concentration, the target molecules are excluded from the bulk solution according to their respective size [4,5]. Conclusively, the effect is enhanced by increasing the size and the concentration of the solutes, i.e., PEG and the target [5]. As the PEG molecules are unable to fill the space of preferential hydration around each target, an increase of water concentration in this region is caused compared to the bulk zone, so that a so-called PEG-deficient zone is formed [9]. By this discontinuity, the free energy of the system is increased, and the unfavorable status is resolved by a reduction of the accessible interface, which forces the targets to associate. Up to this point, the SXC process is no different from conventional precipitation. However, in the chromatographic process, a stationary phase, e.g., a membrane or monolith, is implemented. In other words, the stationary phase is part of the precipitating system, by offering a large surface area, where a PEG-deficient zone can form. Hence, the targets form precipitates at the inner surface area of the stationary phase and are retained [9], making the SXC a bind-and-elute method. Concerning the workflow, the target is combined with a PEG-enriched solution and loaded onto a chromatographic column, e.g., a hydrophilic membrane (Figure 1). Whereas conventional PEG-precipitation aims to maximize selective agglomeration, SXC is based on the retention of the target on the stationary phase by the same exclusion effects and contaminants are washed out throughout the loading of the target. By an omission of PEG in SXC, the target can be eluted from the column with a minimized residual PEG concentration in a purified concentrated manner. At this point, it should be made clear that SXC is not based on any kind of filtration process. In fact, filtration is a limitation to the method. Thus, the balance among rapid precipitation, sufficient retention of the target, and pore blockage by big precipitates must be maintained. Other limitations are an increased viscosity of the PEG-solutions, which can cause reduced diffusion and an increased pressure in the chromatographic system. Apart from the PEG and the target size and concentration, other important factors for the here presented SXC application are the surface characteristics of the targets and the stationary phase (charge [5,9], hydrophilicity [24]), composition of the liquid phase (buffers and salts [5,24–26]), and the contact time of target and PEG [18].

One target that was successfully purified by SXC is the Orf virus (ORFV). The ORFV is a DNA-virus of the genus *Parapoxvirus* that has an ovoid shape of approximately 140–200 nm in width and 220–300 nm in length [27–29]. The pharmaceutical application of the ORFV was shown as a viral vector platform [30–33], an oncolytic and antiviral therapy [34–36], and as an immunomodulatory agent [37–39]. Like many other poxviruses, the ORFV is very stable against degrading forces, and thus an ideal model for purification processes. This work is based on two recent publications, where we reported on the application of SXC in a purification process for ORFV, implemented in a full downstream processing (DSP) train [13,14]. In this process, SXC was employed with yields of >80% and a full recovery from the column as well as a high impurity removal. Here, we describe the process of a SXC adaptation for the purification of infectious ORFV with cellulose

membrane columns, in consideration of these published results. We investigated three parameters: the PEG/ORFV-contact time, the pore size of the membrane stationary phase, as well as the composition and concentration of different salts and buffers. Complimentary to the SXC application of the ORFV, offline aggregation kinetics of the SXC load were performed and analyzed. These data were used to understand the column blockage events and the reduction of yields due to a reduced target retention. We want to give an insight into the adaptation of SXC for a purification task, and equip the reader with pertinent tools to adjust the method for possible new targets with membrane columns. We further discuss the possibility to use precipitation kinetics to predict optimal parameters for a SXC application. With this knowledge, we hope to pave the path for SXC as a possible future purification platform technology.

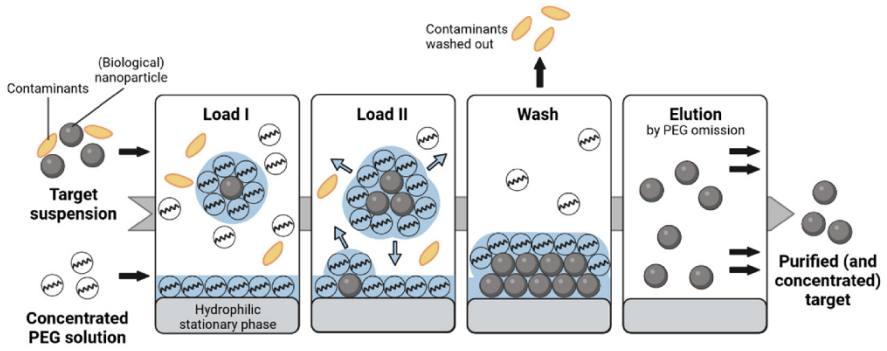

Figure 1. Overview of the working principle of the steric exclusion chromatography (SXC). The target (including impurities from production) is mixed with a concentrated PEG solution. The feed is loaded onto a hydrophilic stationary phase, e.g., cellulose membranes. A PEG-deficient zone (blue) covers the molecules and the stationary phase (load I), while the thickness of this zone is determined by the hydrodynamic diameter and the concentration of the PEG molecules. To reduce the PEG-deficient zones, targets associate/precipitate with each other as well as at the stationary phase (load II) [9,10]. The binding of the targets at the stationary phase allows for a wash-out of smaller contaminants (wash). The binding is reversable by reducing the PEG concentration (elution) so that a purified, concentrated sample can be eluted. The figure was adapted from Eilts et al. [20], and was prepared using biorender.com.

2. Materials and Methods

All chemicals were purchased from Carl Roth, if not stated otherwise.

2.1. Preparation of Virus Stocks

In this study, the attenuated ORFV strain D1701-V, expressing the green fluorescent protein AcGFP [31], was used. The virus was produced in Vero cells, as previously described [32]. After a successful cell infection and incubation, the cell-culture was subjected to one freeze-thaw cycle (−80 °C). A clarification from cell debris was undertaken, using centrifugation (4500× *g*, 30 min). Subsequently, the supernatant was stored at −80 °C until further use. For each set of experiments, several batches from this procedure were pooled to generate one stock.

2.2. SXC Application

The SXC of the ORFV was performed as described several times before [12,15–17] with minor adjustments. In brief, the stationary phase was comprised of single-use regenerated cellulose membranes, combined in a stack of ten sheets with 13 mm in diameter. The nominal pore size was 1 µm (Whatman, Maidstone, UK), and alternatively 3–5 µm (kindly provided by Sartorius Stedim). The column was equilibrated with a run buffer (either 20 mM TRIS-HCl, 0.1 m HEPES, PBS, or 0.1 M citrate phosphate buffer (CPB)), combined with the desired salt (0–600 mM of Na_2SO_4, KCl, NaCl, $NaNO_3$, $MgSO_4$, or $MgCl_2$) and the

appropriate PEG concentration (2–8%) and PEG molecular weight (6000–12,000 Da). For loading, the clarified cell culture supernatant was mixed 1:4 with a concentrated buffer to match the concentrations of the run buffer. To generate the feed, offline or in-line mixing was applied. In detail, for offline mixing, the ORFV/PEG solution was prepared in advance and filled into a superloop (Cytiva, Marlborough, MA, USA) and loaded onto the column. For in-line mixing, the ORFV and the enriched PEG solutions were pumped simultaneously and combined in the mixer (1.4 mL) of the FPLC system (Äkta Pure 25, Cytiva). If not stated otherwise, the feed was loaded onto the membranes until the pressure limit of the respective membrane module was reached, i.e., 2.0 MPa for 1 µm membranes modules and 0.4 MPa for 3–5 µm modules. After loading the sample onto the column, a wash step with the run buffer was undertaken for at least 5 mL. Subsequently, the elution step was performed by omitting the PEG and the additional salts, however, 0.4 M NaCl was added to the buffer. All buffers used in the SXC experiments were of neutral pH (7.4) and their influence on the ORFV infectivity was neglectable for the duration of the SXC runs. A flow rate of 2 mL min^{-1} was used for all runs, unless stated otherwise. Relative recoveries of the infectious ORFV were determined, based on the concentration of each initial load sample.

2.3. ORFV Infectivity Titration

The infectivity of the ORFV samples was determined by a flow cytometry assay using a Guava easycyte HT (Merck Millipore, Darmstadt, Germany). The procedure was adapted from Lothert et al. [14], however, the washing procedure was omitted. Instead, after centrifugation, the cell pellets were resuspended with PBS, containing 1% paraformaldehyde, 2% FCS, and 2 mM EDTA (VWR International, Radnor, PA, USA). The readout was conducted within 48 h. The relative error between samples in one batch was below 10%. The effect of PEG on the ORFV infectivity was assumed to be neglectable, proven by full recoveries of infectious ORFV in previous experiments [13,14]. The presence of all tested buffers and salts (Na_2SO_4, KCl, NaCl, $NaNO_3$, $MgSO_4$, or $MgCl_2$) applied in the SXC experiments had no effect on the virus infectivity (Supplementary Material S1) or the assay (Figure S1).

2.4. Size Measurements

The precipitation behavior of the clarified ORFV solutions was analyzed over time. The cell culture supernatant was mixed with a concentrated PEG/salt-solution in a relation of 1:4 to equal the desired concentrations. Two different buffering systems were used for these experiments: 20 mM TRIS-HCl (pH 7.4) was applied for all experiments with varying salt concentrations (20–200 mM), and 0.1 M CPB of physiological conductivity, on the other hand, was used for screening different PEG concentrations (0–12%) and pH values (4–7.4). Immediately after preparation, the samples were analyzed by dynamic light scattering (DLS), using a Zetasizer ZS90 with the respective Zetasizer software, version 7.13, (both Malvern Panalytical) in micro-cuvettes (Sarstedt, Nümbrecht, Germany). Automatic size measurements were conducted every 5 min over the course of up to 14 h. After the measurement, the precipitates were visualized by bright-field microscopy (MC170HD with Leica Application Suite software, version 3.0.0, both Leica). Next to this data acquisition, a design of experiments (DOE)-based model was generated for the time-dependent size change of the samples under varying pH and PEG_{6000} (molecular weight of 6000 Da) concentrations (see Section 2.5).

2.5. Statistical Analysis

Unless stated otherwise, the experiments were carried out in triplicates ($n = 3$), which were used to calculate the respective mean and standard deviation. For an analysis of significance, an ANOVA with *Tukey* test was performed, where appropriate (Origin Pro 2021b, OriginLab Corporation).

Furthermore, two DOE models were generated with the Design Expert software (version 12, Stat-Ease). These included screening for critical process parameters of the SXC (Section 3.1.1, PEG concentration, and flow rate), as well as a depiction of

the aggregation kinetics of the ORFV in the presence of PEG and varied pH values (Section 3.1.3, time). The statistical evaluation of these designs can be found in the Supplementary Material, S2 and S3, respectively.

3. Results and Discussion

3.1. Influence of the SXC Loading Parameters on the ORFV Recoveries

In this chapter, the loading parameters, i.e., PEG concentration and molecular weight, as well as the flow rate of the SXC experiments with the ORFV, were evaluated. Additionally, the extent of time-dependent precipitation, analyzed by offline size measurements, was compared with the ORFV recoveries and yields in the SXC.

3.1.1. PEG Concentration and Flow Rate

First, using a DOE-approach, different PEG molecular weights were tested in the SXC of the ORFV, according to previously applied concentrations and molecular weights for virus purification [16], i.e., 4–8% PEG of 6000 to 12,000 kDa. For each run, 10 mL ORFV/PEG sample was loaded onto the membrane modules. All experiments were done using a TRIS buffer with 180 mM NaCl. The virus was mixed offline, and the time of mixing, until the entire sample was loaded onto the column, was approximately 20 min. A linear relation was observed, as increased yields were obtained with an increasing PEG concentration and molecular weight from 41% up to 64%, with an optimum at the edge of the design space at 8% PEG_{12000} (Figure 2A). In other words, as the maximum recovery was obtained with the highest chosen PEG concentration and molecular weight, it could be possible that the optimum lies outside the tested range of these parameters. The relation was dominated by the PEG concentration, indicated by a steeper slope for an increasing yield, i.e., a 15% yield increase between 4% and 8% PEG versus a 5% yield increase between 6000 and 12,000 kDa PEG. This was expected, as the precipitation of a target increases in efficiency related to higher PEG concentrations [5] up to a certain point, where precipitation is limited by a compression of the PEG molecules. This causes smaller hydrodynamic radii fo the PEG molecules and reduces the efficiency of exclusion phenomena [7]. In this research work, the maximum applicable PEG concentration for the system was not found. The optimum for an ORFV yield was not covered by the tested design space, presumably lying at higher PEG concentrations and molecular weights. Higher PEG concentrations were not tested, as a high viscosity hampers processing and prevents the application of high flow rates during chromatography.

Overall, the ORFV recoveries in the qabove descibres elution fraction were lower than published before for the same column type of regenerated cellulose membranes with 1 µm pore in diameter [14], i.e., >80% using 8% PEG_{6000}. We assume this to be due to an increased flow rate (Figure S2) and a fixed loading volume of ORFV, which corresponded to only half the dynamic binding capacity of the membrane modules determined with 1.81×10^8 IU (infectious unit) $mL^{-1}_{membrane}$ by Lothert et al. [14].

It should be noted that no extensive pressure increase throughout the sample loading, apart from viscosity-induced increases, was observed with any tested PEG concentration. This led to two conclusions. Firstly, the precipitation in the pore system of the stationary phase, which is the working principle of the SXC, did not reach a maximum to cause a pore blockage. This was not surprising, as the binding capacity of the column was not fully exploited. Secondly, precipitates, which formed throughout the holding time of sample loading, caused no adverse pressure effects. Using offline mixing, as for the experiments in this section, the loading time of the pre-mixed ORFV/PEG solution onto the column took 20 min. Hereafter, this time interval is called *incubation time*. This period is expected to allow for the formation of ORFV precipitates, which increase in size over time while the load is applied. From this description, one might apprehend pore blockage of the stationary phase due to aggregates, which are held back on the upper layers of the membranes. With the here applied set-up, no such filtration effects were indicated by the online pressure monitoring, however, higher loading volumes might reveal the opposite.

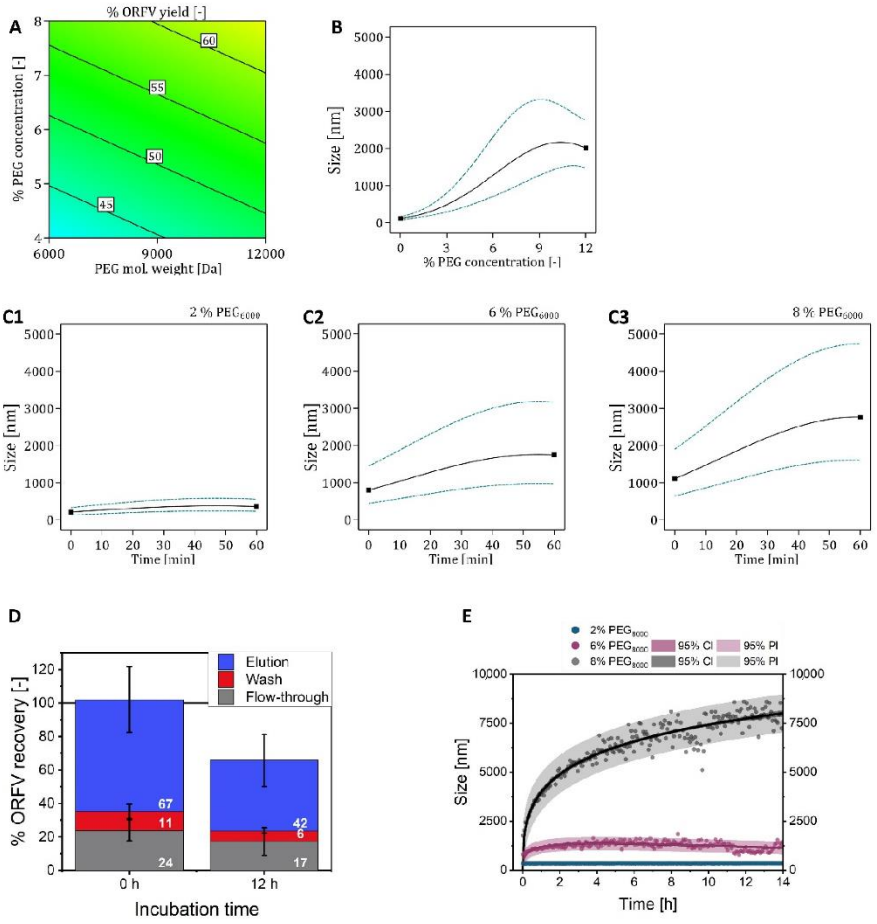

Figure 2. Investigation of loading parameters for steric exclusion chromatography (SXC) of the Orf virus (ORFV). (**A**) The influence of the polyethylene glycol (PEG) molecular weight (6000–12,000 Da) and concentration (4–8%) in a TRIS buffer on the yield of the ORFV was tested, using a design of experiments approach (Supplementary Material S2). The flow rate was set to 2 mL min^{-1} and the elution buffer was composed of 0% PEG + 0.4 M NaCl. (**B**,**C**). According to the conditions chosen in A, the ORFV cell culture supernatant was mixed with concentrated PEG solutions to test the precipitation behavior by size measurements. Samples were incubated in 0–12% PEG_{6000} for 60 min. The resulting kinetics were used to generate a design of experiments-based model (Supplementary Material S3). (**C1**–**3**) represent the kinetics for selected concentrations of 2%, 6%, and 8% PEG_{6000}. (**D**) Using 8% PEG_{8000} in a citrate phosphate buffer, the SXC of the ORFV was operated using different times of contact of the ORFV and the concentrated PEG solutions. The samples were pre-mixed in a superloop and thereafter either loaded onto the column directly (0 h) or after 12 h of incubation time. Representative chromatograms may be found in the Supplementary Material S4.1. (**E**) Additionally, the same concentrations as in **C1**–**C3**, 2%, 6%, and 8%, were applied with PEG_{8000} in a citrate phosphate buffer in a similar set-up, recording the precipitate size of the ORFV. The reference for the calculations of the individual recoveries was the loading sample after the respective incubation time.

3.1.2. Incubation Time Using PEG_{6000}

To further investigate the impact of the incubation time on the ORFV precipitation kinetics, the time-dependent size distribution of the cell culture-derived ORFV, combined

with PEG, was measured in static experiments by DLS. We tested 0–12% PEG_{6000} in CPB, depicted in Figure 2B,C for pH 7.4. Other pH values tested in the DOE-planned size measurements are presented in the Supplementary Material S3, especially Figures S3 and S4.

For all tested PEG concentrations, the aggregate size increased with time. However, the slope, i.e., the velocity of the aggregate size increase, decreased to approximately zero, approaching 60 min for all tested PEG concentrations (Figure 2C). As for the mean sizes after 60 min incubation time, the DOE model predicted the strongest PEG-induced impact between 3% and 8% PEG_{6000} (Figure 2B). The visualization of the ORFV aggregates by bright-field microscopy revealed the same trends as predicted by the statistical model (see Supplementary Material S3.2). The dimensions of the aggregates were of random shape, seemingly consisting of clusters of smaller circular particles (5–10 µm). This leads to the assumption that precipitates form around nuclei, such as cell debris, and grow and randomly attach to each other [40]. The accumulations of smaller precipitates in loose formations might be more sensitive to a shear stress-induced break-up, rather than big dense aggregates [41]. Accordingly, we assume that the actual size of the aggregates loaded onto the membranes is smaller than the size measured in the static experiments shown here. Thus, this effect might be the cause for the precipitates of virus and cell debris to not increase the pre-column pressures significantly by inducing pore blockage in the top membrane layers.

Surely, this set-up is limited by the DLS method itself, as the size distribution often does not resolute different size fractions, especially for aggregates exceeding 6 µm [10]. Methods, investigating the aggregate density and formation, could improve the validity of the aggregation kinetics [40]. However, from these experiments we expect to derive an indicator for the precipitate formation, depending on the changes in the solute composition.

3.1.3. Incubation Time Using PEG_{8000}

Using the knowledge from the previous section, two extrema for the incubation time of an ORFV/PEG_{8000} mixture in CPB were tested in the SXC experiments: No incubation, and 12 h incubation time, both using offline mixing. To facilitate the analysis, the load volume for the column was set again to 10 mL feed. Without incubation, the total ORFV recovery was 102 ± 30%, whereas an incubation time of 12 h revealed 66 ± 20% (Figure 2D). The recoveries were calculated according to the respective load sample. Thus, a mean of 34% was not recovered from the column for the runs after 12 h incubation time. The ORFV yield in the elution fraction with no incubation time showed 67 ± 20%, whereas 12 h incubation time showed 42 ± 8%. The observations were supported by online DLS monitoring, which increased by 100 mV during the loading phase for both incubation times (Figure S6). No differences were observed in the online pressure measurement, similar to the results in the previous section. Thus, no elevated pore blockage is suspected due to increased incubation durations and increased precipitate size. It should be noted that the molecular weight of the PEG was 8000 Da in this set-up (Figure 2D,E), whereas 6000 Da were used for the experiments in Figure 2(A–C1). The increase in molecular weight entailed an increase of the mean size of the precipitates between a mean of 2500 µm up to nearly 4000 µm after 60 min (compare Figure 2C,E).

Nevertheless, the reduction in total recovery and yield indicated remaining virions on the membranes. Adsorption to the cellulose filters was excluded, as they are known to poorly bind viruses [42] and such effects were not observed in previous experiments with the ORFV [13,14]. Therefore, we assume that the increased precipitate sizes after a prolonged incubation time induced a retention of the ORFV on the upper layers of the membrane stationary phase. In other words, the ORFV precipitates were filtered instead of being retained by exclusion effects. A similar, but more pronounced reduction in the total recovery, due to the incubation of the virus/PEG mixture prior to column loading, was reported by Labisch et al. [18] for a lentivirus vector. The authors suspected the difference to originate from the formation of precipitates prior to loading onto the column, which we confirm here for the ORFV vector. Although our previous works with the ORFV showed

no limitations using offline mixing [13,14], and the total virus recovery with offline mixing (0 h incubation time) revealed up to 100% total ORFV recovery, the in-line mixing approach, as recommended by the lentivirus report and other publications [9,17,18], remains to be evaluated for the ORFV.

3.2. Variation of the Pore Size of the Stationary Phase

Based on the results in the previous section, which indicated possible filtration effects for ORFV precipitates in offline mixing, an in-line-mixing set-up was tested for two pore sizes of the cellulose membrane columns, i.e., 1 µm, and 3–5 µm. The mixing of the enriched PEG solution and the virus solution was done in the tubing of the chromatographic system, directly before loading onto the column. According to previous experiments in Section 3.1.1, the buffer was a TRIS buffer with 180 mM NaCl and 8% PEG_{6000}. Surprisingly, the loading of the sample onto the 1 µm cellulose membranes was not possible with a constant backpressure, and the loading volumes varied between 3 and 16 mL, using the same virus stock. However, the yields remained high with 99% ± 17% (Table 1). By changing the pore size from 1 µm to 3–5 µm, the loading volume was increased by more than three-times (Table 1). The virus load that was quantified in the flow-though, however, increased by 30%. Overall, the 3–5 µm membranes showed a robust operation with small standard deviations.

Table 1. Overview of recoveries and load volumes for infective ORFV from SXC experiments with regenerated cellulose membranes as stationary phases. Both column types (1 µm and 3–5 µm pore diameter) were single-use. They consisted of ten stacked membranes, each 13 mm in diameter. Each run consisted of a loading step (the flow-through is analyzed), a wash step, and two elution steps, i.e., a down-flow and an up-flow elution. The down-flow elution was performed in direction of flow, while the up-flow elution was counter-current.

Pore Size	Recoveries					Load	
	Flow-Through	Wash	Down-Flow Elution	Up-Flow Elution	Total	Volume	ORFV Particles
[µm]			[%]			[mL]	[IU]
1	3 ± 1	3 ± 1	99 ± 17	21 ± 10	123 ± 29	8 ± 5	$1.8 \times 10^7 \pm 1.1 \times 10^7$
3–5	37 ± 1	2 ± 1	56 ± 1	5 ± 1	100 ± 2	31 ± 1	$7.0 \times 10^8 \pm 2.2 \times 10^6$

Explanations for these observations for the 1 µm membranes could be sought in the nature of the chromatographic column, which was single-use and assembled manually. Thus, variations in the individual set-up can be expected. Additionally, the 3–5 µm membranes were of reinforced cellulose, adding more stability to the column bed. We assumed that by using in-line mixing, the PEG/ORFV suspension was not completely homogenous, leading to spontaneous increases in pressure due to higher local viscosities. The bigger pores with a lower backpressure might have been less affected by this behavior and allowed for higher loading volumes [11]. Last, the increased virus concentration in the flow-through, and thus reduced yields, could be due to a limited spontaneous encounter of the precipitating targets and the stationary phase inside the matrix with bigger pores, leading to a reduced accretion of the virions.

Another interesting observation throughout this experimental set-up was the recovery in the two elution fractions, i.e., down-flow (in the flow direction of loading) and up-flow (counter direction), which were performed consecutively, as previously described [15]. A considerable fraction of the ORFV was eluted from the 1 µm membranes (20%), whereas the yield from bigger pores increased by only 5%. This leads to the assumption that for the 1 µm membranes, ORFV accumulated in or on the upper layers of the membranes, leading to a limitation similar to an increased incubation time prior to loading (see Section 3.1.3). Presumably, the big size of the Orf virions (up to 200 × 300 nm [27–29]) caused this effect, which has not been reported before for other viruses using in-line mixing, such as for the

bacteriophage M13K07 (7 × 900 nm) [9], the lentivirus (80–100 nm) [18], or the adeno-associated virus (25 nm) [17]. Hence, pore sizes of the stationary phase need a careful validation to prevent filtration effects and to maximize loading capacities in SXC. We further concluded that in-line mixing is a valid alternative to the previously applied offline mixing for the ORFV [13,14].

3.3. Comparison of Buffering Systems in the SXC Process

Throughout our experiments, using CPB and TRIS buffering systems, a tendency for reduced yields using CPB instead of TRIS was observed for different batches of the ORFV. We systematically investigated the SXC performance with different buffers, i.e., CPB, TRIS, PBS, and HEPES (Figure 3). All buffers were of neutral pH, and supplemented with NaCl for a physiological conductivity of 15 mS cm^{-1}. To facilitate a comparison with the 1 µm membrane modules, the load volume was set again to 10 mL. The highest yields were achieved in the presence of PBS (91 ± 19%) and HEPES (82 ± 10%). The application of CPB showed a significantly reduced yield as compared to PBS (Δ 26%) and HEPES (Δ 17%), as well as increased concentrations in flow-through and wash. The online DLS analytics support these trends with according increases (Figure S5). By fractionizing the elution, the major share of the ORFV was detected in the first 4 mL of elution for all buffers (Figure 3). This curtailment allowed for a concentration factor of 2.5× compared to the applied volume of 10 mL The additional elution of 6 mL increased the recovery of infectious ORFV by only 5%. Thus, the total concentration factor with a 4 mL elution volume was 1.9×, considering the 0.25-times dilution of the virus solution to generate the PEG-enriched feed.

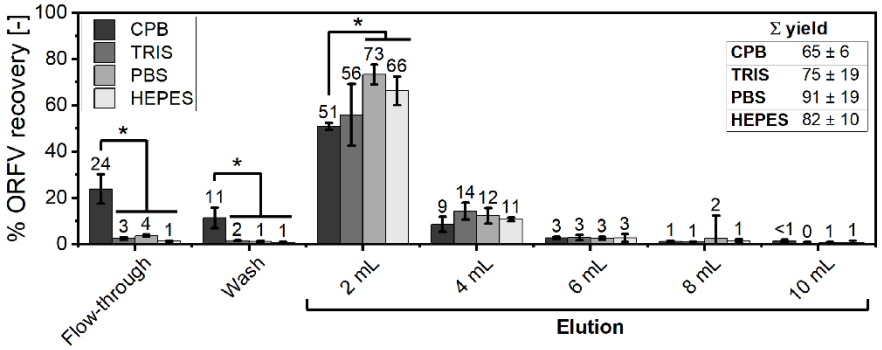

Figure 3. Performance of the steric exclusion chromatography (SXC) depending on the buffer. The Orf virus (ORFV) was processed via SXC (load: 8% PEG_{8000} (polyethylene glycol, 8000 Da); elution: 0% PEG, 0.4 M NaCl) in different buffering systems of neutral pH and physiological conductivity: 0.1 M CPB (dark grey), 20 mM TRIS-HCl (medium grey), PBS (light grey), and 0.1 M HEPES (white). The pre-mixed ORFV/PEG solution was directly applied to the column without an incubation time. The triplicate runs were fractionated into flow-through, i.e., sample application, wash, and elution. The elution itself was fractionated into 5 × 2 mL. Each set of three runs was analyzed regarding the concentration of infectious ORFV. On a volumetric basis, the recoveries were calculated relative to the respective feed. The statistical analysis of the recoveries was performed via ANOVA with a *Tukey* test ($\alpha = 0.05$) for $n = 3$. Asterisks (*) indicate significant differences within the respective group. Representative chromatograms may be found in the Supplementary Material Section S4.2.

Next to the chromatographic experiments, offline precipitation kinetics were conducted. A similar approach was described before by Gagnon et al. [43] for hydrophobic interaction chromatography. The authors pointed towards the positive correlation of precipitation efficiency and retention on such stationary phases. In our study, the differences among the buffers, concerning the ORFV yield, were reflected by offline precipitation kinetics. A slightly smaller size (Δ 500 nm) of the precipitates, incubated in CPB, was measured, as compared to TRIS (data not shown). This observation should be attributable

to the addition of the citrate component as well as the higher concentration (two-times) of phosphate, as PBS showed no analogous deviations. Both, citrate and phosphate, are strongly kosmotropic salts. It was reported before that kosmotropic substances induce a stronger effect in inhibiting the target retention throughout SXC [9]. The complex nature of solute interactions and the influence of such additives is further discussed in Section 3.4. It can be concluded here that the choice of the buffering system has a significant influence on the SXC performance, and should be made with care.

3.4. Changes in the ORFV Yield Depending on Salt Addition in the SXC Load

After the evaluation of different buffering systems, an ion-specific effect on the ORFV yield in the SXC and the precipitation success was expected. To explore this further, we assessed salts with varying concentrations according to their position in the Hofmeister series (Equation (1)) [44] (Figure 4)., i.e., Na_2SO_4, KCl, NaCl, $NaNO_3$, $MgSO_4$, and $MgCl_2$. The salts were combined with 8% PEG_{6000} and were applied, according to the previous findings, in an SXC process with ORFV using 3–5 µm membranes and in-line mixing. To generate a standard procedure for loading, and to facilitate a comparison of the results, the maximum loading volume was determined for the 3–5 µm membranes using "standard" conditions. Here, the feed consisted of a 20 mM TRIS-HCl buffer with 180 mM NaCl, and the elution of the same TRIS buffer, but with 400 mM NaCl. The pressure limit of 0.4 MPa was reached after a 40 mL load. This procedure was adapted to ensure the use of the membrane modules' full binding capacity, thus reducing the relative loss due to unspecific binding.

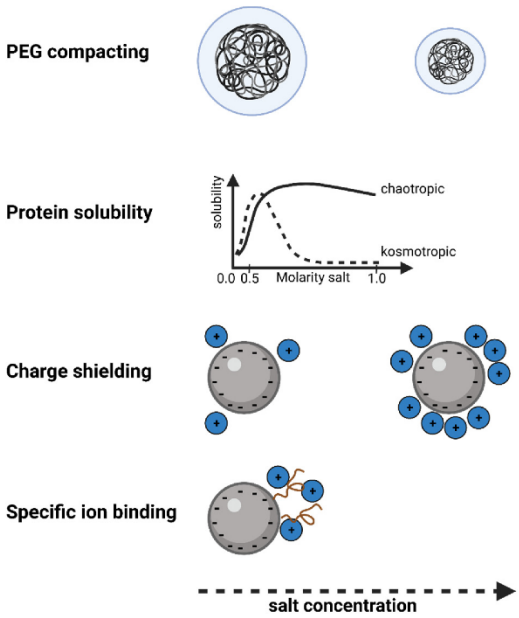

Figure 4. Salt concentration-dependent impact on PEG/salt and salt/protein interactions. Figure prepared using biorender.com.

In contrast to the previous experiments, an additional second elution step after the standard elution in the direction of flow, down-flow (DF), was included in this set-up, using countercurrent flow (up-flow, UF). Comparing the impurity removal of protein (BCA protein assay, Thermo Fisher Scientific) and dsDNA (Quant-iT PicoGreen dsDNA assay, Thermo Fisher Scientific), no differences were detected for the application of the different salts, i.e., less than 1% residual protein and 25–40% residual dsDNA were found in the elution fraction (data not shown).

$$\begin{array}{c} \xrightarrow{\text{chaotropic}} \\ SO_4^{2-} < HPO_4^{2-} < CH3COO^- < Cl^- < NO_3^- < CLO_3^- < I^- \\ NH_4^+ < K^+ < Na^+ < Mg^{2+} < Ca^{2+} \\ \xleftarrow[\text{kosmotropic}]{} \end{array} \quad (1)$$

3.4.1. Influence of Salts on SXC According to the Hofmeister Series

First, the different salts, i.e., Na_2SO_4, KCl, NaCl, $NaNO_3$, $MgSO_4$, and $MgCl_2$, were applied at a 20 mM final concentration in the SXC and in the precipitation studies. The precipitation study revealed two pronounced effects: Compared to a negative control without salt addition (2500 nm), both salts containing 20 mM Mg^{2+} increased the ORFV aggregate size up to 4000 nm after 2 h, whereas Na_2SO_4 reduced the aggregate size to 1500 nm (Figure 5B). Further, NaCl, KCl, and $NaNO_3$ had no impact on the precipitation at a 20 mM concentration. The size of the aggregates correlated with the SXC yields (Figure 5A). The highest ORFV yields were found for 20 mM $MgCl_2$ (84%), followed by $MgSO_4$ (65%). The other four salts, Na_2SO_4, KCl, NaCl, and $NaNO_3$, indicated no significant differences in the individual SXC fractions. However, the addition of 20 mM Na_2SO_4 yielded roughly 10% more infectious ORFV in the elution fraction.

In the presented SXC experimental set-up, PEG is the driving force for precipitation and, after water, the most abundant solute [9]. Thus, changes in the precipitation efficiency should be dominated by the influence of salts on the PEG. In several preceding studies, different salts were applied in the SXC, which were described to mainly cause the following effects, some of them well-known from precipitation [9–11,23] (Figure 4). The first of these effects is the reduction of the target retention at high salt concentrations (approx. > 0.3 M), caused by a compacting of the PEG molecules [9–11]. Hence, the size of the PEG-deficient zone is reduced, suppressing the exclusion effect. This effect has been highlighted with salts following the Hofmeister series, meaning more kosmotropic salts show a stronger negative influence on the retention, as shown for the impact of $(NH_4)_2SO_4$ as compared to NaCl on an immunoglobulin G retention by Lee et al. [9]. Secondly, at low salt concentrations (<0.2 M), the pH is the dominant variable, as it determines the charge (repulsion) of the targets, which is more pronounced for targets with a high charge density, such as phages or nucleic acids [9,10]. By increasing the salt concentration, the process can benefit from charge shielding, which facilitates a higher density packing of the targets [23]. Last, specific ion-binding can alter the charge distribution of the surface proteins of the viral particles, as was described for phosphates [45].

The observation of an increased yield with Na_2SO_4 in the SXC process was unexpected. Theoretically, this kosmotropic salt should have had a negative effect on the yield, as described before [9], which was supported by the precipitation kinetics, showing reduced efficiencies (Figure 5B,C). We propose that the 10% increase in target retention might be due to the ability of strongly kosmotropic salts to retain targets on uncharged surfaces, as was summarized by Arakawa and Gagnon [46] for size exclusion and ion exchange media. It remains to test higher concentrations of Na_2SO_4 to evaluate the effect of the salt-induced target retention on the stationary phase. Such tests could also be insightful for further investigations on the solubility maximum of the ORFV in the presence of kosmotropic salts. The pre-column pressure and loading volumes for the different salts were comparable (Table S5). With the here tested range (20–200 mM) for the ORFV precipitation, we could not make a distinction between the impact of PEG-compacting and the target solubility induced by the salts (Figure 4).

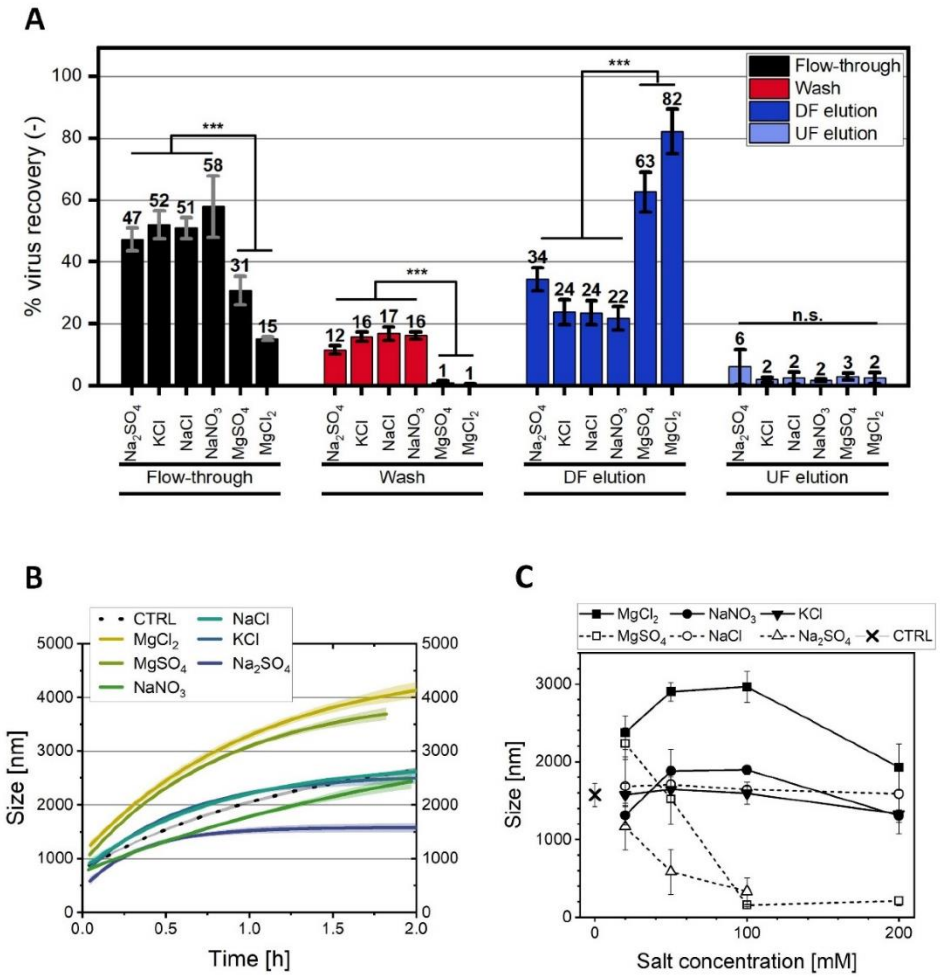

Figure 5. Variation of the salt type throughout the steric exclusion chromatography (SXC). The Orf virus (ORFV) was processed via SXC (load: 8% PEG_{6000} (polyethylene glycol, 6000 Da); elution: 0% PEG, 0.4 M NaCl) in 20 mM TRIS buffer, pH 7.4, supplemented with 20 mM of different salts, i.e., Na_2SO_4, KCl, NaCl, $NaNO_3$, $MgSO_4$, and $MgCl_2$. The load was stopped when the pressure limit of 0.4 MPa was reached or 40 mL PEG/ORFV suspension were loaded. The fractions load (flow-through), wash, and the two elution types, down-flow, DF, (in the direction of loading), and up-flow, UF, (countercurrent) were collected and analyzed for the relative ORFV recovery (**A**). (**B**) depicts the time-dependent precipitation kinetics of the cell culture-derived ORFV supernatant with the same conditions as the SXC loads. Using the same salts at 20–200 mM concentration, (**C**) shows the ORFV precipitate sizes after 0.5 h incubation time. CTRL indicates 8% PEG_{6000} without salt addition. The statistical analysis of the recoveries (**A**) was performed via ANOVA with a *Tukey* test ($\alpha = 0.001$) for $n = 3$. Asterisks (***) indicate significant differences within the respective group.

3.4.2. Concentration-Dependent Precipitation

Next, the precipitation kinetics of the aforementioned salts, Na_2SO_4, KCl, NaCl, $NaNO_3$, $MgSO_4$, and $MgCl_2$, combined with ORFV, was analyzed up to 200 mM. Concerning the Mg^{2+} salts, the increase in the precipitation efficiency remained constant for tests with 20, 50, and 100 mM $MgCl_2$ (~4000 nm), but decreased, as observed before, for 200 mM (3000 nm) (Figure 5C). A similar effect was visible for $NaNO_3$, but with smaller sizes of

1000–1500 nm. $MgSO_4$, on the contrary, revealed a complete prevention of precipitation at 100 and 200 mM. Na_2SO_4 followed the same trend as $MgSO_4$. The other two salts, NaCl and KCl, showed no concentration-dependent impact in the precipitation behavior of the cell culture-derived ORFV.

This picture allows for several salt-specific assumptions. Firstly, PEG-compacting is the dominant variable at the maximum salt concentration (200 mM) for $MgCl_2$ and $NaNO_3$. Secondly, with increasing concentrations, kosmotropic ions (SO_4^{2-}) control the precipitation of the ORFV, instead of the chaotropic ions (Mg^{2+}). Thus, the influence of divalent ions might be stronger, compacting the PEG at a smaller concentration. Divalent ions are also known to be more effective charge-shielding agents, facilitating the precipitation behavior of proteins (Figure S7). Thus, thirdly, this could be the cause for the increase in the precipitation efficiency for $MgCl_2$ and $NaNO_3$, which was not observed for NaCl and KCl. Fourthly, the protein solubility does not dictate the precipitation process. Mg^{2+} was reported to bind to protein surfaces [47], increasing the solubility of viruses [48]. Counteracting this hydration, Mg^{2+} is categorized as more chaotropic, which is known to increase protein solubility (salting-in) up to a maximum plateau [49], preventing the crowding-out (Figure 4). Kosmotropic compounds, on the contrary, themselves undergo a preferential exclusion in a salt-protein system [46,47]. They induce a preferential hydration of the virus surface [47], enhancing the precipitation in a concentration-dependent manner, with a minimum at low molarities (<0.5 M) [49]. Clearly, these solubility effects of the proteins are of an opposite nature for the presented results. We assume that the effects on the PEG are dominant in this system, and the concentrations of the salts were too low to show solubility-dependent effects.

3.4.3. Concentration-Dependent Impact of NaCl and $NaNO_3$

In Figure 5C, three distinct curve progressions were observed for the salt concentration-dependent PEG precipitation of the ORFV: (1) NaCl and KCl did not influence the aggregate size, as compared to the control without a salt addition; (2) $NaNO_3$ and $MgCl_2$ revealed curves with a size maximum between 100 and 200 mM; and (3) the two SO_4^{2-} salts showed a maximum at the lowest tested concentration (20 mM) with an asymptotic decrease.

Here, we selected NaCl and $NaNO_3$ from the group (1) and (2), respectively, to investigate the correlation between the ORFV cell culture precipitate size and the SXC recovery. Just as for the experiments with 20 mM salt, the ORFV retention in the SXC correlated with the aggregate size for $NaNO_3$, but not for NaCl. In detail, for $NaNO_3$, the aggregate size was maximal with 1900 nm at 50 and 100 mM (Figure 5C). The ORFV yield in the SXC processes suggested a similar behavior (Figure 6A) with a maximum of 64% ORFV yield at 100 mM $NaNO_3$. Interestingly, the differences in the aggregate size did not correlate in a quantitative manner with the SXC yields. This was even more pronounced for NaCl. Here, the salt concentration caused no differences in the aggregate size in the range of 0 to 200 mM (Figure 5C). The yield in the SXC process, however, was elevated with increasing concentrations from 26%, to 51%, to 61% for 20, 50, and 200 mM (Figure 6B). The increase in yield was comparative to the findings mentioned by Lee et al. [9] and Levanova and Poranen [23], where reduced mutual charge repulsion led to a higher density packing of the targets. The first study predicted the concentration necessary for a sufficient charge-shielding at 200 mM NaCl for phage M13K07. In our study, the highest yield for NaCl was predicted to be in the range of at least 200 mM.

Observing this complex behavior, precipitation kinetics, as conducted in this research, can indicate increasing or decreasing SXC efficiencies, however, not for every case. More research is necessary to understand the complex interactions within the chromatographic columns, particularly, if additional salts are applied.

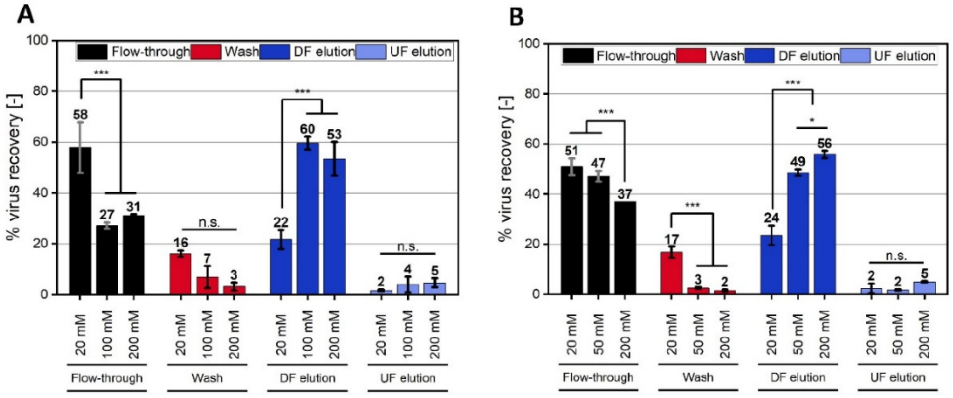

Figure 6. Steric exclusion chromatography (SXC) of the Orf virus (ORFV) with NaCl and $NaNO_3$ at concentrations up to 200 mM. The SXC of the ORFV was performed with 8% PEG_{6000} (polyethylene glycol, 6000 Da) in the loading buffer, 0% PEG, and 0.4 M NaCl in the elution buffer. 20 mM TRIS buffer and pH 7.4 were used for all experiments. The load and wash were supplemented with 20–200 mM of $NaNO_3$ (**A**) or NaCl (**B**). The load was stopped when the pressure limit of 0.4 MPa was reached, or when 40 mL PEG/ORFV suspension were applied. The runs were fractionated into flow-through (load), wash, and the two elutions, up-flow, UF, (in the direction of loading), and down-flow, DF, (counter-flow). Each fraction was analyzed for its relative ORFV recovery. The statistical analysis of the recoveries was performed via ANOVA with a *Tukey* test ($\alpha = 0.001$) for $n = 3$. Asterisks (***) indicate significant differences within the respective group.

4. Conclusions

In this study, we have summarized practical considerations for the application and characterization of the SXC. We focused especially on three factors with a considerable influence on the SXC performance for an ORFV purification, which have not yet been extensively characterized before: (1) the comparison of pore sizes of the stationary phases, (2) the contact time of PEG and the target, and (3) a variety of salts and their concentrations. While smaller pores of the stationary phase reduce the necessary PEG concentrations, bigger pores induce a lower backpressure with similar yields. Especially, if extended contact times of PEG and the target are expected, increased precipitate sizes might cause unwanted filtration effects when using small-pored membranes. Further care should be taken in the selection of buffers and other salts, due to their influence on the precipitation process. Yield losses were encountered when applying kosmotropic substances, such as citrate. However, Mg^{2+}, strongly chaotropic, acted beneficial on the SXC process. To further understand these interactions, we propose that the analysis of the surface protein composition of the target is beneficial for predicting salt-specific effects on the preferential depletion mechanism. Last, although a quantitative prediction was not possible, the precipitation success correlated qualitatively in most cases. Thus, we conclude that offline precipitation kinetics can be a valuable tool to predict the target retention in SXC. In summary, we suggest the use of cellulose membranes with 3–5 µm pore diameter for a stable ORFV purification. Although the impurity removal was not affected, the load volume could be increased with these membranes. Additionally, we expect Mg^{2+} salts to increase the virus binding to the membrane column in SXC without increasing the PEG concentration.

Supplementary Materials: The following supporting information can be downloaded at: https://www.mdpi.com/article/10.3390/membranes12111070/s1, Section S1: Influence of salts on the infectivity assay; Section S2: Screening of relevant process parameters for the SXC with the ORFV; Section S3: Description ORFV aggregation behavior in dependence of PEG_{6000} and pH; Section S4: Chromatograms; Section S5: pH-dependent charge measurements of ORFV with NaCl and $MgCl_2$. References [5,8,9,50] are cited in the supplementary materials.

Author Contributions: Conceptualization, F.E., K.L. and S.O.; Funding acquisition, R.A. and M.W.W.; Investigation, F.E., K.L. and S.O.; Methodology, F.E. and K.L.; Project administration, M.W.W.; Resources, F.P.; Supervision, M.W.W.; Validation, F.E., K.L. and S.O.; Visualization, F.E.; Writing—original draft, F.E.; Writing—review and editing, K.L., F.P., R.A. and M.W.W. All authors have read and agreed to the published version of the manuscript.

Funding: This work was financially supported by the Heinrich Böll Foundation with a doctoral scholarship to FE and the University of Applied Sciences Mittelhessen, Giessen, Germany. Additionally, an EXIST-Forschungstransfer grant (03EFKBW171) of the German Federal Ministry for Economic Affairs and Energy was granted and the project was co-funded by the European Regional Development Fund as part of the Union's response to the COVID-19 pandemic (IGJ-ERDF-Program Hesse-React EU 20008790).

Data Availability Statement: Not applicable.

Acknowledgments: The author would like to thank for the diligent work of Yasmina M.J. Harsy on the ORFV charge characterization and the infectivity assay as well as of Marleen Steger on the time-dependent SXC experiments. The thorough proofreading of the manuscript by Catharine Meckel-Oschmann is greatly acknowledged. We highly appreciate the provision of the regenerated cellulose membranes by Sartorius Stedim. The presented manuscript is part of FE's dissertation at the Graduate Centre for Engineering Sciences under the aegis of the Justus-Liebig University Giessen, Germany, in cooperation with the University of Applied Sciences Mittelhessen, Giessen, Germany.

Conflicts of Interest: RA is CEO of Prime Vector Technologies, a company developing the Orf virus vector platform. FE and KL were employed by Prime Vector Technologies before the time of this study. All other authors declare no conflict of interest. The funders had no role in the design of the study; in the collection, analyses, or interpretation of data; in the writing of the manuscript; or in the decision to publish the results.

References

1. Wolff, M.W.; Reichl, U. Downstream Processing of Cell Culture-Derived Virus Particles. *Expert Rev. Vaccines* **2011**, *10*, 1451–1475. [CrossRef] [PubMed]
2. Hoffmann, D.; Leber, J.; Loewe, D.; Lothert, K.; Oppermann, T.; Zitzmann, J.; Weidner, T.; Salzig, D.; Wolff, M.W.; Czermak, P. Purification of New Biologicals Using Membrane-Based Processes. In *Current Trends and Future Developments on (Bio-) Membranes: Membrane Processes in the Pharmaceutical and Biotechnological Field*; Basile, A.B., Charcosset, C., Eds.; Elsevier: Amsterdam, The Netherlands, 2019; pp. 123–150. ISBN 9780128136065.
3. Morenweiser, R. Downstream Processing of Viral Vectors and Vaccines. *Gene Ther.* **2005**, *12* (Suppl. S1), 103–110. [CrossRef] [PubMed]
4. Atha, D.H.; Ingham, K.C. Mechanism of Precipitation of Proteins by Polyethylene Glycols. Analysis in Terms of Excluded Volume. *J. Biol. Chem.* **1981**, *256*, 12108–12117. [CrossRef]
5. Miekka, S.I.; Ingham, K.C. Influence of self-association of proteins on their precipitation by poly(ethylene glycol). *Arch. Biochem. Biophys.* **1978**, *191*, 525–536. [CrossRef]
6. Ingham, K.C. Precipitation of proteins with polyethylene glycol. In *Guide to Protein Purification*; Deutscher, M.P., Ed.; Elsevier: Amsterdam, The Netherlands, 1990; pp. 301–306.
7. Sim, S.-L.; He, T.; Tscheliessnig, A.; Mueller, M.; Tan, R.B.H.; Jungbauer, A. Branched polyethylene glycol for protein precipitation. *Biotechnol. Bioeng.* **2012**, *109*, 736–746. [CrossRef] [PubMed]
8. Tao, S.-P.; Zheng, J.; Sun, Y. Grafting Zwitterionic Polymer onto Cryogel Surface Enhances Protein Retention in Steric Exclusion Chromatography on Cryogel Monolith. *J. Chromatogr. A* **2015**, *1389*, 104–111. [CrossRef] [PubMed]
9. Lee, J.; Gan, H.T.; Latiff, S.M.A.; Chuah, C.; Lee, W.Y.; Yang, Y.-S.; Loo, B.; Ng, S.K.; Gagnon, P. Principles and Applications of Steric Exclusion Chromatography. *J. Chromatogr. A* **2012**, *1270*, 162–170. [CrossRef] [PubMed]
10. Gagnon, P.; Toh, P.; Lee, J. High Productivity Purification of Immunoglobulin G Monoclonal Antibodies on Starch-Coated Magnetic Nanoparticles by Steric Exclusion of Polyethylene Glycol. *J. Chromatogr. A* **2014**, *1324*, 171–180. [CrossRef]
11. Wang, C.; Bai, S.; Tao, S.-P.; Sun, Y. Evaluation of Steric Exclusion Chromatography on Cryogel Column for the Separation of Serum Proteins. *J. Chromatogr. A* **2014**, *1333*, 54–59. [CrossRef] [PubMed]
12. Lothert, K.; Offersgaard, A.F.; Pihl, A.F.; Mathiesen, C.K.; Jensen, T.B.; Alzua, G.P.; Fahnøe, U.; Bukh, J.; Gottwein, J.M.; Wolff, M.W. Development of a downstream process for the production of an inactivated whole hepatitis C virus vaccine. *Sci. Rep.* **2020**, *10*, 3018. [CrossRef] [PubMed]
13. Lothert, K.; Pagallies, F.; Eilts, F.; Sivanesapillai, A.; Hardt, M.; Moebus, A.; Feger, T.; Amann, R.; Wolff, M.W. A scalable downstream process for the purification of the cell culture-derived Orf virus for human or veterinary applications. *J. Biotechnol.* **2020**, *323*, 221–230. [CrossRef] [PubMed]

14. Lothert, K.; Pagallies, F.; Feger, T.; Amann, R.; Wolff, M.W. Selection of chromatographic methods for the purification of cell culture-derived Orf virus for its application as a vaccine or viral vector. *J. Biotechnol.* **2020**, *323*, 62–72. [CrossRef] [PubMed]
15. Lothert, K.; Sprick, G.; Beyer, F.; Lauria, G.; Czermak, P.; Wolff, M.W. Membrane-Based Steric Exclusion Chromatography for the Purification of a Recombinant Baculovirus and its Application for Cell Therapy. *J. Virol. Methods* **2020**, *275*, 113756. [CrossRef] [PubMed]
16. Marichal-Gallardo, P.; Pieler, M.M.; Wolff, M.W.; Reichl, U. Steric Exclusion Chromatography for Purification of Cell Culture-Derived Influenza A Virus Using Regenerated Cellulose Membranes and Polyethylene Glycol. *J. Chromatogr. A* **2017**, *1483*, 110–119. [CrossRef]
17. Marichal-Gallardo, P.; Börner, K.; Pieler, M.M.; Sonntag-Buck, V.; Obr, M.; Bejarano, D.; Wolff, M.W.; Kräusslich, H.-G.; Reichl, U.; Grimm, D. Single-use capture purification of adeno-associated viral gene transfer vectors by membrane-based steric exclusion chromatography. *Hum. Gene Ther.* **2021**, *32*, 959–974. [CrossRef] [PubMed]
18. Labisch, J.J.; Kassar, M.; Bollmann, F.; Valentic, A.; Hubbuch, J.; Pflanz, K. Steric exclusion chromatography of lentiviral vectors using hydrophilic cellulose membranes. *J. Chromatogr. A* **2022**, *1674*, 463148. [CrossRef] [PubMed]
19. Gränicher, G.; Babakhani, M.; Göbel, S.; Jordan, I.; Marichal-Gallardo, P.; Genzel, Y.; Reichl, U. A high cell density perfusion process for Modified Vaccinia virus Ankara production: Process integration with inline DNA digestion and cost analysis. *Biotechnol. Bioeng.* **2021**, *118*, 4720–4734. [CrossRef]
20. Eilts, F.; Steger, M.; Pagallies, F.; Rziha, H.-J.; Hardt, M.; Amann, R.; Wolff, M.W. Comparison of sample preparation techniques for the physicochemical characterization of Orf virus particles. *J. Virol. Methods* **2022**, *310*, 114614. [CrossRef] [PubMed]
21. Alvim, R.G.F.; Lima, T.M.; Silva, J.L.; de Oliveira, G.A.P.; Castilho, L.R. Process intensification for the production of yellow fever virus-like particles as potential recombinant vaccine antigen. *Biotechnol. Bioeng.* **2021**, *118*, 3581–3592. [CrossRef]
22. Eilts, F.; Steger, M.; Lothert, K.; Wolff, M.W. The Suitability of Latex Particles to Evaluate Critical Process Parameters in Steric Exclusion Chromatography. *Membranes* **2022**, *12*, 488. [CrossRef]
23. Levanova, A.; Poranen, M.M. Application of Steric Exclusion Chromatography on Monoliths for Separation and Purification of RNA Molecules. *J. Chromatogr. A* **2018**, *1574*, 50–59. [CrossRef]
24. Sim, S.-L.; He, T.; Tscheliessnig, A.; Mueller, M.; Tan, R.B.H.; Jungbauer, A. Protein precipitation by polyethylene glycol: A generalized model based on hydrodynamic radius. *J. Biotechnol.* **2012**, *157*, 315–319. [CrossRef]
25. Gagnon, P. Chromatographic Purification of Virus Particles. In *Encyclopedia of Industrial Biotechnology*; Flickinger, M.C., Ed.; John Wiley & Sons, Inc.: Hoboken, NJ, USA, 2009.
26. Broide, M.L.; Tominc, T.M.; Saxowsky, M.D. Using phase transitions to investigate the effect of salts on protein interactions. *Phys. Rev. E* **1996**, *53*, 6325–6335. [CrossRef]
27. Nagington, J.; Horne, R.W. Morphological Studies of Orf and Vaccinia Viruses. *Virology* **1962**, *16*, 248–260. [CrossRef]
28. Nitsche, A.; Gelderblom, H.R.; Eisendle, K.; Romani, N.; Pauli, G. Pitfalls in Diagnosing Human Poxvirus Infections. *J. Clin. Virol.* **2007**, *38*, 165–168. [CrossRef] [PubMed]
29. Wang, R.; Luo, S. Orf Virus: A New Class of Immunotherapy Drugs. In *Systems Biology*; Vlachakis, D., Ed.; IntechOpen: London, UK, 2019.
30. Amann, R.; Rohde, J.; Wulle, U.; Conlee, D.; Raue, R.; Martinon, O.; Rziha, H.-J. A new rabies vaccine based on a recombinant ORF virus (parapoxvirus) expressing the rabies virus glycoprotein. *J. Virol.* **2013**, *87*, 1618–1630. [CrossRef]
31. Rziha, H.-J.; Büttner, M.; Müller, M.; Salomon, F.; Reguzova, A.; Laible, D.; Amann, R. Genomic Characterization of Orf Virus Strain D1701-V (Parapoxvirus) and Development of Novel Sites for Multiple Transgene Ex-pression. *Viruses* **2019**, *11*, 127. [CrossRef]
32. Rziha, H.-J.; Rohde, J.; Amann, R. Generation and Selection of Orf Virus (ORFV) Recombinants. *Methods Mol. Biol.* **2016**, *1349*, 177–200. [CrossRef] [PubMed]
33. Rziha, H.-J.; Büttner, M. Parapoxviruses. In *Reference Module in Life Sciences*; Elsevier: Amsterdam, The Netherlands, 2020; p. 1505.
34. Friebe, A.; Siegling, A.; Weber, O. Inactivated Orf-virus shows disease modifying antiviral activity in a guinea pig model of genital herpesvirus infection. *J. Microbiol. Immunol. Infect.* **2018**, *51*, 587–592. [CrossRef]
35. Rintoul, J.L.; Lemay, C.G.; Tai, L.H.; Stanford, M.M.; Falls, T.J.; de Souza, C.T.; Bridle, B.W.; Daneshmand, M.; Ohashi, P.S.; Wan, Y.; et al. ORFV: A novel oncolytic and immune stimulating parapoxvirus therapeutic. *Mol. Ther.* **2012**, *20*, 1148–1157. [CrossRef]
36. O'Leary, M.P.; Choi, A.H.; Kim, S.-I.; Chaurasiya, S.; Lu, J.; Park, A.K.; Woo, Y.; Warner, S.G.; Fong, Y.; Chen, N.G. Novel oncolytic chimeric orthopoxvirus causes regression of pancreatic cancer xenografts and exhibits abscopal effect at a single low dose. *J. Transl. Med.* **2018**, *16*, 110. [CrossRef] [PubMed]
37. Bergqvist, C.; Kurban, M.; Abbas, O. Orf virus infection. *Rev. Med. Virol.* **2017**, *27*, e1932. [CrossRef] [PubMed]
38. Fleming, S.B.; Wise, L.M.; Mercer, A.A. Molecular genetic analysis of orf virus: A poxvirus that has adapted to skin. *Viruses* **2015**, *7*, 1505–1539. [CrossRef]
39. Friebe, A.; Siegling, A.; Friederichs, S.; Volk, H.-D.; Weber, O. Immunomodulatory effects of inactivated parapoxvirus ovis (ORF virus) on human peripheral immune cells: Induction of cytokine secretion in monocytes and Th1-like cells. *J. Virol.* **2004**, *78*, 9400–9411. [CrossRef]
40. Royo, M.d.C.P.; Beulay, J.-L.; Valery, E.; Jungbauer, A.; Satzer, P. Mode and dosage time in polyethylene glycol precipitation process influences protein precipitate size and filterability. *Process Biochem.* **2022**, *114*, 77–85. [CrossRef]

41. Zumaeta, N.; Byrne, E.P.; Fitzpatrick, J.J. Predicting precipitate particle breakage in a pipeline: Effect of agitation intensity during precipitate formation. *Chem. Eng. Sci.* **2006**, *61*, 7991–8003. [CrossRef]
42. Lukasik, J.; Scott, T.M.; Andryshak, D.; Farrah, S.R. Influence of Salts on Virus Adsorption to Microporous Filters. *Appl. Environ. Microb.* **2000**, *66*, 2914–2920. [CrossRef] [PubMed]
43. Gagnon, P.; Grund, E.; Lindbäck, T. Large Scale Process Development for Hydrophobic Interaction Chromatography, Part 1: Gel Selection and Development of Binding Condition. *BioPharm* **1995**, *8*, 21–29.
44. Hofmeister, F. Zur Lehre von der Wirkung der Salze. *Naunyn-Schmiedeberg's Arch. Exp. Pathol. Pharmakol.* **1888**, *24*, 247–260. [CrossRef]
45. Michen, B.; Graule, T. Isoelectric Points of Viruses. *J. Appl. Microbiol.* **2010**, *18*, 290. [CrossRef] [PubMed]
46. Arakawa, T.; Gagnon, P. Excluded Cosolvent in Chromatography. *J. Pharm. Sci.* **2018**, *107*, 2297–2305. [CrossRef] [PubMed]
47. Arakawa, T.; Timasheff, S.N. Preferential interactions of proteins with salts in concentrated solutions. *Biochemistry* **1982**, *21*, 6545–6552. [CrossRef] [PubMed]
48. Arakawa, T.; Kita, Y.; Ejima, D.; Gagnon, P. Solvent Modulation of Column Chromatography. *Protein Pept. Lett.* **2008**, *15*, 544–555. [CrossRef] [PubMed]
49. Gagnon, P.; Mayes, T.; Danielsson, Å. An adaptation of hydrophobic interaction chromatography for estimation of protein solubility optima. *J. Pharm. Biomed. Anal.* **1997**, *16*, 587–592. [CrossRef]
50. Salgyn, S.; Salgyn, U.; Bahadir, S. Zeta Potentials and Isoelectric Points of Biomolecules: The Effects of Ion Types and Ionic Strengths. *Int. J. Electrochem. Sci.* **2012**, *7*, 12404–12414.

Supplementary Material:

A summary of practical considerations for the application of the steric exclusion chromatography for the purification of the Orf viral vector

S1: Influence of salts on the infectivity assay

Material and Methods

The influence of the implemented salts (KCl, NaCl, $NaNO_3$, $MgCl_2$, $(NH_4)_2SO_4$, Na_2SO_4, and $MgSO_4$) on the infectivity assay was assessed by the change of the infection result, i.e., percentage of virus positive cells compared to a positive control (100 %). For this purpose, Vero cells were prepared as described in **section 2.3** and each well was infected with 50 µL of virus stock (2×10^6 IU mL^{-1}). Immediately afterwards, 100 µL of salt solution was added. The salt solutions, with concentrations of 2 – 200 mM, were prepared in neutral 20 mM TRIS buffer. The positive control (PCTRL) was DMEM with 5 % FCS, known to stabilize the ORFV. Additionally, a negative control (NCTRL) of pure TRIS buffer without salt addition was titrated. Each salt concentration was tested in quadruplicates. The mean readout was normalized to the positive control (100 %). The statistical analysis was performed by ANOVA with a *Tukey* test ($\alpha = 0.05$) (Origin Pro 2021b, OriginLab Corporation).

Results and Discussion

The addition of salts to the infectivity assay indicated a small impact on the readout of infected cells for most tested concentrations (**Figure S1**). KCl, NaCl, $MgCl_2$, and Na_2SO_4 revealed no significant change for 50 – 200 mM. Concerning $NaNO_3$ and $MgSO_4$, only 50 mM and 200 mM affected the assay by lower relative readouts of 12 % and 31 %, respectively. As the addition of the salt-free buffer (NCTRL) revealed a 4 % relative reduction, we assumed that the impact of 50 mM $NaNO_3$ was still in the range of the relative error of the assay (up to 10 %). However, $MgSO_4$ should be diluted at least down to 100 mM to prevent deviating results. Concerning $(NH_4)_2SO_4$, the only salt tested in the full range, 2 – 200 mM, indicated a negative impact on cell viability at concentrations ≥5 mM. In this assay, a destabilizing effect on the virus itself could not be eliminated. Thus, $(NH_4)_2SO_4$ was excluded from further experiments.

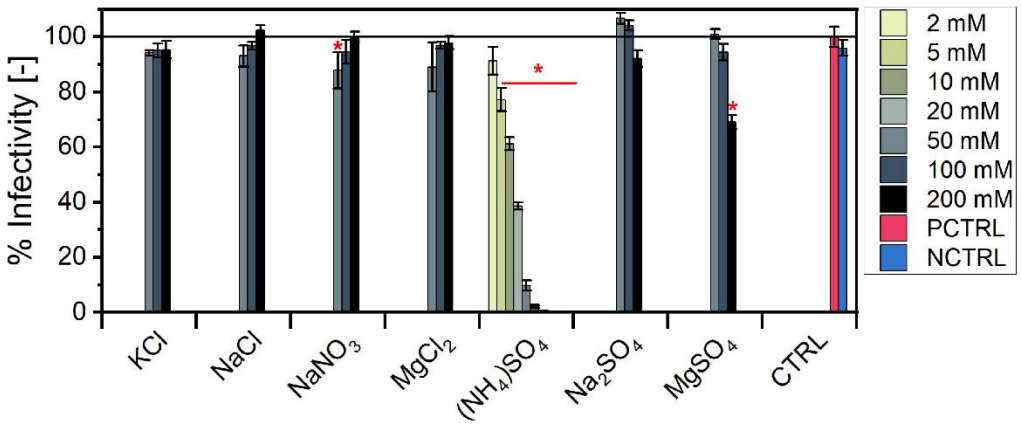

Figure S1: Influence of salts on the infection of Vero cells with the ORFV.

The impact of seven different salts (KCl, NaCl, $NaNO_3$, $MgCl_2$, $(NH_4)_2SO_4$, Na_2SO_4, and $MgSO_4$) on the readout of the infectivity assay with the ORFV was assessed. Therefore, cells were infected with ORFV, and immediately afterwards, salt solutions with concentrations of 2 – 200 mM were applied. After incubation, the percentage of virus-positive cells was measured, and compared to a positive control (PCTRL) (100 %), which consisted of DMEM with FCS. Additionally, a negative control (NCTRL) was prepared with pure TRIS buffer without salt addition. The deviation from the PCTRL was statistically analyzed by ANOVA with a *Tukey* test ($\alpha = 0.05$). Asterisks indicate significance.

S2: Screening of relevant process parameters for SXC with the ORFV

A DOE-based approach was chosen to evaluate the infectious ORFV yield in the SXC process, depending on the PEG concentration (4 – 8 %), the PEG molecular weight (6,000 – 12,000 Da), and the flow rate (0.5 – 6.0 mL min^{-1}). **Table S1** depicts the characteristics of the design, and **Table S2** the ANOVA for the response of infectious ORFV yield.

The resulting model for the response of the ORFV recovery in the elution fraction combines the three factors from **Table S2**. The prediction of the PEG concentration and molecular weight is depicted in **Figure 1A** in the main text. **Figure S2** shows the influence of the flow rate and the PEG precipitation on the SXC performance. A maximum of 60 % ORFV yield was achieved for high PEG concentrations (8 %) and low flow rates (0.5 mL min^{-1}). The recovery was reduced to 35 % for the other extrema of the two factors. Such dependencies of the target retention and the residence time in the SXC were reported before [2]. By reducing the flow rate, the chance of target accretion to the membrane, which is a random process governed by target-surface collisions, is increased. Additionally, shear forces by the passing fluid, which can reverse the accretion, are reduced [3].

Table S1: Model characteristics for the evaluation of the infectious ORFV yield in the SXC process with varying flow rates, PEG concentration, and molecular weight.

Study Type	Response surface
Design Type	I-optimal
Subtype	Randomized
Runs	24
Blocks	No

Table S2: ANOVA of the infectious ORFV yield in the SXC process with varying flow rates, PEG concentration, and molecular weight.

Clarified ORFV cell culture supernatant was processed via SXC with varying PEG concentration (4 – 8 %) (c_{PEG}), PEG molecular weight (MW) (6,000 – 12,000 Da), and flow rates (0.5 – 6.0 mL min^{-1}). The elution fraction of the SXC was analyzed regarding the infectious ORFV concentration and the yield calculated. The data was analysed by ANOVA ($\alpha = 0.05$) for a linear model.

	Infectious ORFV yield [%]	
Source	**F-value**	**p-value**

4

A (PEG MW)	2.67	0.1190	significant
B (% c_{PEG})	10.95	0.0037	significant
C (Flow rate)	10.64	0.0041	significant

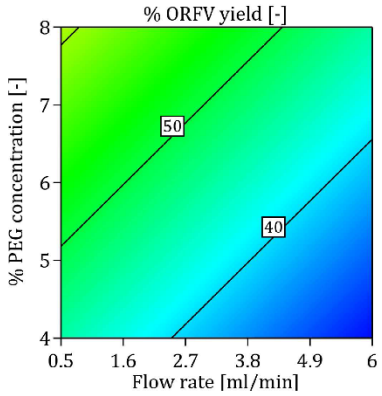

Figure S2: ORFV yield after SXC process with varying PEG concentration and flow rates

Clarified ORFV cell culture supernatant was processed via SXC with varying PEG concentration (4 – 8 %) and flow rate (0.5 – 6.0 mL min^{-1}). The PEG molecular weight was set to 6,000 Da. The elution fraction of the SXC was analyzed regarding the infectious ORFV concentration and the calculated yield. The colouring of the contour plots is coded as follows for the infectious ORFV yield: 30 – 40 % (blue), 40 – 45 % (light blue), and 45 – 60 % (green).

S3: Description of the ORFV aggregation behaviour in dependence of PEG_{6000} and pH

S3.1 Statistical analysis of ORFV aggregation kinetics

Aggregation kinetics, evaluating the influence of time, pH, and PEG_{6000} concentration on the size distribution of ORFV-containing samples, were conducted by dynamic light scattering measurements over the course of 60 min.

Table S3: Model characteristics for the evaluation of ORFV aggregation kinetics with varying pH and PEG concentrations

Study Type	Response surface
Design Type	Historical Data
Subtype	Split-plot
Groups	19
Runs	826
Blocks	No

Table S4: ANOVA of ORFV aggregation kinetics with varying pH and PEG concentrations.

Clarified ORFV cell culture supernatant was mixed 1:4 with concentrated buffers to generate defined pH (4 – 7.4) and PEG_{6000} (0 – 12 %) concentrations (c_{PEG}). The size distribution of the 19 different samples (groups) was measured every 5 min by DLS over the course of 60 min. The data was analyzed by a restricted maximum likelihood ANOVA ($\alpha = 0.05$) for a quadratic split-plot model. The whole-plot represents the unchanged factors (pH and PEG concentration) in each of the groups, and the subplot is used to display the time-dependent changes within.

	Size [nm]		
Source	**F-value**	**p-value**	
Whole-plot	94.08	< 0.0001	significant
a (pH)	27.00	0.0002	significant
b (% c_{PEG})	429.85	< 0.0001	significant
ab	0.28	0.6088	
a^2	4.45	0.0549	
b^2	16.21	0.0015	significant
Subplot	489.33	< 0.0001	significant
C (time)	92.83	< 0.0001	significant
aC	1.33	0.2487	
bC	225.56	< 0.0001	significant
C^2	140.47	< 0.0001	significant

Additional attributes in the statistical analysis were the low variance between the groups (0.125), which rendered the analysis equivalent to a randomized design, as well as the overall small variance (0.145),

the high R^2 (0.99), and the minimal difference between R^2 and the adjusted R^2 ($\Delta = 0.0002$), which indicated a well-fitted model.

The model predicts the design space for the factors PEG_{6000} concentration and pH values, visualized in **Figure S3**. Observing the impact of the pH on the aggregation behavior, a maximum in precipitate size was reached at the highest tested PEG concentration (12 %) and the lowest pH value (pH 4). This pH value is in close proximity of the isoelectric point determined for the applied ORFV genotype in CPB of pH 3.5 (data not shown). At pH 4, omitting PEG, no spontaneous aggregation was observed by DLS. However, an increase of self-association tendencies has to be expected [4].

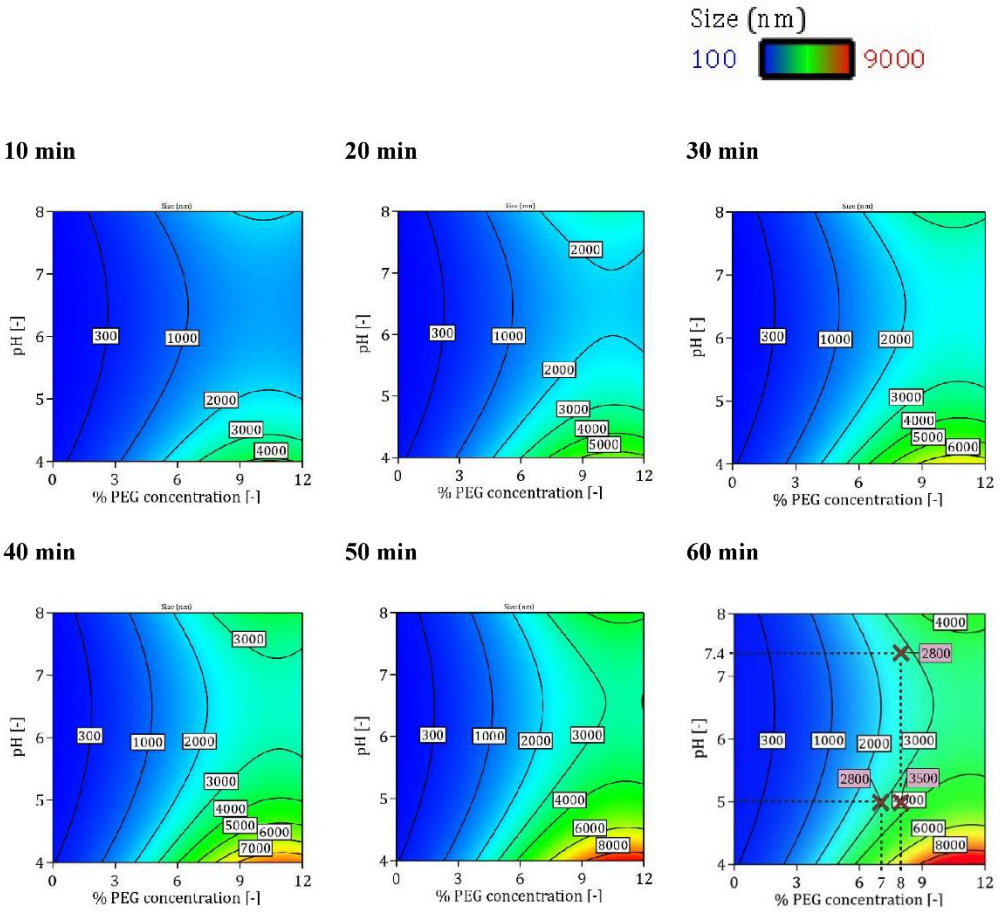

Figure S3: pH-dependent aggregation of cell culture-derived Orf viruses (ORFV) in the presence of polyethylene glycol (PEG).

Aggregation kinetics of the ORFV were analyzed using dynamic light scattering in dependence of the pH (4 – 7.4) and the PEG_{6000} (6,000 Da) concentration (0 – 12 %), mimicking conditions of the steric exclusion

chromatography. Over the course of 60 min, measurements were conducted automatically every 5 min on each sample. After each incubation, the respective sample was visualized by bright-field microscopy (**Figure S4**). Using a design of experiments-based approach, the size response data was statistically analyzed (**Table S4**) and a model was generated. The colouring of the contour plots is coded as follows for the mean size: 100 – 2,000 nm (blue), 2,000 – 3,000 nm (light blue), 3,000 – 6,000 nm (green), 6,000 – 7,000 nm (yellow), and 7,000 – 9,000 nm (red).

S3.2 Visualization of cell culture-derived ORFV aggregates

After the dynamic light scattering measurements, the samples of each run were visualized by bright-field microscopy in a conventional Neubauer chamber in order to control the observed volume. **Figure S4** depicts four of the extrema representing the conducted runs.

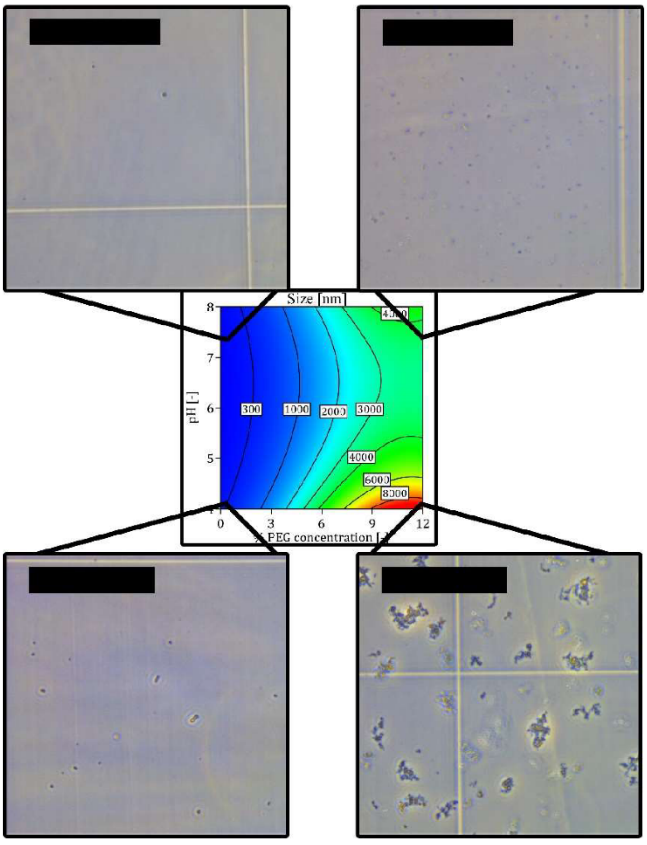

8

Figure S4: Visualization of the influence of the PEG_{6000} concentration and the pH on the ORFV aggregation size.

Clarified ORFV cell culture supernatant was combined with CPB according to a DOE-based plan. The final mixes of deviating pH (4 – 7.4) and PEG_{6000} concentrations (0 – 12 %) were analyzed using dynamic light scattering over the course of 60 min. The kinetic data was statistically analyzed (**Table S4**), and a model was generated of the size response (**Figure S3**). After each measurement run, a defined volume of the sample was visualized by bright-field microscopy in a Neubauer chamber. Here, the contour plot for 60 min incubation time is presented again to facilitate a comparison, augmented by the micrographs of the model's corner points. The bar corresponds to 100 µm.

S4: Chromatograms

S4.1 Application of different buffers

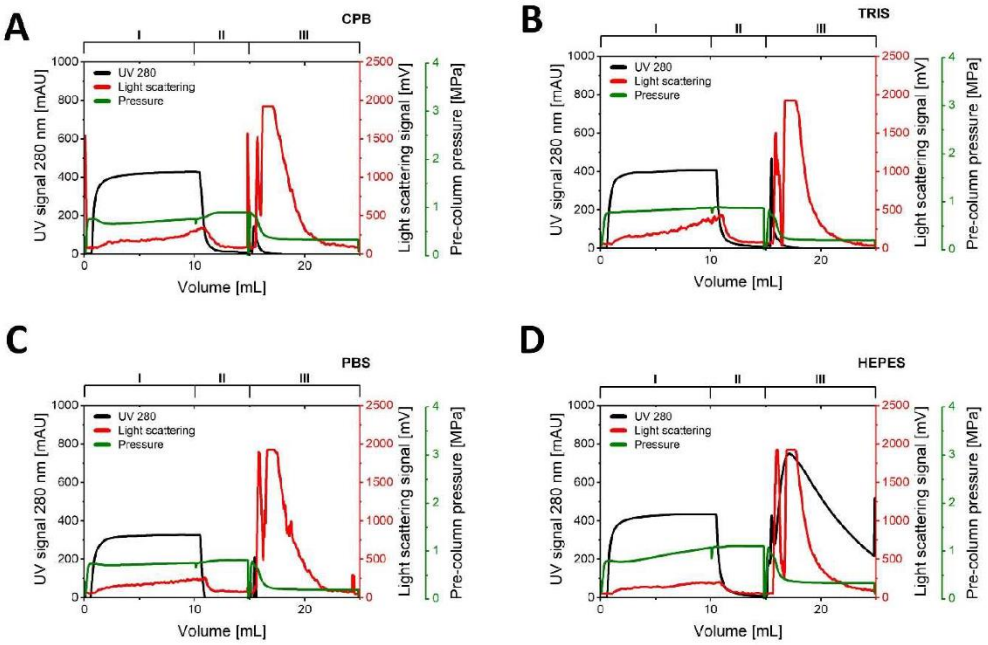

Figure S5: Chromatograms of SXC applications of the ORFV with different buffers

The ORFV was processed via SXC in different buffering systems: 0.1 M citrate phosphate buffer (CPB, **A**), 20 mM TRIS-HCl (**B**), PBS (**C**), and 0.1 M HEPES (**D**). All buffers were of neutral pH and adjusted to a conductivity of 15 mS cm^{-1} with NaCl. Each buffering system was used for all process steps, i.e., the load and wash buffer (8 % PEG_{8000}) as well as the elution buffer (0 % PEG, 0.4 M NaCl). The runs were fractionated into flow-through, i.e., sample application (I), wash (II), and elution (III).

S4.2 SXC with varying incubation times

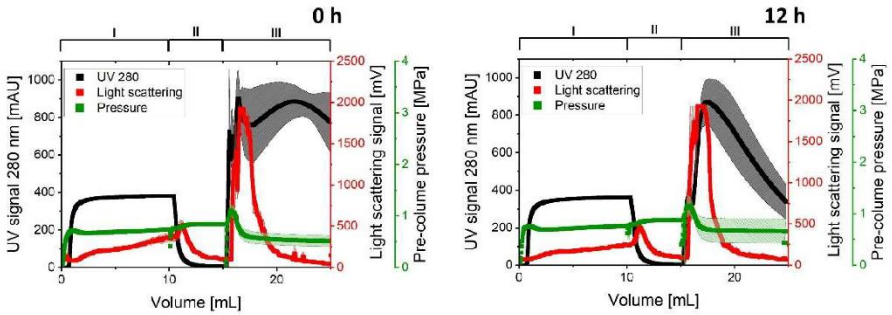

Figure S6: Chromatograms of SXC applications of the ORFV with varying incubation times

The Orf virus (ORFV) was processed via SXC (load: 8 % PEG_{8000} (polyethylene glycol, 8,000 Da); elution: 0 % PEG, 0.4 M NaCl) in citrate phosphate buffer with a pH-value of 7.4. The pre-mixed ORFV/PEG solution was either directly applied to the column (0 h), or incubated for 12 h before loading. The triplicate runs were fractionated into flow-through, i.e., sample application (I), wash (II), and elution (III). The online monitoring included an UV signal at 280 nm (black), light scattering signal (red), and the pre-column pressure (green). The hatched areas indicate the respective standard deviations.

S5: pH-dependent charge measurements of ORFV with NaCl and $MgCl_2$

We tested the impact of the protein-salt interaction by monitoring the pH-dependent zeta potential of the ORFV in the presence of different salt concentrations, under the omission of PEG (**Figure S7**). At 15 mS cm^{-1}, the pH-dependent charge was a similar function for both salts ranging from -6 mV at pH 4.5 to the isoelectric point at pH 3.5. $MgCl_2$ reduced the charge at pH 2.5 by roughly 1 mV compared to NaCl, and lead to a steeper y-intercept passage. With increasing conductivity, the pH of the isoelectric point was reduced to approximately pH 3 at 35 mS cm^{-1} for both salts. Here, the function for NaCl was roughly linear, still down to -6 mV at pH 4.5. $MgCl_2$, on the contrary, diminished the charge to -3 mV at the latter pH, and the charge remained constant (0 mV) at pH values below the isoelectric point. At 45 mS cm^{-1}, the picture was similar to that for 45 mS cm^{-1} for NaCl, with an isoelectric point at pH 2.5. For $MgCl_2$, however, no positive charge was measured at this concentration. This observation implies that charge shielding was more effective for Mg^{2+} than for Na^{+}, as was reported before for divalent ions [5]. Charge shielding increases the efficiency of SXC, as it facilitates target association. This was not observed in the ORFV precipitation kinetics (**Figure 4D+E**). Thus, the effect of charge-shielding was neglectable for the applied salt concentration range. Interestingly, both salts showed specific interactions with the virus surface molecules, demonstrated by the change of the isoelectric point with increasing salt concentrations.

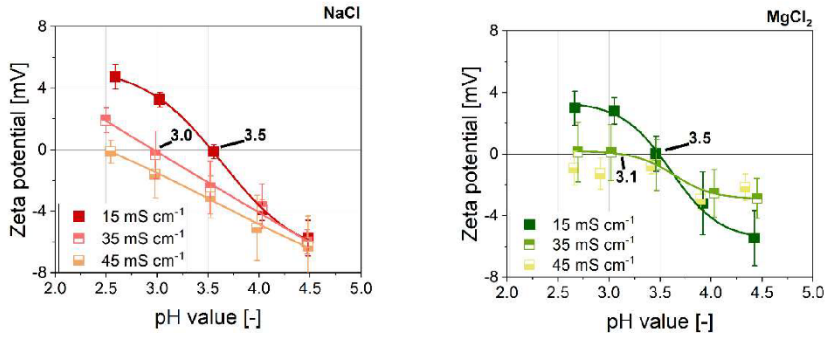

Figure S7: pH-dependent surface charge of the Orf virus (ORFV).

Purified ORFV was titrated to a range of pH values (2.5 – 4.5) with a citrate phosphate buffer, covering the isoelectric point of the virus. The samples were spiked with NaCl (left) and $MgCl_2$ (right) to equal 15, 35, or 45 mS cm^{-1}.

References

[1] H.-J. Rziha, J. Rohde, R. Amann, Generation and Selection of Orf Virus (ORFV) Recombinants, Methods Mol Biol 1349 (2016) 177–200. https://doi.org/10.1007/978-1-4939-3008-1_12.

[2] S.-P. Tao, J. Zheng, Y. Sun, Grafting Zwitterionic Polymer onto Cryogel Surface Enhances Protein Retention in Steric Exclusion Chromatography on Cryogel Monolith, J Chromatogr A 1389 (2015) 104–111. https://doi.org/10.1016/j.chroma.2015.02.051.

[3] J. Lee, H.T. Gan, S.M.A. Latiff, C. Chuah, W.Y. Lee, Y.-S. Yang, B. Loo, S.K. Ng, P. Gagnon, Principles and Applications of Steric Exclusion Chromatography, J Chromatogr A 1270 (2012) 162–170. https://doi.org/10.1016/j.chroma.2012.10.062.

[4] S.I. Miekka, K.C. Ingham, Influence of self-association of proteins on their precipitation by poly(ethylene glycol), Arch Biochem Biophys 191 (1978) 525–536. https://doi.org/10.1016/0003-9861(78)90391-0.

[5] S. Salgyn, U. Salgyn, S. Bahadir, Zeta Potentials and Isoelectric Points of Biomolecules: The Effects of Ion Types and Ionic Strengths, Int. J. Electrochem. Sci. 7 (2012) 12404–12414.

CHAPTER 4: Summary on advancements and future perspectives

The ORFV as a vector platform offers promising pharmaceutical applications as oncolytic, antiviral, immunomodulatory, gene therapeutic or vaccine agent. Therefore, an established production process with high yields of infectious virus, and a facilitated adaption to new genotypes is essential. In this dissertation project, several steps to achieve this goal were investigated.

In the first part of investigations, the ORFV was characterized in detail concerning its susceptibility to different degradation forces and options to maintain its infectivity. For these studies, the virus was prepared by different methods, i.e., ultracentrifugation or SXC. Both approaches performed equally well in terms of reducing impurities, maintaining virus integrity, and yielding infectious virus. While the ultracentrifugation was advantageous for higher infectious ORFV concentrations, the SXC could be performed in a more rapid manner. With virus prepared by either method, the effect of chemical, thermal, and mechanical stress conditions on the ORFV infectivity revealed a high stability compared to other enveloped viruses. In detail, ORFV infectivity was robust within pH 5-7.4 as well as in the presence of all tested buffering substances without citrate component and an ionic strength up to 0.5 M for all tested salts but NH_4Cl. Ammonium salts, however, where shown to affect the infectivity assay, which interfered with the determination of its influence on ORFV infectivity itself. Substances from the groups of amino acids, surfactants, proteins, had no deactivating effect in the commonly applied ranges for pharmaceutical processing. The thermal stability of the ORFV revealed a long-term stability of up to 12 weeks at 4 °C, and increased deactivation with increasing temperature. Nevertheless, short-term storage of 2 d at 37 °C did not affect the very robust virus. Freeze-thawing and storage in frozen form showed no impact. A similar robust picture was observed with mechanical stress. The ORFV has a low shear-sensitivity, but ultrasonication might affect the viral infectivity throughout processing. The addition of proteins, e.g., fetal calf serum or recombinant HSA (rHSA), reduced degradation, especially visible for long-term storage. In studies for stabilization options, additionally several sugars, e.g., sucrose or trehalose, and amino acids, e.g., arginine, were found to increase the ORFV infectivity stability. However, the effect depended on the storage temperature. The highest stability was achieved by protein addition at all temperatures but above 25 °C. Here, sucrose and arginine were able to increase the storage stability of the ORFV. These findings were combined to propose two formulation types: 1 % rHSA and 5 % sucrose for any formulation in liquid and frozen form. If long-term heat is expected, the rHSA is replaced by 150 mM arginine.

With the observed results, conclusions for ORFV production, especially the DSP, can be drawn. While shear-stress due to filtration or pumping is expected to be neglectable for the ORFV, ultrasonication, e.g., to break up virus aggregates or to induce cell lysis, should be evaluated with care. For the choice of chromatographic unit operations, limitation due to salt addition or buffers are not expected if ammonium salts are excluded. The addition of stabilizing substances such as sugars between the DSP unit operations could reduce storage-induced deactivation. Amino acid and protein supplementation are no option throughout the DSP as they would increase the load of protein-related products, which are to be removed. If possible, the processing and storage should

be performed under cooled conditions. The integration of these suggestions in a full DSP train might increase the achievable yield of infectious ORFV in the production process. Furthermore, the stability of infectious ORFV might be increased with a suitable formulation for distribution and pharmaceutical application.

The second focus of the research project was on the SXC as DSP unit operation for ORFV production. The method has been applied for several viral targets, including the ORFV, with high yields. In these studies, several critical process parameters were identified, i.e., the type of PEG, the buffer pH (and charge of the target), the ionic strength, the mixing technique, the flow rate, and the type of the stationary phase. In this work, three unexplored parameters were investigated, i.e., the pore size of the stationary phase, the incubation time and mixing strategy of the PEG / ORFV solution, and the addition of salts. The mode of operation of the parameters was explored by using precipitation kinetics and correlating them with the SXC efficiencies. The experiments revealed filtration effects by using small membrane pores (1 µm) and elongated incubation times. Filtration is an unwanted side effect of the SXC, induced by big precipitates, which cannot pass the pores. However, the size of the precipitates was several times bigger than the pores without causing direct column blockage and pressure surges. Thus, the static precipitation kinetics could only indicate the efficiency of the aggregation in a certain buffer condition. The implementation of the suggested operation modes, adapting the pore size to at least 3-5 µm and operating with in-line mixing, indicated a fail-safe operation of the SXC with reduced back-pressure. With these precautions pore blockage events could be reduced if unexpected holding times occur. Nonetheless, at the same time the ORFV yields were reduced. Thus, an optimization problem with an increased PEG concentration arose. A solution to this was offered by the use of chaotropic salts like Mg^{2+}, which were able to increase the precipitation efficiency and ORFV yield in the SXC at constant PEG concentration. Additionally, the PEG-problem could be approached by adjusting the pH towards the isoelectric point of the ORFV (pH 3.5-4.5), while operating above pH 5 to preserve the ORFV infectivity. To answer these hypotheses, an appropriate model system might improve the sample throughput. As latex particles showed deviating results from ORFV results, functionalization with proteins might solve this issue. This could be supported by offline precipitating kinetics in an agitated system, which represents the SXC operation more accurately.

In conclusion, this work offers a broad overview on degrading forces and stabilizing conditions for the ORFV infectivity, which is essential for the application as pharmaceutical viral vector. By integrating this toolset in any USP and DSP unit operations, a higher preservation of viral infectivity can be expected. Additionally, investigations on the causes of three critical process parameters for the ORFV processing using SXC were described based on the precipitation efficiencies. Here, an optimization problem of the system back-pressure, and ultimately the ORFV yield, was identified, which is balanced by the PEG-induced viscosity, the pore size of the chromatographic media, and the retention time. This advancement might facilitate future adaptions of the SXC to new targets and the development of a suitable model system.

APPENDIX

ANNOTATIONS ON DATA FROM STUDENT THESES

Within the context of this dissertation project, the experimental and theoretical work of several students, aimed to compile a thesis, was supervised. Every one of these students contributed a great deal to the progress of my research projects and my personal development. Data from students' work, which was published in some form, is acknowledged in the very ones. To recognize every student's support, all student theses are listed in the following.

Harsy, Yasmina M. J.: Stabilitätsstudien eines Orf-Virus basierenden Vektorimpfstoffes, practical work thesis, 2021.

Harsy, Yasmina M. J.: Optimierung einer Flüssigformulierung für einen Orf Virus basierten Vektorimpfstoff, Bachelor thesis, 2021.

Kos, Viktor: Correlations of the purification success of a baculovirus using TRPS, $TCID_{50}$ assay, and qPCR, practical work thesis, unfinished.

Orbay, Sabri: Investigation of the ORF virus purification using the steric exclusion chromatography depending on the salt type, ionic strength and buffer, practical work thesis, 2020.

Orbay, Sabri: Investigations of salt effects on the virus loading during the steric exclusion chromatography, Master thesis, 2021.

Schmidt, Jonas S.: Messung der elektrophoretischen Mobilität funktionalisierter Polystyrenpartikel zur Etablierung einer neuen Analytikmethode des isoelektrischen Punktes mittels Tunable Resistive Pulse Sensing, practical work thesis, 2019.

Schmidt, Jonas S.: Entwicklung einer Analytikmethode zur Messung des isoelektrischen Punktes von biologischen Nanopartikeln mittels Tunable Resistive Pulse Sensing, Master thesis, 2020.

Steger, A. Marleen: Studies on variability of the isoelectric point of parapoxviruses, practical work thesis, 2019.

Steger, A. Marleen: Influence of particle charge and aggregation on the steric exclusion chromatography using latex particles as a model for viruses, Master thesis, 2020.

LIST OF PUBLICATIONS RELATED TO THE DISSERTATION

Articles and book chapters

Eilts, F.; Harsy, Y. M. J.; Lothert, K.; Pagallies, F.; Dalby, P.; Amann, R.; Wolff, M. W. (2023). Investigation of excipients for a stable Orf viral vector formulation. Journal of Virus Research 336, 199213. doi: 10.1016/j.virusres.2023.199213

Eilts, F.; Labisch, J. J.; Orbay, S.; Harsy, Y. M. J.; Steger, M.; Pagallies, F.; Amann, R.; Pflanz, K.; Wolff, M. W. (2023). Stability studies for the identification of critical process parameters for a pharmaceutical production of the Orf virus. Vaccine 41 (32), 4731-4742. doi: 10.1016/j.vaccine.2023.06.047

Eilts, F.; Jordan, L. K.; Harsy, Y. M. J.; Bergmann, S. M.; Becker, A. M.; Wolff, M. W. (2023). Purification and concentration of infectious koi herpesvirus using steric exclusion chromatography. Journal of Fish Diseases 46, 873-886. doi: 10.1111/jfd.13800

Dwivedi, R.; Sharma, P.; Eilts, F.; Zhang, F.; Linhardt, R. J.; Tandon, R.; Pomin, V. H. (2023). Anti-SARS-CoV-2 and anticoagulant properties of *Pentacta pygmaea* fucosylated chondroitin sulfate depend on high molecular weight structures. Glycobiology 33 (1), 75-85. doi: 10.1093/glycob/cwac063

Eilts, F.*; Bauer, S.*; Fraser, K.*; Dordick, J. S.; Wolff, M. W.; Linhardt, R. J.; Zhang, F. (2023). The diverse role of heparan sulfate and other GAGs in SARS-CoV-2 infections and therapeutics. Carbohydrate Polymers 299, 120176. doi: 10.1016/j.carbpol.2022.120167

Eilts, F.; Lothert, K.; Orbay, S.; Pagallies, F.; Amann, R.; Wolff, M. W. (2022). A summary of practical considerations for the application of the steric exclusion chromatography for the purification of the Orf viral vector. Membranes 12 (11), 1070. doi: 10.3390/membranes12111070

Eilts, F.; Steger, M.; Pagallies, F.; Rziha, H.-J.; Hardt, M.; Amann, R.; Wolff, M. W. (2022). Comparison of sample preparation techniques for the physicochemical characterization of Orf virus particles. Journal of Virological Methods 310, 114614. doi: 10.1016/j.jviromet.2022.114614

Eilts, F.; Steger, M.; Lothert, K.; Wolff, M. W. (2022). The suitability of latex particles to evaluate critical process parameters in steric exclusion chromatography. Membranes 12 (5), 488. doi: 10.3390/membranes12050488

Lothert, K.; Eilts, F.; Wolff, M. W. (2022): Quantification methods for viruses and virus-like particles applied in biopharmaceutical production processes. Expert Review of Vaccines 21 (8), 1029-1044. doi: 10.1080/14760584.2022.2072302

Eilts, F.; Harnischfeger, J.; Loewe, D.; Wolff, M. W.; Salzig, D.; Czermak, P. (2021). Production of baculovirus and stem cells for baculovirus-mediated gene transfer into human. In: Pfeifer BA, Hill A (eds) Vaccine Delivery Technology: Methods and Protocols, vol 2183. Springer US, New York, NY, 367–390. doi: 10.1007/978-1-0716-0795-4_19

Lothert, K.; Pagallies, F.; Eilts, F.; Sivanesapillai, A.; Hardt, M.; Moebus, A.; Feger, T.; Amann, R.; Wolff, M. W. (2020): A scalable downstream process for the purification of the cell culture-derived Orf virus for human or veterinary applications. Journal of Biotechnology 323, 221-230. doi: 10.1016/j.jbiotec.2020.08.014

Conference contributions: presentations

Eilts, F.; Lothert, K.; Wolff, M. W. The role of target aggregation throughout the steric exclusion chromatography. BioPro22 Himmelfahrtstagung, Mainz, Germany, 23.-25. May 2022.

Eilts, F.; Lothert, K.; Orbay, S.; Pagallies, F.; Amann, R.; Wolff, M. W. Investigations of the salt/PEG-system throughout the steric exclusion chromatography of the Orf virus. 35th International Symposium and Exhibit on Preparative and Process Chromatography (PREP), Baltimore, MD, USA, 15.-18. May 2022.

Lothert, K.; Pagallies, F.; Eilts, F.; Sivanesapillai, A.; Feger, T.; Amann, R.; Wolff, M. W. Development of a scalable downstream purification process for *Parapoxvirus ovis* (ORFV) purification for human and veterinary application. 41st International Symposium on the Separation of Proteins, Peptides and Polynucleotides (ISPPP), Porto, Portugal, 07.-10. November 2021.

Eilts, F.; Orbay, S.; Pagallies, F.; Amann, R.; Wolff, M. W. Investigation of time- and charge-dependent purification of nanoparticles by membrane-based steric exclusion chromatography. 41st International Symposium on the Separation of Proteins, Peptides and Polynucleotides (ISPPP), Porto, Portugal, 07.-10. November 2021.

Eilts, F.; Steger, M.; Wolff, M. W. Investigation of time- and charge-dependent purification of nanoparticles by membrane-based steric exclusion chromatography. ACS Annual Meeting, Atlanta, GA, USA / online, 22.-26. August 2021.

Eilts, F.; Steger, M.; Lothert, K.; Pagallies, F.; Amann, R.; Wolff, M. W. The impact of purification on the particle integrity of the Orf virus analyzed for an established downstream process. ACHEMA Pulse Congress 2021, online, 15.-16. June 2021.

Wolff, M. W.; Lothert, K.; Eilts, F. Development of globally affordable vaccines and gene therapies. Tosoh Bioseparation Forum, Martiensried, Germany, 30. September - 01. October 2020.

Conference contributions: posters

Rotter, M.; Hanselmann, T.; Käßer, L.; Kneitz, J.; Eilts, F; Dekevic, G.; Cremers, G.; Exner, D.; Czermak, P.; Salzig, D. Kombination optischer Rückstreusensorik und Single-Use-Technologie zur Prozessintensivierung von Zellkultur-Prozessen. 15. Dresdner Sensor-Symposium, online, 06.-08. December 2021.

Eilts, F.; Harsy, Y. M. J.; Orbay, S.; Lothert, K.; Pagallies, F.; Amann, R.; Wolff, M. W. Charge-dependent purification of nanoparticles by steric exclusion chromatography. BioPro21 Himmelfahrtstagung, online, 10.-12. May 2021

Jordan, L. K.; Eilts, F; Becker, A. M.; Wolff, M. W. Steric exclusion chromatography as a method for the purification of koi herpesvirus. 19th International Conference on Diseases of Fish and Shellfish, Porto, Portugal, 8.-12. September 2019.

Authors marked with * contributed equally.
For conference contributions, the presenting author is underlined.